International Journal of Proteomics

Proteomics Sample Preparation, Preservation, and Fractionation

Guest Editors: Gary B. Smejkal, William C. Cho, Paul P. Pevsner, and Winston Patrick Kuo

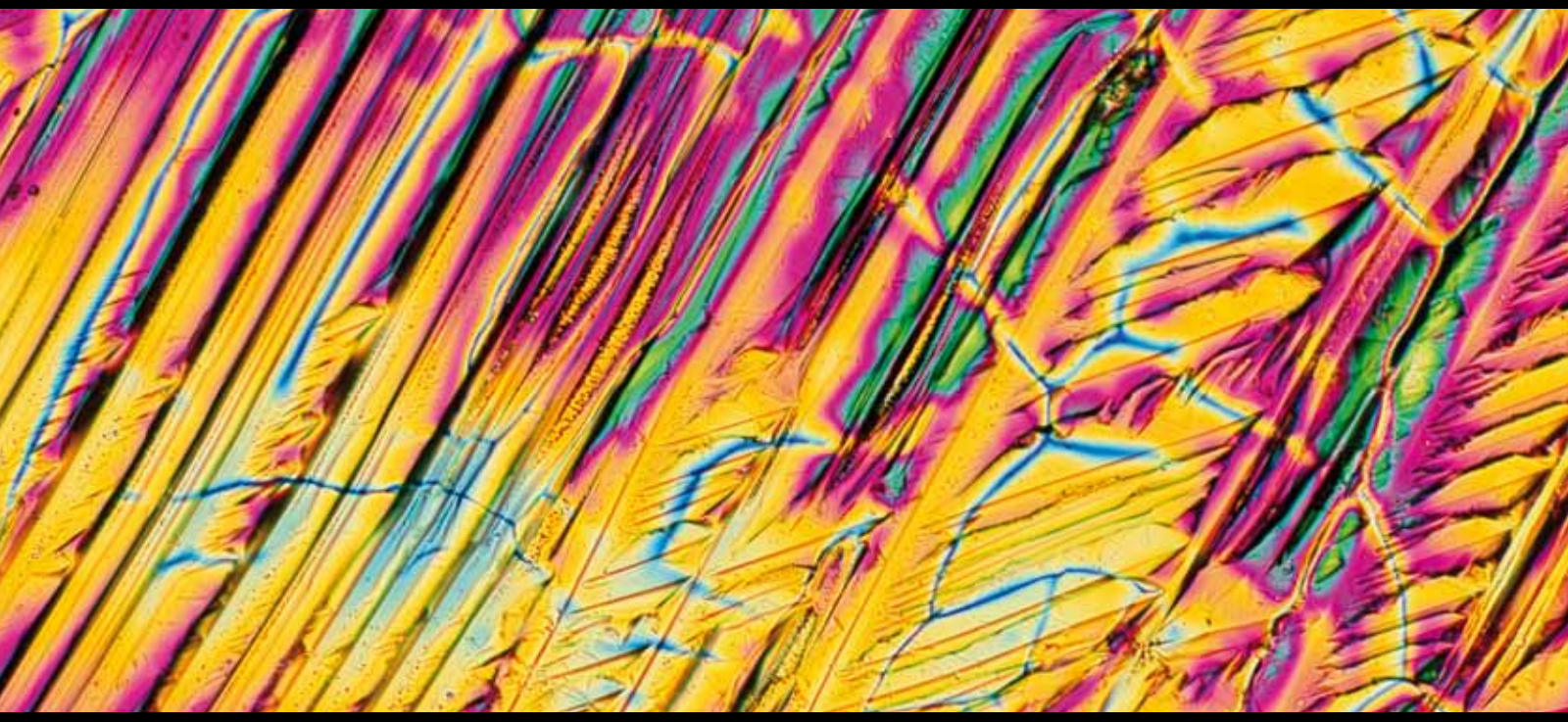

Proteomics Sample Preparation, Preservation, and Fractionation

International Journal of Proteomics

Proteomics Sample Preparation, Preservation, and Fractionation

Guest Editors: Gary B. Smejkal, William C. Cho, Paul P. Pevsner, and Winston Patrick Kuo

Editorial Board

Contents

Hindawi Publishing Corporation
International Journal of Proteomics
Volume 2012, Article ID 701230, 2 pages
doi:10.1155/2012/701230

Editorial

Proteomics Sample Preparation, Preservation, and Fractionation

Gary B. Smejkal[1,2]

[1] *Covaris Inc., 14 Gill Street, Suite H, Woburn, MA 01801, USA*
[2] *Hubbard Center for Genome Studies, University of New Hampshire, Durham, NH, USA*

Correspondence should be addressed to Gary B. Smejkal, gsmejkal@covarisinc.com

Received 16 December 2012; Accepted 16 December 2012

In eukaryotic cells, protein synthesis occurs at the rate of 6–9 amino acid residues per second. With a median length of 360 amino acids, the synthesis of an "average" protein takes about a minute to complete [1]. At this rate, the synthesis of a single molecule of the muscle protein titin, being over 34,000 residues in length, requires over two hours to complete [2]. While this seems slow as biological processes go, the cellular requirement for protein synthesis is satisfied by the huge numbers of ribosomes, which can comprise 30% of a cell's total mass [3]. Human HeLa cells, for example, can contain over nine million ribosomes [4]. Extrapolated from the finding that as many as 80% of the ribosomes can be actively synthesizing protein in metabolically active cells [5], a single cell could theoretically generate 120,000 protein molecules per second.

In its November 2012 release statistics, UniProt/trEMBL reported 28,395,832 sequence entries in its protein database [6]. At the rate of six amino acids per second, a single eukaryotic ribosome working non-stop would require over 48 years to translate the entire database. However, there is protein evidence for only 0.05% and RNA transcript evidence for only 2.21% of the total entries [6]. With fewer than 112,000 sequence entries, *Homo sapiens* comprises only 0.04% of the total sequence entries. It would seem that human proteomics is not in its infancy, it is embryonic.

The number of human proteins is expected to reach into the millions. Immunoglobulins alone are encoded from 70 genes for which there are 320 possible light chain combinations and 10,530 possible heavy chain combinations resulting in 3,369,600 possible quaternary structures [7]. In even the simplest of organisms, the broad concentration of protein expression frequently spanning over nine orders of magnitude compounds the complexity of the proteomic amalgam. An undeterminable number of possible post-translational modifications that produce multiple isoforms of many proteins add another layer of complexity. For instance, there are 3778 distinct genes encoding plasma proteins of which at least 51% of these genes encode more than one protein isoform [8]. Hence, neither genomics nor transcriptomics can reliably predict the protein constituents of cells, tissues, or biological fluids.

The search for biologically important proteins of low abundance is impeded by the enormous range of protein concentrations, as exemplified in human plasma where the mass of albumin is nearly ten billion times greater than that of important signaling proteins such as the interleukins [9, 10]. The diversity of proteins, ranging from very soluble proteins in biological fluids to extremely hydrophobic ones that exist either embedded in lipid membranes or as insoluble aggregates, suggests that the total protein constituency of cells may not be isolated without bias towards or against some protein subpopulations. On the other hand, the complexity of proteomes might be selectively decreased by exploiting the bias toward specific protein subpopulations.

Lessons learned from early computer programmers who coined the phrase "Garbage in, garbage out", downstream proteomics analyses are only as reliable as the upstream sample preparation.

"We now have the technical ability to get the wrong answers with unprecedented speed," commented Carolyn Compton, former Director of the National Cancer Institute, Office of Biorepositories and Biospecimen Research. "If we put the wrong stuff into the front end of our analytical pipeline, we'll pollute the scientific literature with incorrect data that will take us a long time to sort out." [11].

This special issue dedicates to the challenges of sample preparation in the proteomics era. This issue convenes several leaders in the field of proteomics as guest editors,

authors, and reviewers whose contributions have culminated in making this a most substantive work. The articles within this Special Issue are timely and will be of particular interest to the field.

Acknowledgment

The author acknowledges Hamid Khoja and J. D. Herlihy for their helpful suggestions during the preparation of this editorial. G. B. Smejkal is an Affiliate Assistant Professor at the HCGS at UNH.

Gary B. Smejkal

References

[1] L. Brocchieri and S. Karlin, "Protein length in eukaryotic and prokaryotic proteomes," *Nucleic Acids Research*, vol. 33, no. 10, pp. 3390–3400, 2005.

[2] H. Lodish, A. Berk, C. A. Kaiser et al., *Molecular Cell Biology*, W.H. Freeman, New York, NY, USA, 6th edition, 2008.

[3] B. Lewin, *Genes VIII*, Pearson Prentice Hall, New York, NY, USA, 2004.

[4] S. F. Wolf and D. Schlessinger, "Nuclear metabolism of ribosomal RNA in growing, methionine-limited, and ethionine-treated HeLa cells," *Biochemistry*, vol. 16, no. 12, pp. 2783–2791, 1977.

[5] A. Völkl and C. Poort, "Circadian rhythm of protein synthesis activity in the exocrine pancreas of fed and starved rats," *Journal of Cell Science*, vol. 61, pp. 467–473, 1983.

[6] "UniProtKB/TrEMBL Protein Database Release Statistics," 2011, http://www.ebi.ac.uk/uniprot/TrEMBLstats.

[7] T. Paustian and G. Roberts, *Through the Microscope: Adventures in Microbiology*, Textbook Consortia, 4th edition, 2012.

[8] B. Muthusamy, G. Hanumanthu, S. Suresh et al., "Plasma proteome database as a resource for proteomics research," *Proteomics*, vol. 5, no. 13, pp. 3531–3536, 2005.

[9] R. F. Service, "Proteomics: ponders prime time," *Science*, vol. 321, no. 5897, pp. 1758–1761, 2008.

[10] N. L. Anderson and N. G. Anderson, "The human plasma proteome: history, character, and diagnostic prospects.," *Molecular & Cellular Proteomics*, vol. 1, no. 11, pp. 845–867, 2002.

[11] S. Silberman, *Libraries of Flesh: The Sorry State of Human Tissue Storage*, Wired Magazine, 2010.

Hindawi Publishing Corporation
International Journal of Proteomics
Volume 2012, Article ID 515372, 8 pages
doi:10.1155/2012/515372

Research Article

Functional Proteomic Profiling of Phosphodiesterases Using SeraFILE Separations Platform

Amita R. Oka, Matthew P. Kuruc, Ketan M. Gujarathi, and Swapan Roy

ProFACT Proteomics Inc., 1 Deer Park Drive, Suite M, Monmouth Junction, NJ 08852, USA

Correspondence should be addressed to Matthew P. Kuruc, mkuruc@profactproteomics.com

Received 21 March 2012; Revised 29 June 2012; Accepted 2 July 2012

Academic Editor: Winston Patrick Kuo

Functional proteomic profiling can help identify targets for disease diagnosis and therapy. Available methods are limited by the inability to profile many functional properties measured by enzymes kinetics. The functional proteomic profiling approach proposed here seeks to overcome such limitations. It begins with surface-based proteome separations of tissue/cell-line extracts, using SeraFILE, a proprietary protein separations platform. Enzyme kinetic properties of resulting subproteomes are then characterized, and the data integrated into proteomic profiles. As a model, SeraFILE-derived subproteomes of cyclic nucleotide-hydrolyzing phosphodiesterases (PDEs) from bovine brain homogenate (BBH) and rat brain homogenate (RBH) were characterized for cAMP hydrolysis activity in the presence (challenge condition) and absence of cGMP. Functional profiles of RBH and BBH were compiled from the enzyme activity response to the challenge condition in each of the respective subproteomes. Intersample analysis showed that comparable profiles differed in only a few data points, and that distinctive subproteomes can be generated from comparable tissue samples from different animals. These results demonstrate that the proposed methods provide a means to simplify intersample differences, and to localize proteins attributable to sample-specific responses. It can be potentially applied for disease and nondisease sample comparison in biomarker discovery and drug discovery profiling.

1. Introduction

Proteomic profiling based on enzyme activity is assuming significance in drug discovery as it becomes possible to profile selectivity of drugs and their mechanism of action [1]. Such an approach focuses on protein function, an aspect which has been missing from expression proteomics [1]. A functional proteomic profiling approach has the potential not only to help identify targets for diagnosis and therapy [2], specifically in personal medicine [3, 4], but also to reveal the underlying mechanisms of action of disease-sustaining proteins [5].

Methods for global analysis of protein expression and function, including liquid chromatography with mass spectrometry (MS) for shotgun analysis [6, 7], yeast two-hybrid methods [8], and protein microarrays [9], have been crucial in developing the field of proteomics, but they do not provide an accurate assessment of functional states of proteins in cells and tissues [10]. Activity-based protein profiling (ABPP) was first demonstrated for serine hydrolyses [11] and has now been applied to other enzyme classes such as kinases, phosphatases, and histone deacetylates [10, 12]. ABPP typically uses active site-directed covalent probes to interrogate specific subsets (families) of enzymes in complex proteomes to provide a quantitative assessment of the functional state of individual enzymes in the family [10]. The probe-bound enzymes can be visualized with SDS-PAGE or purified using affinity tools for peptide or labeling site identification with MS [10]. Although this approach is promising, it is limited by the availability of suitable synthetic probes. Also, while ABPP categorizes the active site in enzymes, it does not measure the functional kinetics of enzymes and therefore can be considered only as an indirect measure of protein function.

This article proposes a novel approach for localization of a functional enzyme. It forms the central component of the workflow strategy, which has the potential to identify functional biomarkers from natural cellular sources. The proposed method would fill an unmet need for research in drug response and biomarker discovery for investigations

in natural cellular source environments. The physiological relevance of working with natural cellular sources is especially significant for discovery, which targets proteins whose function may be altered by post-translational modification, noncovalent regulatory factors or splice variants. Such an approach may help to reconcile data from high-throughput screening of recombinant proteins to natural cellular sources. It is anticipated that select subproteomes will be subjected to downstream characterization by liquid chromatography mass spectrometry (LC-MS), and other suitable identification methods in common use, so as to annotate sequence and structure to function.

While the term functional proteomics encompasses a variety of phenotypic descriptions of known or measurable functional consequences including cellular response to stimuli [13] and binding interactions [14, 15], etc., the model approach reported herein is limited to characterizing enzyme kinetic properties.

The proposed profiling strategy starts with subfractionation of complex proteomes using SeraFILE [16] (USPTO 20040106131, ProFACT Proteomics, Monmouth Junctions, NJ, USA). This proprietary protein separations platform is configured as a surface library with associated interrogation methods designed to retain bioactivity of the samples. As a result, subproteome pools obtained after SeraFILE separations can be characterized for their enzyme activity properties (e.g., enzyme activity with and without inhibitors, activators, or cosubstrates). Then, a collective functional profile of the original proteome is generated as an integrated profile of the functional properties of the characterized subproteomes. This approach provides multiple data points to characterize and compare samples, thereby increasing the robustness and reliability of analysis. It also allows localization of proteins responsible for sample-specific responses. This profiling method can compare one proteome sample to another (intersample analysis, e,g., tissue type versus tissue type, or normal versus diseased tissue) and can compare different subproteomes of the same complex proteome (intrasample analysis).

The cyclic nucleotide phosphodiesterases (PDEs) enzyme family has been used in this study as a model class of proteins to demonstrate the proposed strategy. PDEs are enzymes that hydrolyze the second messenger adenosine 3′, 5′-cyclic monophosphate (cAMP) or guanosine 3′, 5′-cyclic monophosphate (cGMP), or both. These small molecules along with other nucleotides, lipids, and ions function as secondary messengers [17]. The second messenger cAMP mediates a wide variety of actions of hormones and neurotransmitters and influences cell growth, differentiation, survival, and inflammatory processes [18]. Class I PDEs (found in protozoa and metazoa) are cAMP specific (PDE4, 7 and 8) or cGMP specific (PDE5, 6 and 9) or can hydrolyze both cAMP and cGMP (PDE1, 2, 3, 10, and 11) [17, 19, 20]. A comprehensive review of PDEs can be found in [17, 19, 21].

PDEs are widely acknowledged and explored as drug targets in pulmonary, neurodegenerative, and vascular diseases, and in diabetes, osteoporosis, cancer, rheumatoid arthritis, and depression [22]. Inhibitors of PDE5 and PDE3 are already in clinical use [23], but numerous other PDE inhibitors have not been used for therapeutic purposes due to side effects such as nausea and emesis [24]. The proposed approach to proteomic profiling is guided by the principle that, by discriminating and characterizing PDE variants in natural sources, greater disease-specific therapeutic inhibition/activation can be achieved along with a better understanding of disease pathway dynamics.

This research article demonstrates functional proteomic profiling of cAMP-hydrolyzing phosphodiesterases from bovine and rat brains. Although earlier studies have documented the presence of different types of PDEs in rat and bovine brains, a comprehensive comparative profile of PDE proteomes based on function and content/identity has not been established. It is known that bovine brain exhibits calmodulin-activated PDE activity (PDE1), as well as PDE2, and PDE4 activity [25, 26]. The cAMP hydrolysis activity of PDEs in bovine brain can be stimulated [27] or inhibited [28] by cGMP. Studies on rat brain have identified calmodulin-stimulated PDEs [29–31] (PDE1), as well as PDE4 isoforms [32–34].

SeraFILE was first applied for fractionation of each brain homogenate (sample proteome) into subproteomes, in order to reduce the complexity of PDEs in the sample proteome. Then, these subproteomes were interrogated for cAMP hydrolysis activity in the presence and absence of cGMP. cGMP is another substrate of PDEs and is used as a challenge condition in these experiments. The results were compiled into a signature profile of cAMP hydrolysis characteristics of each sample proteome, defined as an integrated profile of characteristics of SeraFILE-generated subproteomes. The hypothesis was that SeraFILE and associated interrogation methods would generate distinct profiles of enzyme catalyzed cAMP hydrolysis-activities from bovine brain and rat brain homogenates because these are different mammalian species.

2. Materials and Methods

2.1. SeraFILE Surfaces. The SeraFILE inventions [16] encompass the surface characteristics and protocols suitable for differential proteomic fractionation. Each surface architecture was designed to have moderate binding capacity and was prepared with Nugel Epoxy (Biotech Support Group Inc., Monmouth Junction, NJ, USA). The epoxy-coated silica was modified by reacting it with different ligands to generate unique surfaces selectivities and was based on the premise that important ligand protein interactions include hydrogen bonds, ionic interactions (salt bridges), hydrophobic interactions and ring structures. Table 1 illustrates the differences in the properties of the surfaces in the library; however for proprietary protection, details of the surface chemistries remain undisclosed.

An initial screen of 13 surfaces from the library (Table 1) and one underivatized control was performed. Further study was limited to a set of five surfaces (A, B, D, M, and N) from the surface library because the subproteomes obtained from these surfaces had the most distinguishing characteristics (enzyme activity and its response to

Table 1: Mixed-mode properties of SeraFILE surface structures[a]. Table shows potential numbers of hydrogen bond donor/acceptor groups, numbers of cationic/anionic groups, and number of ring structures in the surface ligands, along with relative hydrophobicity of the ligands.

	Surface	Hydrogen bond		Cationic groups	Anionic groups	Relative hydrophobicity[b]	Rings
		Donor groups	Acceptor groups				
Surfaces used in the study	A	1	2		1	2	
	B	1	6		3	2	1
	D	1	4		2	2	1
	M	Multipolymer				1	
	N			1		1	
Surfaces initially screened, but not used in the study	PN	3		3		3	1
	E			Multipolymer		3	
	AP				Multipolymer	1	
	AM	1	2	1		1	
	S				Multipolymer	5	Multipolymer
	F			1		4	
	C	1	2		1	5	1
	PL			1		3	
	PA	1	1		1	4	1
	PC			1		5	1

[a] In cases of polymers, only predominant effect is considered.
[b] Scale 1–5: low-high.

rolipram/vinpocetine/calmodulin, protein concentrations, and SDS profile, data not shown).

2.2. Preparation of Brain Homogenates. Rat brain homogenate (RBH) and bovine brain homogenate (BBH) were supplied by Lampire Biologicals (Pipersville, PA, USA). Whole bovine or rat brain was homogenized in a prechilled blender using 100 mL of extraction buffer for every 50 g of brain tissue. Extraction buffer for BBH was 0.1 M Tris, 2 mM EDTA, and pH 7.5, and for RBH it was 1 mM EDTA, 10 mM HEPES, and pH 7.4. Each extraction buffer was made with protease inhibitor cocktail (Roche, Indianapolis, IN, U.S.A.). Homogenized brain-buffer mixtures were centrifuged at 4°C, and the supernatant was used for the experiments.

2.3. Brain Homogenate Pretreatment (Clarification). RBH and BBH samples were mixed with Cleanascite (Biotech Support Group, Monmouth Junction, NJ, U.S.A.) in a 1 : 16 ratio of Cleanascite-to-homogenate, to remove lipids and particulates. Clarified homogenates were obtained by following mixing and centrifugation steps as given in the manufacturer's protocol.

2.4. Sample Separation. The pretreated homogenates were each subjected to separation by five SeraFILE surfaces (A, B, D, M, and N) [35–38]. For separation of each homogenate, 50 mg of each surface contained in a Spin-X tube (Corning Inc., Corning, NY, U.S.A.) was equilibrated with binding buffer (0.05 M HEPES, 1 mM $MgCl_2$, and pH 6.5). Clarified BBH and RBH were diluted in the binding buffer, to pH 6.5-6.6, and 200 μL of each diluted homogenate (load, 1.16 mg of total protein) was added separately to each of the five surfaces, mixed for 10 mins, and then centrifuged. (Note that the total protein amounts used for SeraFILE separations were based on the sensitivity of the cAMP hydrolysis assay used in our experiments for downstream analysis. The SeraFILE methodology is nevertheless amenable to protocols that can use μg amounts of protein loads). The flowthrough was collected as the 1st SeraFILE fraction, represented as subproteomes A1, B1, D1, M1, and N1, from surfaces A, B, D, M, and N, respectively. The proteins bound on the surfaces were eluted with 200 μL of elution buffer (0.05 M HEPES, 1 mM $MgCl_2$, 0.5 M NaCl, and pH 8.0) using mixing and centrifugation steps as above. The flow-through collected in this process was the 2nd SeraFILE fraction, represented as subproteomes A2, B2, D2, M2, and N2, from surfaces A, B, D, M, and N, respectively. Mixing steps were performed using a MixMate (Eppendorf, Hauppauge, NY, U.S.A.) at 1150 rpm following an initial pulse of mixing on a vortex mixer. Centrifugation steps were performed using a tabletop centrifuge at 16873 rcf for 3 mins. Each brain homogenate, bovine and rat, was used for separations in triplicates.

2.5. cAMP Hydrolysis Activity Assays and Protein Assays. Activity of cAMP hydrolysis in each subproteome was measured using a real-time kinetic assay [39, 40]. This assay links cAMP hydrolysis to NADH oxidation using coupling enzymes (adenylate kinase, pyruvate kinase, and lactate dehydrogenase), and NADH loss can be measured at 340 nm. For each assay, a mixture of reaction buffer and coupling enzymes was equilibrated at room temperature for 16 mins (stage I). Then, subproteomes were each individually added to the reaction mix, and loss in absorbance was measured for 16 mins (stage II). Finally, substrate cAMP or a mix of cAMP and cGMP was added to the assay, and

the loss in absorbance was measured as above (stage III). Final concentrations of assay components were as follows: 9 mM $MgCl_2$, 0.46 mM $CaCl_2$, 46 mM KCl, 46 mM HEPES, 1 mM phosphoenolpyruvate, 46 μM ATP, 0.4 μM NADH, 50 μM cAMP, 0.8 units pyruvate kinase, 4 units lactate dehydrogenase, and 0.06 units adenylate kinase (Sigma, St. Louis, MO, U.S.A.) with 6.25 μL of each enzyme sample. The cAMP hydrolysis activity of each sample was measured as the basal activity (in the absence of cGMP) and as challenged activity (in presence of 25 μM cGMP or 50 μM cGMP). Final volume of the assay was 0.1 mL. Volume-normalized enzyme assays were performed on each replicate subproteomes in a 96-well format using a Multiskan MMC346 plate reader (Thermo Scientific, Hudson, NH, U.S.A.).

To measure cAMP hydrolysis activity in the unfractionated brain homogenates, the clarified homogenates were diluted with binding buffer to obtain 5-6 dilutions of each homogenate, which were then used for the assays as described above.

Protein content of all RBH and BBH proteomes and subproteomes was measured using a BCA assay kit (Pierce, Rockford, IL, U.S.A.). Replicate subproteomes were pooled before protein analysis.

2.6. Calculations. (a) The cAMP hydrolysis activity of each sample was calculated as follows:

$$\text{Enzyme activity } \left(\text{nmoles mL}^{-1}\,\text{min}^{-1}\right) = \frac{\text{Path length correction factor} \times \text{corrected PDE rate } \left(\text{min}^{-1}\right) \times \text{reaction volume (mL)} \times \text{dilution factor}}{\text{Molar absorption coeffcient } \left(\text{M}^{-1}\,\text{cm}^{-1}\right) \times \text{sample volume (mL)}}, \quad (1)$$

where corrected PDE rate is $\Delta A_{340\,\text{nm}}(\text{min}^{-1})$ of stage III $-\Delta A_{340\,\text{nm}}(\text{min}^{-1})$ stage II, molar absorption coefficient is $1.25 \times 10^4\,\text{M}^{-1}\,\text{cm}^{-1}$, dilution factor is 1, and path length correction (to 10 mm) is 3.16.

(b) The % change in cAMP hydrolysis activity of each sample was calculated as follows:

$$\%\ \text{Change in cAMP hydrolysis activity} = \frac{(\text{Challenged enzyme activity} - \text{Basal enzyme activity}) \times 100}{\text{Basal enzyme activity}}, \quad (2)$$

where challenged enzyme activity is cAMP hydrolysis activity in presence of cGMP, and basal enzyme activity is cAMP hydrolysis activity in absence of cGMP.

3. Results and Discussion

3.1. Sample Pretreatment. Cleanascite [41–44], a solid-phase, nonionic adsorbent for lipid removal, significantly improved the clarity of brain homogenates and eliminated clogging of the surfaces during the SeraFILE process. A 1 : 16 ratio of Cleanascite to untreated BBH gave optimal results, with minimum loss of cAMP hydrolysis activity. Consequently, the same ratio of Cleanascite to brain homogenate was used for RBH clarification.

3.2. cAMP Hydrolysis Activity in the Sample Proteomes. Enzyme activity and protein analysis of the unfractionated brain homogenates showed that the mean specific activity of clarified RBH and BBH was comparable, between 8 and 8.8 units/mg, measured at 50 μM cAMP concentration.

3.3. Effect of cGMP on cAMP Hydrolysis of Unfractionated Brain Homogenates. A comparison of the basal and challenged cAMP hydrolysis activities in the dilutions of each homogenate is shown in Figure 1. As expected, increase in activity (basal and cGMP challenged) was observed with increasing concentration of clarified homogenates. The comparison also shows that at relatively lower concentrations of the homogenates, cGMP inhibited cAMP hydrolysis, while, at higher concentrations, cAMP hydrolysis activity increased. In addition, the change in cAMP hydrolysis activity was more pronounced in the presence of 50 μM cGMP than 25 μM cGMP. Specifically, at 50 μM cGMP (Figures 2(a) and 2(b)), the change from inhibition to activation of cAMP hydrolysis activity occurred above ~1.5 mg/mL protein in RBH and above 4 mg/mL protein in BBH proteomes. Thus, it is a characteristic in the PDEs of RBH and BBH, that the effect of cGMP on cAMP hydrolysis is a function both of the concentration of the homogenate and of the concentration of cGMP.

3.4. SeraFILE-Derived Subproteomes and Generation of Enzyme Activity Profiles. Buffer-diluted, protein-normalized, and clarified RBH and BBH samples were used for separations. Each subproteome obtained was analyzed for protein content and cAMP hydrolysis activity under basal and cGMP-challenged conditions, and then the change in cAMP hydrolysis activity was calculated.

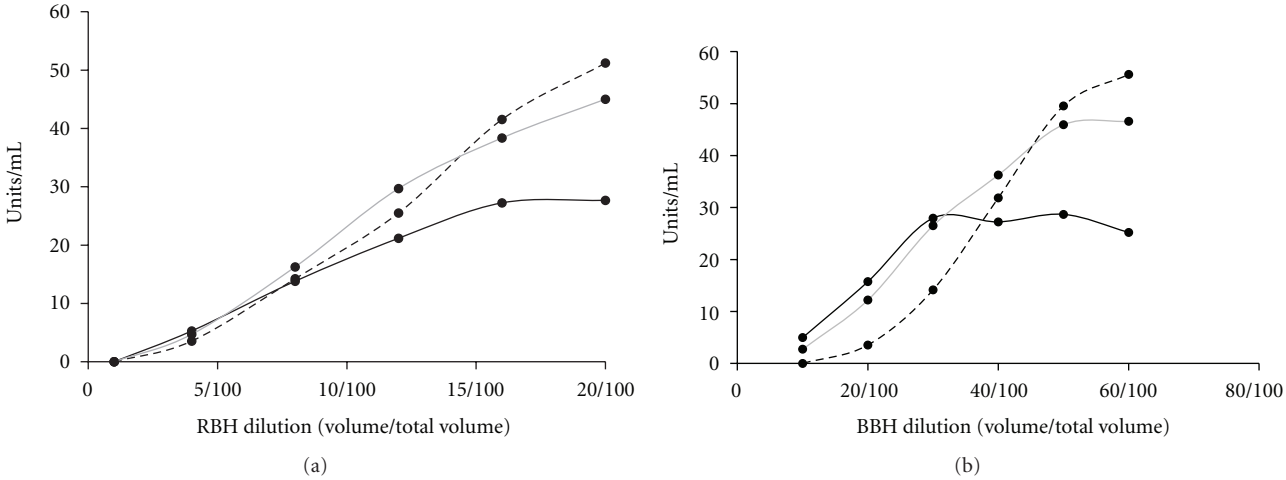

Figure 1: The cAMP hydrolysis activity in clarified rat brain homogenate (RBH), (a), and bovine brain homogenate (BBH), (b), proteomes. The cAMP hydrolysis activity was measured by using dilutions of the clarified homogenates in the absence of cGMP (solid black) or in presence of 25 μM cGMP (solid gray) or 50 μM cGMP (dashes).

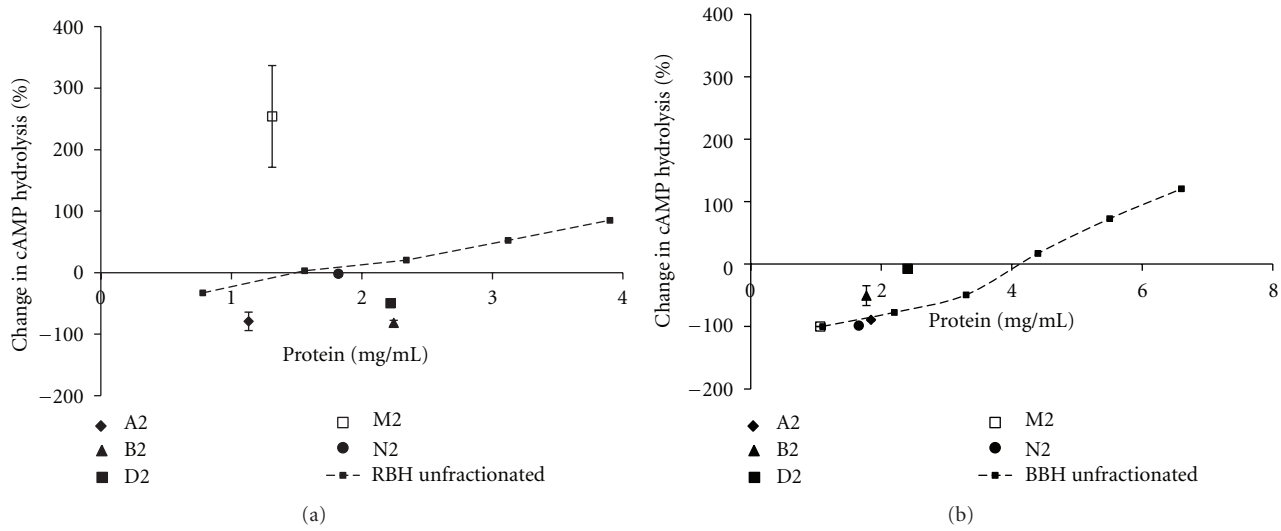

Figure 2: Relationship between change in cAMP hydrolysis activity and protein content of the unfractionated brain homogenates and SeraFILE-generated subproteomes. The figure shows change in cAMP hydrolysis of rat brain homogenate (RBH) and generated subproteomes, (a), and bovine brain homogenate (BBH) and generated subproteomes, (b). *X*-axis represents protein concentration. *Y*-axis represents percentage change in cAMP hydrolysis activity due to the challenge of 50 μM cGMP, as compared to basal cAMP hydrolysis activity. A2, B2, D2, M2, and N2 represent subproteomes from the homogenates.

To ensure that the observed properties of the subproteomes were not an effect of the dilution of the sample proteome, the properties of RBH and BBH proteomes and their respective SeraFILE subproteomes were compared (Figures 2(a) and 2(b)). The data in Figure 2(a) show that not all RBH subproteomes follow the activity versus protein content relationship of the RBH proteome. Similar observations were made with respect to BBH (Figure 2(b)). These outliers indicate that SeraFILE produces differential subproteomes. Data show that some subproteomes do share the activity versus protein content relationship of the sample proteome, likely indicating a comparable distribution of cAMP hydrolyzing PDEs to total proteins.

To generate an intersample functional proteomic profile of RBH and BBH proteomes, the change in cAMP hydrolysis activity of each subproteome due to cGMP challenge was calculated and plotted as shown in Figure 3. A functional proteomic profile of the brain homogenates in these experiments is defined by the collective response of individual SeraFILE subproteomes to cGMP challenge. A comparison between the functional profiles of the two homogenates (Figure 3) shows that, overall, these two profiles have a similar pattern (i.e., % change in cAMP hydrolysis is similar, positive or negative, in comparable fractions of the two homogenates). However, a major difference is found in subproteome M2 of RBH and BBH (refer to Figure 3(a) versus Figure 3(e),

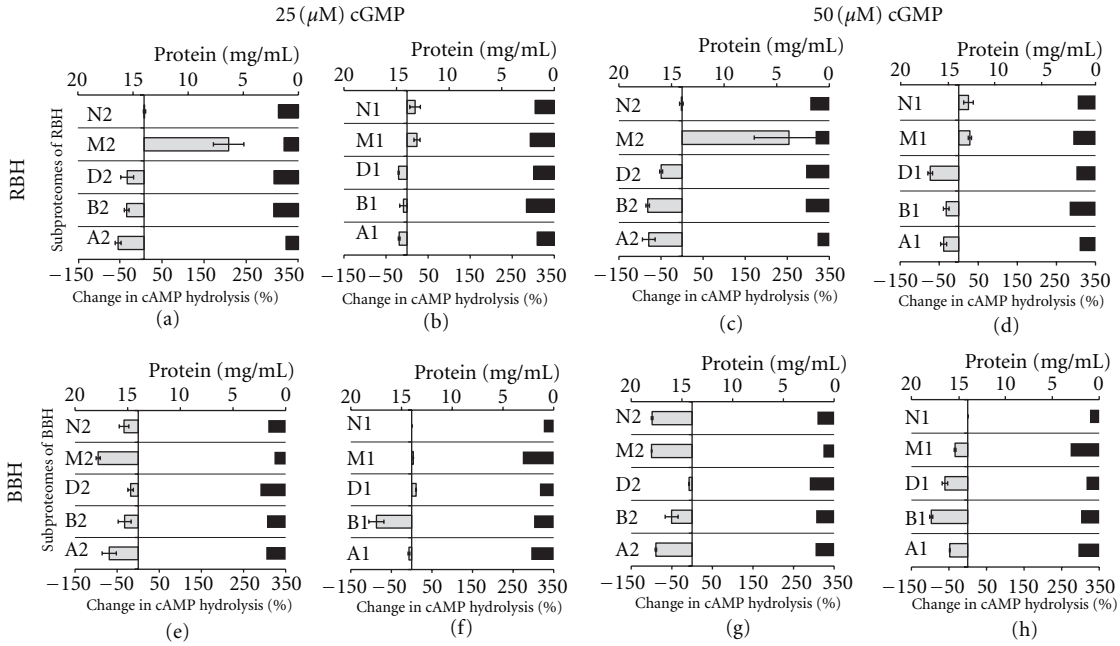

Figure 3: Comparison of functional profiles of rat brain homogenate (RBH) and bovine brain homogenate (BBH). Figure shows percentage change in cAMP hydrolysis activity in each subproteome of RBH ((a)–(d)) and BBH ((e)–(h)) due to cGMP challenge of 25 μM or 50 μM. In each panel, the primary X-axis represents the change in cAMP hydrolysis due to cGMP, the secondary X-axis represents protein concentration, and the Y-axis represents subproteomes. The pair of subproteomes A1 and A2 (and similarly others) was derived sequentially from the same surface in the library as described in the protocol. Grey bars represent mean percent change ($n = 3$), in cAMP hydrolysis of each subproteome due to presence of cGMP. Error bars represent (± 1) std. Black bars represent protein concentration of each subproteome.

and Figure 3(c) versus Figure 3(g). Subproteome M2 of RBH shows over 190% increase in cAMP hydrolysis in the presence of cGMP (both 25 μM and 50 μM), while subproteome M2 of BBH shows over 90% decrease in cAMP hydrolysis in the presence of cGMP (both 25 μM and 50 μM). Thus, subproteome M2 is a differentiating feature of this intersample analysis and therefore can be used for further sample characterization.

These model data demonstrate that our proposed methods of protein separation generate subproteomes that are sufficiently differentiated for intersample functional analysis. As a result, these methods can be potentially applied to effectively differentiate functional properties of complex proteomes and can be used to localize subset of proteins attributable to sample-specific responses. The localized proteins can then be used for further analysis, characterization, and subsequent MS identification (gene sequence annotation/reconciliation).

SeraFILE separations use mild-to-moderate elution conditions with buffers like phosphate or HEPES that are commonly used in the laboratory. In addition, the solid-phase surface (50 μ derivatized silica) can be easily removed by filtration. Thus SeraFILE separations methods do not introduce substances like urea or SDS that may restrict downstream compatibility with existing reporting assay and LC-MS detection methodologies [45]. Therefore, the proposed methodology is considered to have a broad scope of applicability within the pathway to identification and can be potentially applied to profile narrowly defined therapeutically important classes of enzymes such as Kinases or cyclic nucleotide phosphodiesterases.

Another important characteristic of SeraFILE separations methodology is its reproducibility at different protein loads. In separate experiments, surface separation of 0.25 mg to 1 mg protein per 50 mg of surface was shown to have only 10% variation (data not shown, [35]). The reproducibility in sample separation can be significant for heterogeneous samples of clinical origin.

In addition to separations, SeraFILE can also be applied for enrichment of proteins. Incremental increase in pH was applied for enrichment of alkaline phosphatase (data not shown, [35]) with an enrichment factor up to 20X.

The applications of SeraFILE separations can be based on two basic types of sample and data analysis of (i) intersample analysis whereby samples such as tissues, cellular models, or biofluids are compared and contrasted and (ii) intrasample analyses, or differential analysis within a sample whereby the subproteomes are monitored with respect to a challenging modulation condition such as in drug response profiling. It is envisioned that these will complement one another for personalized medicine applications.

Inter-sample analysis of complex proteomes, as demonstrated, potentially applies to disease and nondisease comparisons, to identify differences in samples by compartmentalizing the most distinctive subproteomes associated with disease. Deeper characterization of these fractions with enrichment (e.g., with pH optimization of SeraFILE separations, or with conventional separations 2DE or HPLC),

followed by LC-MS analyses, can help identify prospective biomarkers. It is important to recognize that any biomarker panel selected in this context would require more characterization, with larger sample sets and statistical validation.

Intra-sample analysis, on the other hand, can be used to catalogue or index the effects of functional modulation of the daughter subproteomes. This will be especially valuable for establishing localized panels of proteins that are responsive to modulation with drug compounds, with the same caveats as the aforementioned inter-sample analyses.

The two data analysis strategies, profiling between samples, and cataloging within samples, are complementary insofar as molecular profiles that characterize and compartmentalize drug-responsive proteins from complex mixtures, can potentially, through coincident iterations with disease profiling, create a bulls-eye effect for drug repurposing.

We envision that, for the drug development industry, the proposed methods for localizing proteins with known functional attributes offer new resources for biomarker discovery, complementing conventional methods of identification and sequence annotation. For drug compounds, a challenge/response method, as described, can help address the problems of drug promiscuity and discern the subtleties of protein attributes; when the same or similar underlying sequences, have multiple conformations and functions, and when different sequences sometimes perform the same or similar function.

As a way to begin sifting through these biological complexities, a more efficient method to characterize protein function and corresponding modulation is now possible. Starting with the enrichment of prospective functional biomarkers in localized subproteomes, we suggest that structural and sequence relationships can be determined. Such an approach has the potential to provide new and useful service to biomarker discovery and personalized medicine.

Conflict of Interests

The authors declare that there is no conflict of interests.

Acknowledgments

The authors would like to thank Dr. Miles Houslay, University of Glasgow, for his guidance in the initial development of this project. The authors are also thankful to Dr. Faribourz Payvandi, NeoloMed BioSciences, for providing facility for sample treatment and for his continuous guidance throughout the project. The authors would like to acknowledge work of Dr. Meghan Tierney on reproducibility of separations and enrichment of proteins with SeraFILE library. This work was funded in part by NJCST Post-Doctoral Fellowship Grant (10-2042-014-54) to A. R. Oka for work at ProFACT Proteomics Inc. (2009-2010), and in part by the IRS Qualifying Therapeutic Discovery Grant to ProFACT Proteomics Inc. (2009-2010).

References

[1] P. Mallick and B. Kuster, "Proteomics: a pragmatic perspective," *Nature Biotechnology*, vol. 28, no. 7, pp. 695–709, 2010.

[2] S. Pitteri and S. Hanash, "A systems approach to the proteomic identification of novel cancer biomarkers," *Disease Markers*, vol. 28, no. 4, pp. 233–239, 2010.

[3] A. H. J. Danser, W. W. Batenburg, A. H. van den Meiracker, and S. M. Danilov, "ACE phenotyping as a first step toward personalized medicine for ACE inhibitors. Why does ACE genotyping not predict the therapeutic efficacy of ACE inhibition?" *Pharmacology and Therapeutics*, vol. 113, no. 3, pp. 607–618, 2007.

[4] S. M. Danilov, I. V. Balyasnikova, R. F. Albrecht, and O. A. Kost, "Simultaneous determination of ACE activity with 2 substrates provides information on the status of somatic ACE and allows detection of inhibitors in human blood," *Journal of Cardiovascular Pharmacology*, vol. 52, no. 1, pp. 90–103, 2008.

[5] M. Sanchez-Carbayo, "Antibody array-based technologies for cancer protein profiling and functional proteomic analyses using serum and tissue specimens," *Tumor Biology*, vol. 31, no. 2, pp. 103–112, 2010.

[6] S. P. Gygi, B. Rist, S. A. Gerber, F. Turecek, M. H. Gelb, and R. Aebersold, "Quantitative analysis of complex protein mixtures using isotope-coded affinity tags," *Nature Biotechnology*, vol. 17, no. 10, pp. 994–999, 1999.

[7] M. P. Washburn, D. Wolters, and J. R. Yates, "Large-scale analysis of the yeast proteome by multidimensional protein identification technology," *Nature Biotechnology*, vol. 19, no. 3, pp. 242–247, 2001.

[8] T. Ito, K. Ota, H. Kubota et al., "Roles for the two-hybrid system in exploration of the yeast protein interactome.," *Molecular & Cellular Proteomics*, vol. 1, no. 8, pp. 561–566, 2002.

[9] G. MacBeath, "Protein microarrays and proteomics," *Nature Genetics*, vol. 32, supplement 5, pp. 526–532, 2002.

[10] B. F. Cravatt, A. T. Wright, and J. W. Kozarich, "Activity-based protein profiling: from enzyme chemistry to proteomic chemistry," *Annual Review of Biochemistry*, vol. 77, pp. 383–414, 2008.

[11] Y. Liu, M. P. Patricelli, and B. F. Cravatt, "Activity-based protein profiling: the serine hydrolases," *Proceedings of the National Academy of Sciences of the United States of America*, vol. 96, no. 26, pp. 14694–14699, 1999.

[12] M. Bantscheff, D. Eberhard, Y. Abraham et al., "Quantitative chemical proteomics reveals mechanisms of action of clinical ABL kinase inhibitors," *Nature Biotechnology*, vol. 25, no. 9, pp. 1035–1044, 2007.

[13] D. Kültz, D. Fiol, N. Valkova, S. Gomez-Jimenez, S. Y. Chan, and J. Lee, "Functional genomics and proteomics of the cellular osmotic stress response in 'non-model' organisms," *Journal of Experimental Biology*, vol. 210, no. 9, pp. 1593–1601, 2007.

[14] R. D. Gietz, B. Triggs-Raine, A. Robbins, K. C. Graham, and R. A. Woods, "Identification of proteins that interact with a protein of interest: applications of the yeast two-hybrid system," *Molecular and Cellular Biochemistry*, vol. 172, no. 1-2, pp. 67–79, 1997.

[15] M. Fromont-Racine, J. C. Rain, and P. Legrain, "Toward a functional analysis of the yeast genome through exhaustive two- hybrid screens," *Nature Genetics*, vol. 16, no. 3, pp. 277–282, 1997.

[16] S. Roy, J. Krupey, and M. Kuruc, "Composition and methods for proteomic investigations," in *US Patent and Trade Mark*

Office, P. Proteomics, Ed., ProFACT Proteomics, Monmouth Junction, NJ, USA, 2003.

[17] M. Conti and J. Beavo, "Biochemistry and physiology of cyclic nucleotide phosphodiesterases: essential components in cyclic nucleotide signaling," *Annual Review of Biochemistry*, vol. 76, pp. 481–511, 2007.

[18] K. M. Torgersen, E. M. Aandahl, and K. Taskén, "Molecular architecture of signal complexes regulating immune cell function.," *Handbook of Experimental Pharmacology*, no. 186, pp. 327–363, 2008.

[19] J. A. Beavo, M. Conti, and R. J. Heaslip, "Multiple cyclic nucleotide phosphodiesterases," *Molecular Pharmacology*, vol. 46, no. 3, pp. 399–405, 1994.

[20] C. Lugnier, "Cyclic nucleotide phosphodiesterase (PDE) superfamily: a new target for the development of specific therapeutic agents," *Pharmacology and Therapeutics*, vol. 109, no. 3, pp. 366–398, 2006.

[21] J. Beavo, S. H. Francis, and M. D. Houslay, *Cyclic Nucleotide Phosphodiesterases in Health and Disease*, CRC Press, Boca Raton, Fla, USA, 2006.

[22] J. Beavo, S. H. Francis, and M. D. Houslay, *Cyclic Nucleotide Phosphodiesterases in Health and Disease*, CRC Press/Taylor & Francis, Boca Raton, Fla, USA, 2007.

[23] Y. H. Jeon, Y. S. Heo, C. M. Kim et al., "Phosphodiesterase: overview of protein structures, potential therapeutic applications and recent progress in drug development," *Cellular and Molecular Life Sciences*, vol. 62, no. 11, pp. 1198–1220, 2005.

[24] M. D. Houslay, P. Schafer, and K. Y. J. Zhang, "Keynote review: phosphodiesterase-4 as a therapeutic target," *Drug Discovery Today*, vol. 10, no. 22, pp. 1503–1519, 2005.

[25] R. K. Sharma, A. M. Adachi, K. Adachi, and J. H. Wang, "Demonstration of bovine brain calmodulin-dependent cyclic nucleotide phosphodiesterase isozymes by monoclonal antibodies," *Journal of Biological Chemistry*, vol. 259, no. 14, pp. 9248–9254, 1984.

[26] T. Kyoi, M. Oka, K. Noda, and Y. Ukai, "Phosphodiesterase inhibition by a gastroprotective agent irsogladine: preferential blockade of cAMP hydrolysis," *Life Sciences*, vol. 75, no. 15, pp. 1833–1842, 2004.

[27] S. Murashima, T. Tanaka, S. Hockman, and V. Manganiello, "Characterization of particulate cyclic nucleotide phosphodiesterases from bovine brain: purification of a distinct cGMP-stimulated isoenzyme," *Biochemistry*, vol. 29, no. 22, pp. 5285–5292, 1990.

[28] K. Sankaran, I. Hanbauer, and W. Lovenberg, "Heat-stable low molecular weight form of phosphodiesterases from bovine pineal gland," *Proceedings of the National Academy of Sciences of the United States of America*, vol. 75, no. 7, pp. 3188–3191, 1978.

[29] S. Kakiuchi, R. Yamazaki, Y. Teshima, and K. Uenishi, "Regulation of nucleoside cyclic 3':5' monophosphate phosphodiesterase activity from rat brain by a modulator and Ca^{2+}," *Proceedings of the National Academy of Sciences of the United States of America*, vol. 70, no. 12, 1973.

[30] J. A. Smoake, S. Y. Song, and W. Y. Cheung, "Cyclic 3',5' nucleotide phosphodiesterase. Distribution and developmental changes of the enzyme and its protein activator in mammalian tissues and cells," *Biochimica et Biophysica Acta*, vol. 341, no. 2, pp. 402–411, 1974.

[31] R. S. Hansen and J. A. Beavo, "Differential recognition of calmodulin-enzyme complexes by a conformation-specific anti-calmodulin monoclonal antibody," *Journal of Biological Chemistry*, vol. 261, no. 31, pp. 14636–14645, 1986.

[32] I. McPhee, L. Pooley, M. Lobban, G. Bolger, and M. D. Houslay, "Identification, characterization and regional distribution in brain of RPDE-6 (RNPDE4A5), a novel splice variant of the PDE4A cyclic AMP phosphodiesterase family," *Biochemical Journal*, vol. 310, no. 3, pp. 965–974, 1995.

[33] F. Ohsawa, M. Yamauchi, H. Nagaso, S. Murakami, J. Baba, and A. Sawa, "Inhibitory effects of rolipram on partially purified phosphodiesterase 4 from rat brains," *Japanese Journal of Pharmacology*, vol. 77, no. 2, pp. 147–154, 1998.

[34] M. Shepherd, T. McSorley, A. E. Olsen et al., "Molecular cloning and subcellular distribution of the novel PDE4B4 cAMP-specific phosphodiesterase isoform," *Biochemical Journal*, vol. 370, no. 2, pp. 429–438, 2003.

[35] ProFACT Proteomics, Reproducibility Of SeraFILE Derived Functional Proteomic Profiles, ProFACT Proteomics, http://www.profactproteomics.com/technical_notes.html, 2007.

[36] ProFACT Proteomics, Molecular profiling with SeraFILE, Nature Methods, Application Notes, ProFACT Proteomics, http://www.profactproteomics.com/technical_notes.html, 2008.

[37] ProFACT Proteomics, SeraFILE—A Biomarker and Drug Discovery Engine, ProFACT Proteomics, http://www.profactproteomics.com/serafile.html, 2004.

[38] ProFACT Proteomics, Functional Proteomic Signatures of the Ubiquitin/Proteasome Pathway, ProFACT Proteomics, http://www.profactproteomics.com/technical_notes.html, 2007.

[39] S. P. Chock and C. Y. Huang, "An optimized continuous assay for cAMP phosphodiesterase and calmodulin," *Analytical Biochemistry*, vol. 138, no. 1, pp. 34–43, 1984.

[40] A. B. Burgin, O. T. Magnusson, J. Singh et al., "Design of phosphodiesterase 4D (PDE4D) allosteric modulators for enhancing cognition with improved safety," *Nature Biotechnology*, vol. 28, no. 1, pp. 63–70, 2010.

[41] M. S. S. Alhamdani, C. Schröder, and J. D. Hoheisel, "Analysis conditions for proteomic profiling of mammalian tissue and cell extracts with antibody microarrays," *Proteomics*, vol. 10, no. 17, pp. 3203–3207, 2010.

[42] A. Farina, J. M. Dumonceau, J. L. Frossard, A. Hadengue, D. F. Hochstrasser, and P. Lescuyer, "Proteomic analysis of human bile from malignant biliary stenosis induced by pancreatic cancer," *Journal of Proteome Research*, vol. 8, no. 1, pp. 159–169, 2009.

[43] B. Chen, J. Q. Dong, Y. J. Chen et al., "Two-dimensional electrophoresis for comparative proteomic analysis of human bile," *Hepatobiliary and Pancreatic Diseases International*, vol. 6, no. 4, pp. 402–406, 2007.

[44] T. Z. Kristiansen, J. Bunkenborg, M. Gronborg et al., "A proteomic analysis of human bile," *Molecular and Cellular Proteomics*, vol. 3, no. 7, pp. 715–728, 2004.

[45] E. I. Chen, D. Cociorva, J. L. Norris, and J. R. Yates, "Optimization of mass spectrometry-compatible surfactants for shotgun proteomics," *Journal of Proteome Research*, vol. 6, no. 7, pp. 2529–2538, 2007.

Hindawi Publishing Corporation
International Journal of Proteomics
Volume 2012, Article ID 536963, 10 pages
doi:10.1155/2012/536963

Research Article

Optimization of an Efficient Protein Extraction Protocol Compatible with Two-Dimensional Electrophoresis and Mass Spectrometry from Recalcitrant Phenolic Rich Roots of Chickpea (*Cicer arietinum* L.)

Moniya Chatterjee, Sumanti Gupta, Anirban Bhar, and Sampa Das

Division of Plant Biology, Bose Institute, Centenary Campus, P 1/12, CIT Scheme VII-M, Kankurgachi, West Bengal, Kolkata 700054, India

Correspondence should be addressed to Sampa Das, sampa@bic.boseinst.ernet.in

Received 15 March 2012; Accepted 4 September 2012

Academic Editor: Paul P. Pevsner

Two-dimensional electrophoresis and mass spectrometry are undoubtedly two essential tools popularly used in proteomic analyses. Utilization of these techniques however largely depends on efficient and optimized sample preparation, regarded as one of the most crucial steps for recovering maximum amount of reliable information. The present study highlights the optimization of an effective and efficient protocol, capable of extraction of root proteins from recalcitrant phenolic rich tissues of chickpea. The widely applicable TCA-acetone and phenol-based methods have been comparatively evaluated, amongst which the latter appeared to be better suited for the sample. The phenol extraction-based method further complemented with sodium dodecyl sulphate (SDS) and pulsatory treatments proved to be the most suitable method represented by greatest spot number, good resolution, and spot intensities. All the randomly selected spots showed successful identification when subjected to further downstream MALDI-TOF and MS/MS analyses. Hence, the information obtained collectively proposes the present protein extraction protocol to be an effective one that could be applicable for recalcitrant leguminous root samples.

1. Introduction

Presence of intricate photosynthetic machinery, cell wall and other organelles, complex primary and secondary metabolic processes, and their cellular regulation adds to the complexity of functional biology of plants. In recent years, proteomics has become one of the most enthralling fields in molecular biology as it targets the molecular link in the information chain from protein to its coding sequence and its manifestation in the form of phenotype. In contrast to the relative ease of mRNA isolation, c-DNA synthesis and analysis, protein extraction presents numerous challenges due to its heterogeneous nature, structural complexity and instability. Such features dramatically complicate their extraction, solubilization, handling, separation, and ultimately identification. Moreover no technology currently exists that is equivalent to PCR, which can amplify low abundance proteins [1].

The most critical step in any proteomic study is protein extraction and sample preparation. However, the difficulties involving plant protein extractions especially from roots are quite complicated as compared to other organisms. Root tissues are highly vacuolated with relatively low protein content. They are often rich in proteases, storage polysaccharides, lipids, phenolics and a broad array of secondary metabolites [2–4]. Such contaminants cause major obstacles for two-dimensional electrophoresis (2DE) resulting in horizontal and vertical streaking, smearing, and reduction in the number of distinctly resolved protein spots [5].

The present investigation deals with protein extraction from chickpea roots. Chickpea is the most important legume crop in India and ranks third in the world's list of important

legumes. Its production is greatly hampered by different abiotic and biotic factors. Major yield loss is caused by root invading pathogens like *Sclerotium rolfsii* (collar rot), *Fusarium solani* (black root rot), *Thielaviopsis basicola* (black streak root rot), *Phytophthora* sp. (*Phytophthora* root rot), *Fusarium* sp. (*Fusarium* root rot), *Fusarium oxysporum* f.sp. ciceris (*Fusarium* wilt), and so forth. Hence, root proteins serve to be excellent target to study early signaling in plant-pathogen interaction involving root invading pathogens in particular.

Most common and basic protocols used for protein extraction from plant tissue are TCA-acetone and phenol-based extraction methods. TCA-acetone precipitation was initially developed by Damerval et al. [6]. This method increases the protein concentration and helps removing contaminants, although some polymeric contaminants are often coextracted. This appears as a problem with tissues that are rich in compounds such as soluble cell wall polysaccharides and polyphenols. Another method involves protein solubilization in phenol, with or without using SDS followed by precipitation with methanol and ammonium acetate and subsequent resolubilization in IEF (isoelectric focusing) sample buffer [5, 7, 8]. This method can efficiently generate protein extracts from resistant tissues such as wood [9], olive leaves [10], maize roots [11], and hemp roots [12], and so forth. Similar studies also suggested that phenol-based method reduces protein degradation during extraction and helps in solubilizing membrane proteins and glycoproteins [5, 13]. However, requirement of extensive time appears to be the major limitation of this method. Thus, these extraction protocols demand optimization for particular organisms, tissue or cell compartment.

In current study attempts were made to optimize the phenol SDS method along with sonication for protein extraction from small amount of recalcitrant chickpea roots. Evaluations of other different extraction methods were also done in comparison to the optimized phenol SDS sonication method and its compatibility with high throughput method like mass spectrometry analysed.

2. Materials and Methods

2.1. Plant Material. Experiments were performed using chickpea seeds (JG62) obtained from International Crops Research Institute for the Semi Arid Tropics (ICRISAT), Patancheru, Andhra Pradesh, India. Seeds sown in a mixture of sand and synthetic soil (1 : 1) were allowed to grow in natural green house conditions suited for the crop [14]. Roots of 15–20 days old seedlings were thoroughly washed, frozen in liquid nitrogen, and stored at −80°C prior to extraction of protein.

2.2. Extraction Protocols

(A) TCA-Acetone Precipitation Method. TCA-acetone precipitation was carried out according to Damerval et al. with some modifications [6]. One gram of root material was ground in a precooled mortar in the presence of liquid nitrogen. Approximately 100–150 mg of ground tissue powder was precipitated overnight with freshly prepared 2 mL of 10% TCA, 0.07%β-mercaptoethanol in cold acetone. Following precipitation the set was centrifuged at 10,000 g for 15–20 min at 4°C and the supernatant discarded. The obtained pellet was rinsed twice in ice-cold acetone with 0.07%β-mercaptoethanol. An additional modification was introduced between the rinsing steps by incubating the sample for 60 min at −20°C [15]. The pellet was air dried, resuspended in 100 μL sample buffer (8 M Urea, 2% CHAPS, 50 mM DTT, 0.2% Biolyte 3/10 Ampholyte, 0.001% Bromophenol Blue) (Biorad), and vortexed for 1 hour at room temperature. The supernatant was used for downstream analyses (Figure 1).

(B) Phenol Extraction Method. Phenol extraction method was used both singly and in combinations of extraction buffer and SDS along with variations of with and without sonication (Figure 1).

(B.1) Phenol-SDS Buffer Extraction with Sonication (PSWS). Phenol extraction of proteins was carried out as described by Hurkman and Tanaka [7] in the presence of SDS buffer designated as phenol-SDS extraction by Wang et al. [10]. One gram of root tissue was ground in a mortar in the presence of liquid nitrogen and extracted with 3 mL of SDS buffer (30% sucrose, 2% SDS, 0.1 M Tris-Cl, 5% β-mercaptoethanol, and 1 mM phenyl methyl sulfonyl fluoride (PMSF), pH 8.0). The extract was sonicated 6 times for 15 seconds at 60 amps. Following sonication 3 mL of Tris buffered phenol was added to the mixture and vortexed for 10 mins at 4°C. The set was centrifuged at 8,000 g for 10 min at 4°C, phenolic phase collected and reextracted with 3 mL SDS buffer and shaken for 3–10 min. Centrifugation was further repeated using the same settings, phenolic phase collected and precipitated overnight with four volumes of 0.1 M ammonium acetate in methanol at −20°C. Precipitate obtained by centrifugation at 10,000 g for 30 min at 4°C was washed thrice with cold 0.1 M ammonium acetate and finally with cold 80% acetone. The pellet was dried and resuspended in 100 μL sample buffer (Biorad) and used for further analyses.

(B.2) Phenol-SDS Buffer Extraction without Sonication (PSWOS). This method was same as mentioned in case of PSWS only with the elimination of the sonication step.

(B.3) Phenol-Extraction Buffer with Sonication (PEWS). One gram of frozen root tissue was homogenized in liquid nitrogen and was extracted with ice-cold extraction buffer (500 mM Tris-Cl, 50 mM EDTA, 700 mM sucrose, 100 mM KCl, pH 8.0) at 4°C. The extract was sonicated 6 times at 60 amps for 15 sec and further extracted with Tris buffered phenol as described in PSWS.

(B.4) Phenol-Extraction Buffer without Sonication (PEWOS). Protein extraction was carried out in the same way as described in case of PEWS with elimination of the sonication step.

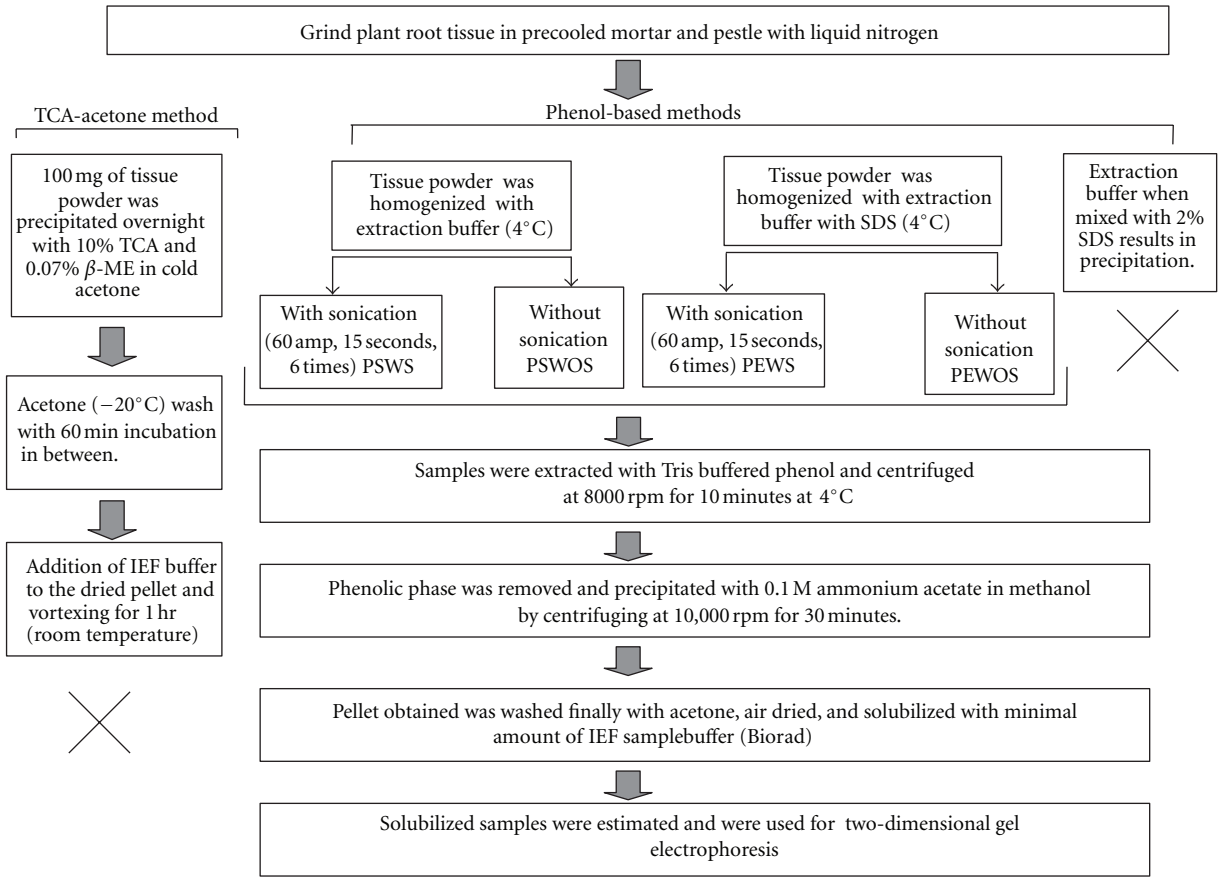

Figure 1: Schematic representation of extraction of protein from chickpea roots using TCA-acetone and phenol based extraction protocols.

(B.5) Phenol-Extraction Buffer with SDS. This protocol was similar to phenol extraction method. The buffer composition was the same as mentioned in PEWS pH 8.0 with 2% SDS as an additional component. However appearance of a white precipitate following SDS addition to the basal phenol extraction buffer prevented further processing of the sample using this buffer (Figure 1).

2.3. Protein Quantification. Protein concentrations were quantified using the Bradford protein assay method using BSA as a standard [16].

2.4. Two-Dimensional Electrophoresis (2DE). IPG strips (11 cm, 3–10 nonlinear, Readystrip, Biorad) were passively rehydrated overnight with rehydration sample buffer containing 250 μg of isolated protein. IEF was carried out on PROTEAN IEF Cell (Biorad) at field strength of 600 V/cm and 50 mA/IPG strip. The strips were focused at 250 V for 20 mins, 8000 V for 2 hours 30 mins with linear voltage amplification, and finally to 20,000 volt hour with rapid amplification. Following IEF, the strips were reduced with 135 mM DTT in 4 mL of equilibration buffer (20% (v/v) glycerol, 0.375 M Tris-Cl, 6 M urea, 2% (w/v) SDS, pH 8.8) for 15 mins and alkylated with 135 mM iodoacetamide in 4 mL equilibration buffer for 15 mins. The 2DE was performed using 12% polyacrylamide gels (13.8 cm × 13.0 cm × 1 mm) in an AE-6200 Slab Electrophoresis Chamber (Atto Biosciences and Technology, China) at constant volt (200 V) for 3 hours 30 mins in Tris glycine-SDS running buffer. All 2DE gel separation was performed in triplicates for all the methods. The gels were stained with 0.1% (w/v) coomassie brilliant blue R-250 (Sigma) overnight, destained, and stored in 5% acetic acid at 4°C for further analysis.

2.5. Image Analysis of 2D PAGE Gels. Coomassie stained 2-D gels were visualized using Versa Doc (Model 4000) Imaging System (Biorad) and analyzed with PD Quest Advanced 2-D Analysis software (version 8.0.1, Biorad). Spots were detected automatically by the Spot Detection Parameter Wizard using the Gaussian model with standard parameters. Comparison between spot quantities across gels was performed accurately, and normalization was done using local regression model. Only spots present in each of the three replicate gels, with high and low intensity, were randomly chosen for subsequent analyses. Selected protein spots were subjected to in-gel digestion for identification by MALDI-TOF MS and MS/MS analyses.

2.6. MALDI-TOF MS and MS/MS Analysis and Database Search. Spots were excised from protein gels, and in-gel digestion was performed as described by Shevchenko et al.

Table 1: Protein yield/fresh weight of root tissue (μg/gm) using Bradford method.

Methods	Protein yield (μg/gm)
PSWS	603 ± 6.08
PSWOS	406 ± 5.77
PEWS	302 ± 5.51
PEWOS	408 ± 7.64
TCA	73 ± 2

Table 2: Total number of spots using different methods.

Methods	Average number of spots
PSWS	446 ± 9.07
PSWOS	287 ± 6.43
PEWS	338 ± 6.11
PEWOS	348 ± 1.53

with minor modifications [17]. Proteins were digested in gel using porcine trypsin (Promega) and were extracted using 25% acetonitrile and 1% trifluoroacetic acid. One microlitre of sample and matrix (α-cyano-4-hydroxy cinnamic acid, HCCA) (Bruker, Daltonics) was loaded in a Anchor Chip MALDI Plate (Bruker, Daltonics).

Mass spectra were obtained on an Autoflex II MALDI TOF/TOF (Bruker, Daltonics, Germany) mass spectrometer equipped with a pulsed nitrogen laser (λ-337 nm, 50 Hz). Then the spectra were analysed with Flex Analysis Software (version 2.4, Bruker, Daltonics). The processed spectra were then searched using MS Biotools (version 3.0) program, against the taxonomy of Viridiplantae (green plants) in the MSDB database using MASCOT search engine (version 2.2). The peptide mass fingerprinting parameters included peptide mass tolerance (≤100 ppm); proteolytic enzyme (trypsin); global modification (carbamidomethyl, Cys); variable modification (oxidation, Met); peptide charge state (1+) and maximum missed cleavage 1. The significance threshold was set to a minimum of 95% ($P \leq 0.05$). The criteria used to accept protein identification were based on molecular weight search (MOWSE) score, the percentage of the sequence coverage, and match with minimum five peptides. MS/MS was performed to confirm the identification with matched peptides, selected on the basis of suitability for fragmentation (signal strength and relative isolation).

3. Results

3.1. Protein Quantification

3.1.1. TCA-Acetone Precipitation Method. Protein yield using the classical TCA-acetone precipitation method was extremely low (data not shown). However a modification of incubating the sample at −20°C for 60 minutes in-between the rinsing step yielded a measurable amount of protein. Approximately seventy-three micrograms of protein were obtained from one gram of root tissue using this method (Table 1). However, when the obtained protein was subjected to electrophoresis in SDS PAGE (polyacrylamide gel electrophoresis) gel, no banding profile was visualized (data not shown). Hence, this protocol was eliminated from further downstream analysis.

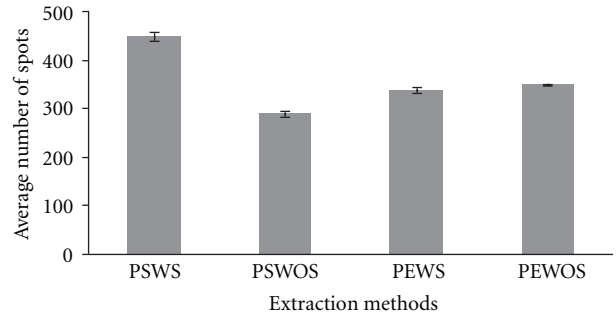

Figure 2: A comparative graphical representation showing the average number of protein spots detected in 2DE gels using PSWS, PSWOS, PEWS, and PEWOS protein extraction protocols.

3.1.2. Phenol-Based Methods. In case of phenol-based methods, protein yields obtained from PSWS, PSWOS, PEWS, and PEWOS were 600 μg, 406 μg, 408 μg, and 300 μg, respectively, (Table 1). One gram of fresh chickpea roots yielded maximum amount of protein with PSWS method as compared to protein obtained by methods PSWOS, PEWS, and PEWS.

3.2. Data Analysis of 2DE Gels. The 2DE patterns of extracted protein when compared with equal amount of initial protein load revealed that protein extracted by PSWS method displayed a comparatively good resolution with lesser contamination, whereas proteins extracted with methods PSWOS, PEWS and PEWOS resolved fewer protein spots (Figure 2). Approximately 446 detectable spots (as estimated by PD Quest software) were obtained by PSWS method while 287 spots by PSWOS method, 338 by PEWS, and 348 by PEWOS method were detected (Table 2). The number of spots described in Table 2 is the average number of spots across the triplicates. In addition we also found that many spots were diffused or absent in these methods (PSWOS, PEWS, PEWOS) as indicated in the marked areas (Figures 3A, 3B, 3C, and 3D). Intensities of all the spots randomly selected for downstream MS and MS/MS were more in PSWS method as compared to other methods (Figures 4 and 5).

3.3. MALDI-TOF MS and MS/MS Analysis for Protein Identification. All the 9 spots selected for MALDI analysis (Figures 4 and 5), consisting of both less abundant (sp 36, 80, 212) and more abundant (sp 19, 55, 109, 165, 248, 267) proteins, were successfully identified and listed in Table 3 (Figure 6). Data listed in the table include assigned spot number, spot identity, protein identity (MSDB database), number of peptide matches, sequence coverage (%), MOWSE score, accession number, experimental and theoretical molecular weight and pI.

Table 3: Proteins identified by MALDI-TOF MS analyses.

S no.	Spot ID.	Protein identity	Peptides matched	Sequence coverage (%)	MOWSE score	Accession number (NCBI)	Mr(kDa)/pI experimental (theoretical)	Plant species
1	sp 165	NADP specific isocitrate dehydrogenase	10	17%	70	Q9XGU7_ORYSA	46.4/6.29 (46.0/6.0)	*Oryza sativa*
2	sp 212	Glyceraldehyde 3 phosphate dehydrogenase	9	24%	86	Q6K5G8_ORYSA	36.716/7.68 (37/6.5)	*Oryza sativa*
3	sp 109	Triose phosphate isomerase	6	20%	71	Q38IW8_SOYBN	27.4/5.87 (25/5.5)	*Glycine max*
4	sp 55	Fructokinase-like protein	9	40%	94	Q8LPE5_CICAR	26.26/5.03 (35.5, 4.5)	*Cicer arietinum*
5	sp 36	ATP synthase (subunit D chain)	13	36%	88	ATPQ_ARATH	19.4/5.09 (20/5.0)	*Arabidopsis thaliana*
6	sp 267	Porin of Pea, channel protein	2	11%	134	T12558	29.7/8.56 (30/9.5)	*Phaseolus coccineus*
7	sp 19	Plasma membrane intrinsic polypeptide	10	38%	74	Q9SMK5_CICAR	23.3 /4.95 (24.5/5.0)	*Cicer arietinum*
8	sp 248	Unidentified protein	11	35%	80	CAA06491	22.12/9.91 (44.0,9.0)	*Cicer arietinum*
9	sp 80	Putative pyruvate dehydrogenase E1 beta subunit isoform 1 protein	2	6%	55	Q6Z1G7_ORYSA	40.2/5.25 (38.5/5.3)	*Oryza sativa*

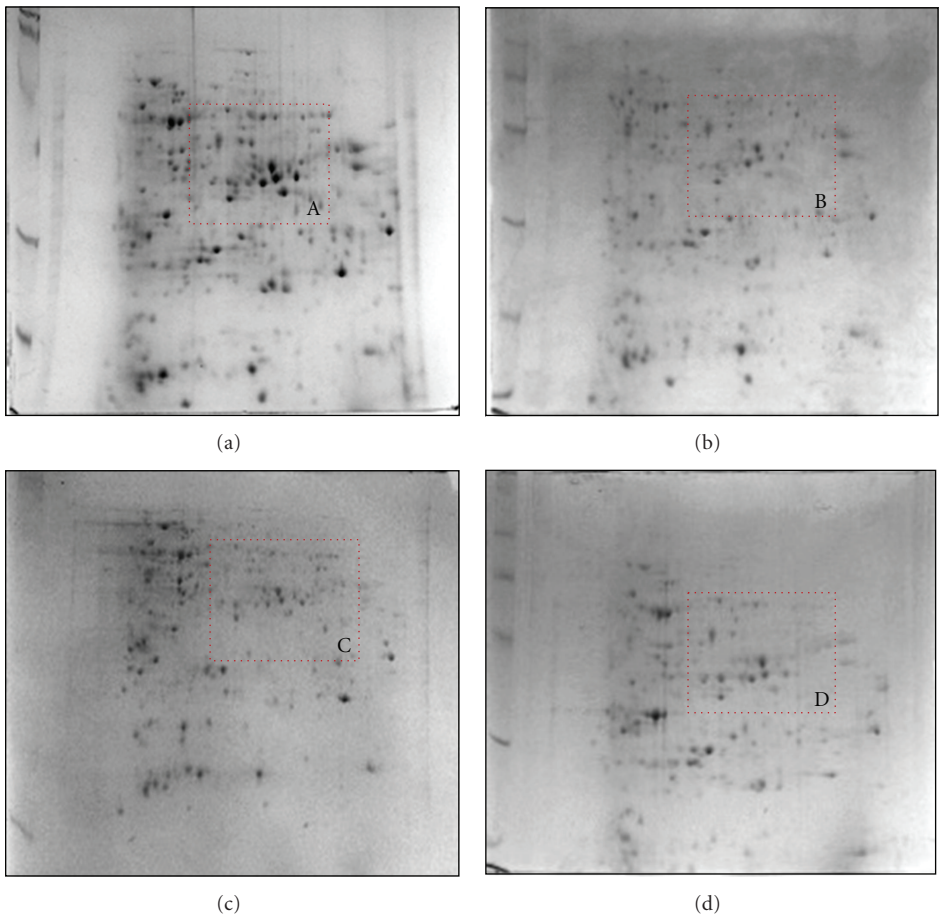

Figure 3: 2DE profiles of chickpea root proteins of JG 62. Profile of proteins isolated using PSWS (a), PSWOS (b), PEWS (c), and PEWOS (d) extraction protocols. Inset A, B, C, D represents a close-up view of an area showing spot resolution: in PSWS (a), PSWOS (b), PEWS (c), and PEWOS (d), respectively.

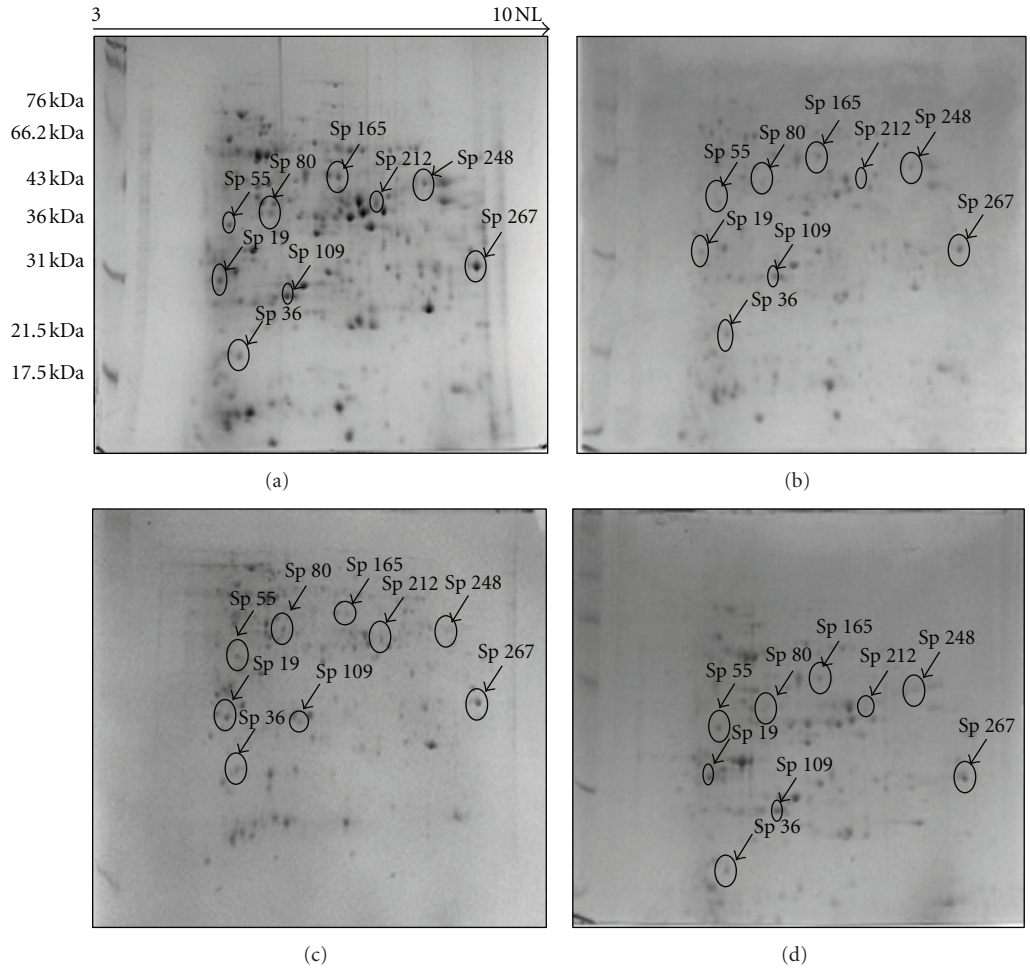

Figure 4: 2DE profiles with marked spots selected for MALDI-TOF MS and MS/MS. (a) 2DE profile using PSWS, (b) 2DE profile using PSWOS, (c) 2DE profile using PEWS, and (d) 2DE profile using PEWOS.

4. Discussion

Secondary metabolites are known to play important role in structural composition and defense of plants. These metabolites accumulate in various soluble forms in vacuoles and cause severe interference in protein extraction as well as separation in 2DE gels [18, 19]. Chickpea roots are rich in phenolic compounds like tannic acid, gallic acid, o-coumaric acid, chlorogenic acid, cinnamic acid; flavanoids, isoflavanoids like daidzein, genistein, as well as tannins, lignins, and carbohydrates [20, 21]. These compounds form hydrogen bonds with proteins. Besides they also form irreversible complexes with proteins by oxidation and covalent condensation which leads to charge heterogeneity resulting in streaking of gels [22]. Carbohydrates block gel pores causing precipitation and prolonged focusing time, which also results in loss of protein spots and streaks in the gels [15]. Although the amount of these secondary metabolites is comparatively low in etiolated tissues like roots, but low protein content and limiting tissue amounts demand for a competent protein extraction method. In our study TCA-acetone method and phenol-based method using two different extraction buffers (SDS buffer and extraction buffer without SDS) with and without sonication were evaluated. Comparison was done on the basis of protein yield, spot focusing, resolution, number of resolved spots, and also intensities of the spot and their downstream analysis using high throughput technology (MALDI/MS) of the optimized method.

Quantitative comparison of protein extracts revealed that phenol-based methods gave higher protein yield as compared to TCA-acetone method. The major reason for low protein yield in TCA-acetone method which constrained it for further downstream processing could probably be attributed to the insolubility of protein pellet in IEF buffer as compared to phenol-based methods [23]. Moreover TCA-acetone protocol is known to be effective with tissues from young plants and was found not to be the best choice for more complex tissues [5, 10, 15].

In case of phenol extraction, the proteins were first homogenized in two different extraction buffers; both the buffers contained sucrose which was added to create phase inversion. These buffers formed the aqueous lower phase containing carbohydrates, nucleic acid, insoluble cell debris, while the upper phenol phase contained cytosolic and

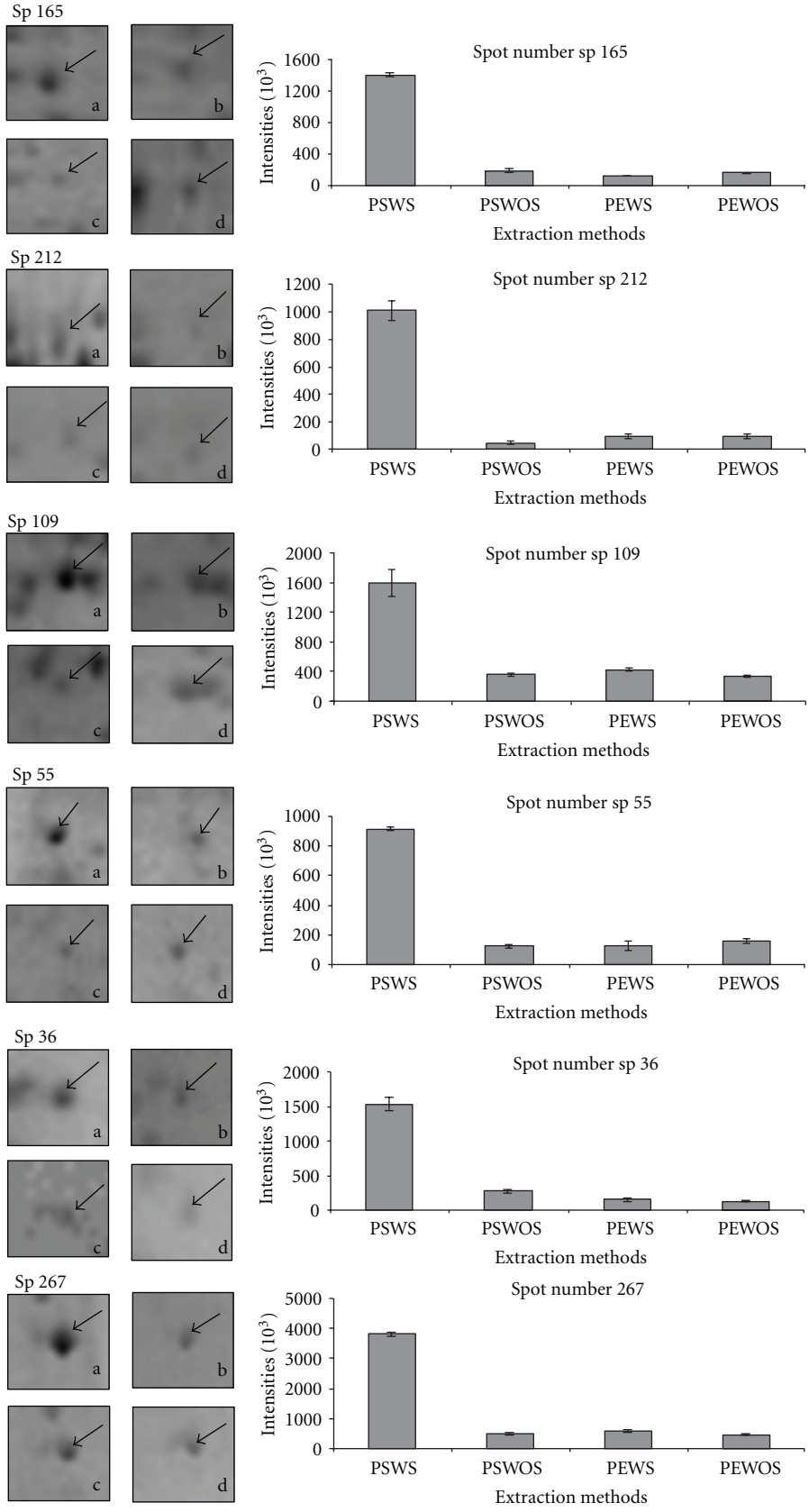

Figure 5: Continued.

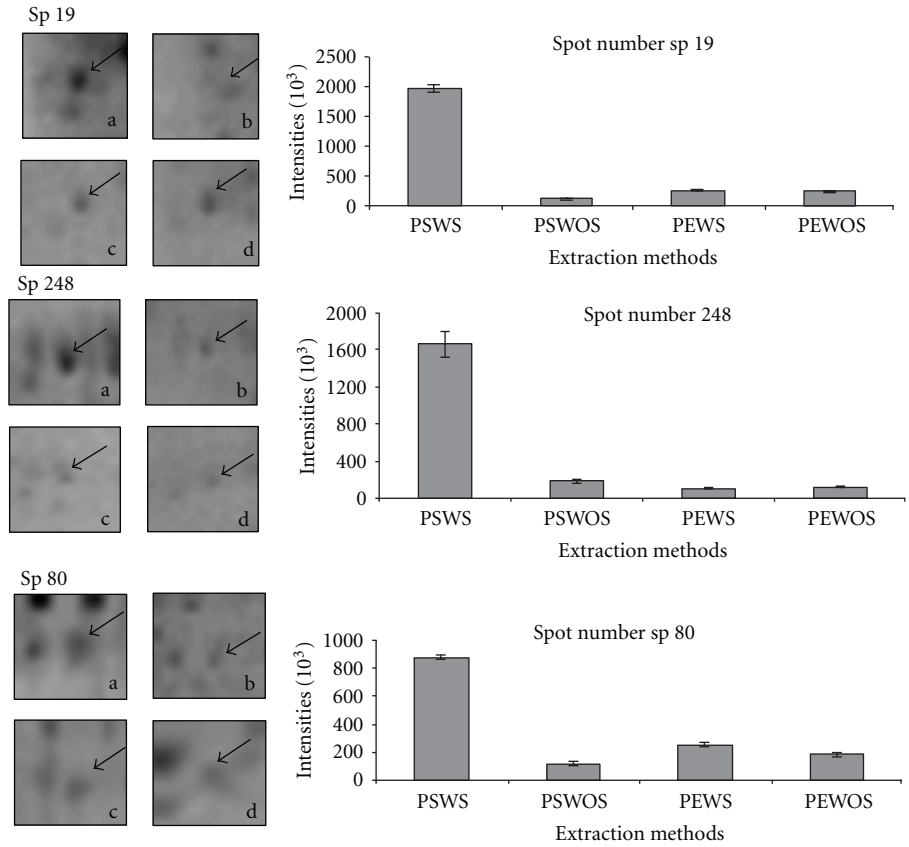

Figure 5: 2DE gel profiles showing individual spots and their relative intensities in graphical form using PSWS, PSWOS, PEWS, and PEWOS protein extraction protocols. (a), (b), (c), (d) represent the spot obtained by PSWS, PSWOS, PEWS, and PEWOS, respectively.

membrane proteins, lipids, and pigment [15]. SDS buffer contained about 30% sucrose which helped in better phase separation as compared to extraction buffer (24%). The high pH buffers inhibit common activity of the proteases [24] and cause ionization of phenolic compounds, thus preventing them from forming hydrogen bonding with the protein [22]. It also neutralizes the acids that are released by disrupted vacuoles. PMSF and β-mercaptoethanol which were used in both buffers in the present study were reported to irreversibly inhibit serine protease action and act as a reducing agent which prevents protein oxidation, respectively. KCl and EDTA were used in case of extraction buffer without SDS (PEWS and PEWOS). KCl facilitates the extraction of proteins by its salting in effect and EDTA inhibits metalloprotease and polyphenoloxidase by chelating metal ions [15]. Although the salting in effect or chelation of metal ions could not improve the protein yield as compared to SDS buffer with sonication, SDS is known to act as an excellent solubilizing agent, which allows the recovery of membrane-bound proteins [10]. The solubilization of protein was found to increase with sonication as evident from the increase in protein yield and spot resolution after sonication in PSWS compared to PSWOS. Sonication results in better disruption of cell membrane and release of intracellular proteins and thus provides explanation for SDS to have efficiently solubilized the protein in PSWS method. In contrary, in case of extraction buffer, sonication could not improve protein yield or resolution, presumably due to the interference with constituents of buffer (KCl or EDTA) or due to lack of better solubilizing agent like SDS and/or both.

The phenol used in this method was buffered to pH 8.0 to ensure that nucleic acids are partitioned to the buffer phase and not to phenol-rich phase [25], and thus proteins in phenol phase were purified and concentrated simultaneously by subsequent methanol ammonium acetate precipitation. Phenol acts as one of the strongest dissociaters known to decrease molecular interaction between proteins and other materials [15]. It can minimize protein degradation resulting from endogenous proteolytic activity [26]. Phenol extraction method though with high clean-up capacity has a little tendency to dissolve polysaccharides and nucleic acids.

We found that in PSWS method the spots obtained were well resolved and showed high intensity (Figures 3 and 5) as compared to PSWOS, PEWS, and PEWOS. About 25% unique spots were obtained in PSWS and the rest 75% spots though existed in PSWOS, PEWS, and PEWOS, however, resolved with variable clarity. Streaking was absent in all the gels. We could see that the difference in number of spots between PSWS and PSWOS was more as compared to PEWS and PEWOS, which confirmed that the effectivity of SDS increased in presence of sonication. However in the latter case (PEWS, PEWOS) sonication did not have much influence.

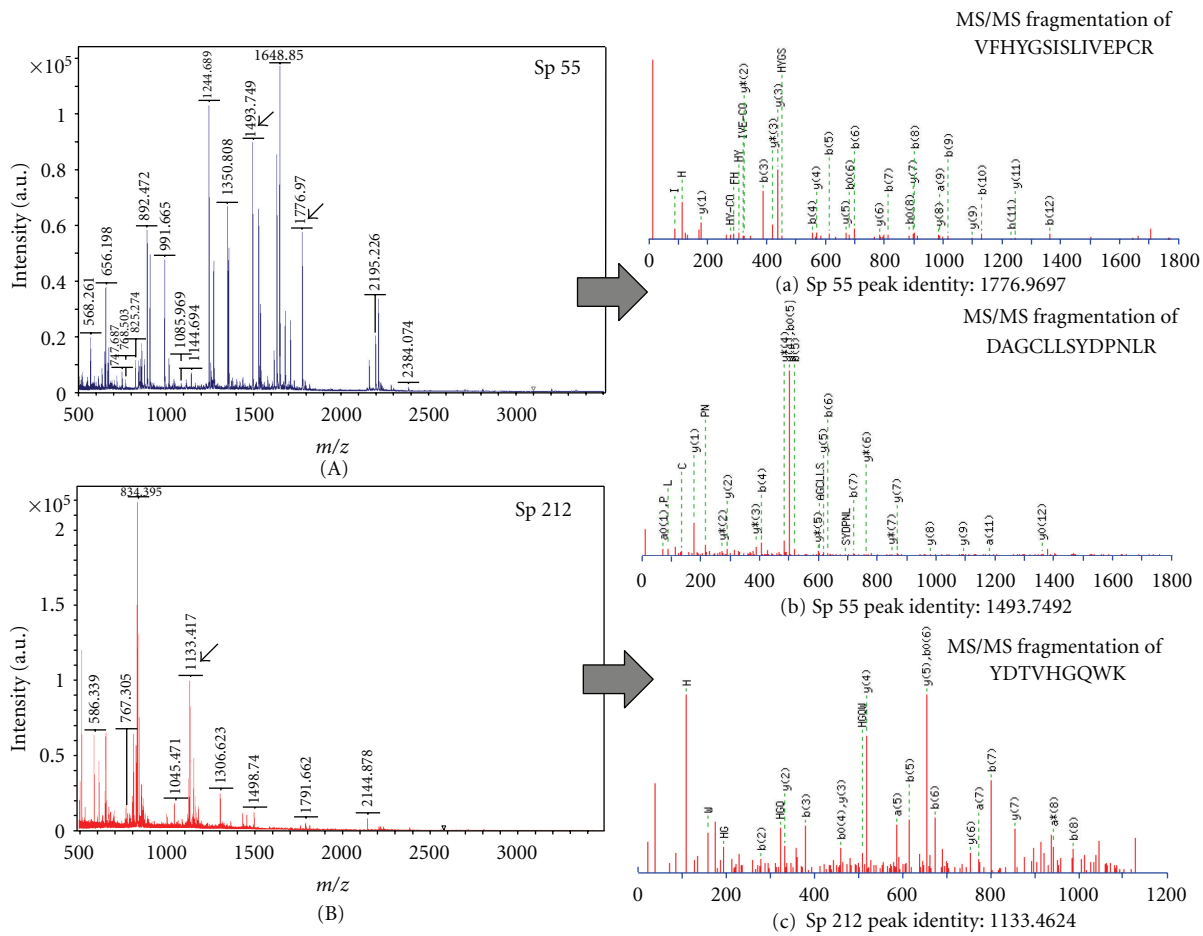

Figure 6: Spectral profiles obtained by MALDI-TOF MS and MS/MS. (A) MALDI spectra of sp 55 and (a), (b), show MS/MS spectra of two selected peaks of sp 55 (1776.9697 and 1493.7492). (B) MALDI spectra of sp 212 and (c) shows MS/MS spectra of the selected peak of sp 212 (1133.4624).

Improvisation of the extraction buffer was also made by adding 2% SDS, which resulted in precipitation. Interference between constituents of the extraction buffer and SDS was assumed to be the cause of such precipitation. However further experimentation needs to be performed for confirmation of such predictions.

All protein spots selected for MALDI-TOF/MS and MS/MS from PSWS resulted in successful identification. High intense spot like sp 55, (fructokinase-like protein) and less intense spot like sp 212, (glyceraldehyde 3-phosphate dehydrogenase) both resulted in high quality spectra with low background noise (Figure 6). These results further indicated the compatibility of PSWS method with both MS and MS/MS and its reliability for downstream processing.

5. Conclusion

The present study emphasizes PSWS as the optimized phenol-based method for chickpea root protein extraction. This method successfully isolated high quality protein suitable for downstream processing. Hence, the data obtained projects this protocol as an effective and efficient one that could be applied for other recalcitrant leguminous root tissues as well. Nevertheless, it should be kept in mind that one generalized protein extraction protocol applicable for global protein profiling of variable tissues irrespective of their origins though theoretically conceivable, but fails to meet practical feasibility.

Acknowledgments

M. Chatterjee is thankful to NMTILI, Council of Scientific and Industrial Research for financial support. S. Gupta is thankful to Department of Biotechnology, Government of India for financial assistance. A. Bhar is also thankful to Council of Scientific and Industrial Research for financial support. Besides, all the authors are thankful to Bose Institute for infrastructure. Special thanks are offered to Rajesh Vashisth (Bruker Daltonics) for providing technical help for conducting mass spectrometry. The help provided by the Central Instrumentation Facility, Bose Institute on proteomic services is duly acknowledged. The authors would also like to thank International Crops Research Institute for the Semi Arid Tropics (ICRISAT), Patancheru, Andhra Pradesh, for seeds. Finally the authors thank Mr. Arup Kumar Dey for providing backup support.

References

[1] J. K. C. Rose, S. Bashir, J. J. Giovannoni, M. M. Jahn, and R. S. Saravanan, "Tackling the plant proteome: practical approaches, hurdles and experimental tools," *The Plant Journal*, vol. 39, no. 5, pp. 715–733, 2004.

[2] P. Gegenheimer, "Preparation of extracts from plants," *Methods in Enzymology*, vol. 182, pp. 174–193, 1990.

[3] A. Tsugita and M. Kamo, "2-D electrophoresis of plant proteins," *Methods in Molecular Biology*, vol. 112, pp. 95–97, 1999.

[4] W. Wang, F. Tai, and S. Chen, "Optimizing protein extraction from plant tissues for enhanced proteomics analysis," *Journal of Separation Science*, vol. 31, no. 11, pp. 2032–2039, 2008.

[5] R. S. Saravanan and J. K. C. Rose, "A critical evaluation of sample extraction techniques for enhanced proteomic analysis of recalcitrant plant tissues," *Proteomics*, vol. 4, no. 9, pp. 2522–2532, 2004.

[6] C. Damerval, D. D. Vienne, M. Zivy, and H. Thiellement, "Technical improvements in two-dimensional electrophoresis increase the level of genetic variation detected in wheat-seedling proteins," *Electrophoresis*, vol. 7, no. 1, pp. 52–54, 1986.

[7] W. J. Hurkman and C. K. Tanaka, "Solubilization of plant membrane proteins for analysis by two-dimensional gel electrophoresis," *Plant Physiology*, vol. 81, no. 3, pp. 802–806, 1986.

[8] Y. Meyer, J. Grosset, Y. Chartier, and J. C. Cleyet-Marel, "Preparation by two-dimensional electrophoresis of proteins for antibody production: antibodies against proteins whose synthesis is reduced by auxin in tobacco mesophyll protoplasts," *Electrophoresis*, vol. 9, no. 11, pp. 704–712, 1988.

[9] K. V. Mijnsbrugge, H. Meyermans, M. Van Montagu, G. Bauw, and W. Boerjan, "Wood formation in poplar: identification, characterization, and seasonal variation of xylem proteins," *Planta*, vol. 210, no. 4, pp. 589–598, 2000.

[10] W. Wang, M. Scali, R. Vignani et al., "Protein extraction for two-dimensional electrophoresis from olive leaf, a plant tissue containing high levels of interfering compounds," *Electrophoresis*, vol. 24, no. 14, pp. 2369–2375, 2003.

[11] T. Isaacson, C. M. B. Damasceno, R. S. Saravanan et al., "Sample extraction techniques for enhanced proteomic analysis of plant tissues," *Nature Protocols*, vol. 1, no. 2, pp. 769–774, 2006.

[12] T. J. Raharjo, I. Widjaja, S. Roytrakul, and R. Verpoorte, "Comparative proteomics of *Cannabis sativa* plant tissues," *Journal of Biomolecular Techniques*, vol. 15, no. 2, pp. 97–106, 2004.

[13] A. M. Schuster and E. Davies, "Ribonucleic acid and protein metabolism in pea epicotyls: II. Response to wounding in aged tissue," *Plant Physiology*, vol. 73, no. 3, pp. 817–821, 1983.

[14] S. Gupta, D. Chakraborti, A. Sengupta, D. Basu, and S. Das, "Primary metabolism of chickpea is the initial target of wound inducing early sensed *Fusarium oxysporum* f. sp. *ciceri* race I," *PLoS ONE*, vol. 5, no. 2, Article ID e9030, 2010.

[15] S. C. Carpentier, E. Witters, K. Laukens, P. Deckers, R. Swennen, and B. Panis, "Preparation of protein extracts from recalcitrant plant tissues: an evaluation of different methods for two-dimensional gel electrophoresis analysis," *Proteomics*, vol. 5, no. 10, pp. 2497–2507, 2005.

[16] M. M. Bradford, "A rapid and sensitive method for the quantitation of microgram quantities of protein utilizing the principle of protein-dye binding," *Analytical Biochemistry*, vol. 72, no. 1-2, pp. 248–254, 1976.

[17] A. Shevchenko, H. Tomas, J. Havliš, J. V. Olsen, and M. Mann, "In-gel digestion for mass spectrometric characterization of proteins and proteomes," *Nature Protocols*, vol. 1, no. 6, pp. 2856–2860, 2007.

[18] F. Granier, "Extraction of plant proteins for two-dimensional electrophoresis," *Electrophoresis*, vol. 9, no. 11, pp. 712–718, 1988.

[19] C. M. Vâlcu and K. Schlink, "Reduction of proteins during sample preparation and two-dimensional gel electrophoresis of woody plant samples," *Proteomics*, vol. 6, no. 5, pp. 1599–1605, 2006.

[20] S. Maurya, U. P. Singh, D. P. Singh, K. P. Singh, and J. S. Srivastava, "Secondary metabolites of chickpea (*Cicer arietinum*) and their role in pathogenesis after infection by *Sclerotium rolfsii*," *Journal of Plant Diseases and Protection*, vol. 112, no. 2, pp. 118–123, 2005.

[21] M. Chérif, A. Arfaoui, and A. Rhaiem, "Phenolic compounds and their role in bio-control and resistance of chickpea to fungal pathogenic attacks," *Tunisian Journal of Plant Protection*, vol. 2, no. 1, pp. 7–21, 2007.

[22] W. D. Loomis and J. Battaile, "Plant phenolic compounds and the isolation of plant enzymes," *Phytochemistry*, vol. 5, no. 3, pp. 423–438, 1966.

[23] S. X. Chen and A. C. Harmon, "Advances in plant proteomics," *Proteomics*, vol. 6, no. 20, pp. 5504–5516, 2006.

[24] D. F. Hochstrasser, M. G. Harrington, A. C. Hochstrasser, M. J. Miller, and C. R. Merril, "Methods for increasing the resolution of two-dimensional protein electrophoresis," *Analytical Biochemistry*, vol. 173, no. 2, pp. 424–435, 1988.

[25] A. Pusztai, "Interactions of proteins with other polyelectrolytes in a two-phase system containing phenol and aqueous buffers at various pH values," *Biochemical Journal*, vol. 99, no. 1, pp. 93–101, 1966.

[26] A. Schuster and E. Davies, "Ribonucleic acid and protein metabolism in pea epicotyls II. Response to wounding in aged tissue," *Plant Physiology*, vol. 73, no. 3, pp. 817–821, 1983.

Hindawi Publishing Corporation
International Journal of Proteomics
Volume 2012, Article ID 290457, 8 pages
doi:10.1155/2012/290457

Research Article

Miniaturized Mass-Spectrometry-Based Analysis System for Fully Automated Examination of Conditioned Cell Culture Media

Emanuel Weber,[1,2] Martijn W. H. Pinkse,[1] Eda Bener-Aksam,[1] Michael J. Vellekoop,[2] and Peter D. E. M. Verhaert[1,3]

[1] *Department of Biotechnology, Netherlands Proteomics Centre, Delft University of Technology, Julianalaan 67, 2628BC Delft, The Netherlands*
[2] *Institute of Sensor and Actuator Systems, Vienna University of Technology, Gusshausstrasse 27-29/E366, 1040 Vienna, Austria*
[3] *Biomedical Research Institute (BJOMED), Hasselt University, Agoralaan building C, 3590 Diepenbeek, Belgium*

Correspondence should be addressed to Peter D. E. M. Verhaert, p.d.e.m.verhaert@tudelft.nl

Received 29 February 2012; Accepted 6 September 2012

Academic Editor: Paul P. Pevsner

We present a fully automated setup for performing in-line mass spectrometry (MS) analysis of conditioned media in cell cultures, in particular focusing on the peptides therein. The goal is to assess peptides secreted by cells in different culture conditions. The developed system is compatible with MS as analytical technique, as this is one of the most powerful analysis methods for peptide detection and identification. Proof of concept was achieved using the well-known mating-factor signaling in baker's yeast, *Saccharomyces cerevisiae*. Our concept system holds 1 mL of cell culture medium and allows maintaining a yeast culture for, at least, 40 hours with continuous supernatant extraction (and medium replenishing). The device's small dimensions result in reduced costs for reagents and open perspectives towards full integration on-chip. Experimental data that can be obtained are time-resolved peptide profiles in a yeast culture, including information about the appearance of mating-factor-related peptides. We emphasize that the system operates without any manual intervention or pipetting steps, which allows for an improved overall sensitivity compared to non-automated alternatives. MS data confirmed previously reported aspects of the physiology of the yeast-mating process. Moreover, matingfactor breakdown products (as well as evidence for a potentially responsible protease) were found.

1. Introduction

In the field of proteomics/peptidomics mass spectrometry has become a well-established tool for protein/peptide sequencing [1–3]. Its steadily increasing performance (sensitivity as well as resolution) enables the analysis of thousands of different molecules at the same time which is of big advantage for "shotgun" approaches, where complex mixtures of unknown samples are targeted for identification. In combination with sophisticated separation methods, protein/peptide analysis has become much faster and more efficient [4–6].

Nevertheless, the whole analysis cycle, starting with peptide extraction from the medium of interest, sample pretreatments (chromatographic purification, digestion) prior to the ultimate injection in the MS instrument requires many time consuming and tedious steps, often done manually. Furthermore, the need for pipetting induces unavoidable sample losses, resulting in a decrease of the overall method sensitivity.

The goal of this work was the design and realization of a system, capable of performing sample extraction, protein/peptide enrichment, purification, and sample preparation for MALDI MS analysis in a fully automated and controlled manner. With the elimination of all previously necessary sample handling steps requiring pipetting, the sensitivity achievable by the system is boosted. Furthermore, using MALDI MS instead of direct connection to an ESI instrument allows for decoupling of the cell cultivation and the actual sample analysis. In that way those two parts can be

performed independently from each other, even at different locations.

In addition, sample volumes are kept at a minimum. Reasons to pursue miniaturization include reagent costs. In many studies, different chemicals or additives are needed at certain concentrations to reveal activities of different components in the cell culture. The investment for additives is evidently reduced if the total sample volume is small. Besides these "economy" factors, evolution towards microscale is an essential step to a possible future design of a fully integrated, on-chip analysis system [7]. Once integrated on a single chip, all the advantages of those can be exploited, including (but not limited to) faster analysis cycles, implementation of extrasensing elements (e.g., viability analysis [8]) and on-chip temperature control [9, 10].

As a possible application of this system the analysis of cell-to-cell communication in *Saccharomyces cerevisiae* (baker's yeast) cultures based on peptide secretion was investigated. It is long known that peptides play an important role in cell-to-cell communication in yeast cultures [11]. As best documented example, we selected the mating process as model to evaluate the performance of our novel system. During mating, two yeast cells of opposite haplotype secrete a 13 amino acid pheromone called alpha-mating factor (secreted by alpha-type cells) and a 12 amino acid residue a-mating factor (released by a-haplotypes), respectively. This initiates alpha- and a-haplotype cell fusion to form a diploid cell [12]. In the course of this study the focus was on the detection, accumulation, and analysis of this peptide at different stages during cell culture growth. Therefore, cells were cultivated at small scale (1 mL) while continuously extracting and analyzing the extracellular conditioned medium. As a result a chronological sequence of MS spectra was obtained that could be nicely correlated to the corresponding growth stages. In a second study the effects of an enzyme inhibitor on potential peptidase activity cleaving alpha-mating factor was investigated. This experiment enabled us to collect evidence supporting the hypothesis for the involvement of a yapsin-like protease in an easy and fast way [13].

2. Materials and Methods

2.1. Strains and Growth Conditions. A WT *Saccharomyces cerevisiae* strain (CEN.PK 113-1A) mating-type alpha was used [14]. Cells were grown in mineral medium (MM) with addition of glucose (2%, w/v) as sole carbon source [15]. Prior to the transfer into the actual analysis chamber, yeast cells were precultivated in shaker flasks (10 mL MM, 30°C, 200 rpm). Such 24-hour culture has a typical optical density of 19-20 at a measuring wavelength of 600 nm (OD_{600}). Dilution to an OD_{600} of 0.1 yielded the initial cell density chosen for all experiments. For every analysis, 1 mL of initial culture was transferred into a custom modified 2 mL glass vial which was prepared for connection to the analysis system.

In the protease inhibition experiments, 10 μM pepstatin (Sigma Aldrich) was added to the culture flask after precultivation.

2.2. Miniaturized Cell Culture Chamber. A modified 2 mL glass vial with cap including septum (Agilent Technologies, USA) was used as a basic module for the miniaturized cell culture chamber. Fused silica tubings (inner diameter 100 μm; BGB Analytik AG, Switzerland) were inserted through the perforated septum, to provide two liquid in- and three liquid outlets (Figure 1). All tubings inside the vial were fitted with a porous glass ending to allow cell culture medium to pass through, while preventing cells to leave the vial and enter the analysis system. Airtight closure of the vial, essential for the functionality of the system, was achieved by deposition of a silicone rubber-based sealant (Bison, Netherlands) on top of the cap. To obtain efficient mixing of the cell suspension the cell culture chamber was equipped with a small magnet and kept on a magnetic stirrer (500 rpm).

Sampling of supernatant from the culture was done by creating an overpressure inside the vial. One of two inlets ("pressure", Figure 1) was connected to a pressurized air system. The second inlet ("MM", Figure 1) was connected to the medium reservoir (via syringe pump 1, SP1, Figure 2) for a constant supply of fresh mineral medium (MM, 0.5 μL/min). In operation only one of the three outlets ("sampling", Figure 1) was opened at a time, with the overpressure inside the chamber resulting in a steady sampling of supernatant.

2.3. Automated Setup for In-Line Sampling of Extracellular Medium System Components. The complete system consists of the cell culture chamber placed on a magnetic stirrer (IKA Labortechnik, Germany), two syringe pumps (Fusion 200; Chemyx, USA), a six-port valve (Rheodyne, USA) controlled by an external interface, three capillary columns packed with 5 μm silica-based C4 beads (300 Å pore size, ReproSil; Dr. Maisch GmbH, Germany) for peptide enrichment/concentration and pressure stabilization, an electrospray unit for sample deposition, a MALDI target plate, and an *x-y-z* motion controller (MM4005; Newport, USA; Figure 2). The syringe pumps supply solvent for elution (SP2) and MM (SP1), keeping the volume in the vial constant. In the current experiments, no additional glucose or vitamins were supplied via SP1. The MALDI plate was accurately micropositioned by the motion controller. An in-house software program was developed and loaded into the microcontroller of the MM4005 for synchronization with the six-port valve. Real-time determination of optical density was realized with a fiber spectrophotometer (Avaspec-2048) and suitable light source (DH-2000; Avantes, Netherlands). MS analysis was performed directly from the spotted samples in a MALDI Q-TOF mass spectrometer (QTof Premier; Waters, Manchester, UK), equipped with a solid state NdYag laser.

2.4. Real-Time Optical Density Measurement inside the Miniaturized Cell Culture Chamber. The optical density was measured with a fiber spectrophotometer setup especially conceived for use with 2 mL glass vials. Initial linearity of the device at 600 nm was established for ODs between 0.1 up to 1.5. An extended calibration curve was recorded to get

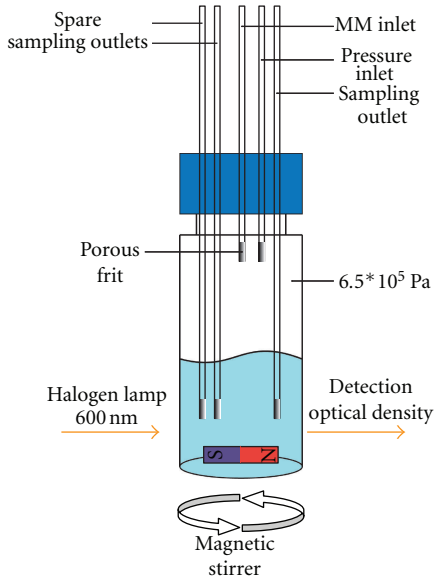

Figure 1: Schematic of miniaturized cell culture chamber: a modified 2 mL glass vial. Five fused silica tubings inserted through perforated cap provide liquid in- and outlets. Endings of fused silica tubings are fitted with a porous frit to prevent cells from leaving the vial and contaminating the analysis system. Overpressure of approximately $6.5 * 10^5$ Pa inside chamber operates as pumping system. Efficient mixing of culture is ensured by minimagnet at vial bottom in combination with underlying magnetic stirrer. Light path for OD determination goes straight through vial between magnet and endings of fused silica.

valid data at higher densities as well. After averaging of more than 200 individual measurements for one data point and curve fitting (Matlab, The MathWorks, USA) linearity was obtained for values up to OD_{600} 13, fully covering the range of interest (Figure 3).

2.5. Sampling Cycle Operation. Operation of the sampling system was basically divided into two parts: (i) sample accumulation/concentration and (ii) elution. The temporal resolution of the setup in the current configuration is approximately 2 hours. Keeping in mind the life cycle of *S. cerevisiae* (reproduction/cell division each 75–120 minutes [16]) this resolution gives chronological information about the state the whole culture is going through rather than information at the single-cell level. In the accumulation step (90 min) the analysis column C1 was connected directly with the open outlet of the cell culture chamber via valve V1 (Figure 2). The outflow of solution in that time was spotted onto a waste position on the MALDI plate. The flow was adjusted to 0.4–0.6 μL/min resulting in a sampling volume of 36 to 54 μL over the 90 minutes accumulation/concentration period. During this step solvent was pumped through column C2 (Figure 2) connected via the valve to waste. The inclusion of column C2 proved necessary for maintaining constant backpressure inside the system and hence constant (out-) flow. After accumulation, elution followed by switching the valve, which simultaneously triggered the motion controller to position the first spot on the MALDI plate exactly under the electrospray unit. Solvent (water/acetonitrile/acetic acid; 10 : 90 : 0.6, v/v/v) was pumped through the column C1 at a flow rate of 1 μL/min. Eluates were deposited for 1.5 min per spot (corresponding to 1.5 μL). Ten sample spots were collected in a row to ensure complete elution of the column. Carryover between consecutive analysis runs can be excluded as empty MS spectra (no peptide ion peaks) were obtained for the last sample spots of each series. Extraction of supernatant out of the cell culture chamber continued during the elution step as well. The sample was continuously pushed through a second waste column (C3, Figure 2) for flow stabilization reasons. Both, accumulation and elution step, were repeated up to 11 times, equivalent to more than 19 hours of total analysis time. Throughout the experiment the optical density was measured at a 2 hours interval, and the resulting growth curve was recorded (see e.g., Figure 5).

2.6. Preparation of Target Plate for MALDI Mass Spectrometry. Prior to sample spotting, the MALDI plate was ultrasonically cleaned in ammonium bicarbonate solution (10 mM) followed by water/methanol/trifluoroacetic acid (50/50/0.1, v/v/v). Alpha-cyano-4-hydroxycinnamic acid was used as matrix (dissolved at 6 mg/mL in water/acetonitrile/trifluoroacetic acid; 50/50/0.1, v/v/v). After electrospray deposition of the samples, 0.8 μL of matrix solution was added to each spot on the MALDI plate. The plate was analyzed in the MS system, i.c. MALDI Q-TOF after air-drying and complete crystallization of the matrix.

Direct connection of the presented setup to an ESI MS instrument is feasible but requires both parts, cell cultivation as well as sample analysis, to be physically linked which prohibits independent operation and requires all instruments to be placed at the same location.

3. Results

3.1. Detection of S. cerevisiae Mating Factor. Alpha-pheromone (TrpHisTrpLeuGlnLeuLysProGlyGlnProMetTyr, monoisotopic mass 1682.84 Da) is detected in our MALDI Q-TOF MS as $[M + H]^+$ at *m/z* 1683.85. Associated with this ion often a peak at *m/z* 1699.84 is observed, corresponding to the peptide oxidized at position Met_{12} (a very common posttranslational modification (PTM)). The identity of the peptide could be confirmed by CID of the 1699.84 precursor ion (MS/MS spectrum given in Figure 4).

The alpha-mating-factor-related peptides were detected nearly throughout the whole analysis indicating that alpha factor is expressed and secreted constitutively (also in the absence of opposing-mating-type cells/pheromone). The appearance of alpha-mating factor was more obvious at the late exponential growth phase (corresponding to the diauxic shift, when conditions get less favorable, after nutrient consumption). Two major fragments of the alpha-mating factor (the aminoterminal hexapeptide and the carboxyterminal heptapeptide) were detected in the medium (verified by MS/MS, data not shown) besides the intact pheromone.

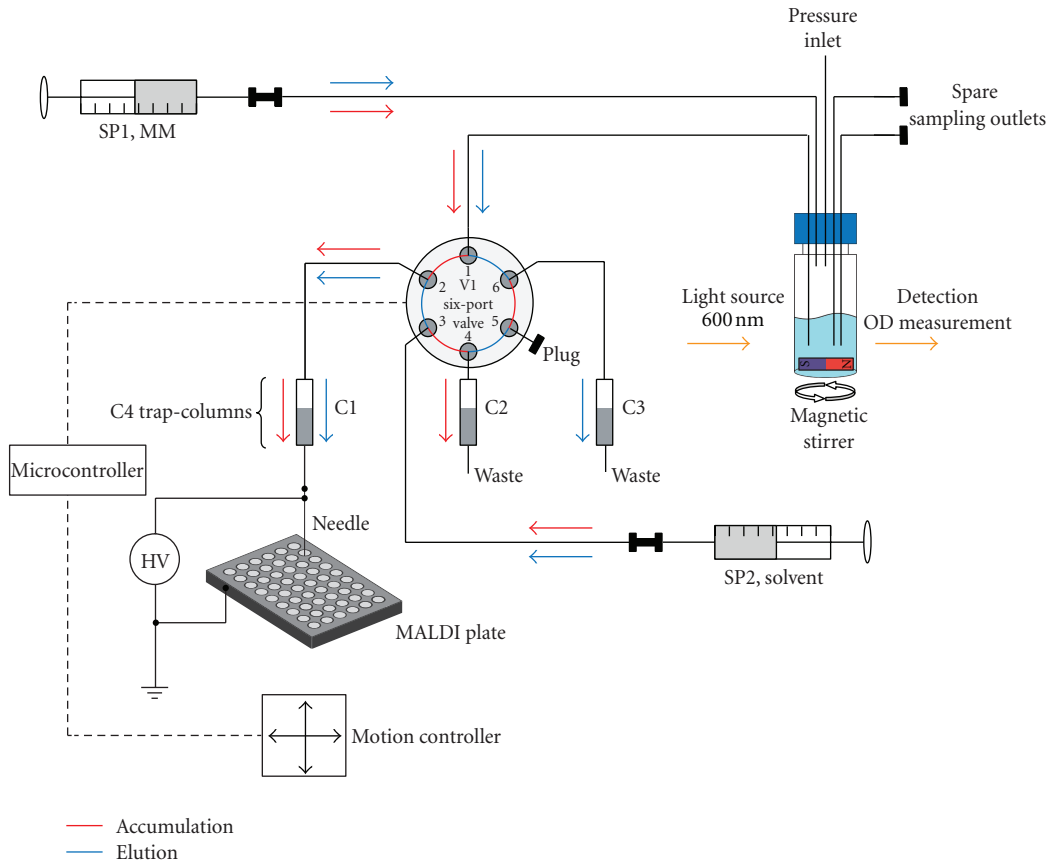

Figure 2: Overall analysis setup incorporating two syringes for MM and solvent supply and a switching valve for alternating between concentration/accumulation and elution steps. Cell culture chamber, placed on a magnetic stirrer, is connected via six-port valve with one of three C4 columns, which maintain a stable system backpressure. Via an electrospray needle held at 1.2 kV, sample is deposited onto a MALDI target plate.

These two mating-factor (degradation-) fragments may be products of a protease which cleaves the intact pheromone in two pieces (see Section 3.4 [17]). The fact that their amounts increase in time while intact pheromone decreases at later stages of growth would agree with this.

3.2. Real-Time Monitoring of S. cerevisiae Growth in Cell Culture Chamber. The objective of this study was to develop an automated setup for the analysis of conditioned media of *Saccharomyces cerevisiae* cultures at different growth stages at a miniature scale. To obtain reproducible results and to allow valid comparisons between experiments, it is important to keep the cells at the same physiological/growth state for all experiments. The growth state of the cells was monitored robustly by measuring cell density. For this a fiber spectrophotometer was integrated in our setup, specifically designed for use with 2 mL glass vials. This allowed real-time noninvasive determination of culture ODs. To cover the whole range of ODs a typical yeast culture under the applied conditions goes through (0.1 to 13), a thoroughly elaborated calibration including multiple individual measurements was generated. The real-time recorded growth curves were accurate, as they were in excellent accordance with calibration curves obtained from standard OD determination techniques (diluting the culture to ODs in the linear range of the spectrophotometer and recalculating the actual OD, data not shown). Our analyses confirmed that different batches of yeast cultures show very similar growth behaviors (Figure 5). However, for a meaningful comparison between cultures at various time points/growth stages a perfect match of the two curves is essential. Parameters like small variations in the initial ODs of the inoculated culture or the addition of a test compound may result in slightly delayed or shifted initiation of cell growth. This can be corrected for by software-wise adjustment ("warping") of one of the two curves onto the other (a simple shift along the time axis often being sufficient). The finally obtained diagram shows a perfect match in terms of cell growth of both investigated conditions (Figure 6). All timepoints of both series overlap on a single curve which facilitates a valid comparison.

3.3. Time-Resolved Detection of Mating Factor (and Other Peptide-Like Compounds) in Yeast Cell Culture Media under Standard Growth Conditions. To study the cell culture medium during a standard yeast growth, samples were collected at 2 hours intervals starting at an OD_{600} of approx.

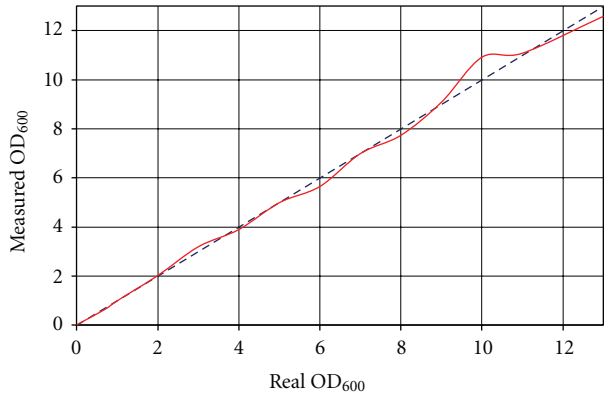

Figure 3: Calibration curve for linearization of OD_{600} measurement. Blue dashed line represents optimal behavior. Solid red curve illustrates actually determined OD_{600} after measuring, averaging, and calibration.

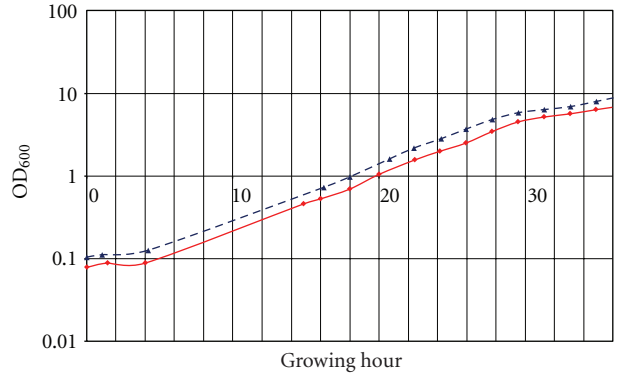

Figure 5: Growth curves recorded from two cultures grown under different conditions (blue, dashed curve represents standard growing conditions; red, solid curve with addition of protease inhibitor pepstatin). A small time lag between both curves is evident and makes a comparison based on absolute time points inaccurate.

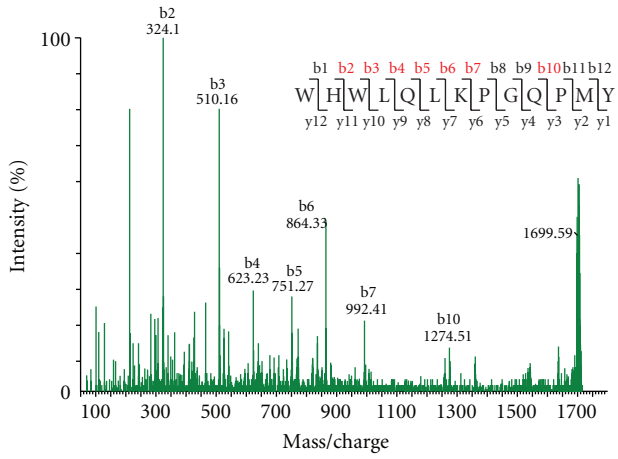

Figure 4: MS/MS spectrum of alpha-mating factor (oxidized at Met_{12}). Insert: amino-acid sequence with detected sequence ions indicated in red. Note virtually complete b-ions series.

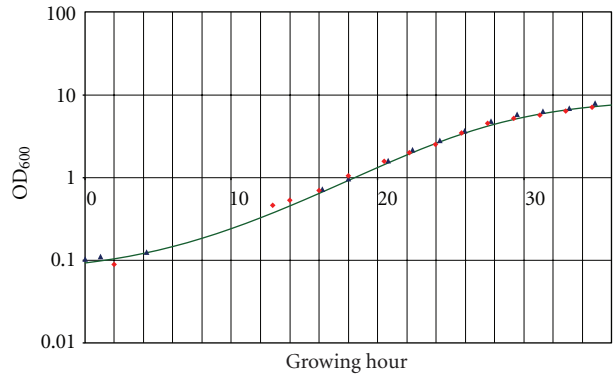

Figure 6: After PC-supported adjustment of measurement series of pepstatin-containing culture a perfect matching of both growth curves was obtained. All points lie on fitted sigmoid function (solid, green curve), allowing a valid comparison.

1, which typically is reached 18 to 20 hours after inoculation of the initial culture (OD_{600} of 0.1).

Up to 11 consecutive samples were analyzed by MALDI Q-TOF MS(/MS) yielding chronologically classified MS spectra ("peptide profiles"). Figure 7 shows representative spectra at every second time point sampled (resulting in a difference of 4 hours between each consecutive spectrum displayed). Several different peptide-like signals are evident in the mass spectra acquired. To assist in the interpretation of these profiles, 5 mass over charge (m/z) values of interest are highlighted throughout all the spectra, (four between 1520 and 1720 m/z and one at about half the m/z). MS/MS analysis confirmed that the peaks at m/z 1683.85, 1699.83, and 1536.75 represent the mating factor, its oxidized version, and a C terminally truncated species (loss of Tyr residue), respectively. The peak in the lower m/z region, at 882.45, represents one of the two mating-factor cleavage products (the aminoterminal hexapeptide). The complementary peptide fragment (the carboxyterminal heptapeptide) was not readily identified.

One of the most distinct peptide peaks shows up at 1628.74 Da (Figure 7). MS/MS analysis and Mascot database searching (using "no enzyme" as parameter) identified it as the soluble fragment of a cell wall protein; exo-1,3-beta-glucanase (EXG1). EXG1 is known to be involved in cell wall organization by enabling beta-glucan assembly [18]. Literature data [19] and our time-course analysis confirm its presence in the culture medium just before alpha-mating-factor secretion. This suggests that this protein fragment is shed from the membrane just prior to, or simultaneously with, mating-factor release, which may imply a potential role of this protein fragment in mating.

For the time-resolved detection of mating-factor, cells were grown in MM without addition of any special component except those needed for cell growth. It was observed that none of the four mating-factor-related peaks appear early during growth. First unequivocal detection is between hour

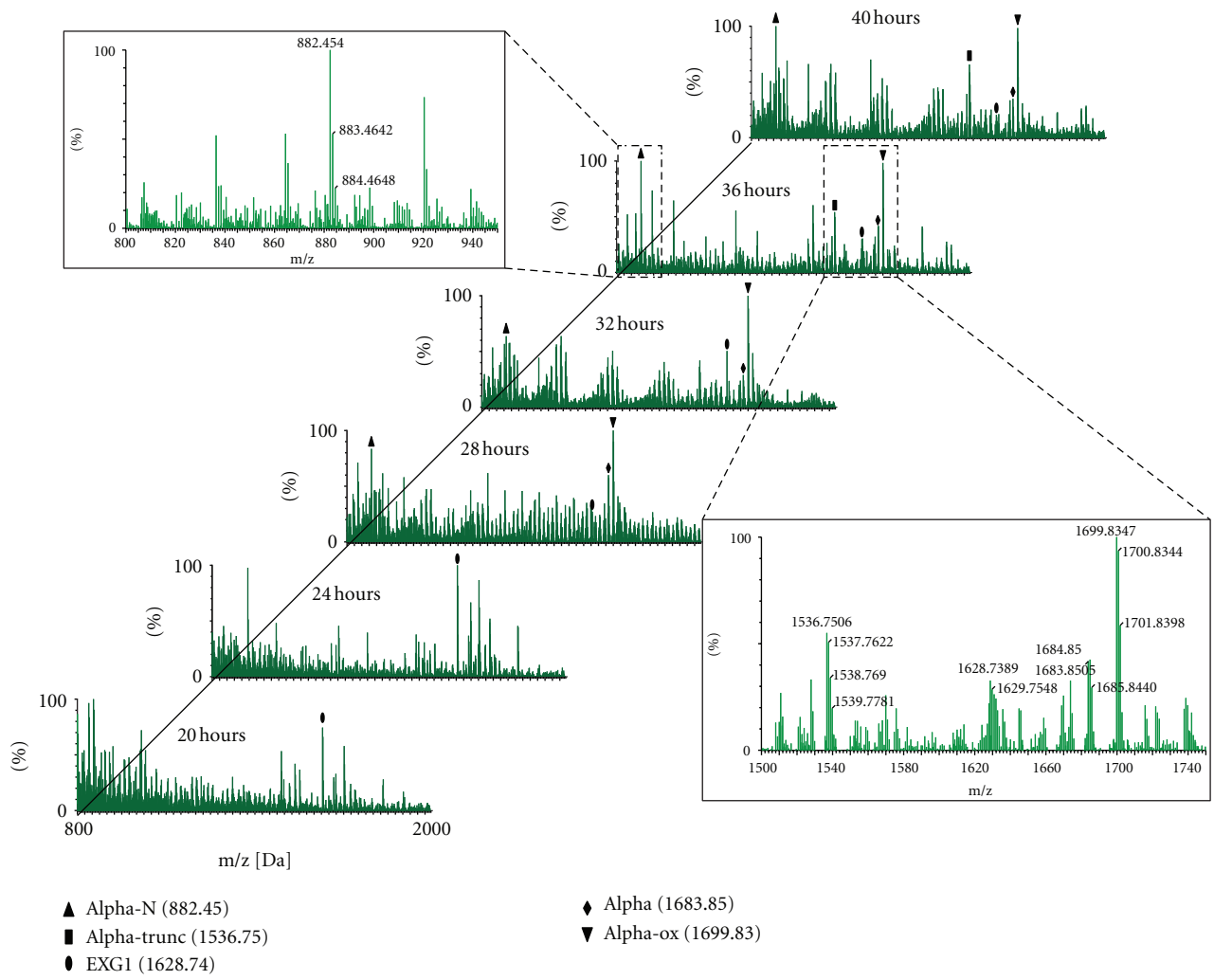

Figure 7: MS spectra at 2 hours intervals during standard yeast growth (for figure clarity, every 2nd spectrum is omitted resulting in a 4 hours interval). Marked peaks (legend insert) indicate peptide ions of interest (alpha-N, 882.45 Da: $[M + H]^+$ of aminoterminal mating factor hexapeptide; alpha-trunc, 1536.75 Da: carboxy terminally truncated oxidized mating factor (oxidized alpha factor minus C-terminal tyrosine residue); EXG1, 1628.74 Da: fragment of EXG1 membrane protein; alpha, 1683.85 Da and alpha-ox, 1699.83 Da: alpha-mating factor and its oxidized version). Mating-factor-related peptides do not appear at early time points, whereas they become the most abundant ion peaks at later growth stages, which fits with physiological data. Inserts (top left; bottom right) show magnifications of a spectrum with annotated peaks of interest and their isotopes.

26 and 28, that is, at an OD_{600} of approx. 3.5. Mating-factor concentrations significantly increase in the later growth stages. It is remarkable that both intact mating factor and one of its fragments (the aminoterminal hexapeptide) are detected virtually simultaneously. Multiple repetitions (exceeding 5) confirmed the above-stated behavior. Figure 7 should be understood as an illustrative sequence of MS spectra of a single continuous (40 hours) analysis run.

3.4. Effect of Pepstatin (Inhibition of Aspartic Proteases). To illustrate the usefulness of the miniature culture media analysis system, a simple experiment was designed looking at the effect of a protease inhibitor on the appearance of selected peptide fragments detected above. The proteolytic cleavage of mating factor at the Leu/Lys peptide bond suggests involvement of an aspartic protease. Hence a general aspartic protease inhibitor was selected to study its effect on the appearance of the peptides/peptide fragments observed [20]. Pepstatin was added to the culture at a concentration of 10 μM. The anticipated effect reduced appearance of the 881.45 Da fragment ($[M + H]^+$ at *m/z* 882.45) during the whole experiment. Besides the addition of 10 μM of pepstatin all conditions were kept strictly the same as for the other experiments. The first appearance of intact mating factor and its oxidized variant was observed at the same time point as for the culture without inhibitor. This indicates that the addition of pepstatin at the chosen concentration had no effect on the actual secretion of alpha factor (MS data not shown). The abundance of the 881.45 Da fragment on the other

hand was significantly lower in all spectra (Figure 8, right scale). The red, dashed line in Figure 8 (left scale) depicts the growth curve (in terms of optical density (light absorbance) at 600 nm) at the time of sampling. Data shown represent values from a complete analysis run lasting over 40 hours. Values plotted are representative as biological repetitions of the experiment over shorter time frames showed the very same trend.

4. Discussion

4.1. Alpha-Mating-Factor Profiles at Different Growth Stages. During the yeast life cycle, mating factor is the trigger for two haploid cells of opposite mating type (alpha and a) to mate and form one single diploid cell. This happens in nature once the growth conditions get unfavorable, for example, lack of nutrition. The strain used in this study is incapable of changing its sex/haplotype [14]. This precludes the formation of diploid cells in the culture flask. However, it is clear that these haploid cells still produce their pheromone in the absence of an opposing mating type or pheromone. The obtained MS spectra in Figure 7 illustrate that the cells "signal for mating" particularly at the later stages of growth, that is, at the end of and after the exponential growth phase. In the early stages of growth no peaks representing the mating factor were identified.

4.2. Alpha-Mating-Factor Detection in Pepstatin-Containing Cultures. Comparing the growth curves of the pepstatin containing with those of "standard" cultures confirmed that the growth behavior of the cells was similar in both conditions, justifying a valid time-based peptide profile comparison (Figure 6).

We hypothesized that if mating factor is secreted already at an earlier cell growth stage but readily cleaved by a protease, inhibition or inactivation of this protease could promote the detection of intact mating factor at an earlier time point in the growth curve. This was not observed. The intact mating factor appeared at the same time in both experiments. However, it should be noted that the time resolution of the current setup was 2 hours. Small shifts within this interval may still have been missed.

4.3. Effect of Pepstatin on Mating-Factor Fragment Appearance. The comparison of cell cultures with and without pepstatin showed significant differences in terms of the extracellular peptide profiles. The presumed aspartic protease responsible for the formation of the 881.45 Da fragment clearly seems to be inhibited by pepstatin. At all examined time points the ratio between the overall count of the 881.45 Da fragment and that of the intact mating factor (both native (1682.84 Da) and oxidized (1698.83 Da)) was significantly decreased in the culture containing the protease inhibitor (Figure 8). Only at the latest points of inspection, the stationary stage of cell growth, a noticeable count of the 881.45 Da fragment was detected but still far below the intensity level of that in the pepstatin-free culture. Given that the conditions for both cultures were kept identical, the

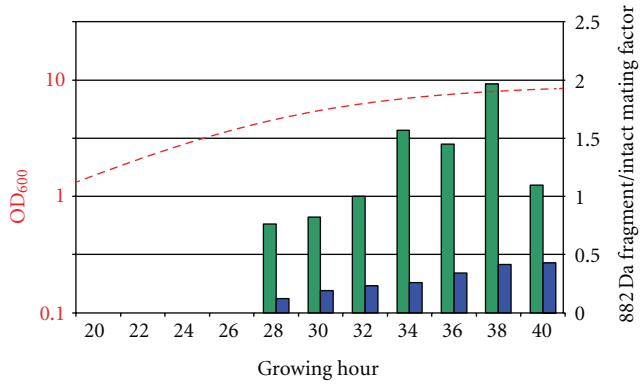

Figure 8: Ratio of 881.45 Da fragment to intact mating factor (1682.84 Da plus 1698.83 Da; right scale). No mating factor or fragments are detected in first 4 investigated time points. At later time points ratios between 0.8 and 2 for culture grown under standard conditions were obtained (right scale, green bars). Note significant reduction of relative amount of 881.45 Da fragments in pepstatin-containing culture (blue bars). Dashed, red curve (left, logarithmic scale) plots growth curve of cells.

disappearance or drastic reduction of the fragment in the extracellular medium is clearly to be attributed primarily to the addition of pepstatin. This suggests that pepstatin inhibits the potential protease responsible for "normal" alpha-mating-factor peptide cutting.

4.4. Additional Mating-Factor-Related Peptide Ions. In the obtained MS spectra additional mating-factor-related ions were identified. The detection of oxidized mating factor missing the tyrosine at the C-terminus at the later growth stages (*m/z* 1536.75; Figure 7) may reflect the action of an (carboxyterminal) exopeptidase in the extracellular medium. Concurrently, the amount of intact mating factor inside the culture decreases.

4.5. Other Nonmating Factor-Related Peptide Ions. Besides ions related to mating factor, another peptide possibly involved in the secretion process was identified (*m/z* 1628.74; Figure 7). Database searching identified it as the soluble part of the exo-b-1,3-glucanase EXG1 (a cell wall protein). The role of this protein in peptide secretion remains elusive, but comparing its appearance in both experiments showed marked differences. In standard cultures, the peptide was found most abundant prior to secretion of mating factor and slightly reduced at later growth stage. In-pepstatin containing cultures this peptide was not found prior to mating peptide secretion, and it appeared considerably less prominently present at later growth stages as well (data not shown).

5. Conclusion

The presented automated system allows in-line sampling of microliter amounts of extracellular conditioned cell culture media, preparing them for MALDI MS analysis. The minimal

amount of cell culture required for this has advantages in terms of handling and cost reduction. For example, compared to standard flask cultivation, an enzyme inhibition study during cell growth could be completed with 10 times less amount of the commercial compound (i.c. pepstatin). In particular when effects on cultured cells of more expensive compounds have to be tested, the experiment cost savings related to the reduced culture chamber volume will become more substantial.

Implementation of the real-time optical density measurement in-line (without disturbing the cell culture) made many tedious extra sample collection and dilution steps redundant and resulted in an overall increase of the practicability of the system.

In summary, we have realized a fully automated setup which eliminates all manual pipetting interventions. This reduces the risk for losses of peptides sticking to microtip or tubing/column wall materials, which often drastically reduces the overall sensitivity of the analysis.

Acknowledgments

This project was financed by European Marie Curie Research Training Network "CellCheck", Grant no. MCRTN-CT-2006-035854. Also The Netherlands Proteomics Center (Project T3.1b) and The Netherlands Genomics Initiative are gratefully acknowledged for their support.

References

[1] M. A. Baldwin, "Protein identification by mass spectrometry: issues to be considered," *Molecular and Cellular Proteomics*, vol. 3, no. 1, pp. 1–9, 2004.

[2] T. Nilsson, M. Mann, R. Aebersold, J. R. Yates Jr., A. Bairoch, and J. J. M. Bergeron, "Mass spectrometry in high-throughput proteomics: ready for the big time," *Nature Methods*, vol. 7, no. 9, pp. 681–685, 2010.

[3] B. Ma and R. Johnson, "De novo sequencing and homology searching," *Molecular & Cellular Proteomics*, vol. 11, no. 2, Article ID O111.014902, 2012.

[4] J. R. Wiśniewski, A. Zougman, N. Nagaraj, and M. Mann, "Universal sample preparation method for proteome analysis," *Nature Methods*, vol. 6, no. 5, pp. 359–362, 2009.

[5] H. D. Meiring, E. van der Heeft, G. J. ten Hove, and A. de Jong, "Nanoscale LC-MS(n): technical design and applications to peptide and protein analysis," *Journal of Separation Science*, vol. 25, no. 9, pp. 557–568, 2002.

[6] P. M. Van Midwoud, L. Rieux, R. Bischoff, E. Verpoorte, and H. A. G. Niederländer, "Improvement of recovery and repeatability in liquid chromatography-mass spectrometry analysis of peptides," *Journal of Proteome Research*, vol. 6, no. 2, pp. 781–791, 2007.

[7] M. Stangegaard, S. Petronis, A. M. Jørgensen, C. B. V. Christensen, and M. Dufva, "A biocompatible micro cell culture chamber (μCCC) for the culturing and on-line monitoring of eukaryote cells," *Lab on a Chip*, vol. 6, no. 8, pp. 1045–1051, 2006.

[8] E. Weber, M. Rosenauer, W. Buchegger, P. D. E. M. Verhaert, and M. J. Vellekoop, "Fluorescence based on-chip cell analysis applying standard viability kits," in *Proceedings of the 15th International Conference on Miniaturized Systems for Chemistry and Life Science (microTAS '11)*, pp. 1716–1718, Seattle, Wash, USA, 2011.

[9] A. Jain and K. E. Goodson, "Thermal microdevices for biological and biomedical applications," *Journal of Thermal Biology*, vol. 36, no. 4, pp. 209–218, 2011.

[10] S. Petronis, M. Stangegaard, C. B. V. Christensen, and M. Dufva, "Transparent polymeric cell culture chip with integrated temperature control and uniform media perfusion," *BioTechniques*, vol. 40, no. 3, pp. 368–376, 2006.

[11] T. Tanaka, H. Kita, T. Murakami, and K. Narita, "Purification and amino acid sequence of mating factor from *Saccharomyces cerevisiae*," *Journal of Biochemistry*, vol. 82, no. 6, pp. 1681–1687, 1977.

[12] Y. Wang and H. G. Dohlman, "Pheromone signaling mechanisms in yeast: a prototypical sex machine," *Science*, vol. 306, no. 5701, pp. 1508–1509, 2004.

[13] D. J. Krysan, E. L. Ting, C. Abeijon, L. Kroos, and R. S. Fuller, "Yapsins are a family of aspartyl proteases required for cell wall integrity in *Saccharomyces cerevisiae*," *Eukaryotic Cell*, vol. 4, no. 8, pp. 1364–1374, 2005.

[14] J. P. Van Dijken, J. Bauer, L. Brambilla et al., "An interlaboratory comparison of physiological and genetic properties of four *Saccharomyces cerevisiae* strains," *Enzyme and Microbial Technology*, vol. 26, no. 9-10, pp. 706–714, 2000.

[15] C. Verduyn, E. Postma, W. A. Scheffers, and J. P. Van Dijken, "Effect of benzoic acid on metabolic fluxes in yeasts: a continuous-culture study on the regulation of respiration and alcoholic fermentation," *Yeast*, vol. 8, no. 7, pp. 501–517, 1992.

[16] T. Boekhout and V. Robert, *Yeasts in Food: Beneficial Detrimental Aspects*, Behr's, Hamburg, Germany, 2003.

[17] V. L. MacKay, S. K. Welch, M. Y. Insley et al., "The *Saccharomyces cerevisiae* BAR1 gene encodes an exported protein with homology to pepsin.," *Proceedings of the National Academy of Sciences of the United States of America*, vol. 85, no. 1, pp. 55–59, 1988.

[18] A. R. Nebreda, T. G. Villa, J. R. Villanueva, and F. Del Rey, "Cloning of genes related to exo-β-glucanase production in *Saccharomyces cerevisiae*: characterization of an exo-β-glucanase structural gene," *Gene*, vol. 47, no. 2-3, pp. 245–259, 1986.

[19] C. Cappellaro, V. Mrsa, and W. Tanner, "New potential cell wall glucanases of *Saccharomyces cerevisiae* and their involvement in mating," *Journal of Bacteriology*, vol. 180, no. 19, pp. 5030–5037, 1998.

[20] A. V. Azaryan, M. Wong, T. C. Friedman et al., "Purification and characterization of a paired basic residue-specific yeast aspartic protease encoded by the YAP3 gene. Similarity to the mammalian pro- opiomelanocortin-converting enzyme," *Journal of Biological Chemistry*, vol. 268, no. 16, pp. 11968–11975, 1993.

Hindawi Publishing Corporation
International Journal of Proteomics
Volume 2012, Article ID 735132, 10 pages
doi:10.1155/2012/735132

Research Article

An Economical High-Throughput Protocol for Multidimensional Fractionation of Proteins

David John Tooth, Varun Gopala Krishna, and Robert Layfield

School of Biomedical Sciences, University of Nottingham Medical School, Queen's Medical Centre, Nottingham NG7 2UH, UK

Correspondence should be addressed to David John Tooth, david.tooth@nottingham.ac.uk

Received 17 February 2012; Revised 6 July 2012; Accepted 24 July 2012

Academic Editor: Paul P. Pevsner

A sequential protocol of multidimensional fractionation was optimised to enable the comparative profiling of fractions of proteomes from cultured human cells. Differential detergent fractionation was employed as a first step to obtain fractions enriched for cytosolic, membrane/organelle, nuclear, and cytoskeletal proteins. Following buffer exchange using gel-permeation chromatography, cytosolic proteins were further fractionated by 2-dimensional chromatography employing anion-exchange followed by reversed-phase steps. Chromatographic fractions were shown to be readily compatible with 1- and 2-dimensional gel electrophoresis or with direct analysis by mass spectrometry using linear-MALDI-TOF-MS. Precision of extraction was confirmed by reproducible SDS-PAGE profiles, MALDI-TOF-MS spectra, and quantitation of trypsinolytic peptides using LC-MS/MS (MRM) analyses. Solid phases were immobilised in disposable cartridges and mobile-phase flow was achieved using a combination of centrifugation and vacuum pumping. These approaches yielded parallel sample handling which was limited only by the capacities of the employed devices and which enabled both high-throughput and experimentally precise procedures, as demonstrated by the processing of experimental replicates. Protocols were employed at 10 mg scale of extracted cell protein, but these approaches would be directly applicable to both smaller and larger quantities merely by adjusting the employed solid- and mobile-phase volumes. Additional potential applications of the fractionation protocol are briefly described.

1. Introduction

Protein identification and quantitation are major steps towards full characterization of a proteome. Many proteomic projects classically employ 2-dimensional gel electrophoresis (2DE) and are limited by both the precision of the technique and by well-documented limitations in pI and molecular size constraints [1]. Proteome fractionation is desirable in potentially yielding reduced complexity and increased dynamic range and there have been numerous approaches developed including affinity-depletion [2] and immune depletion of major components [3], liquid isoelectric focussing (IEF) [4], GelC-MS [5], and multidimensional column liquid chromatographic (MDLC) protocols [6].

Differential detergent fractionation (DDF) has long been proposed a suitably robust alternative to more challenging and costly differential ultracentrifugation approaches [7] and indeed its use was recently commercialised [8].

For several decades, liquid chromatography has been a powerful tool for separating proteins, peptides, and other molecules in complex mixtures [9]. Users employ exclusively pumped systems, disadvantages of which are inherently low throughput and no opportunity for parallel processing; the applications of such approaches have been reviewed [10–12]. Two-dimensional systems were also commercialised and their uses have been cited in several proteomics applications [13, 14]. MDLC has been commonly employed more recently for increased separation of complex peptide mixtures to enable increased mass-spectrometer experimental time and so maximised protein structural analysis, either incorporating offline MDLC [15] automated online [16] or using biphasic columns in MuDPIT approaches [17]. Potential

disadvantages of these latter peptide MDLC experiments are the disparate nature of peptide analyses and the potential transparency of some posttranslational processing which may be overcome by alternatively using or combining prior protein fractionation.

Gel permeation chromatography (GPC) separates proteins and smaller components on the basis of molecular weight and three-dimensional shape [18]. Components move through a bed of porous beads, with smaller molecules diffusing further into pores and moving more slowly, whilst larger molecules enter less or not at all, so passing through more quickly. GPC has been used analytically or for buffer exchange in preparative work flows.

Ion-exchange chromatography separates proteins based on differences between pI and net charge [9]. Proteins must have a charge opposite that of the functional group attached to the resin in order to bind. For example, at pH 10, proteins with pI below approximately 9 have a net negative charge and bind to anion exchangers which contain positively charged functional groups. Because this interaction is ionic, binding must take place under low ionic conditions and elution is achieved either by increasing the ionic strength or decreasing the pH of the mobile phase. Mobile phases typically employed in ion exchange are well suited to direct orthogonal second-dimensional separation using reversed-phase chromatography and there are numerous published examples [6, 13, 14].

Reversed-phase chromatography has been and is commonly employed as the final chromatographic stage in proteomics workflows due to the volatile nature of the mobile phase which makes it compatible with both on- and off-line mass spectrometric analyses. Example potential applications include analyses of tissue specimens using MALDI-TOF-MS in studies to design discriminatory disease biomarkers [19] and quantitative proteomic studies employing LC-MS/MS methods such as multireaction monitoring (MRM) which has been recently reviewed [20]. Reversed-phase fractions are suitably stable samples for storage, at least in the short term, and may be readily dried or lyophilised using vacuum devices for longer-term storage or additionally to be made compatible with electrophoretic methods. Another approach to which this protocol, using all described dimensions, could potentially be applied is GeLCMS whereby regions of SDS-PAGE profiles are proteolysed and subsequently analysed using mass-spectrometry [21].

Here, using human cell extracts as an exemplar we demonstrate how a number of these fractionation approaches can be combined to afford the multidimensional separation of protein mixtures in an economical and high-throughput protocol, which is broadly applicable to a range of experimental scales.

2. Methods

2.1. Cell Harvesting and Protein Extraction. Samples of cultured human Neuro-2A cells were harvested in triplicate. Each set of triplicates represented cells in which wild-type or mutant malin or laforin proteins were transiently over-expressed [22] although for the purposes of this paper the malin/laforin phenotype is irrelevant. Similar to 5×10^7 cells, sufficient to yield approximately 10 mg of total protein were removed from culture dishes using trypsin and then pelleted by centrifugation. Following washing with phosphate-buffered saline (PBS) twice, pellets were rapidly frozen using liquid nitrogen and stored at −70°C.

Differential detergent fractionation (DDF) was performed with optimised modifications to published methods [7, 8]. Cells were initially washed with 1-cell-pellet-volume of PBS containing 1 : 100 protease inhibitor cocktail (Sigma; P8340) and 5 $\mu g \cdot mL^{-1}$ proteasome inhibitor MG132. Pellets were resuspended with 2.5 volumes freshly prepared 0.01% (w/v) digitonin in extraction buffer (5 mM EDTA, 1 : 200 phosphatase inhibitor [Roche; PhosStop] 1 : 100 protease inhibitor and 5 $\mu g \cdot mL^{-1}$ MG132 in 50 mM HEPES, 150 mM sodium chloride pH 7.4) and following a brief agitation incubated on ice for 10 minutes. Supernatants enriched in cytosolic proteins were recovered and the extraction repeated. Membrane/organelle protein-enriched fractions were obtained in a similar procedure but using 1% (w/v) IGEPAL in the same extraction buffer. Nuclear extracts were prepared using 1.5 volumes of 0.25% (w/v) deoxycholate, 0.1% (w/v) SDS, and 500 units$\cdot mL^{-1}$ benzonase, in extraction buffer. Finally, cytoskeletal protein-enriched fractions were obtained using 1.5 volumes of 0.25% (w/v) deoxycholate, 1.0% (w/v) SDS in extraction buffer. All protein quantitation was performed using a commercially available (Sigma) Bicinchoninic acid (BCA) kit, which was determined to demonstrate similar to 100–120% accuracies using the described DDF and anion-exchange buffers (data not shown).

2.2. Anion-Exchange Fractionation. Buffer exchange was firstly performed upon cytosolic protein extracts by (centrifugally) passing through GPC columns prepared using 1 g resin (GE Healthcare, G-25 Sepharose) per mL of sample, preequilibrated with (10 mL per gramme of resin) chromatography load buffer (8 M urea, 20 mM Tris, pH 10.0). A strong anion-exchange resin was selected (BioRad; UNOsphere-Q) which has a monoquaternary amine functional group with 120 μm bead diameter and protein binding capacities in excess of 100 mg$\cdot mL^{-1}$. Anion-exchange columns were prepared using 0.2 mL resin per mg cytosolic proteins, preconditioned with 10 resin volumes of load buffer; extracts were sequentially passed 3 times and retained components were washed thrice with 3 resin volumes of load buffer. Selective elution was achieved using a sequential application of 0.15, 0.25, 0.40, and 1.0 M potassium chloride (in load buffer) and all flow-through, wash and eluate fractions were retained. Disposable columns were prepared using fritted polypropylene extraction tubes (Supelco), although centrifugal filtration microtubes or filter-microplates would be suitable for smaller-scale or higher-throughput applications, respectively. Chromatographic flow was achieved using centrifugation (1000 ×g) for typically 1 minute or until columns were emptied.

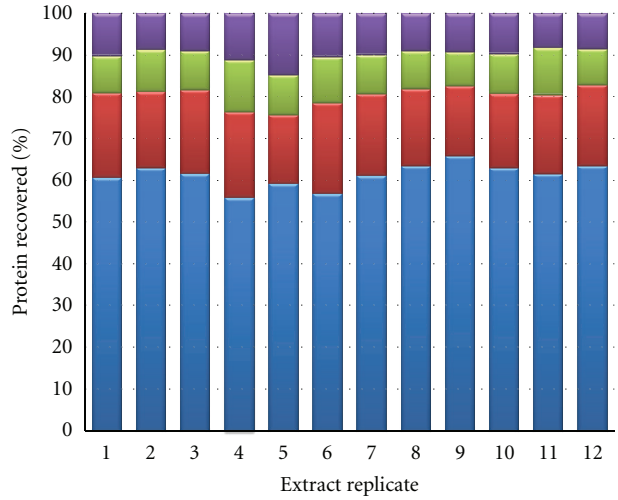

Figure 1: The distribution of extracted proteins in subcellular proteome fractions from twelve samples of cultured human Neuro-2A cells using the described DDF protocol (cellular phenotypes randomised and denoted replicates 1–12). Proteins were quantitated using a BCA method and quantities were normalised as a percentage of total extracted protein. Fractions denoted are cytosolic (blue), membrane/organelle (red), nuclear (green), and cytoskeletal (violet).

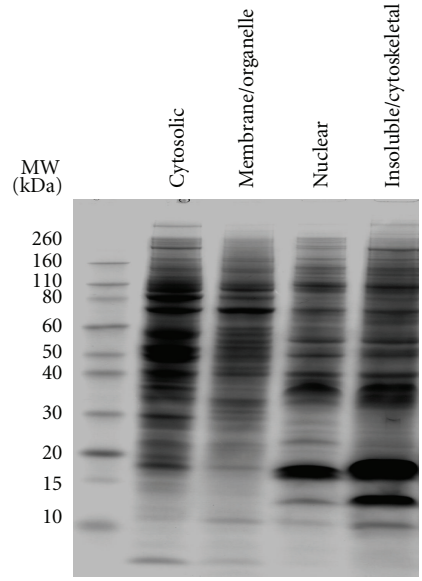

Figure 2: Exemplary analytical SDS-PAGE showing the profiles of proteins in subcellular proteome fractions extracted from a single sample of cultured human Neuro-2A cells, using the described DDF protocol. Similar to 20 μg of protein in each fraction was loaded and subsequently chemically stained using Coomassie Blue G-250. Partial differential fractionation is clearly evident.

2.3. Reversed-Phase Fractionation. Polymeric large-pore reversed-phase SPE cartridges (IST ISOLUTE, PDVB, 1000 Å, 25 mg) were selected and had previously been assessed to display broad binding selectivities with capacities of similar to 0.1 mg·mg^{-1} (data not shown). Solid phase was initially "wetted" with 1 mL (per 25 mg) 70% (v/v) acetonitrile, 0.1% (v/v) trifluoroacetic acid (TFA) in water and preconditioned with 1 mL 0.1% (v/v) TFA in water. Anion-exchange fractions were loaded, washed with 0.1% (v/v) TFA in water and sequentially eluted with 1 mL of 30, 35, 40, 43, 45, 48, 50, and 90% (v/v) acetonitrile, 0.1% (v/v) TFA in water. Chromatographic flow was achieved using vacuum pumping and the target mobile-phase flow-rate was 1 mL·min^{-1}.

2.4. Protein Electrophoresis. DDF extracts were loaded directly on to SDS-PAGE gels (Invitrogen, 4–12% Bis-Tris, MES) following dilution in sample buffer. MDLC fractions were first dried to residue using vacuum centrifugation then resolubilised in sample buffer. Protein components were visualised using Coomassie Blue G-250 [23] chemical staining. 2DE was performed using IPG-strip IEF gels (BioRad, 11 cm, 3–10) with dried samples resuspended in

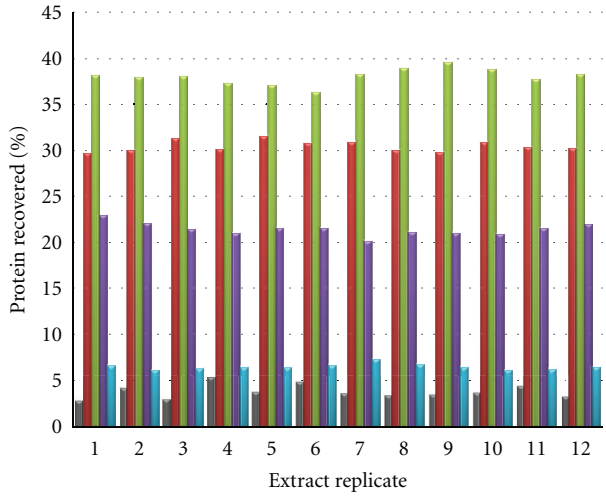

Figure 3: The distribution of cytosolic proteins, extracted from twelve samples of cultured human Neuro-2A cells, in anion-exchange chromatographic fractions. Proteins were quantitated using a BCA method and quantities were normalised as a percentage of total extracted protein. The flow-through (grey), 0.15 M (red), 0.25 M (green), 0.4 M (violet) and 1.0 M (blue) potassium chloride eluate chromatographic fractions display high between sample precision using the anion-exchange protocol described.

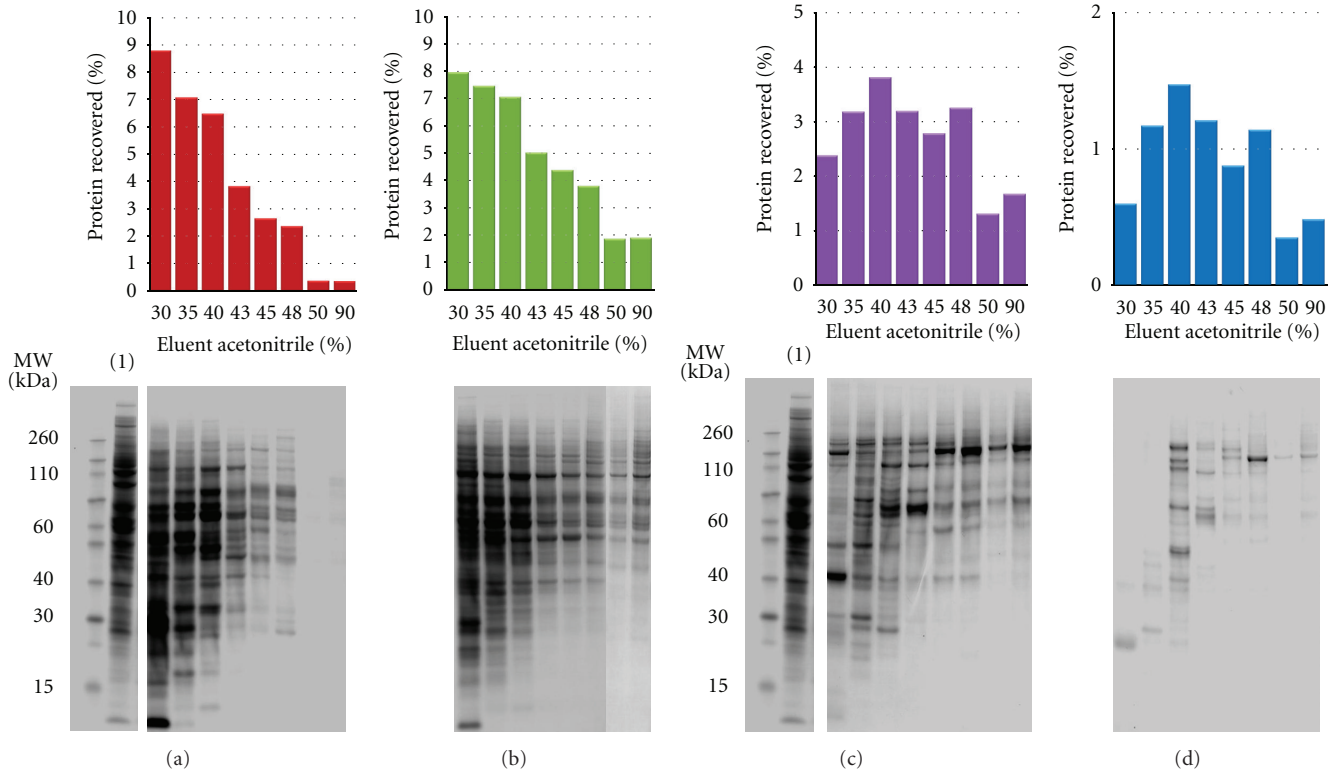

Figure 4: The distribution of cytosolic proteins in reversed-phase chromatographic fractions of 0.15 M (a), 0.25 M (b), 0.4 M (c), and 1.0 M (d) potassium chloride anion-exchange fractions, derived from a single DDF extract of cultured human Neuro-2A cells. Proteins were quantitated using a BCA method and quantities were normalised as a percentage of total extracted protein (top). Samples of all fractions were analysed using SDS-PAGE stained with Coomassie Blue G-250 (bottom) and total cytosolic extract is also shown (1) for comparison. It is evident that proteins from each of the anion-exchange fractions eluted over a broad range of hydrophobicity using the reversed-phase protocol and were therefore further fractionated.

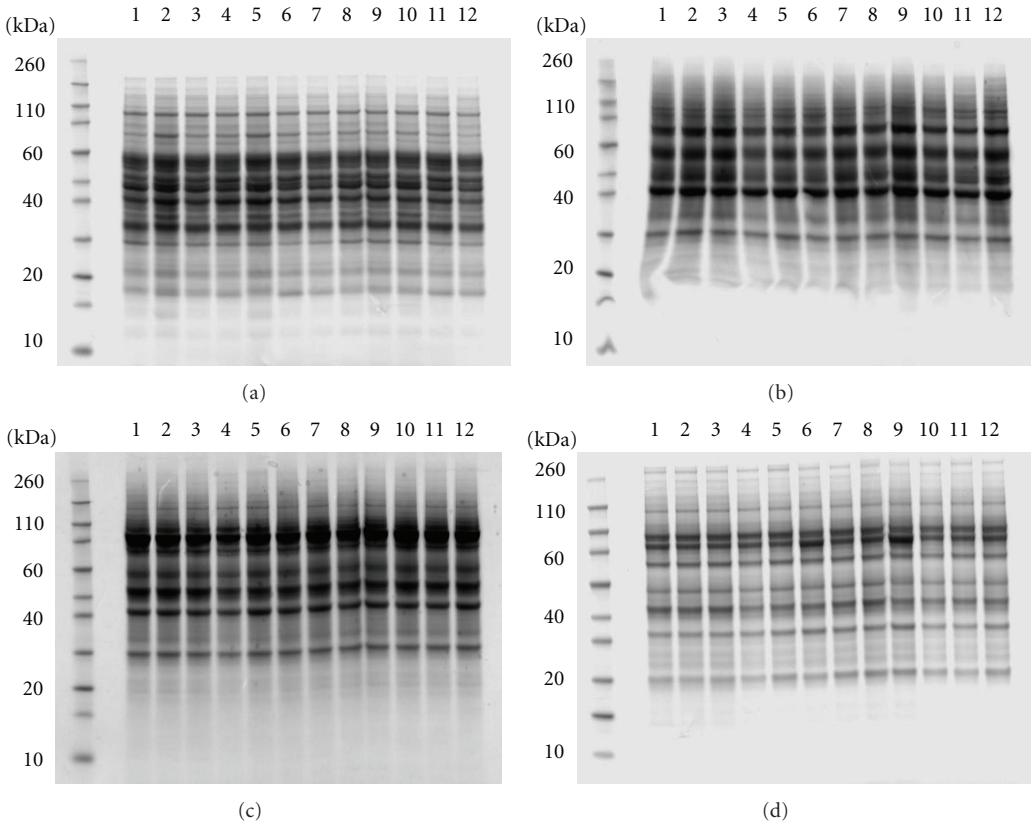

Figure 5: Representative comparative Coomassie Blue G250-stained analytical SDS-PAGE analyses of four MDLC fractions. These are in all cases the 45% (v/v) acetonitrile reversed-phase chromatographic fractions of 0.15 M (a), 0.25 M (b), 0.4 M (c), and 1.0 M (d) potassium chloride anion-exchange fractions, originally derived from cytosolic DDF extracts of twelve samples of cultured human Neuro-2A cells.

8 M urea, 2% (w/v) CHAPS, 50 mM DTT and subsequent IEF for in excess of 30,000 Vh. Second-dimensional SDS-PAGE was as described previously and proteins were silver-stained using a standard protocol [24].

2.5. MALDI-TOF Mass-Spectrometric Analysis. Mass spectrometric profiling of MDLC fractions, using linear-MALDI-TOF-MS, was performed by direct cospotting of reversed-phase SPE eluates with saturated solutions of sinapic acid (Fluka) or alpha-cyano-4-hydroxy-cinnamic acid (Sigma-Aldrich) in 50% (v/v) acetonitrile, 0.1% (v/v) TFA in water. A LaserToF TT (SAI Ltd.) operated in positive ion and linear modes was used to acquire spectra over the 1,000–300,000 m/z range and was calibrated against a range of protein standards.

2.6. Liquid-Chromatography-Tandem-Mass-Spectrometric Analysis. Trypsinolytic peptides recovered from selected MDLC fractions were analysed by microcapillary-LC-MS/MS using a hybrid Q-TOF instrument (Waters QToF2) equipped with a nanoelectrospray ion-source and controlled using MassLynx 4.0 software. Data-dependent product ion experiments were performed and protein identifications were ascertained using the MS/MS Ion Search program in the MASCOT search engine (http://www.matrixscience.com/). Selected signature peptides identified in MDLC fractions were analysed quantitatively by LC-MS/MS using a triple-quadrupole instrument (Waters Quattro Ultima) using analytical scale HPLC and controlled using MassLynx 4.0 software. MRM experiments were performed using previously identified precursor and product ions.

3. Results

3.1. Fractionation Achieved Using Differential Detergent Protocol. Reproducible protein extraction and fractionation was achieved for triplicates of the 4 experimental cell phenotypes using the described DDF protocol, evidenced from comparable percentage protein distribution in the resulting fractions (Figure 1). SDS-PAGE profiling of DDF extracts demonstrated clear differences in protein constituents of the fractions, providing evidence of successful subcellular fractionation (Figure 2).

3.2. Anion-Exchange Fractionation of Cytosolic Proteins. Each of the twelve cytosolic protein fractions was further fractionated by anion-exchange chromatography using the described protocol. Less than 5% of protein was unretained and the chromatographed cytosolic proteomes were distributed throughout the four eluted fractions. Again, precise and

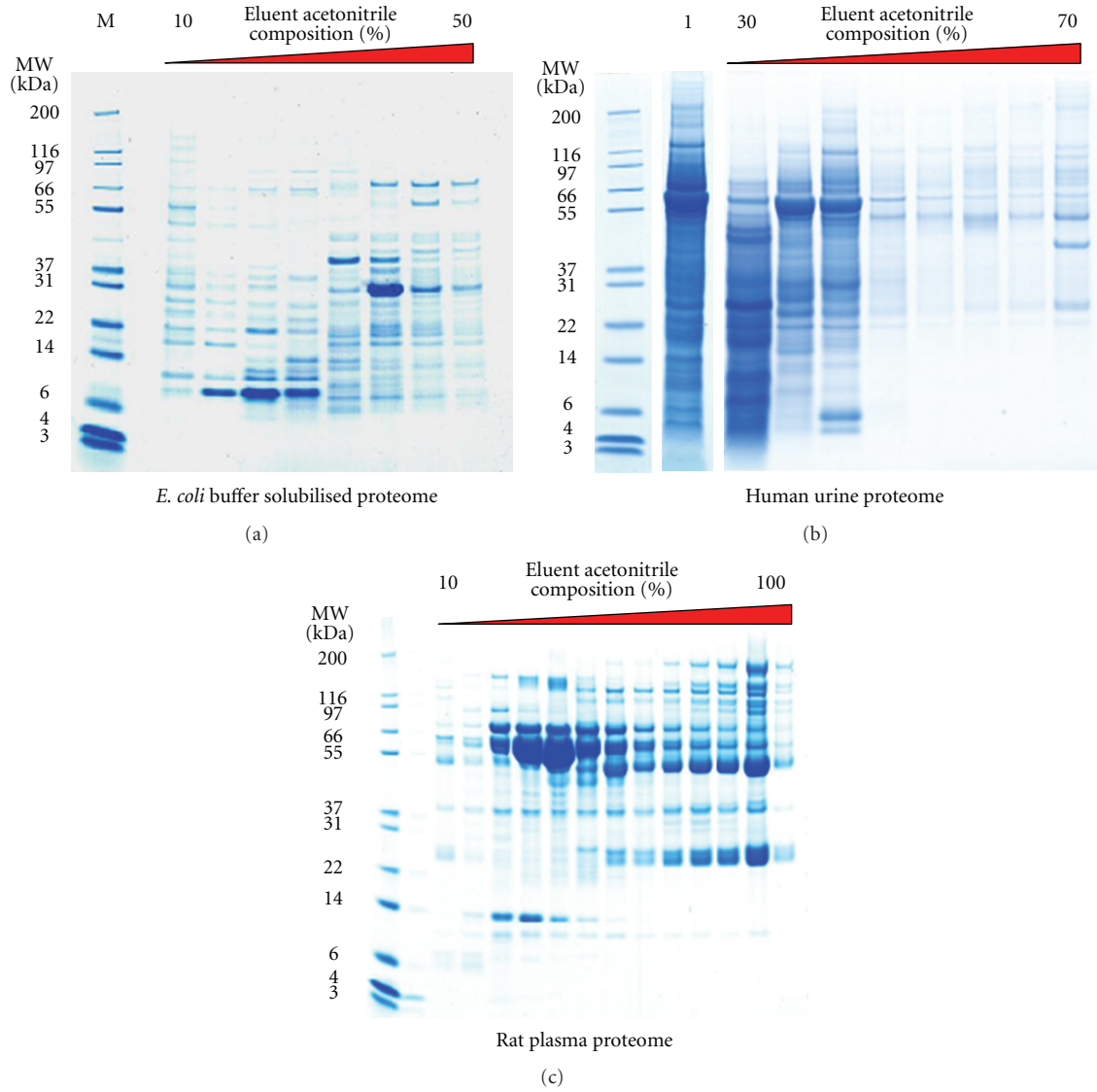

Figure 6: Versatile applicability of reversed-phase SPE alone which enables the concentration, desalting and partial fractionation of complex proteome samples. Coomassie Blue G250-stained analytical SDS-PAGE of reversed-phase SPE fractionated samples equivalent to (a) approximately 50 μg of *E. coli* whole cell lysate, (b) 1 mL of human urine, also unfractionated (1), and (c) 0.01 mL of rat plasma.

reproducible protein fractionation was achieved, evidenced from comparable percentage protein distribution in the resulting fractions (Figure 3). In this case, the employed eluent compositions had been optimised empirically but further improved fractionation, by more refined choice of eluent, would clearly be possible so yielding either increased fractionation or more equally distributed mass quantities of proteins as required.

3.3. Second-Dimensional Reversed-Phase Separation. Proteome distribution in reversed-phase fractions of exemplary anion-exchange fractions (derived from a single cytosolic protein fraction) is shown in Figures 4(a)–4(d). Again the chosen eluent compositions were optimised empirically; however, very similar performance was achieved when this protocol had been previously applied to a range of alternative proteome samples. Comparative analysis of experimental test cell types was enabled using the methods described here. Examples of analytical SDS-PAGE of various MDLC fractions are shown in Figures 5(a)–5(d). The high precision of the fractionation protocols is apparent (note the reproducibility of the gel band profiles) and the potential for comparative proteome analysis is clearly evident. Figures 6(a)–6(c) show fractionation of plasma, urine, and bacterial cell lysate and highlight that this protocol on its own offers a powerful and broadly applicable fractionation strategy.

3.4. Proteome Profiling Using MALDI-TOF-Mass-Spectrometric Analysis. As proof-of-concept, selected MDLC fractions derived from the cultured cells were profiled using mass-spectrometric approaches, as indicated from the linear

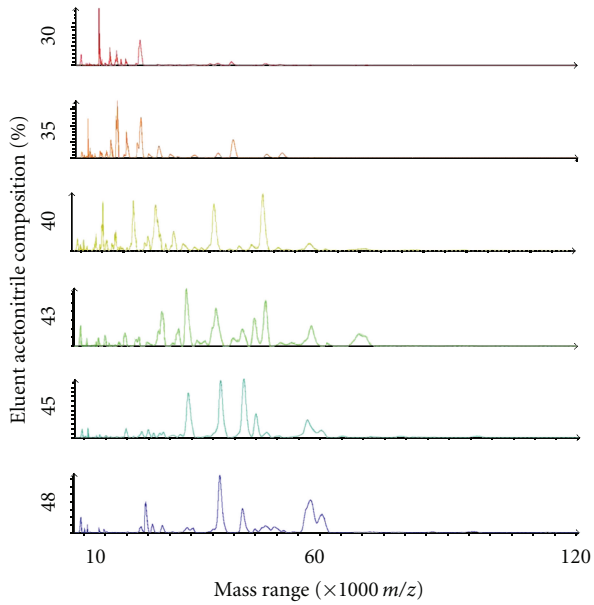

Figure 7: Exemplary linear-MALDI-TOF mass spectra of proteins in several different reversed-phase SPE fractions of a 0.25 M potassium chloride eluted anion-exchange fraction, derived from a DDF cytosolic extract of cultured human Neuro-2A cells. Proteins in fractions were directly cospotted with sinapic acid matrix and it is evident that such analysis is directly compatible with the MDLC fractionation protocol described herein.

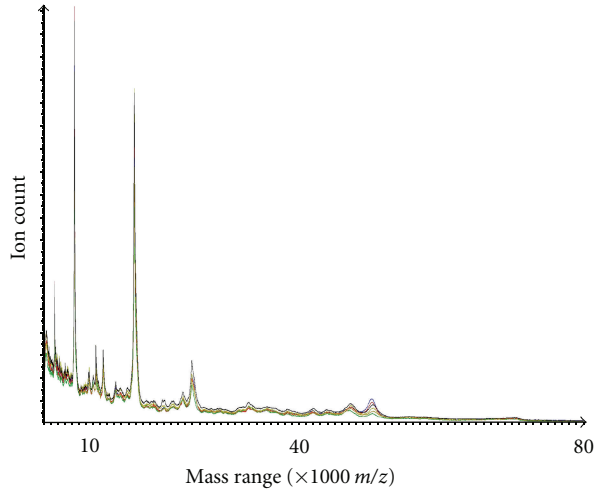

Figure 8: Exemplary comparative linear-MALDI-TOF mass spectra of proteins in 40% (v/v) acetonitrile eluted reversed-phase SPE fractions of 0.4 M potassium chloride eluted anion-exchange fraction, derived from DDF cytosolic extracts of six samples of cultured human Neuro-2A cells. Proteins in fractions were directly cospotted with alpha-cyano-4-hydroxy-cinnamic acid matrix. This data serves to show the high between sample extract precision with which some proteins were recovered and could be analysed.

mass spectra shown in Figure 7. Clearly, reversed-phase purified proteins are entirely amenable to analysis using MALDI-TOF-MS and whilst this has not thus far been routinely applied by us in our workflows, it does suggest that relatively low-cost, rapid, and high-throughput analyses could be achievable if desired. The high between sample extract precision with which some proteins were recovered and could be analysed is shown for six test samples derived from different cell samples (Figure 8). These results confirm the potential suitability of the described workflow for application to discovery profiling proteomic projects such as disease biomarker investigations. Similarly reversed-phase-SPE purified intact proteins have been readily analysed by us using Electrospray-TOF-MS demonstrating further applicability (data not shown).

3.5. Protein Quantitation Using Liquid-Chromatography-Tandem-Mass-Spectrometric Analysis. Overlaid peptide MRM

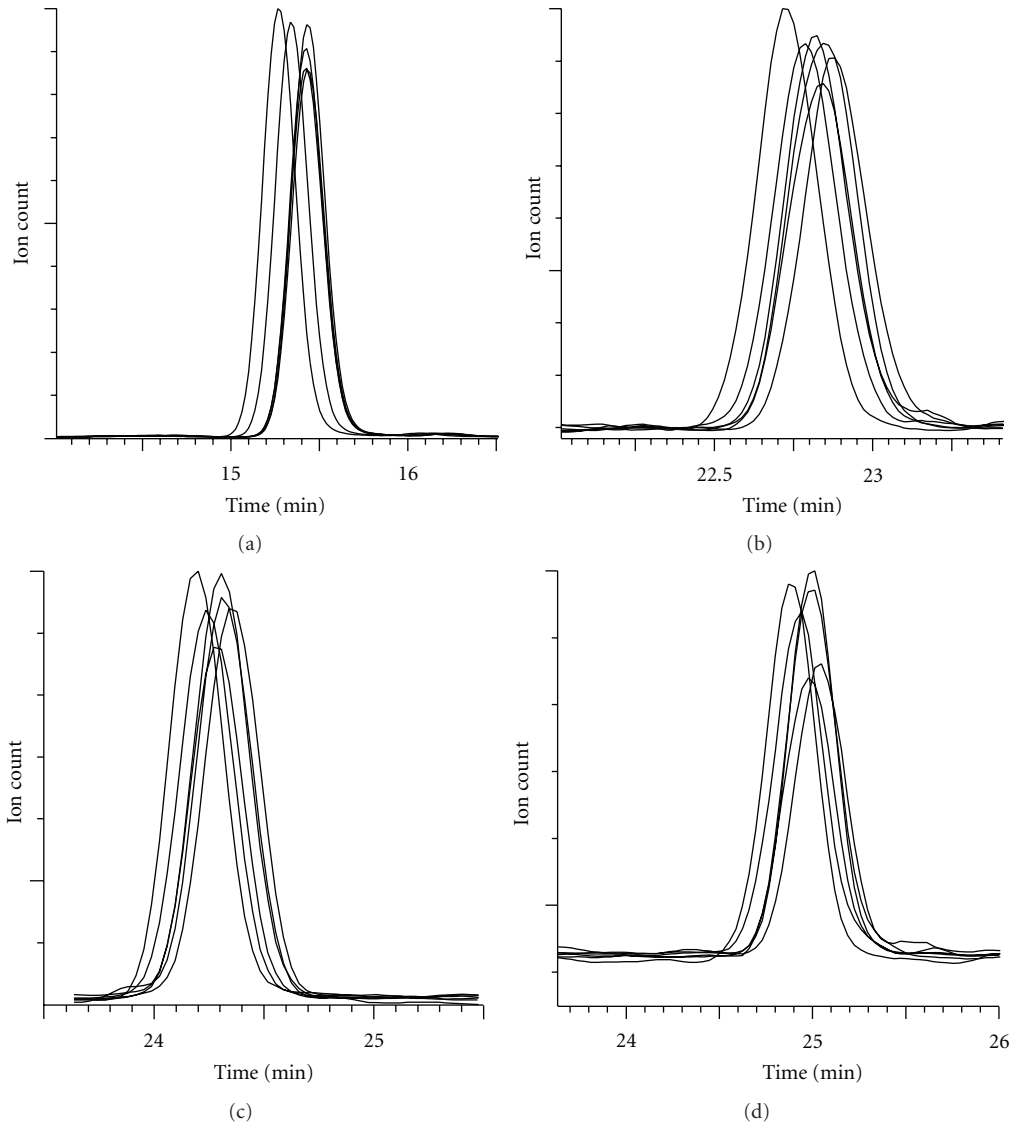

Figure 9: Exemplary LC-MS/MS (MRM) chromatogram peptide peaks from analyses of four candidate proteins in 35% (v/v) acetonitrile eluted reversed-phase SPE fractions of 0.15 M potassium chloride eluted anion-exchange fractions, derived from DDF cytosolic extracts of six samples of cultured human Neuro-2A cells. Target protein trypsinolytic signature peptides and the employed MRM transitions were (a) Ubiquitin $[TITLEVEPSDTIENVK+2H]^{2+}$; 894.8 > 1002.5, (b) 60 s ribosomal subunit L30 $[VCTLAIIDPGDSDIIR+2H]^{2+}$; 879.8 > 872.4, (c) serine-arginine-rich splicing factor 3 $[NPPGFAFVEFEDPR+2H]^{2+}$; 811.8 > 1410.7, and (d) PML protein $[NMSERSAMAAVLAMR+2H]^{2+}$; 827.3 > 933.5. This data serves to show the high between sample extract precision with which some proteins were recovered and confirms the potential suitability of the described workflow for application to quantitative proteomic projects.

chromatogram peaks, measured for four proteins identified in 35% (v/v) acetonitrile eluted reversed-phase SPE fractions of 0.15 M potassium chloride eluted anion-exchange fractions, show similar peak properties (Figure 9). Note that differences in peak areas, for different test samples, indicate peptide (protein) abundance differences and so the relative quantification of specific proteins in the purified fractions is possible. This data serves to show the high between sample extract precision with which some proteins were recovered and confirms the potential suitability of the described workflow for application to quantitative proteomic projects subsequent to either direct proteolysis of MDLC fractions or to regions of SDS-PAGE profiled fractions (GeLC-MS) with subsequent LC-MS/MS.

3.6. Profiling Chromatographic Fractions Using 2-Dimensional Gel Electrophoresis. Whilst the multidimensional fractionation procedures described herein were developed to circumvent the application of classical 2DE and to achieve parallel and robust arraying of extracts, it was of interest to assess the compatibility of these protocols with 2DE. Figures 10(a) and 10(b) show exemplary 2DE gel profiles of two MDLC fractions and serve to highlight that less

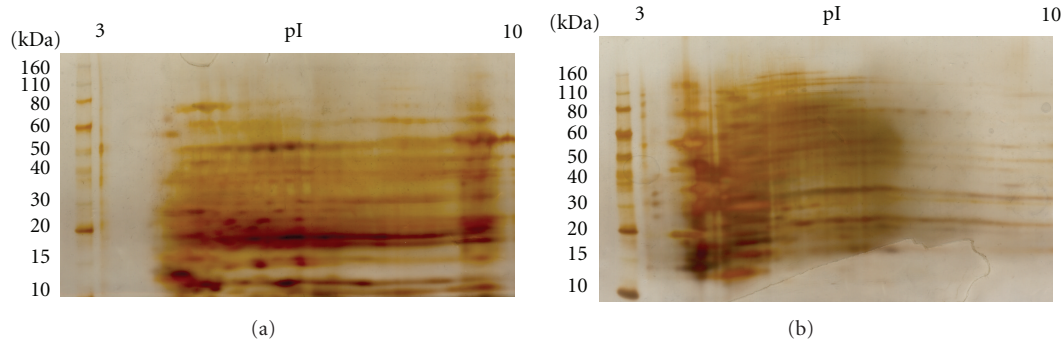

Figure 10: Representative examples of 2DE analysis (silver-stained) of two MDLC fractions. These are in both cases the 45% (v/v) acetonitrile reversed-phase SPE fractions of 0.25 M (a) and 0.4 M (b) potassium chloride eluted anion-exchange fractions, derived from a cytosolic DDF extract of cultured human Neuro-2A cells.

heterogeneous proteome fractions are obtainable using the described protocols and that fractions from this workflow are entirely compatible with 2DE. Differences in component pI in the two anion-exchange fractions are apparent, the average pI being lower in the 0.4 M anion-exchange fraction and this clearly demonstrates the resolving power of the protocol. Common anomalies associated with 2DE are apparent in the images of these gels further highlight the need for the development of new multidimensional protein separation approaches as described herein.

4. Discussion

In summary, we present an economical and high-throughput protocol for multidimensional fractionation of proteins, in this case extracted cytosolic proteins, which is compatible with various workflows and applicable to a range of experimental approaches. Initial fractionation using the DDF protocol yields four fractions, which (as demonstrated for the cytosolic fraction) can be further fractionated by anion-exchange chromatography. An additional dimension of separation is readily achieved by reversed-phase SPE separation of anion-exchange fractions, a method which we also demonstrate in its own right can be used to concentrate, desalt, and partially fractionate other complex proteome samples (shown for plasma, urine, and bacterial cell lysates). Where required, reversed-phase SPE fractions, in this case derived from anion-exchange fractions, can also be profiled by MALDI-TOF-MS or 2DE, offering an additional 1- or 2-dimensional separation, respectively and may also be used in quantitative proteomic projects where proteolytic peptides can be analysed using LC-MS techniques. Thus, precise 3-, 4-, or 5-dimensional protein separations can be easily achieved, largely without the requirement for specialist equipment, with the precision that should also allow comparative proteome analyses to be performed.

Acknowledgments

This work was funded by the BioPharm2020 India-UK Science Bridge and UK-India Science Bridge. The authors are grateful to Dr. Subramaniam Ganesh and Ms Sweta Singh Department of Biological Sciences and Bioengineering, Indian Institute of Technology, Kanpur, India for project design discussions and provision of cell samples.

References

[1] B. Cañas, C. Piñeiro, E. Calvo, D. López-Ferrer, and J. M. Gallardo, "Trends in sample preparation for classical and second generation proteomics," *Journal of Chromatography A*, vol. 1153, no. 1-2, pp. 235–258, 2007.

[2] C. Greenough, R. E. Jenkins, N. R. Kitteringham, M. Pirmohamed, B. K. Park, and S. R. Pennington, "A method for the rapid depletion of albumin and immunoglobulin from human plasma," *Proteomics*, vol. 4, no. 10, pp. 3107–3111, 2004.

[3] N. Zolotarjova, P. Mrozinski, H. Chen, and J. Martosella, "Combination of affinity depletion of abundant proteins and reversed-phase fractionation in proteomic analysis of human plasma/serum," *Journal of Chromatography A*, vol. 1189, no. 1-2, pp. 332–338, 2008.

[4] K. S. Dhugga and P. M. Ray, "Isoelectric focusing of plant plasma membrane proteins: further evidence that a 55 kilodalton polypeptide is associated with β-1,3-glucan synthase activity from pea," *Plant Physiology*, vol. 95, no. 4, pp. 1302–1305, 1991.

[5] R. L. J. Graham, M. K. Sharma, N. G. Ternan, D. B. Weatherly, R. L. Tarleton, and G. McMullan, "A semi-quantitative GeLC-MS analysis of temporal proteome expression in the emerging nosocomial pathogen *Ochrobactrum anthropi*," *Genome Biology*, vol. 8, no. 6, article R110, 2007.

[6] S. Zheng, K. A. Schneider, T. J. Barder, and D. M. Lubman, "Two-dimensional liquid chromatography protein expression mapping for differential proteomic analysis of normal and O157:H7 *Escherichia coli*," *BioTechniques*, vol. 35, no. 6, pp. 1202–1212, 2003.

[7] M. L. Ramsby, G. S. Makowski, and E. A. Khairallah, "Differential detergent fractionation of isolated hepatocytes: biochemical, immunochemical and two-dimensional gel electrophoresis characterization of cytoskeletal and noncytoskeletal compartments," *Electrophoresis*, vol. 15, no. 2, pp. 265–277, 1994.

[8] A. Abdolzade-Bavil, S. Hayes, L. Goretzki, M. Kröger, J. Anders, and R. Hendriks, "Convenient and versatile subcellular extraction procedure, that facilitates classical protein expression profiling and functional protein analysis," *Proteomics*, vol. 4, no. 5, pp. 1397–1405, 2004.

[9] S. R. Himmelhoch, "Chromatography of proteins on ion-exchange adsorbents," *Methods in Enzymology*, vol. 22, pp. 273–286, 1971.

[10] Y. Shi, R. Xiang, C. Horváth, and J. A. Wilkins, "The role of liquid chromatography in proteomics," *Journal of Chromatography A*, vol. 1053, no. 1-2, pp. 27–36, 2004.

[11] I. Neverova and J. E. Van Eyk, "Role of chromatographic techniques in proteomic analysis," *Journal of Chromatography B*, vol. 815, no. 1-2, pp. 51–63, 2005.

[12] X. Zhang, A. Fang, C. P. Riley, M. Wang, F. E. Regnier, and C. Buck, "Multi-dimensional liquid chromatography in proteomics-A review," *Analytica Chimica Acta*, vol. 664, no. 2, pp. 101–113, 2010.

[13] W. H. Jin, J. Dai, S. J. Li, Q. C. Xia, H. F. Zou, and R. Zeng, "Human plasma proteome analysis by multidimensional chromatography prefractionation and linear ion trap mass spectrometry identification," *Journal of Proteome Research*, vol. 4, no. 2, pp. 613–619, 2005.

[14] J. H. Deford, J. E. Nuss, J. Amaning, R. D. English, D. Tjernlund, and J. Papaconstantinou, "High-throughput liquid-liquid fractionation of multiple protein post-translational modifications," *Journal of Proteome Research*, vol. 8, no. 2, pp. 907–916, 2009.

[15] M. Vollmer, P. Hörth, and E. Nägele, "Optimization of two-dimensional off-line LC/MS separations to improve resolution of complex proteomic samples," *Analytical Chemistry*, vol. 76, no. 17, pp. 5180–5185, 2004.

[16] K. Fujii, T. Nakano, H. Hike et al., "Fully automated online multi-dimensional protein profiling system for complex mixtures," *Journal of Chromatography A*, vol. 1057, no. 1-2, pp. 107–113, 2004.

[17] D. A. Wolters, M. P. Washburn, and J. R. Yates, "An automated multidimensional protein identification technology for shotgun proteomics," *Analytical Chemistry*, vol. 73, no. 23, pp. 5683–5690, 2001.

[18] J. Porath and P. Flodin, "Gel Filtration: a method for desalting and group separation," *Nature*, vol. 183, no. 4676, pp. 1657–1659, 1959.

[19] K. Yanagisawa, S. Tomida, K. Matsuo et al., "Seven-signal proteomic signature for detection of operable pancreatic ductal adenocarcinoma and their discrimination from autoimmune pancreatitis," *International Journal of Proteomics*, vol. 2012, Article ID 510397, 11 pages, 2012.

[20] P. Picotti and R. Aebersold, "Selected reaction monitoring-based proteomics: workflows, potential, pitfalls and future directions," *Nature Methods*, vol. 9, no. 6, pp. 555–566, 2012.

[21] A. Vasilj, M. Gentzel, E. Ueberham, R. Gebhardt, and A. Shevchenko, "Tissue proteomics by one-dimensional gel electrophoresis combined with label-free protein quantification," *Journal of Proteome Research*, vol. 11, no. 7, pp. 3680–3689, 2012.

[22] S. Singh, P. Satishchandra, S. K. Shankar, and S. Ganesh, "Lafora disease in the Indian population: EPM2A and NHLRC1 gene mutations and their impact on subcellular localization of laforin and malin," *Human Mutation*, vol. 29, no. 6, pp. E1–E12, 2008.

[23] G. Candiano, M. Bruschi, L. Musante et al., "Blue silver: a very sensitive colloidal Coomassie G-250 staining for proteome analysis," *Electrophoresis*, vol. 25, no. 9, pp. 1327–1333, 2004.

[24] J. X. Yan, R. Wait, T. Berkelman et al., "A modified silver staining protocol for visualization of proteins compatible with matrix-assisted laser desorption/ionization and electrospray ionization-mass spectrometry," *Electrophoresis*, vol. 21, no. 17, pp. 3666–3672, 2000.

Hindawi Publishing Corporation
International Journal of Proteomics
Volume 2012, Article ID 473843, 7 pages
doi:10.1155/2012/473843

Research Article

Rapid Screening of the Epidermal Growth Factor Receptor Phosphosignaling Pathway via Microplate-Based Dot Blot Assays

Amedeo Cappione III, Janet Smith, Masaharu Mabuchi, and Timothy Nadler

EMD Millipore, Merck KGaA, 17 Cherry Hill Drive, Danvers, MA 01923, USA

Correspondence should be addressed to Amedeo Cappione III, amedeo.cappione@merckgroup.com

Received 4 June 2012; Accepted 15 July 2012

Academic Editor: Gary B. Smejkal

Expression profiling on a large scale, as is the case in drug discovery, is often accomplished through use of sophisticated solid-phase protein microarrays or multiplex bead technologies. While offering both high-throughput and high-content analysis, these platforms are often too cost prohibitive or technically challenging for many research settings. Capitalizing on the favorable attributes of the standard ELISA and slot blotting techniques, we developed a modified dot blot assay that provides a simple cost-effective alternative for semiquantitative expression analysis of multiple proteins across multiple samples. Similar in protocol to an ELISA, but based in a membrane bound 96-well microplate, the assay takes advantage of vacuum filtration to expedite the tedious process of washing in between binding steps. We report on the optimization of the assay and demonstrate its use in profiling temporal changes in phosphorylation events in the well-characterized EGF-induced signaling cascade of A431 cells.

1. Introduction

Signaling through receptor tyrosine kinases (RTKs) is a highly conserved cellular mechanism, controlling fate determination, proliferation, survival, and migration [1, 2]. In most instances, ligand binding initiates conformational changes in the externally facing receptor molecule leading to autophosphorylation on the internal portion of the receptor. A subsequent chain of phosphorylation events propagates the signal to the nucleus culminating in the transcription of genes required to direct changes in cell function (the EGFR cascade is outlined in Figure 1). Given the dynamic interplay of cells with their surrounding microenvironment and owing to the presence of a myriad of other simultaneously activated paths, this process must be tightly regulated to ensure proper responses occur. The broad importance of RTK signaling is highlighted by the well-documented role of pathway dysregulation in human disease, most notably cancer. RTK mutations have been implicated in a variety of cancers, specifically, members of the epidermal growth factor receptor (EGFR) family in brain, lung, and breast cancer. In fact, thirty percent of all solid tumors possess Ras or Raf mutations, including almost 90% of pancreatic adenocarcinomas [3, 4].

Due to the inherent complexity of the global signaling network and the involvement of their constituents in malignancy, these pathways have been extensively studied by researchers looking for insight into the mechanisms underlying both normal and aberrant growth. Detecting alterations in phosphorylation patterns within signaling profiles is a technique commonly employed to map the dose dependence and specificity of small-molecule inhibitors targeting upstream components. Traditionally, compound screening was performed in cell-free assays using purified enzymes as the target. More recently, a greater significance has been placed on the use of cell-based approaches where multiple components in a single pathway and multiple signaling cascades can be monitored simultaneously. Such analyses require complex and expensive detection platforms such as flow cytometers or high-content imaging systems. While well suited for the high throughput needs of large-scale screens at the industrial level, such platforms may not fit the workflow

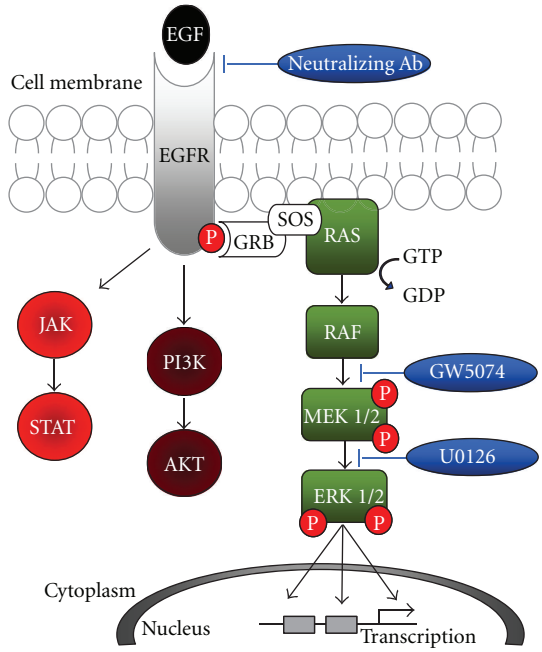

Figure 1: The EGFR signaling cascade. The binding of EGF to the EGF receptor (EGFR) results in receptor dimerization and conformational changes triggering autophosphorylation. Under proper conditions, phosphorylated EGFR activates any number of three downstream signaling pathways through Ras, PI3K, and JAK, respectively. The work performed in this study focuses on the Ras cascade (highlighted in green). The three inhibitors (blue) are shown acting at their specific sites of signal interruption.

or demand of smaller research groups. Alternative detection systems offering semiquantitative measurement of multiple proteins in parallel include the enzyme-linked immunosorbent assay (ELISA), multiplex bead arrays, western blots, and slot blots. Although plate based, a fact that simplifies setup and signal detection, ELISAs require a pair of protein-specific antibodies which identify unique epitopes and are also quite time consuming due to multiple binding steps and extensive washing. Slot blotting apparatuses have been developed that offer increased throughput over standard western blots yet retain the same overall labor-intensive protocol that is not amenable to automation. In addition, signal quantitation for both blotting techniques is limited by the dynamic range of the developing film and method of densitometric analysis.

In this paper, we present a modified dot blotting technique for protein detection where purified proteins or cell lysates are applied directly to membrane-based 96-well microplates. This dot blot assay combines the plate-based ease of handling offered by ELISAs with vacuum filtration to greatly expedite the process of semiquantitative analysis of protein expression. Following the addition of protein sample, a two-step antibody binding process using an HRP-conjugated secondary detection antibody is performed. In the final step, the conversion of chemiluminescent substrate provides the signal in each well that can be quantified using a standard plate reader. For a 96-well plate, the entire process, from sample addition to data acquisition, requires less than 90 minutes. Our assay was validated using lysates derived from the extensively studied EGFR signaling cascade of the A431 epidermal carcinoma cell line. Temporal changes in phosphoactivation of three proteins (EGFR, MEK1/2, and ERK1/2) were measured at five-minute intervals across a twenty-minute time course of EGF stimulation. Pathway mapping was further interrogated using a set of three site-specific inhibitors of the EGFR cascade.

2. Materials and Methods

2.1. Cell Culture. A431 (CRL-1555, ATCC, Manassas, VA), a human skin carcinoma cell line, was maintained in complete media (DMEM + 10% FBS) and passaged routinely by trypsinization (TrypLESelect, GIBCO/Life Technologies, Grand Island, NY) to ensure log phase growth. For induction experiments, 100 K live cells were seeded per well in 6-well plates, cultured for 2 days, and then serum-starved for 20 HR. Following synchronization, cells were exposed to 100 ng/mL human EGF (Cell Signaling Technology, Danvers, MA) for 5–20 minutes. For inhibitor studies, cultures were pre-incubated with 10 μm U0126 (Cell Signaling Technology), 5 μm GW5074 (Sigma-Aldrich, St. Louis, MO), or 10 μg/mL anti-EGFR neutralizing Ab (EMD Millipore), for 2 hrs prior to EGF exposure. Following induction, total cell lysates were prepared as described below (for the EGFR pathway schematic, see Figure 1).

2.2. Cell Counting and Viability. 10 μL sample was mixed with 190 μL guava ViaCount reagent and incubated for 5 minutes at RT. Sample data was acquired on a guava easyCyte HT instrument and analyzed using guava ViaCount software (all EMD Millipore).

2.3. Cell Lysis. Lysis was performed using two buffers: (1) Cytobuster Protein Extraction Reagent (EMD Millipore) and a modified RIPA buffer (25 mM Tris-HCl pH 7.6, 150 mM NaCl, 1% NP-40, 1% sodium deoxycholate, and 0.1% SDS). All buffers were supplemented with protease inhibitors and phosphatase inhibitors (EMD Millipore). All buffers were chilled on ice prior to use. Following induction, cells were washed twice with ice-cold PBS. 400 μL of lysis buffer was added to each well. Samples were incubated on ice for 5 minutes with occasional swirling. To pellet cellular debris, resulting extracts were centrifuged at 16000 g $\times$ 15 min at 4°C. Cell lysates were removed, aliquoted, and stored at −20°C until assayed.

2.4. IR-Based Protein Quantitation. Proteins were quantified using the Direct Detect assay-free sample card and Direct Detect Spectrometer (EMD Millipore). Each card contained four hydrophilic polytetrafluoroethylene (PTFE) membrane positions, each surrounded by a hydrophobic ring to retain analyzed sample within the device's IR beam. All measurements were performed using 2 μL of sample per membrane position. A "buffer only" sample was also analyzed as a reference blank. Sample concentration was determined in reference to a calibration method. For all experiments, the system was initially calibrated using National-Institute-of-Standards-&-Technology- (NIST-) certified BSA SRM927d in phosphate-buffered saline (PBS). A series of ten concentration points (0.125–5 mg/mL) was used to generate the instrument calibration curve.

2.5. Antibody Validation. One of the limiting factors in biochemistry is the availability and quality of antibodies. Prior to use in the dot blot assay, each candidate antibody was subjected to a stringent validation procedure [5]. As part of the initial screening process, we reviewed the certificate of analysis for each of the four antibodies: anti-phospho-EGFR (TYR1069, clone 9H2), anti-phospho-Mek1/2 (SER218/SER222, clone E237), anti-phospho-Erk 1/2 (THR202/TYR204, clone 12D4), and anti-GAPDH (clone 6C5) employed in this study (all Abs are from EMD Millipore). All four were validated for use in western blotting analysis as part of the standard quality control testing by EMD Millipore. Staining with each of the four antibodies resulted in detection of a single prominent band at the approximate molecular weight and the lack of any nonspecific binding. In addition, all four were validated using lysates derived from A431 cells, the only cell line employed in this study. Antibodies against phosphorylated epitopes had to demonstrate specificity to stimulated (ex. EGF) or inhibited (anti-EGF neutralizing Ab) to yield phosphorylated (signal) or nonphosphorylated forms (no signal) of the protein, respectively.

2.6. Dot Blot Protocol (see Figure 2). Prewet PVDF membrane Multiscreen plates (EMD Millipore) with 100 uL 70% Ethanol for 15 seconds then immediately wash 2X with 100 μL Milli-Q H_20 by vacuum filtration using the Multiscreen$_{HTS}$ Vacuum Manifold (EMD Millipore) with pressure set to 4″Hg. In all wash steps use vacuum filtration. Add diluted lysate (50 μL/well) and incubate for 30 minutes at RT on a plate shaker at low speed. Wash plates 2X with Tris-Buffered Saline (TBS). Block sample wells in 0.5% nonfat dried milk (in TBS) for 5 minutes on the shaker then remove blocking agent by vacuum filtration. Add 50 μL/well diluted primary antibody and incubate on a shaker for 10 minutes. Each antibody was previously titrated to optimize performance. The antibodies included anti-phospho-EGFR (TYR1069, clone 9H2), anti-phospho-Mek1/2 (SER218/SER222, clone E237), anti-phospho-Erk1/2 (THR202/TYR204, clone 12D4), and anti-GAPDH (clone 6C5). Wash plates 3X with TBS + 0.1% Tween-20 (TBST). Add 50 μL/well diluted goat anti-rabbit IgG HRP (EMD Millipore) and incubate on a shaker for 10 minutes. Wash plates 3X as above. Add 100 μL/well of Luminata Forte Western HRP Reagent (EMD Millipore) and incubate for 5 minutes on a shaker. Read signal using BioTek Synergy microplate reader (BioTek, Winooski, VT). For each well, chemiluminescent signal was measured and presented as counts per second (CPS).

3. Results

Initial feasibility studies and optimization of the dot blot assay were performed using purified Glyceraldehyde-3-Phosphate Dehydrogenase (GAPDH) protein in PBS buffer. Representative results from a serial dilution of GAPDH are presented in Figure 3. From the graph, the assay was able to detect down to ~4 ng and was linear in response up to 100 ng protein loaded. The assay shows a robust signal:noise ratio and does not appear to be limited by binding capacity of the membrane; the theoretical binding capacity of a single well (0.3 cm^2) of membrane is approximately 90 μg [6]. The assay was optimized as follows for each step: 30 min protein binding, 10 min primary Ab binding, and 10 min secondary Ab binding. All binding steps were performed with low-speed agitation at room temperature. Overall assay time is 90 minutes. It is possible that protein range could be increased with greater Ab input or increased binding reaction times although this may lead to elevations in nonspecific binding. Due to differences in binding kinetics, optimization of reaction conditions may be required for each protein analyzed.

For the dot blot assay to have broader application, it must perform in the context of total cell lysates where relative protein concentration, buffering conditions, and lysate clarity may impact not only membrane binding but also antibody detection characteristics. To assess such issues, we first extracted lysates from A431 cells using two distinct lysis buffers, a modified RIPA buffer and a nondetergent-based commercial extraction reagent. Following extraction, protein samples were quantified using the Direct Detect IR-based quantitation system. On average, the RIPA buffer liberated five times greater total protein than the nondetergent buffer (data not shown); this may be due to the presence of harsher detergent in the RIPA buffer resulting in greater protein solubilization.

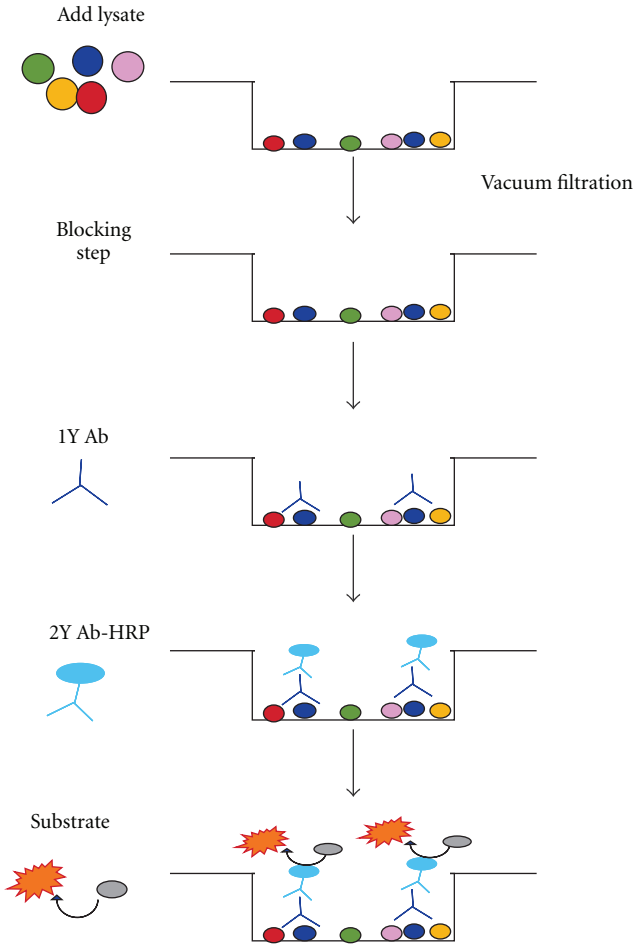

Figure 2: The dot blot protocol. Depicted in the diagram is the assay for one representative well from a 96-well microplate. After protein binding, a blocking step is performed to reduce nonspecific Ab binding to any unoccupied region of membrane. The remaining portion of the assay is similar to ELISA except that all wash steps are performed via vacuum filtration.

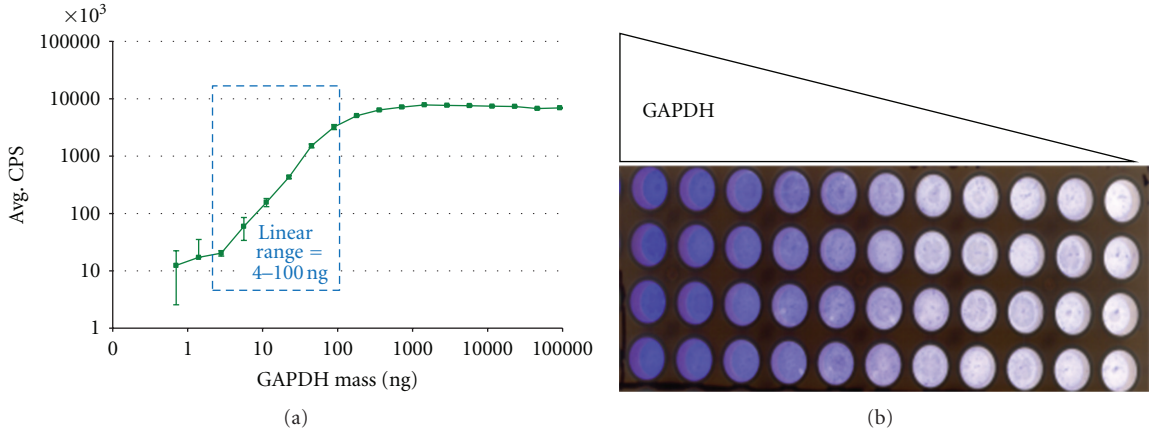

Figure 3: Dot blot assay feasibility—titration of pure GAPDH. (a) The titration curve demonstrates a range 4–100 ng input protein whereby linear signal could be detected. Each point represents the mean of 4 replicates. (b) Coomassie staining of membrane wells after protein loading. Four replicates are shown for each concentration point.

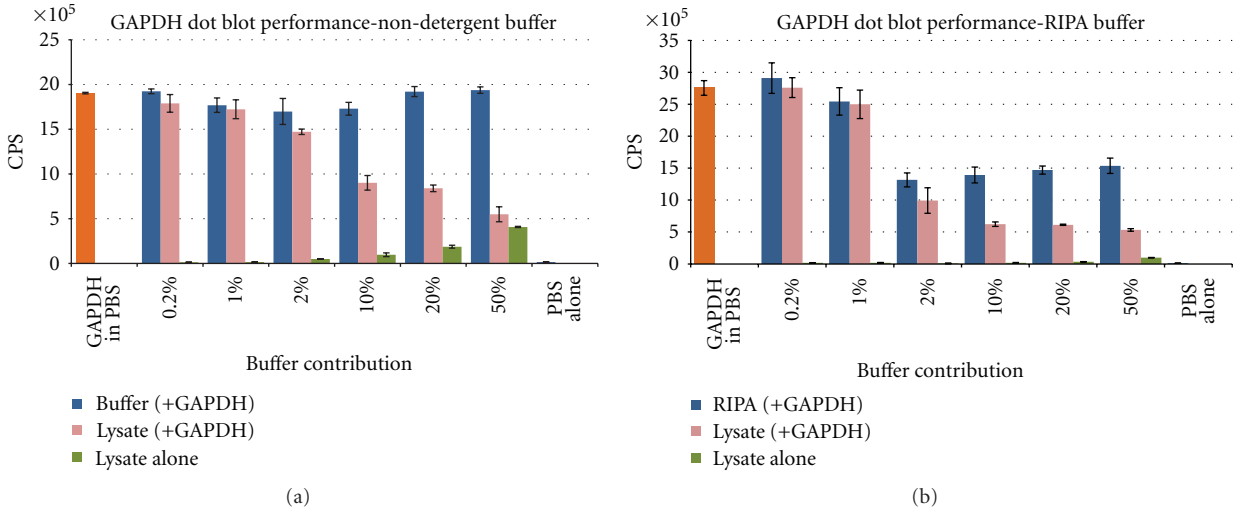

Figure 4: Impact of lysis buffer components on dot blot performance—Detergents. Lysates (pink bars) or buffers alone (blue) were diluted in PBS, spiked with 100 ng GAPDH and assayed for changes in GAPDH detection. The green bars show detection of the native GAPDH present in A431 lysates (no GAPDH was spiked into these samples). The CPS signal for GAPDH in PBS is displayed by the orange Bar. Each bar represents the average of 3 individual replicates. Protein concentrations for the lysates used were determined to be (a) nondetergent buffer, 494 ng/μL, and (b) RIPA buffer, 2443 ng/μL. The RIPA buffer was diluted to 494 ng/μL prior to setup. Total protein lysate loaded was as follows: 0.2% = 49 ng; 1% = 295 ng; 2% = 494 ng; 10% = 2950; 20% = 4940 ng; 50% = 12350 ng.

Total lysates from each extraction condition were used to assess the potential effects of protein concentration and buffer components on dot blot assay performance. The results of this experiment are outlined in Figure 4. Briefly, lysates, or buffers alone, were diluted to varying degrees with PBS. Samples were spiked with 100 ng purified GAPDH and loaded onto microplates. A standard dot blot assay was then performed. For the RIPA buffer, any contribution greater than 1% (0.5 μL in 50 μL reaction volume) caused a significant decrease in GAPDH signal; this is most likely due to detergents interfering with membrane binding and limiting protein-protein interactions. By contrast, the nondetergent-based buffer alone had little or no effect on GAPDH signal even at 50% sample dilution; this result may be important for situations where either total protein concentrations are low or the protein of interest is expressed at relatively low levels. We also found a reduction in GAPDH signal in both buffer types when lysate load/well was increased. Signal reduction was slightly greater in the homebrew samples due to the contributing detergent effect. Signal loss is most likely due to protein crowding and/or competition for membrane binding. More importantly, native GAPDH was easily detected in nondetergent-derived samples with signal >100X over background for 12.5 μg lysate loaded.

We sought to determine the assay's linear range and define the optimal concentration of primary antibody required for protein detection. Given the wide variability in relative protein expression within a cell and between different cells, such optimization may be required for each protein (and each cell type's lysate) to be measured. The graphs in Figure 5 depict the results for titration curves performed on EGF-stimulated A431 lysates using antibodies specific for the house-keeping GAPDH protein and phosphorylated ERK1/2. The dot blot assay demonstrated a linear range of detection for 400–6000 ng/well. Irrespective of primary Ab concentration, little to no signal could be detected below 400 ng lysate. The assay also failed to detect any greater signal levels in wells with ≥6000 ng lysate. In fact, at higher sample loads, counts per second (CPS) values tended to decrease; this was most likely due to the higher complexity of the lysate solution as well as increased competition for membrane binding. In both cases, a 1 : 500 dilution of primary antibody (2 μg/mL GAPDH Ab, 1 μg/mL pERK1/2 Ab) provided optimal detection.

We next applied the dot blot assay in a proof-of-concept study to track changes in protein phosphorylation for the EGFR signaling cascade of A431 cells cultured with EGF. Ligand binding activates a chain of signaling events, which includes successive phosphorylation of the EGFR, MEK, and ERK proteins. Given the temporal nature of phosphoactivation within the cascade, synchronized A431 cells were exposed to EGF and harvested at 5 minute intervals for a total of 20 minutes. The time course was performed with EGF stimulus alone and in the presence of three pathway inhibitors. In the absence of inhibition, a clear temporal order of phosphorylation events is seen (Figure 6). EGF stimulation resulted in an almost immediate increase in the presence of phosphorylated EGFR, which was maintained at high levels for the entire 20 minutes. Among the four proteins measured, the phospho-EGFR signal was by far the highest level detected; this finding is not unexpected given that the A431 cell line expresses abnormally high levels of EGFR [7]. Phosphorylated Mek1/2 was first detected at 10 minutes followed by ERK1/2 at 15 minutes. For the latter two proteins, the phosphorylated state was far more transient appearing to decrease soon after initial appearance.

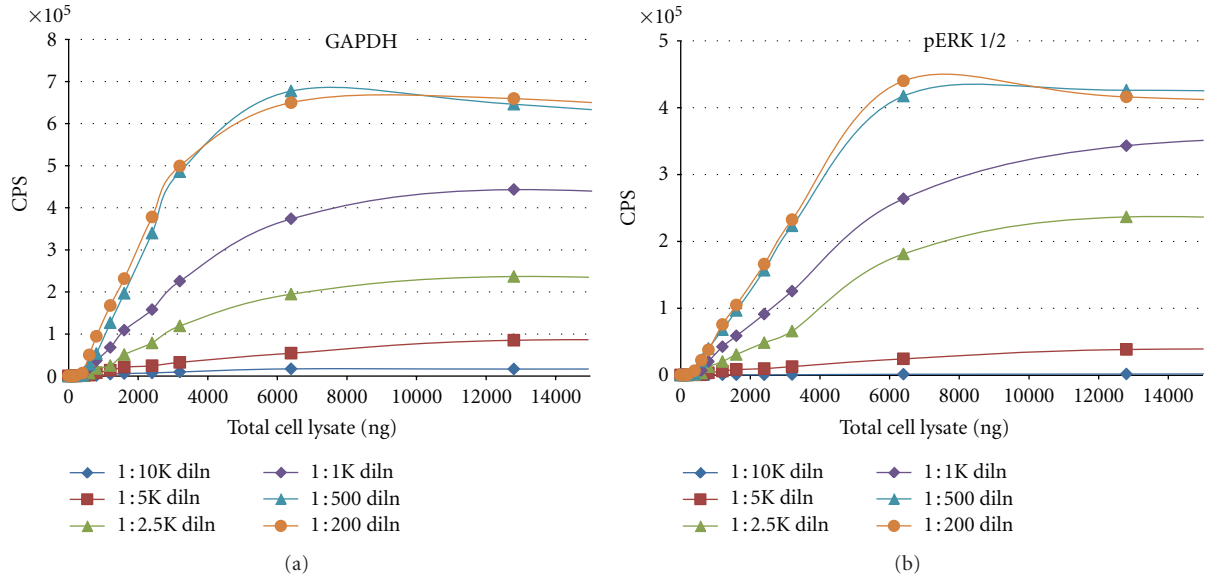

Figure 5: Native protein detection—primary antibody optimization. Serum-starved A431cells were stimulated with EGF for 20 min and harvested and lysates prepared as described previously. Dot blot assays were performed to optimize detection by (a) GAPDH and (b) phospho-ERK1/2 antibodies. A series of seven lysate concentrations (100–10000 ng/well) was used to assess six different dilutions of each primary antibody. All points were run in triplicate.

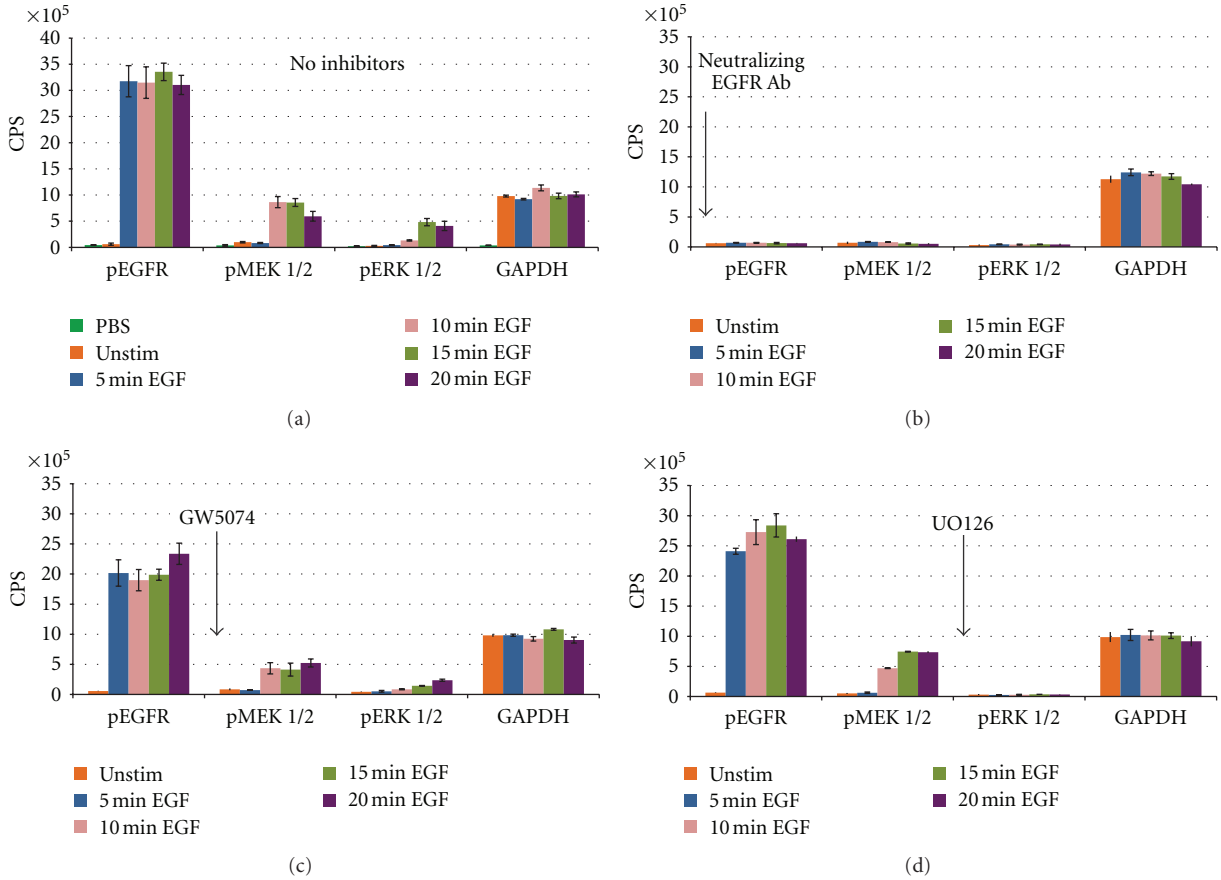

Figure 6: Temporal mapping of the EGFR cascade using site-specific inhibitor molecules. The four bar graphs represent results for the following: (a) EGF stimulation, no inhibitor, and EGF stimulation in the presence of (b) neutralizing EGFR Ab, (c) GW5074—an inhibitor of Raf kinase activity, and (d) U0126—a highly selective inhibitor of MEK1/2. For each inhibitor, the arrow indicates the point of pathway inhibition. Each graph contains the time course (0–20 minutes) of expression profiles for each of the four proteins analyzed. Each bar value represents the average of three replicates.

GAPDH detection was included in each data set as a loading control to permit cross-sample comparisons. Overall, for 60 GAPDH wells analyzed across 20 experimental conditions (3 replicates for each), the mean CPS value was 1,026,671 ± 87,405 with a coefficient of variation of 8.5%. Pre-incubation with the EGFR blocking antibody completely abolished all downstream phosphorylation events. U0126 treatment prevented phosphorylation of ERK1/2 without affecting either upstream event. At the concentration applied, GW5074 caused only partial inhibition of MEK1/2 and ERK1/2. Interestingly, GW5074 also caused a reduction in EGFR phosphorylation suggesting a potential positive feedback loop involving intermediary signaling proteins. A more extensive study involving challenges with various concentrations of GW5074 may offer greater insight into this phenomenon.

4. Discussion

Standard dot blotting is a method of protein detection similar to the western blot technique but differing in that protein samples are not initially separated electrophoretically on polyacrylamide gels but simply applied directly onto the membrane's surface. Once applied, proteins are driven to bind the membrane through either active pressure (vacuum) or gentle agitation and passive absorption. Dot and slot blotting techniques have been used extensively by molecular biology researchers to affix proteins and nucleic acids on membranes for the purpose of quantitation, DNA homology assessment, protein-DNA/RNA interactions, enzymatic activity, and the study of ligand-receptor binding. The standard device is comprised of three main parts: the upper block with an array of slots for sample loading, a middle component that holds the inserted membrane, and a bottom block with a connector permitting vacuum filtration. A set of screws clamps the assembled device in place thereby minimizing sample bleed-over. Given this format, slot blots offer greater throughput capacity than the standard western blot and are therefore ideal for screening applications. However, the device's main value is in sample loading; all subsequent steps are performed in the same labor-intensive manner as a western blot. To expedite the process without sacrificing throughput, our modified dot blot takes advantage of 96-well microplates equipped with PVDF membrane. The plate-based format minimizes sample bleed-over and permits easy reagent loading at each step. Since the plate is membrane based, all wash steps can be performed via vacuum filtration. The plate format and simple reaction steps are also well suited for automation and expanded screening needs. A final benefit is being able to use a standard plate reader for chemiluminescent signal detection; this format offers greater dynamic range than film densitometry enhancing quantitative capacity of the assay.

The work presented here clearly demonstrates the feasibility of the plate-based dot blot application for semiquantitative detection or comparative analyses of multiple proteins and/or multiple samples in parallel. The assay performed well on pure protein samples but more importantly worked for total cell lysates although the linear ranges of detection were considerably different. The assay is, however, quite sensitive to detergent interference, an important consideration when choosing extraction reagents. As well, samples with high viscosity or large amounts of debris had a tendency to cause a reduction in filtration flow rate and, in more severe cases, complete clogging of the membrane. Dilution of viscous samples or precentrifugation to clear particulates ameliorated clogging issues. In summary, the dot blot assay offers a cost-effective protein expression screening tool for researchers with moderate throughput needs.

Acknowledgment

We would like to thank Dr. Elene Chemokalskaya for manuscript review, advice, and assistance with the submission process.

References

[1] J. Schlessinger, "Cell signaling by receptor tyrosine kinases," *Cell*, vol. 103, no. 2, pp. 211–225, 2000.

[2] I. Rebay, "Keeping the receptor tyrosine kinase signaling pathway in check: lessons from *Drosophila*," *Developmental Biology*, vol. 251, no. 1, pp. 1–17, 2002.

[3] G. Pearson, F. Robinson, T. B. Gibson et al., "Mitogen-activated protein (MAP) kinase pathways: regulation and physiological functions," *Endocrine Reviews*, vol. 22, no. 2, pp. 153–183, 2001.

[4] G. L. Johnson and R. Lapadat, "Mitogen-activated protein kinase pathways mediated by ERK, JNK, and p38 protein kinases," *Science*, vol. 298, no. 5600, pp. 1911–1912, 2002.

[5] R. Tibes, Y. H. Qiu, Y. Lu et al., "Reverse phase protein array: validation of a novel proteomic technology and utility for analysis of primary leukemia specimens and hematopoietic stem cells," *Molecular Cancer Therapeutics*, vol. 5, no. 10, pp. 2512–2521, 2006.

[6] A. Weiss, "Overview of membranes and membrane plates used in research and diagnostic ELISPOT assays," *Methods in Molecular Biology*, vol. 792, pp. 243–256, 2012.

[7] R. Fabricant, J. Delarco, and G. Todaro, "Nerve growth factors on human melanoma cells in culture," *Proceedings of the National Academy of Sciences of the United States of America*, vol. 74, pp. 565–569, 1977.

Hindawi Publishing Corporation
International Journal of Proteomics
Volume 2012, Article ID 630409, 12 pages
doi:10.1155/2012/630409

Research Article

Chromatin-Associated Proteins Revealed by SILAC-Proteomic Analysis Exhibit a High Likelihood of Requirement for Growth Fitness under DNA Damage Stress

Han Wang,[1] Pornpimol Tipthara,[2] Lei Zhu,[2] Suk Yean Poon,[2] Kai Tang,[1] and Jianhua Liu[2,3]

[1] *School of Biological Science, Nanyang Technological University, Singapore 637551*
[2] *Systems Biology, Genome Institute of Singapore, Singapore 138672*
[3] *Department of Biochemistry, Yong Loo Lin School of Medicine, National University of Singapore, Singapore 119077*

Correspondence should be addressed to Kai Tang, ktang@pmail.ntu.edu.sg and Jianhua Liu, liujh@gis.a-star.edu.sg

Received 11 February 2012; Accepted 9 June 2012

Academic Editor: Winston Patrick Kuo

Chromatin-associated nonhistone proteins (CHRAPs) are readily collected from the DNaseI digested crude chromatin preparation. In this study, we show that the absolute abundance-based label-free quantitative proteomic analysis fail to identify potential CHRAPs from the CHRAP-prep. This is because that the most-highly abundant cytoplasmic proteins such as ribosomal proteins are not effectively depleted in the CHRAP-prep. Ribosomal proteins remain the top-ranked abundant proteins in the CHRAP-prep. On the other hand, we show that relative abundance-based SILAC-mediated quantitative proteomic analysis is capable of discovering the potential CHRAPs in the CHRAP-prep when compared to the whole-cell-extract. Ribosomal proteins are depleted from the top SILAC ratio-ranked proteins. In contrast, nucleus-localized proteins or potential CHRAPs are enriched in the top SILAC-ranked proteins. Consistent with this, gene-ontology analysis indicates that CHRAP-associated functions such as transcription, regulation of chromatin structures, and DNA replication and repair are significantly overrepresented in the top SILAC-ranked proteins. Some of the novel CHRAPs are confirmed using the traditional method. Notably, phenotypic assessment reveals that the top SILAC-ranked proteins exhibit the high likelihood of requirement for growth fitness under DNA damage stress. Taken together, our results indicate that the SILAC-mediated proteomic approach is capable of determining CHRAPs without prior knowledge.

1. Background

Chromatin is a complex of DNA and proteins, in which the histones H2A, H2B, H3, and H4 are the major protein constituents [1, 2]. Chromatin remodeling through post-translational modification of histones plays an important role in modulation of DNA-protein interaction and thus regulates various biological processes such as replication, DNA damage repair, and transcription [3]. Hence, identification of the chromatin associated nonhistone proteins (CHRAPs) would permit understanding the molecular mechanisms for chromatin remodeling and regulation of various biological processes.

Fission yeast is a useful model for analysis of RNA interference (RNAi) directed heterochromatin formation [4, 5]. Many CHRAPs have been identified by using the high-throughput proteomic analysis of protein complexes purified through the chromatin immunoprecipitation (ChIP) coupled with the tandem affinity protein purification (TAP) tagging method in which the known CHRAP is used as bait [6–12]. However, it is limited to the identification of the CHRAPs that are associated with the complexes containing the previously known CHRAPs.

A traditional assay for testing whether a protein of interest is associated with the chromatin includes the preparation of CHRAPs extracts (or CHRAP-prep) through collection of the released proteins from the DNaseI digested crude chromatin and western blot analysis [13–16]. By using this method, components of the origin recognition complex such as Orc1, Orc2, and Orc5 are found to be associated with the chromatin throughout the cell cycle [13, 14]. On the other hand, the ATR-like kinase Rad3 and the mitotic activator phosphatase Cdc25 are found to be temporally associated with chromatins upon DNA damage [15, 16]. The relative

level of a CHRAP of interest in CHRAP-prep is clearly higher than that of whole cell extract (WCE) [13–16]. Nevertheless, it is unclear if highly abundant cytoplasm-localized proteins are effectively depleted from the CHRAP-prep. Effectively, depletion of the highly abundant non-CHRAPs such as ribosomal proteins is essential for *de novo* identification of CHRAPs through proteomic analysis of CHRAP-prep based on their absolute abundances.

We found that the top ranked proteins by levels of abundance in CHRAP-prep were predominated by the ribosomal proteins, suggesting that the highly abundant non-CHRAPs are not effectively removed in CHRAP-prep. Hence, simply based on the level of protein abundance in CHRAP-prep by using the high-throughput proteomic analysis is unlikely to reveal CHRAP candidates without prior knowledge. SILAC (stable isotope labeling with amino acids in cell culture)-mediated proteomic analysis has shown to permit the quantitative analysis of the relative protein levels between those labeled with and without heavy isotopes [17], allowing estimation of ratios between individual protein levels in CHRAP-prep versus WCE. By applying the SILAC-mediated high-throughput proteomic analysis, we show, in this study, that the highly abundant non-CHRAP ribosomal proteins are significantly depleted in the top ranked proteins by SILAC-ratio between CHRAP-prep and WCE. The top ranked proteins by SILAC-ratio are enriched for potential CHRAP candidates such as nucleus-localized proteins and CHRAP-associated functions such as chromatin structure organization, DNA replication and repair, transcription according to gene ontology analysis. Phenotypic assessment shows that the SILAC-enriched but not depleted nucleus-localized proteins exhibit the high likelihood of requirement for growth fitness in MMS (methyl methanesulfonate)-induced DNA damage stress. Taken together, our results indicate that SILAC-mediated proteomic analysis of CHRAP-prep is capable of identifying CHRAP candidates without prior knowledge. We propose that our approach can be complementary to the ChIP method coupled with TAP-tagging for identification of CHRAP-interacting partners.

2. Results and Discussion

In the SILAC proteomic analysis, SILAC-labeled samples are required to be fully incorporated with the heavy stable isotope-coupled lysine (e.g., $^{13}C_6$-lysine or heavy-lysine) or arginine (e.g., $^{13}C_6$-arginine or heavy-arginine) or both. To avoid the arginine-conversion problem [18], we applied heavy lysine alone in this study. The rate of incorporation with heavy-lysine in cells after various numbers of passages or subcultures in minimal medium supplemented with heavy-lysine was tested. In this test, each subculture was maintained for a day (i.e., equivalent to ~3 generations) before subsequent subculturing (Figure 1(a)).

The relative level of light versus heavy peptides/proteins was exemplified by the Eno1 peptide AVGNVNNIIAPVVK in various subcultures. As expected, no Eno1 peptide was detected to contain heavy-lysine in the initial culture (p0) prior to subculturing with the heavy lysine-containing medium (Figure 1(b), see p0). On the other hand, ~90% of the peptides were detected to contain heavy-lysine in the first subculture (p1) with the heavy lysine-containing medium (Figure 1(b), see p1). Hardly any light lysine-containing peptides were detected in the second (p2) or the third (p3) subcultures (Figure 1(b), see p2 and p3). This result indicates that heavy lysine is effectively incorporated into cellular protein in fission yeast.

To further test whether the heavy lysine was uniformly incorporated in all peptides/proteins besides Eno1, a slice of SDS-PAGE gel containing proteins derived from the first subculture was subjected to LC-MS/MS analysis. The ratio between light and heavy peptide levels in all of the ~100 peptides detected was found to be close to −3 in log 2 scale, indicating that the heavy lysine is uniformly incorporated in all proteins in the culture (Figure 1(c)). To ascertain proteins were fully incorporated with heavy lysine, cells derived from the third subculture (i.e., ~9 generations in the heavy-lysine-containing medium) were applied for SILAC analysis in this study.

Next, we wanted to assess the sensitivity by varying the ratios of light and heavy peptides/proteins in the given premixed samples. A slice of SDS-PAGE gel (i.e., containing >100 peptides) from each given sample was subjected to the proteomic analysis after in-gel trypsinization. To this end, the distribution of ratios of all peptides detected in SILAC analysis correlated well with the expected ratio in the given samples, suggesting that our SILAC protocol is adequate for the quantitative proteomic analysis (Figure 2(a)). This is consistent with the notion that SILAC methodology is excellent for quantitative proteomic analysis [17]. The correlation was apparent when the medians of ratios of all peptides detected in SILAC analysis were compared to the expected ratios of the given samples (Figure 2(b)). To estimate the ratios between light and heavy proteins, the median of the unique peptides levels was applied (see Section 4). Based on this estimation, protein ratios detected in SILAC analysis correlated well with the expected ratios of the given samples (Figure 2(c)). Hence, the median of unique peptide levels was used to estimate the level of proteins in this study.

It has been shown that a given proteins can be tested for its association with the chromatins by enriching the CHRAPs [13, 14]. Based on the protocols, we obtained CHRAP-prep (Figure 3(a)). It was clear that soluble proteins such as tubulin were depleted only in the soluble fraction (sup1) and chromatin-associated proteins such as histone H4 were enriched in the CHRAP-prep (or sup2) (Figures 3(b) and 3(c)). To test if the most abundant proteins in CHRAP-prep were CHRAPs, CHRAP-prep was subjected to the non-SILAC protein analysis. We found that the top 10% ranked proteins by absolute abundance in CHRAP-prep were overrepresented by the non-CHRAP ribosomal proteins when compared to the background level (i.e., 51.4% versus 14.9%; P value $= 2.21e-07$) (see Supplementary Table S3 in Supplementary Material available online at doi:10.1155/2012/630409 and also see Section 4). This result indicates that the highly abundant non-CHRAPs ribosomal proteins are not effectively removed in CHRAP-prep.

We judged that the absolute abundance of the majority enriched CHRAPs might not be higher than that of the

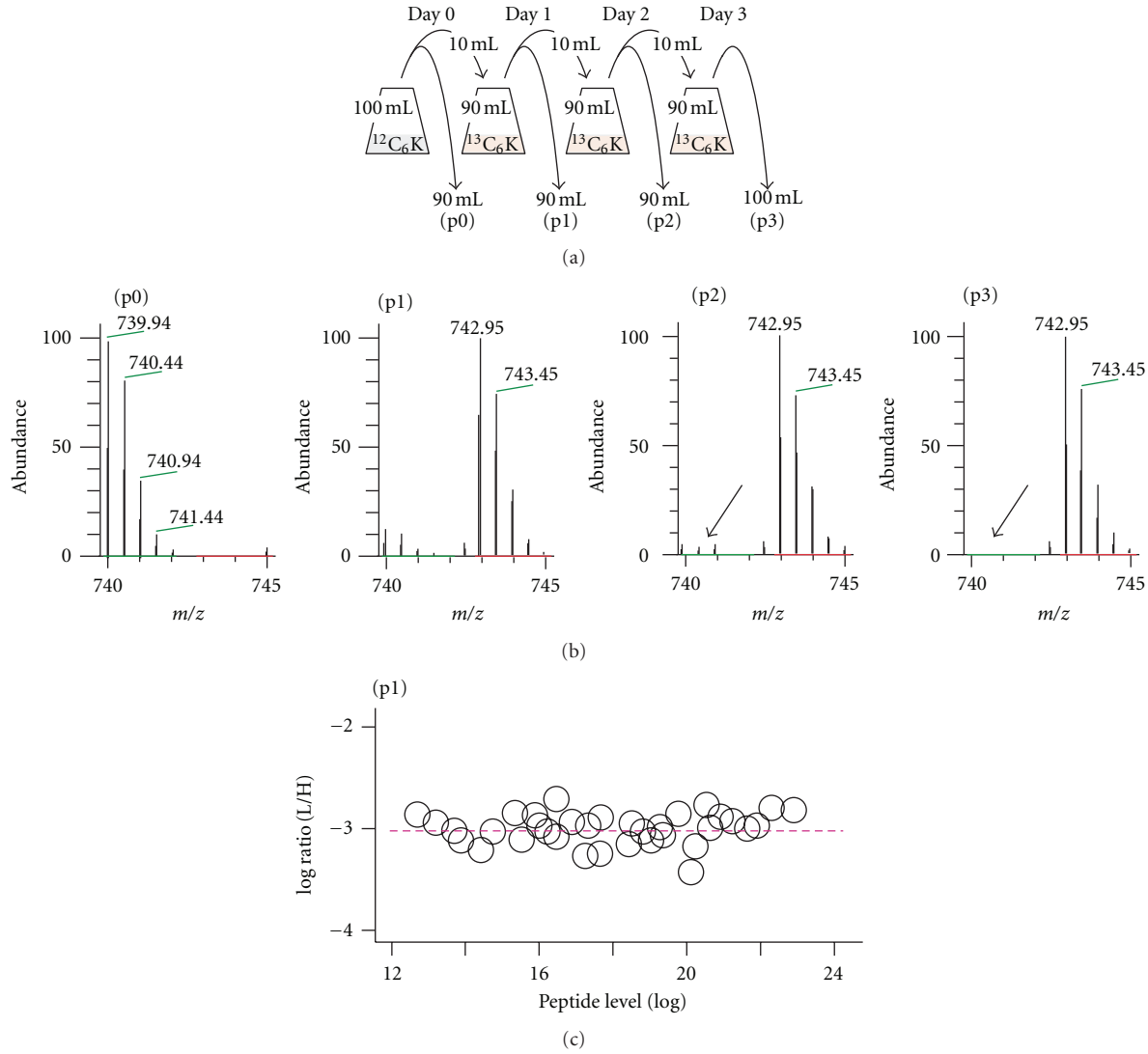

Figure 1: Heavy lysine is efficiently incorporated in fission yeast. (a) A schematic diagram shows the consecutive subculturing of cells in heavy lysine containing medium. (b) An MS spectrum of the Eno1 peptide AVGNVNNIIAPVVK. The spectrum of the peptide resulted from passages p0, p1, p2, and p3 is shown. Green and red lines indicate the *m/z* of light and heavy peptides, respectively. Arrow indicates the position of light peptide undetected in p2 and p3 cells. (c) The scatter plot shows the ratio of light and heavy peptides in the first passage (sample p1). *X*- and *Y*-axis indicate the abundance of individual peptides and the ratio of light and heavy peptide, respectively. Each dot represents a peptide.

depleted ribosomal proteins due to their high abundance prior to the enrichment. On the other hand, CHRAPs would be top ranked by comparing levels of enrichment or ratios between CHRAP-prep (after enrichment) and WCE (before enrichment). To test this possibility, equal amounts of CHRAP-prep and heavy lysine-labeled WCE proteins were mixed and subjected to LC-MS/MS analysis using LTQ Orbitrap mass spectrometry (see Section 4).

A total of 507 proteins were identified based on the presence of paired light (i.e., CHRAP-prep) and heavy (i.e., WCE) peptides after selection of high quality peptide through the Trans-Proteomic Pipeline (http://tools.proteomecenter.org/) (Supplementary Table S2; see Section 4). By ranking the proteins using SILAC-ratios, we found that the occurrence of ribosomal proteins in the top 10% (or top 50) ranked proteins was ~35% lower than the background level (6% versus 9.5%). We found that the ribosomal protein occurrence in the top 10% ranked proteins by SILAC ratios was significantly lower than that in the top 10% ranked proteins by absolute abundances (6% versus 51.4%; *P*-value $= 9.32e - 12$). This result indicates that the abundant ribosomal proteins can be effectively reduced from the top 10% ranked proteins in SILAC analysis (Figure 3(d)).

We noted that the occurrence of ribosomal proteins in the second top 10% ranked proteins by SILAC ratios was not reduced when compared to the background level (i.e., 14% versus 9.5%). This result suggests that the enrichment for CHRAPs in the second top 10% ranked proteins was

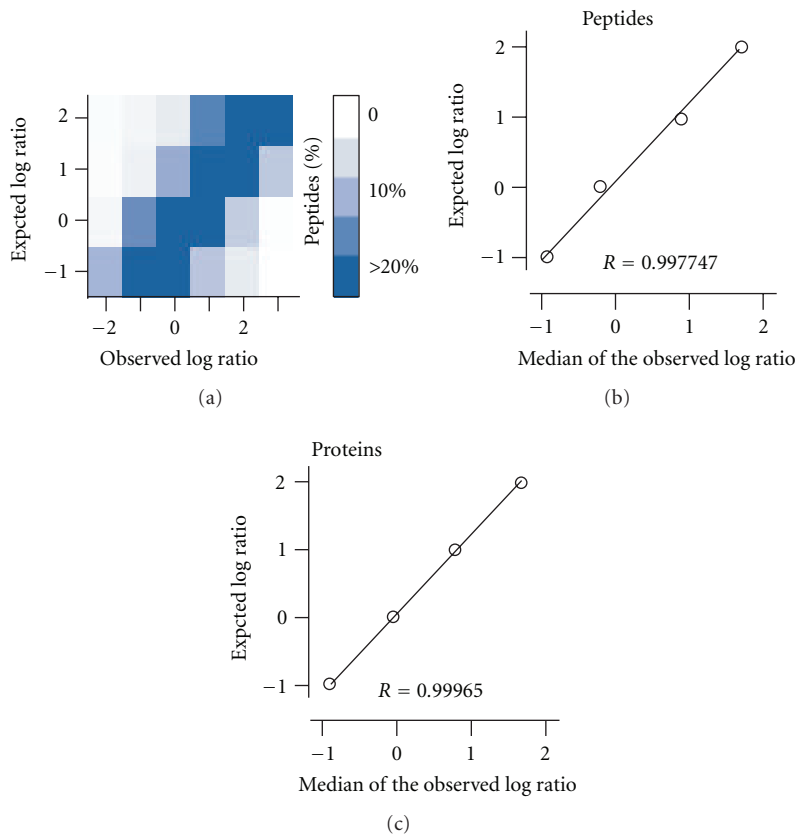

Figure 2: High sensitivity of peptide/protein ratio detection by SILAC analysis. (a) Distribution of detected ratios by SILAC is correlated with the expected ratio in the given samples. X- and Y-axis indicate the detected peptide ratios by SILAC and the expected ratio of the given samples, respectively. Color key is shown in (a). (b) The median of detected peptide ratios by SILAC is highly correlated with the expected ratio in the given samples. The correlation coefficient (R) is shown. (c) The median of protein ratios is highly correlated with the expected ratio.

less effective. Hence, only the first top 10% ranked proteins by SILAC ratio were considered for enriching CHRAP candidates and were further analyzed in this study.

CHRAPs would have nucleus-localization due to their association with chromatin. We, therefore, wanted to examine if the nucleus-localized proteins were particularly enriched in the top ranked proteins by SILAC ratios. Based on the subcellular localization characterized by Matsuyama et al. [19] and gene ontology (http://www.geneontology.org/), we found that the nucleus-localized proteins were significantly enriched in the top 10% ranked proteins by SILAC ratios when compared to the background level (i.e., 24% versus 9.47%; P-value $= 2.0e - 03$) (Figure 4(a)). This result supports the notion that the top 10% ranked proteins by SILAC ratios are enriched for CHARP candidates, suitable for CHRAP discovery without prior knowledge.

Next, we wanted to know if the CHRAP-associated functions such as chromatin modification and DNA replication and repair would be enriched in the top ranked proteins by SILAC ratios. Based on the gene ontology (i.e., biological process terms), gene functions such as transcription, chromatin modification, DNA replication and repair were over-represented in the top 10% ranked proteins (P value < 0.05) (Figure 4(b)). These results are consistent with a notion that the top ranked proteins by SILAC were enriched for CHRAP functions.

In the top 10% ranked proteins by SILAC ratios, we found Psm3, Cbh2, and C27f1.06c that are involved in chromosome organization and chromatin remodeling; Ddb1, Msh3, Spp1, and Uve1 that are involved in DNA replication and repair, and Eri1, C947.08c, Rpb1, and C530.05 that are involved in transcription (see Supplementary Table S2). These proteins would represent a small subset of CHRAPs that are relatively soluble, abundant, and constitutively associated with the chromatin. Deep analysis of CHRAP-prep using SILAC proteomics should allow identifying more proteins with CHRAP-associated functions without prior knowledge.

We also found Prp16, Smb1, and Mug161 that are involved in proteolysis and Ubr1, P8b7.11, and Rpt2 that are involved in mRNA splicing in the top ranked proteins by SILAC ratios. In fact, it is not unusual to find components of the proteolysis machinery that are associated with the chromatin. For instance, the ubiquitin E3 ligase Pcu4 is found to be associated with the RNA-induced transcriptional silencing (RITS) complex involved in heterochromatin assembly [20]; and the E3 ligase Ubr1 is associated with the Set1 complex

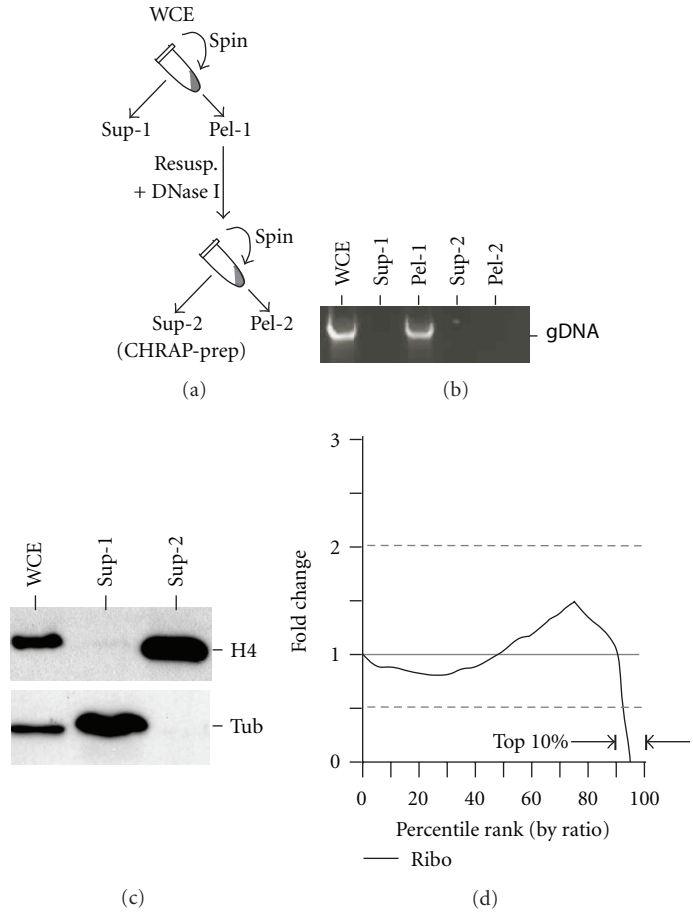

Figure 3: Abundant ribosomal proteins are effectively depleted in CHRAP-prep by SILAC. (a) A schematic diagram shows the steps of CHRAP preparation. WCE stands for whole cell extract; sup for supernatant; pel for pellet; and resusp. for resuspension. (b) The image of the agarose gel shows the presence or absence of genomic DNA (gDNA) in various samples indicated as in (a). (c) The image of western blot shows the presence or absence of histone H4 and soluble protein tubulin (tub). (d) Top 10% ranked proteins by SILAC ratios are depleted of ribosomal proteins. *X*-axis indicates the percentile ranks by SILAC ratios and *Y*-axis indicates the level of the ribosomal proteins.

involved in histone H3 methylation [21, 22]. On the other hand, proteins involved in mRNA splicing have been found to be assembled into the cotranscriptional spliceosome on chromosome [23].

We noted that some nucleus-localized proteins were not listed in the top 10% ranked proteins by SILAC ratios. Those nucleus-localized proteins might not be associated with the chromatins. To test this possibility, randomly selected 3 top SILAC-ranked proteins Msh3, Prp16, and C18.05c (e.g., their SILAC ratios were 5.86, 4.72, and 4.19 in $\log 2$ scale, resp.) and 2 other proteins Srp2 and Kap95 (e.g., their SILAC ratios are -0.46 and -1.30 in $\log 2$ scale) (see Supplementary Table S2) were subjected to the traditional assay for CHRAPs (see Section 4). The analysis indicated that the SILAC most enriched nucleus-localized proteins were the true CHRAPs (Figure 5(a)). On the other hand, the SILAC depleted nucleus-localized proteins were not CHRAPs (Figure 5(b)). To ascertain that the subcellular localization of the HA epitope-tagged protein used in the traditional CHRAP assay would not be altered by the epitope, we performed the indirect immunofluorescence microscopic analysis (Figure 5(c)). Clearly, the HA-tagged proteins remained to be nuclear. Hence, we conclude that the SILAC enriched nucleus-localized proteins are CHRAP candidates.

Some of the dual-localized proteins were found in the top ranked proteins by SILAC ratios (see Supplementary Table S2). To test if they were the true CHRAPs, the 3 randomly selected proteins Uve1, Hsp16, and C530.05 were subjected to the traditional CHRAP assay. The analysis indicated that all 3 proteins exhibited apparent enrichment in the CHRAP-prep when compared to WCE (Figure 5(d)). On the other hand, the presence in the soluble fraction was detected in 2 out of 3 dual-localized proteins, consistent with their dual subcellular localization. This result indicates that most of the top ranked proteins by SILAC ratios are true CHRAP candidates.

Of the 507 proteins identified in the SILAC analysis, 413 were found to be either SILAC enriched (i.e., $\log 2$ SILAC-ratio > 0.585) or depleted (i.e., $\log 2$ SILAC-ratio < -0.585). We wanted to test if the SILAC-enriched proteins have a likelihood of requirement for growth fitness in DNA

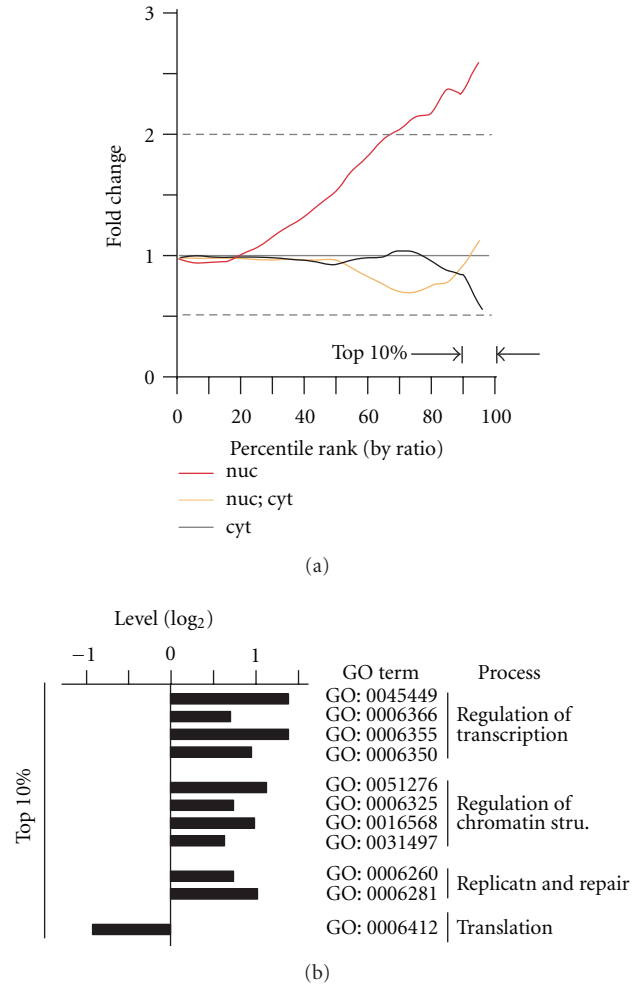

Figure 4: Top ranked proteins by SILAC ratios are enriched for nucleus-localized proteins and CHRAP-associated functions. (a) Nucleus-localized proteins are enriched in the top 10% ranked proteins by SILAC. Display is identical to Figure 3(d). Levels of nucleus-localized (nuc), dual-localized (nuc; cyt), and cytoplasm-localized (cyt) proteins are shown. (b) Top 10% ranked proteins by SILAC are enriched for CHRAP-associated functions based on gene ontology analysis.

damage stress, one of the CHRAP-associated functions. For this reason, 188 (~45.5%) *S. pombe* gene deletion strains from the Bioneer deletion strains set (version 1) were subjected to the phenotypic assessment using the mini-growth curve assay [24]. Level of growth fitness under MMS stress was estimated by the growth fitness score (GFS_{MMS}) that was calculated based on the difference of T_{50} (the time at the half-maximal concentration) between cultures supplemented with and without MMS (see Section 4).

The growth fitness score GFS_{MMS} was proportional to the level of requirement for growth fitness under MMS stress. It was apparent that, among the nucleus-localized proteins, the median GFS_{MMS} of the SILAC-enriched proteins was significantly higher than that of the SILAC-depleted ones (1.43 versus 0.79; P value < 0.05; Supplementary Table S4). This result indicates that the top SILAC-ranked nucleus-localized proteins are *bona fide* CHRAP candidates that exhibit a high likelihood of requirement for growth fitness under DNA damage stress (Figure 6(a)). On the other hand, among the cytoplasm-localized or dual-localized proteins, the median GFS_{MMS} of the SILAC-enriched proteins showed no apparent differences from that of the SILAC-depleted ones (i.e., 0.93 versus 0.98 or 1.05 versus 1.02) (Figures 6(b) and 6(c)). This is consistent with the observation that the cytoplasm-localized or dual-localized proteins were not overrepresented in the top ranked proteins by SILAC ratios (see Figure 4(a)). Hence, SILAC proteomic analysis of CHRAP-prep is capable of identifying CHRAP candidates without prior knowledge.

We noted that, however, hardly any chromo-domain or bromo-domain containing chromatin remodelers are found in our SILAC analysis of CHRAP-prep. This is probably a result of using the physiological salt concentration in this analysis (see Section 4). It is known that extraction of chromo-domain and bromo-domain proteins requires high salt concentrations [25]. Alternatively, these proteins could also escape the detection in LC-MS/MS due to their relatively low abundance and high level of interference from the

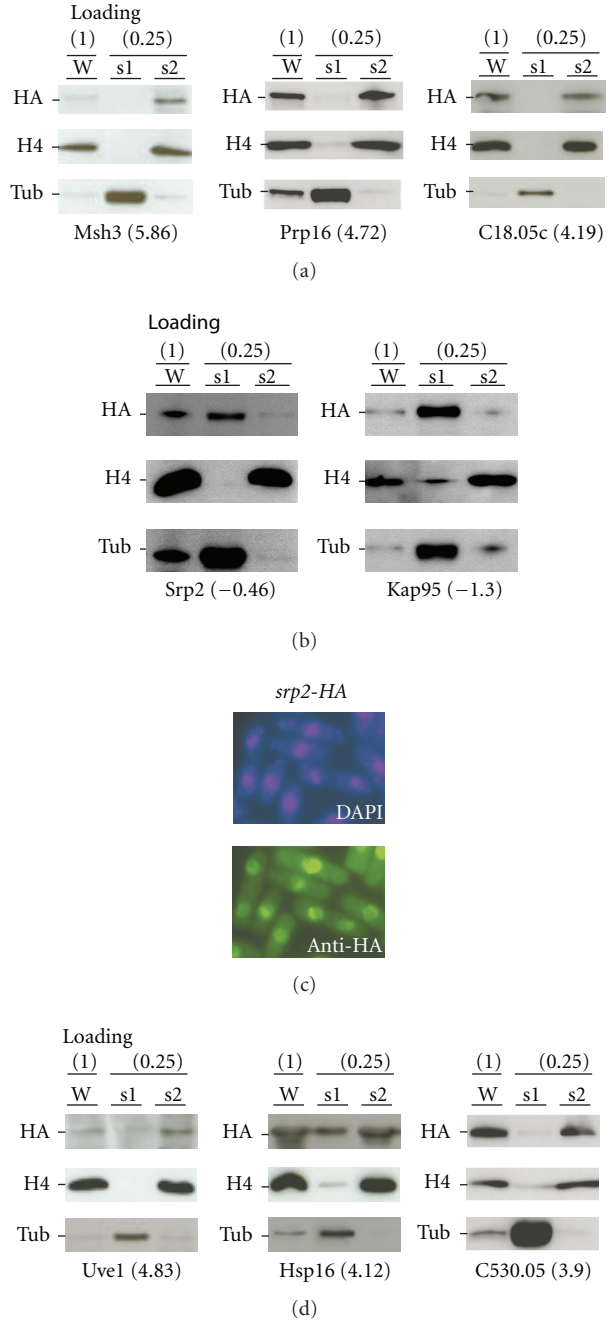

Figure 5: Traditional CHRAP assay to validate SILAC-enriched/depleted proteins. (a) SILAC-enriched nucleus localized proteins are association with the chromatin. Loading quantity of various protein samples such as whole cell extract (W), supernatant-1 (s1) and supernatant-2 (s2; the CHRAP-prep) is indicated in parentheses on the top. Tested proteins and their SILAC ratio in parentheses are indicated at the bottom. (b) SILAC-depleted proteins are unassociated with the chromatin. The display is identical to (a). (c) Subcellular localization of the HA-tagged Srp2 proteins. (d) SILAC-enriched dual-localized proteins are associated with the chromatin. The display is identical to (a).

cytoplasm-localized abundant proteins. It could be improved by better chromatographic separation of the trypsinized peptides using a longer column or UPLC separation before mass spectrometric analysis. Modification of CHRAP preparation and improvement of SILAC proteomic analysis should allow identification of the chromo-domain and bromo-domain proteins in future studies.

3. Conclusion

We show that the CHRAP-prep used in traditional assays for CHRAPs is predominated by the abundant cytoplasmic proteins such as ribosomal proteins based on the absolute abundance of proteins. On the other hand, we show that proteomic analysis of CHRAP-prep together with the

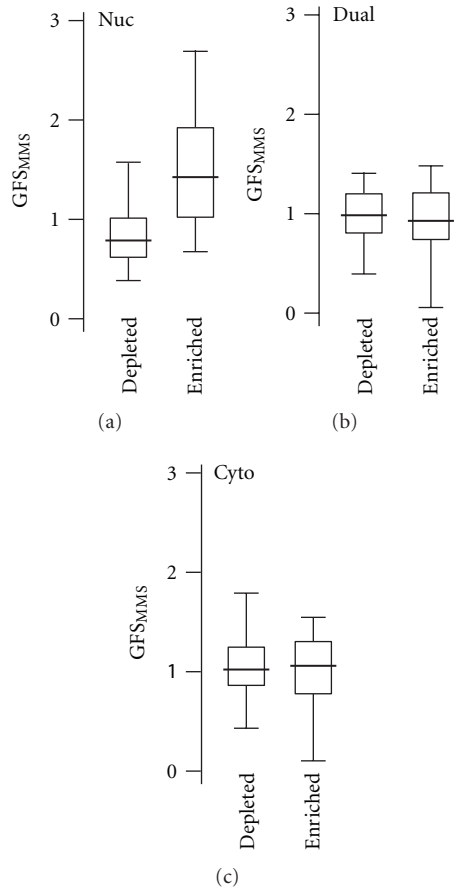

Figure 6: SILAC-enriched nucleus-localized proteins exhibit the high likelihood of requirement for growth fitness under DNA damage stress. The boxplots show the level of growth fitness in various mutant strains. Cells containing a deletion allele of the SILAC-enriched or depleted proteins are indicated. Nucleus-localized (Nuc), dual-localized (Dual), or cytoplasm-localized (Cyto) are shown in (a), (b), or (c), respectively.

SILAC-labeled WCE is able to effectively deplete the ribosomal proteins from the top ranked proteins by SILAC ratios. Significantly, we show that the top ranked proteins by SILAC ratios enrich for nucleus-localized proteins that display a high likelihood of requirement for growth fitness under DNA damage stress. Hence, the SILAC-mediated proteomic analysis is capable of determining CHRAPs without prior knowledge. We propose the method shown in this study can be complementary to the proteomic analysis of protein complexes purified via ChIP with TAP-tagged CHRAPs for identification of CHRAP-interacting partners.

4. Methods

4.1. Strain Construction and Cell Culture Manipulation. Strains used in this study are listed in Table 1 except for Bioneer deletion strains (Bioneer Corporation, Daejeon, Korea). The strain *lys1-131* was used in preparation of the SILAC-labeled cells. Hemagglutinin (HA)-tagged strains for western blot analysis were constructed based on the protocol reported previously [26]. The Bioneer deletion strains used in this study are listed in Supplementary Table S1. Cultures in minimal medium (MM) supplemented with normal or heavy lysine ($^{13}C_6$-lysine; Cat. No. CLM-2247-0.25; Cambridge Isotope Laboratories, Andover, MA, USA) was used in proteomic analysis. Cultures in rich medium (YES) supplemented with or without methyl methanesulfonate (MMS) at the final concentration of 1 mM were used in growth fitness assays.

4.2. Enrichment of Chromatin-Associated Proteins (CHRAPs). To enrich the CHRAPs, CHRAP-prep was obtained as described elsewhere with some modification [13, 14]. In brief, ~500 mL (for LC-MS/MS analysis) or 50–100mL (for western blot analysis) log-phase growth cells (OD_{600} = ~0.8) were harvested and washed once with STOP Buffer (0.9% NaCl, 1 mM NaN_3, 50 mM NaF, 10 mM EDTA). The washed cells were then protoplasted by resuspending in protoplast buffer (35.5 mM BME, 50 mM sodium citrate, 40 mM EDTA, and 1.2 M sorbitol) supplemented with 8 mg/mL zymolyase-20T (MP Biomedicals Inc., Solon, OH, USA). Protoplasting of cells were monitored frequently under microscope (protoplasts turned dark when treated with 1% SDS). The reaction was stopped by addition of an equal volume of ice-cold 1.2 M sorbitol pH 7.5 when ~90% of the cells were protoplasted. The washed protoplasts were resuspended in

Table 1: List of strains used in this study[a].

ID	Relevant genotype	Comment
LJY3766	*lys1-131 ura4-D18h-*	Laboratory stock
LJY188	*leu1-32 ura4-D18h-*	Laboratory stock
LJY4383	*hsp16*$^+$*-3HA-6His::ura4+ ura4-D18 leu1-32 h-*	This study
LJY4384	*1c8.05c*$^+$*-3HA-6His::ura4+ ura4-D18 leu1-32 h-*	This study
LJY4385	*msh3*$^+$*-3HA-6His::ura4+ ura4-D18 leu1-32 h-*	This study
LJY4386	*uve1*$^+$*-3HA-6His::ura4+ ura4-D18 leu1-32 h-*	This study
LJY3236	*c530.05*$^+$*-3HA-6His::ura4+ ura4-D18 leu1-32 h-*	This study
LJY4224	*prp16*$^+$*-3HA-6His::ura4+ ura4-D18 leu1-32 h-*	This study
LJY4429	*kap95*$^+$*-HA-6His::ura4+ ura4-D18 leu1-32 h-*	This study
LJY4430	*srp2*$^+$*-HA-6His::ura4+ ura4-D18 leu1-32 h-*	This study

Note: [a]Bioneer deletion strains used in this study are listed in the Supplementary Table S1.

450 μL 1.2 M sorbitol for generating CHRAPs-prep or snap-frozen in liquid nitrogen and stored at -80°C for later use. The resuspended protoplasts were lysed by addition of 50 μL 10x lysis buffer (500 mM KAc, 20 mM $MgCl_2$, 200 mM HEPES pH 7.9) supplemented with the 1x complete protease inhibitors EDTA-free tablet (Roche, Basel, Switzerland) and 1% Triton X-100 (TX-100) (Promega, Fitchburg, WI, USA). The lysate was incubated on ice for 10 min with occasional mixing. Ten percent of the lysate was preserved as whole cell extract (WCE). The remaining was centrifuged at 12,000 g for 15 min at 4°C. Supernatant (sup-1) containing soluble proteins was transferred to a fresh tube and the pellet (pel-1) was washed twice and resuspended in lysis buffer without TX-100 to yield the crude chromatin extract. The resulting crude chromatin fraction was digested with DNaseI (Stratagene, La Jolla, CA, USA) at the concentration of 10 unit/μg DNA in digestion buffer (40 mM Tris-HCl pH 7.5, 6 mM $MgCl_2$, 150 mM NaCl, 2 mM $CaCl_2$ and protease inhibitors) at 37°C for 30 min with vigorous shaking.The DNaseI-digested crude chromatin extract was centrifuged at 14,000 g for 5 min. The supernatant (sup-2) was referred as the CHRAP-prep and separated from the pellet (pel-2).

4.3. SDS-PAGE and Western Blot Analysis. A desired amount of proteins was taken and mixed with standard loading buffer for SDS-PAGE analysis. Proteins in gel were electro-transferred onto nitrocellulose membranes for probing with primary antibodies against HA (Santa Cruz Biotechnology, Santa Cruz, CA, USA), histone H4 (Upstate Biotechnology, Lake Placid, NY, USA), and β-tubulin (TAT1 antibody; a gift of K. Gull, University of Oxford, London, UK). Secondary antibodies conjugated with horse radish peroxidase (GE Healthcare, Piscataway, NJ, USA) were used for detection of chemiluminescence signals using the ECL Plus System (GE Healthcare).

4.4. Sample Preparation and LC-MS/MS Analysis. Prior to MS analysis, protein samples were fractionated in SDS-PAGE gels. Gels were sliced into ~50 pieces from top to bottom of a lane. Proteins in gel slices were destained and trypsinized in-gel in 25 mM NH_4HCO_3 supplemented with 12.5 ng/μL trypsin (Promega, Madison, WI, USA). The resulting peptides were cleaned using C18 ZipTip (Millipore, Medford, MA, USA) and ready for mass spectrometry analysis.

Mass spectrometry analysis was performed using a nanoflow high-performance liquid chromatography (HPLC) system (Eksigent, Dublin, CA) connected to a hybrid LTQ-Orbitrap (Thermo Scientific, Bremen, Germany) equipped with a nanoelectrospray ion source (Thermo Scientific). The peptides were separated with a 15 cm long and 75 μm inner diameter PicoFrit column with an integrated tip (New Objective Inc, Woburn, MA) packed with 4 μm reverse-phase C12 resins (Jupiter Proteo Phenomenex, Torrance, CA, USA). HPLC mobile phase consists of (A) 2% acetonitrile 0.1% formic acid and (B) 98% acetonitrile 0.1% formic acid. Approximately 10 μL peptide solution was loaded onto a nano trap column (300SB-C18, Agilent) with 100% mobile phase A and washed for 10 min at a flow rate of 20 μL/min. The trap column was then brought in-line with the nano column using the CN2 nano volume switching valve (VICI Valco Cheminert, Switzerland) and the peptides were eluted by 2–35% mobile phase B over 70 min and 35–90% over 6 min with a constant flow rate of 300 nL/min. Finally the column was washed for 10 min with high concentration of organic solvent (90% mobile phase B) and re-equilibrate with another 15 min with 98% mobile-phase A prior to loading of the next sample. Eluted peptides from HPLC column were directly electrosprayed into the LTQ-Orbitrap mass spectrometer for analysis. The spray voltage was set to 2.0 kV and the temperature of the heated capillary was set to 250°C. The MS instrument was operated in a data-dependent mode by automatically switching between the full survey scan and MS/MS acquisition. High resolution precursor spectra (m/z 300–2,000) were acquired in the Orbitrap with resolution of 60,000 at m/z 400 (after accumulation to a target value of 10^6 ions in the linear ion trap). The 5 most intense ions with ion intensity above 1,000 counts and charged state ≥ 2 were sequentially isolated for fragmentation in the linear ion trap using collision induced dissociation (CID; normalized collision energy 35%, activation Q 0.250, and activation time 30 ms) at a target value of 10,000 ions. The dynamic exclusion list was restricted to a maximum retention period of 90 sec and a relative mass window of 10 ppm. The MS and

MS/MS spectra were recorded by the mass spectrometer as raw files using the Xcalibur software 2.0SR2 (Thermo Fisher Scientific).

4.5. SILAC-Mediated Proteomic Data Analysis. TPP (Trans-Proteomic Pipeline version 4.2.1, Seattle Proteome Centre, Institute of Systems Biology, Seattle, WA, USA) was used to perform database searching and peptide assignment and validation. For this purpose, all RAW spectra files were converted to mzXML-format. Uninterpreted MS/MS spectra were searched against the *S. pombe* protein databases UniProt Knowledgebase, including Swiss-Prot and TrEMBL using SEQUEST algorithm [27]. The database includes forward protein (target) and reverse protein (decoy) sequences that were generated by Bioworks 3.3.1 (Thermo Scientific). Search parameters used in this study were the requirement of tryptic cleavage (allowing 1 missed cleavage site), minimum peptide length of 7 amino acids, maximal precursor ions mass deviation of 10 ppm, peptide mass tolerance of ±0.5 Da, static modification on Cys of +57.0215 Da, differential modification on Met of 15.9945 Da, and heavy isotope coupling on Lys of +6.0201 Da. The output was in pepXML-format. All assigned peptides were validated using PeptideProphet [28] and the cutoff was set to the probability of 90% or greater. The qualified peptides (probability ≥ 90%) were quantified by the XPRESS software [29]. The elution profile of the $^{12}C_6$-Lys and $^{13}C_6$-Lys containing peptides from the qualified peptides were isolated and quantified based on the area of peaks by XPRESS. Protein levels were approximated by the median level of unique peptides. A total of 507 proteins with a ratio between light (CHRAP-prep) and heavy (WCE) protein levels were listed in Supplementary Table S2.

4.6. Non-SILAC Proteomic Data Analysis. To test whether the CHRAP candidates (e.g., nucleus-localized proteins) could be dominated in the most abundant proteins (i.e., based on the absolute abundance) in the CHRAP-prep, proteomic analysis of the CHRAP-prep proteins without SILAC was performed. In determination of the absolute abundance, the PeptideProphet-qualified peptides (probability ≥ 90%) were quantified by PepQuan and the abundance of proteins was estimated by the median abundance of the respective unique peptides. A total of 376 proteins whose abundance level was approximated by the median level of their unique peptides were listed in Supplementary Table S3. Based on the absolute abundance, nucleus-localized proteins were not overrepresented in the top 10% most abundant proteins (Supplementary Figure S1). Notably, on the other hand, the ribosomal proteins were dominated in the top 10% most abundant proteins, suggesting that the highly abundant non-CHRAP ribosomal proteins are not effectively depleted in the CHRAP-prep.

4.7. Miniculture Growth Curve Assay. Of 507 proteins identified in the SILAC-mediated analysis, 413 were either enriched or depleted (i.e., ratio ≥ ±1.5 fold) in CHRAP-prep when compared to WCE. Out of 413 deletion strains, 188 (45.5%) were found in the Bioneer deletion strain collection (Version 1, Bioneer Corporation). Therefore, 188 deletion mutant strains (see Supplementary Table S1) were subjected to minigrowth curve assays using the Bioscreen miniculture growth curve system (Growth Curves USA, Piscataway, NJ) for growth fitness in 1 mM MMS stress. All tests were done in triplicate. Minigrowth curve assay settings used were identical to the previous study [24].

Growth fitness score in MMS (GFS_{MMS}) is calculated based on the formula $(GFS_{MMS}) = 100\ (\Delta T_{50\_mut}/\Delta T_{50\_wt})$, in which T_{50} is the time at the half-maximal cell concentration based on the growth curve, and ΔT_{50} is the difference of the half-maximal time between cultures supplemented with and without MMS. mut stands for mutant strains and wt for the wild type strain. The average GFS_{MMS} of tested strains is listed in Supplementary Table S4.

4.8. Statistical Analysis. Binomial test was used to test the nonrandom distribution. In analysis of enrichment or depletion of the nuclear or cytoplasmic proteins, the protein localization information in a genome-wide study by Matsuyama et al. [19] was used, in which 4,387 proteins whose subcellular localization has been characterized. Localization of additional 321 proteins is based on the GO terms (i.e., cellular components; http://www.genedb.org/ or http://amigo.geneontology.org/). The subcellular localizations are briefly categorized into three types: the nucleus (it includes the nucleus, nucleolus, spindle pole body, and nuclear envelope), cytoplasm (it includes cytosol, mitochondrion, Golgi, ER, cytoskeleton, plasma membrane, and other cytoplasmic organelles), or both. Thus, 4,708 proteins (i.e., ~93% of *S. pombe* proteome) have well defined localization types: 763 (~16.2%) are localized at the nucleus, 2180 (46.3%) at the cytoplasm, and 1765 (37.5%) at both the nucleus and cytoplasm.

Biological process terms were only considered in gene ontology analysis when the occurrence was 15 or greater in the group of 300–500 proteins.

Unpaired two-sample *t*-test was used to test the difference of GFS_{MMS} between the SILAC-enriched and depleted proteins with nucleus or cytoplasm or both localizations.

Original mass spectrometric data are deposited in Tranche database (https://proteomecommons.org/) and can be accessed by a hash "ap/3Mk3fjF/4aY8SslwNzqzdi9FDeoA WmmB9oZ3th0cnj807UrbPmSG/s+HWzM4MAzdrmmMh Qxi10xe5jO2jaQtfSsEAAAAAAAAEMQ==" or at the author's website at http://pombe.gis.a-star.edu.sg/.

List of Abbreviations

ChIP:	Chromatin immunoprecipitation
CHRAP:	Chromatin-associated non-histone proteins
CHRAP-prep:	Preparation of proteins enriched for CHRAPs
GFS:	Growth fitness score
GO:	Gene ontology
LC:	Liquid chromatography
LTQ:	Linear trap quadrupole
MS/MS:	Tandem mass spectrometry

SILAC: Stable isotope labeling with amino acids in cell culture
WCE: Whole cell extract.

Authors' Contributions

All authors read and approved the final manuscript. H. Wang, P. Tipthara, K. Tang, and J. Liu participated in research design. H. Wang, and P. Tipthara conducted experiments. SYP contributed new reagents. H. Wang, P. Tipthara, L. Zhu, K. Tang, and J. Liu performed data analysis. J. Liu wrote the paper. H. Wang and P. Tipthara are contributed equally to the paper.

Conflict of Interests

The authors declare that there are no conflict of interests.

Acknowledgments

The authors are grateful to Dr. J. Li (Nanyang Technological University, Singapore) for his assistance in processing the peptide datasets, Dr. K. Gull (University of Oxford, UK) for the TAT1 antibody, and Dr. A. Lin for the helpful comments. This work was supported by the Agency for Science, Technology, and Research (A-STAR), Singapore to J. Liu and a Nanyang Technological University Ph.D. Studentship to H. Wang.

References

[1] K. E. Van Hoide, C. G. Sahasrabuddhe, and B. R. Shaw, "A model for particulate structure in chromatin," *Nucleic Acids Research*, vol. 1, no. 11, pp. 1579–1586, 1974.

[2] K. Luger, A. W. Mäder, R. K. Richmond, D. F. Sargent, and T. J. Richmond, "Crystal structure of the nucleosome core particle at 2.8 Å resolution," *Nature*, vol. 389, no. 6648, pp. 251–260, 1997.

[3] B. D. Strahl and C. D. Allis, "The language of covalent histone modifications," *Nature*, vol. 403, no. 6765, pp. 41–45, 2000.

[4] E. Bernstein and C. D. Allis, "RNA meets chromatin," *Genes and Development*, vol. 19, no. 14, pp. 1635–1655, 2005.

[5] M. Bühler and D. Moazed, "Transcription and RNAi in heterochromatic gene silencing," *Nature Structural and Molecular Biology*, vol. 14, no. 11, pp. 1041–1048, 2007.

[6] A. J. Link, J. Eng, D. M. Schieltz et al., "Direct analysis of protein complexes using mass spectrometry," *Nature Biotechnology*, vol. 17, no. 7, pp. 676–682, 1999.

[7] M. Brajenovic, G. Joberty, B. Küster, T. Bouwmeester, and G. Drewes, "Comprehensive proteomic analysis of human par protein complexes reveals an interconnected protein network," *Journal of Biological Chemistry*, vol. 279, no. 13, pp. 12804–12811, 2004.

[8] R. M. Ewing, P. Chu, F. Elisma et al., "Large-scale mapping of human protein-protein interactions by mass spectrometry," *Molecular Systems Biology*, vol. 3, article 89, 2007.

[9] A. C. Gavin, P. Aloy, P. Grandi et al., "Proteome survey reveals modularity of the yeast cell machinery," *Nature*, vol. 440, no. 7084, pp. 631–636, 2006.

[10] Y. Ho, A. Gruhler, A. Heilbut et al., "Systematic identification of protein complexes in Saccharomyces cerevisiae by mass spectrometry," *Nature*, vol. 415, no. 6868, pp. 180–183, 2002.

[11] N. J. Krogan, G. Cagney, H. Yu et al., "Global landscape of protein complexes in the yeast Saccharomyces cerevisiae," *Nature*, vol. 440, no. 7084, pp. 637–643, 2006.

[12] E. H. Bayne, S. A. White, A. Kagansky et al., "Stc1: a critical link between RNAi and chromatin modification required for heterochromatin integrity," *Cell*, vol. 140, no. 5, pp. 666–677, 2010.

[13] D. Griffiths, M. Uchiyama, P. Nurse, and T. S. F. Wang, "A novel mutant allele of the chromatin-bound fission yeast checkpoint protein Rad17 separates the DNA structure checkpoints," *Journal of Cell Science*, vol. 113, part 6, pp. 1075–1088, 2000.

[14] Z. Lygerou and P. Nurse, "The fission yeast origin recognition complex is constitutively associated with chromatin and is differentially modified through the cell cycle," *Journal of Cell Science*, vol. 112, no. 21, pp. 3703–3712, 1999.

[15] D. Hermand and P. Nurse, "Cdc18 enforces long-term maintenance of the S phase checkpoint by anchoring the Rad3-Rad26 complex to chromatin," *Molecular Cell*, vol. 26, no. 4, pp. 553–563, 2007.

[16] S. P. Selvanathan, A. G. Thakurta, J. Dhakshnamoorthy, M. Zhou, T. D. Veenstra, and R. Dhar, "Schizosaccharomyces pombe Dss1p Is a DNA damage checkpoint protein that recruits Rad24p, Cdc25p, and Rae1p to DNA double-strand breaks," *Journal of Biological Chemistry*, vol. 285, no. 19, pp. 14122–14133, 2010.

[17] S. E. Ong, B. Blagoev, I. Kratchmarova et al., "Stable isotope labeling by amino acids in cell culture, SILAC, as a simple and accurate approach to expression proteomics," *Molecular & Cellular Proteomics*, vol. 1, no. 5, pp. 376–386, 2002.

[18] C. C. Bicho, F. D. L. Alves, Z. A. Chen, J. Rappsilber, and K. E. Sawin, "A genetic engineering solution to the "arginine conversion problem" in stable isotope labeling by amino acids in cell culture (SILAC)," *Molecular and Cellular Proteomics*, vol. 9, no. 7, pp. 1567–1577, 2010.

[19] A. Matsuyama, R. Arai, Y. Yashiroda et al., "ORFeome cloning and global analysis of protein localization in the fission yeast Schizosaccharomyces pombe," *Nature Biotechnology*, vol. 24, no. 7, pp. 841–847, 2006.

[20] P. J. Horn, J. N. Bastie, and C. L. Peterson, "A Rik1-associated, cullin-dependent E3 ubiquitin ligase is essential for heterochromatin formation," *Genes and Development*, vol. 19, no. 14, pp. 1705–1714, 2005.

[21] A. Roguev, S. Bandyopadhyay, M. Zofall et al., "Conservation and rewiring of functional modules revealed by an epistasis map in fission yeast," *Science*, vol. 322, no. 5900, pp. 405–410, 2008.

[22] A. Roguev, A. Shevchenkon, D. Schaft, H. Thomas, A. F. Stewart, and A. Shevchenko, "A comparative analysis of an orthologous proteomic environment in the yeast Saccharomyces cerevisiae and Schizosaccharomyces pombe," *Molecular and Cellular Proteomics*, vol. 3, no. 2, pp. 125–132, 2004.

[23] S. A. Lacadie and M. Rosbash, "Cotranscriptional spliceosome assembly dynamics and the role of U1 snRNA:5′ss base pairing in yeast," *Molecular Cell*, vol. 19, no. 1, pp. 65–75, 2005.

[24] M. Eshaghi, J. H. Lee, L. Zhu et al., "Genomic binding profiling of the fission yeast stress-activated MAPK sty1 and the bZIP transcriptional activator Atf1 in response to H_2O_2," *PLoS ONE*, vol. 5, no. 7, Article ID e11620, 2010.

[25] J. P. Lambert, L. Mitchell, A. Rudner, K. Baetz, and D. Figeys, "A novel proteomics approach for the discovery of chromatin-associated protein networks," *Molecular & Cellular Proteomics*, vol. 8, no. 4, pp. 870–882, 2009.

[26] A. Bimbó, Y. Jia, L. P. Siew et al., "Systematic deletion analysis of fission yeast protein kinases," *Eukaryotic Cell*, vol. 4, no. 4, pp. 799–813, 2005.

[27] J. K. Eng, A. L. McCormack, and J. R. Yates, "An approach to correlate tandem mass spectral data of peptides with amino acid sequences in a protein database," *Journal of the American Society for Mass Spectrometry*, vol. 5, no. 11, pp. 976–989, 1994.

[28] A. Keller, A. I. Nesvizhskii, E. Kolker, and R. Aebersold, "Empirical statistical model to estimate the accuracy of peptide identifications made by MS/MS and database search," *Analytical Chemistry*, vol. 74, no. 20, pp. 5383–5392, 2002.

[29] D. K. Han, J. Eng, H. Zhou, and R. Aebersold, "Quantitative profiling of differentiation-induced microsomal proteins using isotope-coded affinity tags and mass spectrometry," *Nature Biotechnology*, vol. 19, no. 10, pp. 946–951, 2001.

Hindawi Publishing Corporation
International Journal of Proteomics
Volume 2012, Article ID 123076, 12 pages
doi:10.1155/2012/123076

Research Article

A Comprehensive Subcellular Proteomic Survey of *Salmonella* Grown under Phagosome-Mimicking versus Standard Laboratory Conditions

Roslyn N. Brown,[1] James A. Sanford,[2] Jea H. Park,[1] Brooke L. Deatherage,[1] Boyd L. Champion,[1] Richard D. Smith,[1] Fred Heffron,[3] and Joshua N. Adkins[1]

[1] *Biological Sciences Division, Pacific Northwest National Laboratory, 902 Battelle Boulevard, Richland, WA 99352, USA*
[2] *Biomedical Sciences Graduate Program, University of California San Diego, 9500 Gilman Dive, La Jolla, CA 92063, USA*
[3] *Department of Molecular Microbiology and Immunology, Oregon Health and Science University, 3181 SW Sam Jackson Park Road, Portland, OR 97239, USA*

Correspondence should be addressed to Joshua N. Adkins, joshua.adkins@pnnl.gov

Received 16 March 2012; Accepted 6 June 2012

Academic Editor: Gary B. Smejkal

Towards developing a systems-level pathobiological understanding of *Salmonella enterica*, we performed a subcellular proteomic analysis of this pathogen grown under standard laboratory and phagosome-mimicking conditions *in vitro*. Analysis of proteins from cytoplasmic, inner membrane, periplasmic, and outer membrane fractions yielded coverage of 25% of the theoretical proteome. Confident subcellular location could be assigned to over 1000 proteins, with good agreement between experimentally observed location and predicted/known protein properties. Comparison of protein location under the different environmental conditions provided insight into dynamic protein localization and possible moonlighting (multiple function) activities. Notable examples of dynamic localization were the response regulators of two-component regulatory systems (e.g., ArcB and PhoQ). The DNA-binding protein Dps that is generally regarded as cytoplasmic was significantly enriched in the outer membrane for all growth conditions examined, suggestive of moonlighting activities. These observations imply the existence of unknown transport mechanisms and novel functions for a subset of *Salmonella* proteins. Overall, this work provides a catalog of experimentally verified subcellular protein locations for *Salmonella* and a framework for further investigations using computational modeling.

1. Introduction

The pursuit of a systems-level understanding of bacterial physiology requires not only knowledge about the identity, function, and relative abundance of proteins, but also insight into the subcellular localization of these proteins. Subcellular protein localization is linked to protein function, potential protein-protein interactions, and to interactions between a cell and its exterior environment. The observation of proteins in unexpected cellular compartments gives clues about the presence of possible alternate functions. Hence, there is a growing appreciation for the presence of bacterial "moonlighting proteins," that is, those proteins that have a secondary function depending on subcellular location [1–3]. Experimentally verified localization also provides a foundation for describing proteins that are "hypothetical," uncharacterized, or that contain domains of unknown function. Furthermore, with the increasing use of systems biology approaches, including genome-scale models of metabolism [4] and regulation to study microbial functions, experimentally founded protein localization on a global scale is necessary to produce more accurate model constraints.

Subcellular proteomics has emerged as a powerful tool for large-scale profiling of protein subcellular location [5–9]. Unlike traditional Western blot or high-resolution microscopy methods that rely on the use of antibodies or molecular tags to identify individual proteins, proteomic methods enable high-throughput, unbiased, and large-scale

identification of the protein complement of subcellular fractions [5, 6, 10]. Moreover, interrogation of the subcellular proteome under different growth or environmental conditions allows for the investigation of changes in protein abundance and possibly protein location.

Subcellular proteomic analysis of bacterial pathogens holds promise for identifying novel virulence determinants and potential therapeutic targets [11–13]. For Gram-negative pathogens such as *Salmonella enterica*, each of the four main protein-containing compartments—the outer and inner membranes, periplasm, and cytoplasm—is a potential source of virulence determinants. Outer membrane/cell surface proteins mediate adhesion, cell-cell communication, immune evasion, sequestration, transport (including antibiotic efflux), and secretion, whereas inner membrane proteins accomplish transport and assembly of complex structures, such as flagella and secretion apparati. Periplasmic proteins sense and respond to the host environment, and cytoplasmic proteins include secretion substrates, chaperones, and housekeeping proteins important in maintaining the pathogenic lifestyle. Comprehensive characterization of these subcellular fractions can provide insight into the potential for virulence-related interactions with the host as well as fundamental information on the subcellular architecture of this organism.

Our present goals were twofold: (1) to survey the localization of proteins in *Salmonella* cells as a reference of protein localization in this bacterium and (2) to observe changes in protein abundance or location upon growth under phagosome-mimicking conditions relative to standard laboratory conditions to generate new biological insights, as well as improved data for computational modeling. Towards this end, cytoplasmic (CYT), inner membrane (IM), periplasmic (PERI), and outer membrane (OM) fractions were analyzed using liquid chromatography-tandem mass spectrometry (LC-MS/MS). We did not analyze the secretome as we recently completed an extensive analysis of the proteins secreted by *Salmonella* under phagosome-mimicking conditions [14]. In the present study, over 25% of the theoretical *Salmonella* proteome was represented, and confident assignment of subcellular locations was achieved for most proteins. In addition, we assigned subcellular-level localization to the response of the bacteria to growth under conditions that mimic the host macrophage intracellular environment. This study represents the most comprehensive global survey of subcellular localization in *Salmonella* to date and affords a resource to others interested in protein location, improving location predictions and systems computational models.

2. Methods

2.1. Rationale for Media and Strains Used in This Study. Growth to mid-logarithmic phase in Luria-Bertani broth represents a standard laboratory growth condition in this study and is noninducing for *Salmonella* pathogenicity island 2 (SPI-2) gene expression [15]. Growth of *Salmonella* in defined, acidic media with low concentrations of phosphate and magnesium induces expression of SPI-2 genes that are required for intracellular survival and replication [15–19]. mLPM has been shown to induce expression and secretion of SPI2-related virulence factors [14] and was used in this study to mimic the environment of a macrophage phagosome.

We previously identified flagellin (especially FliC) as one of the most abundant proteins secreted by *Salmonella* into culture media [14] and also in cell envelope fractions (Supplemental Table 1, supplementary material available online at doi: no# 10.1155/2012/123076). *Salmonella* flagellins are downregulated during the intracellular stage of infection, and SPI-2-expressing bacteria are not motile [20]. Since flagella are not relevant to the stage of infection we intended to mimic, we deleted flagellin genes *fliC* and *fljB* from wildtype *Salmonella enterica* serovar Typhimurium (*S.* Typhimurium) ATCC 14028 in an attempt to achieve better sensitivity by depleting these abundant proteins.

2.2. Bacterial Strains, Media, and Chemicals. Bacteria were maintained in LB broth (Difco, Franklin Lakes, NJ, USA) or on LB plates. Unless otherwise noted, components of mLPM [14] and other chemicals were purchased from Sigma (St. Louis, MO, USA). Protein concentrations were determined by bicinchoninic acid (BCA) assay (Pierce, Rockford, IL, USA) using bovine serum albumin as standards. Trypsin used for protein digestions was purchased from Promega (Madison, WI, USA).

2.3. Deletion of Flagellin Genes. In an attempt to achieve better sensitivity by depleting a nonessential abundant protein (Supplemental Table 1), a double-flagellin mutant (Δ*fliC*Δ*fljB*) was created using λ Red recombination [21]. *fliC* was deleted using oligos FliC P1: AGCCCAATAACATCAAGTTGTAATTGATAAGGAAAAGATCGTGTAGGCTGGAGCTGCTTC and FliC P2: CCTTGATTGTGTACCACGTGTCGGTGAATCAATCGCCGGACATATGAATATCCTCCTTAG.

For deleting *fljB*, oligos FljB P1: GATTTTCTCCTTTACATCAGATAAGGAAGAATTTTAGTCGGTGTAGGCTGGAGCTGCTTC and FljB P2: CTCGCCCGTAGGAAATATCATTTACAGCCATACATTCCATCATATGAATATCCTCCTTAG were used. Underlined portions of the above oligos represent pKD4 sequences. Insertion of the kanamycin resistance cassette was confirmed using oligos FliC test1: AATGATGAAATTGAAGCCAT and K1: CAGTCATAGCCGAATAGCCT for *fliC* and using FljB test1: AACGCCACCAGGTTTTTCAC and K1 for *fljB*. The kanamycin resistance gene was removed using pCP20 as previously described [21]. The flagellin mutant was tested for lack of motility, compared to the wildtype, using 0.4% agar plates.

2.4. Subcellular Fractionation. Overnight starter cultures of WT and the Δ*fliC*Δ*fljB* mutant were grown in LB broth at 37°C with shaking at 200 rpm. The cultures were diluted 1 : 100 into LB and grown to mid-log phase (OD600 ~ 0.6) for the "LB-log" condition or diluted 1 : 10 into mLPM and grown for 4 or 20 h for "LPM4" and "LPM20," respectively.

The cell fractionation protocol was adapted from that described by Brown et al. [9]. Unless otherwise noted, centrifugation steps were performed at 4°C. Cells were collected via centrifugation (10,000 ×g, 10 min) and washed with 10 mL of 50 mM Tris-HCl (pH 8.0). PERI fractions were generated by suspending cell pellets in 10 mL spheroplasting buffer (50 mM Tris-HCl, pH 8, 250 mM sucrose, 2.5 mM EDTA) and incubating at room temperature for 5 min, after which they were centrifuged at 11,500 ×g for 10 min. Pellets were then suspended in 1.3 mL cold 5 mM $MgSO_4$ and kept on ice for 10 min with occasional mixing. After centrifugation (11,500 ×g, 10 min), the supernatant was retained as the soluble PERI fraction, while the pelleted spheroplasts were suspended in 1.0 mL 20 mM NaH_2PO_4.

Half of the spheroplasts from each condition were then used to perform fractionation into CYT, IM, and OM fractions. The volumes were adjusted to 3.0 mL in 20 mM NaH_2PO_4 and lysed by passing three times through a prechilled French Press (8,000 PSI). Cell lysate suspensions were adjusted to 10 mL using 20 mM NaH_2PO_4 and centrifuged at 5,000 ×g for 30 min to pellet unbroken cells. Supernatants were then centrifuged at 45,000 ×g for 60 min to separate the soluble CYT fraction from the crude membrane pellet. The CYT fractions were centrifuged again to remove residual membrane contaminants. After tubes containing membrane pellets were inverted to dry, the pellets were suspended in 10 mL 20 mM NaH_2PO_4 containing 0.5% Sarkosyl and shaken at 200 rpm for 30 min at room temperature. This mixture was then centrifuged at 45,000 ×g for 60 min to pellet the OM fraction, and the supernatant containing the IM fraction was removed. OM fractions were washed once by suspending in 5 mL NaH_2PO_4 and repeating the centrifugation.

2.5. Tryptic Digests. Tryptic digests of the soluble CYT and PERI fractions were prepared as follows. To 75 μg of protein from each sample, urea and DTT were added to final concentrations of 7 M and 5 mM, respectively, followed by incubation at 60°C for 30 min. Samples were then diluted 7-fold with 100 mM NH_4HCO_3, and $CaCl_2$ was added to a final concentration of 1 mM. Trypsin was then added in a 1 : 50 trypsin : protein ratio, and digestions were performed at 37°C with shaking at 600 rpm for 3 hours. Following digestion, samples were cleaned using 1 mL, 50 mg Discovery DSC-18 solid phase extraction (SPE) columns (Supelco, St. Louis, MO, USA). Briefly, each column was conditioned with methanol and then rinsed with 0.1% TFA in water. Digested samples were run through the columns under vacuum and rinsed with 95 : 5 H_2O : ACN with 0.1% TFA. Excess liquid was removed from the columns, and peptides were eluted using 80 : 20 ACN : H_2O containing 0.1% TFA. Peptides were collected and concentrated using a SpeedVac (Thermo-Savant) to a final volume of 50–100 μL, after which final peptide concentrations were determined by BCA protein assay.

Tryptic digests of the insoluble IM and OM fractions were prepared as follows. To 75 μg of protein from each sample, urea, DTT, and CHAPS were added to final concentrations of 7 M, 10 mM, and 1%, respectively, followed by incubation at 60°C for 30 min. Samples were then diluted 7-fold with 100 mM NH_4HCO_3, and $CaCl_2$ was added to a final concentration of 1 mM. Digestion was performed as described for the soluble fractions. Digested samples were then cleaned using 1 mL, 50 mg Discovery SCX strong cation exchange SPE columns (Supelco, St. Louis, MO, USA). Briefly, columns were conditioned with methanol and then rinsed in varying sequences and amounts of 10 mM ammonium formate in 25% ACN (pH 3.0), 500 mM ammonium formate in 25% ACN (pH 6.8), and nanopure water. Peptide samples were acidified to pH < 4 with formic acid, centrifuged at 10,000 ×g for 5 min, applied to the columns, and washed with 10 mM ammonium formate in 25% ACN (pH 3.0). Peptides were eluted using 80 : 15 : 5 MeOH : H_2O : NH_4OH and concentrated to a final volume of 50–100 μL using a SpeedVac. Final peptide concentrations were calculated by BCA protein assay.

2.6. SDS-PAGE. For visualization of the protein fractions, 5 μg of each protein sample was suspended in NuPAGE LDS sample buffer (Invitrogen, Carlsbad, CA, USA), heated at 70°C for 10 min, and resolved on NuPAGE Novex 4–12% Bis-Tris gradient gels (Invitrogen). Gels were run at a constant voltage of 200 V for 35 min and subsequently stained with GelCode Blue stain (Pierce) to observe protein profiles.

2.7. Capillary LC-MS/MS Analysis. The high-performance liquid chromatography (HPLC) system and method used for nanocapillary liquid chromatography have been described in detail elsewhere [19, 22]. Analysis was performed using an LTQ-Orbitrap mass spectrometer (Thermo Fisher Scientific, San Jose, CA, USA) with electrospray ionization. The HPLC column was coupled to the mass spectrometer using an in-house manufactured interface. The heated capillary temperature and spray voltage were 200°C and 2.2 kV, respectively. Data acquisition began 20 min after the sample was injected and continued for 100 min over an *m/z* range of 400–2000. For each cycle, the six most abundant ions from MS analysis were selected for MS/MS analysis, using a collision energy setting of 35 eV. A dynamic exclusion time of 60 s was used to discriminate against previously analyzed ions. All subcellular fractions from the Δ*fliC*Δ*fljB* mutant were analyzed in addition to the PERI of the WT (Supplemental Table 2) to ensure that the loss of flagellins did not alter periplasmic proteome expression. Each sample was analyzed in triplicate.

2.8. Data Analysis. Peptides were identified by using SEQUEST to search the mass spectra from LC-MS/MS analyses. These searches were performed using the annotated *S.* Typhimurium 14028 FASTA file, containing 5590 protein sequences [23]. Porcine trypsin protein sequences were included in the search to detect trypsin autocleavage contaminants. The SEQUEST parameter file contained no modifications to amino acid residues and a mass error window of 3 *m/z* units for precursor mass and 0 *m/z* units

for fragmentation mass. The searches allowed for all possible peptide termini, that is, not limited by tryptic terminus state. Results were filtered using the MS-Generating Function [24], a software tool that assigns *P* values (spectral probabilities) to spectral interpretations. The prescribed spectral probability cutoff ($1E^{-10}$) was used. This corresponded to a false-positive rate of 0.88% at the unique peptide level and 0.16% and the spectrum level using a traditional decoy approach, that is, searching against a reversed FASTA database [25].

The number of peptide observations from each protein (spectral count) was used as a measure of relative abundance. Multiple charge states of a single peptide were considered as individual observations, as were the same peptides detected in different mass spectral analyses. Similar approaches for quantitation have been described previously [9, 14, 19, 26]. A protein was considered present in a sample (subcellular fraction) only if observed in at least 2 of 3 technical replicates, and means of triplicate samples were adjusted to zero if this rule was not satisfied.

Statistical analyses were performed using Microsoft Excel and R (http://www.r-project.org/). K-means clustering and construction of heat maps were done using OmniViz 6.0.

3. Results

3.1. Protein Identification in Salmonella Subcellular Fractions. To survey the localization of proteins in *Salmonella* cells as a reference of protein localization and to observe changes in protein abundance upon growth under phagosome-mimicking conditions relative to standard laboratory conditions, *S.* Typhimurium 14028 flagellin mutant (see Section 2 for rationale) was grown in Luria-Bertani broth (LB) to log phase or in a low-phosphate, low-magnesium, low-pH minimal medium (LPM) for 4 or 20 h. Subcellular fractionation based on osmotic shock, differential centrifugation, and differential detergent solubilization yielded CYT, IM, PERI, and OM fractions (Figure 1) from which tryptic peptides were identified using LC-MS/MS (see Section 2). The total number of peptide observations from each protein (spectral count) was used as an estimate of relative abundance, and a protein was considered present in a sample only if observed in at least two of three replicates. This step served the dual purpose of globally removing proteins with only one peptide observation and increasing confidence in peptide identifications within each subcellular fraction. The average sequence coverage for each protein was ~30%. Similar numbers of proteins were identified in LB (993), LPM-4h (1102), and LPM-20h (1006) growth conditions.

3.2. Subcellular Fraction Enrichment. Each subcellular fraction contained a unique protein profile (Supplemental Figure 1), although the IM contained a larger proportion of cofractionating CYT proteins, as noted previously [9]. We avoided high-pH treatment of membrane fractions [27] in an attempt to maintain physiologically relevant protein-protein and protein-membrane interactions; thus, peripheral membrane proteins were not removed in our protocol.

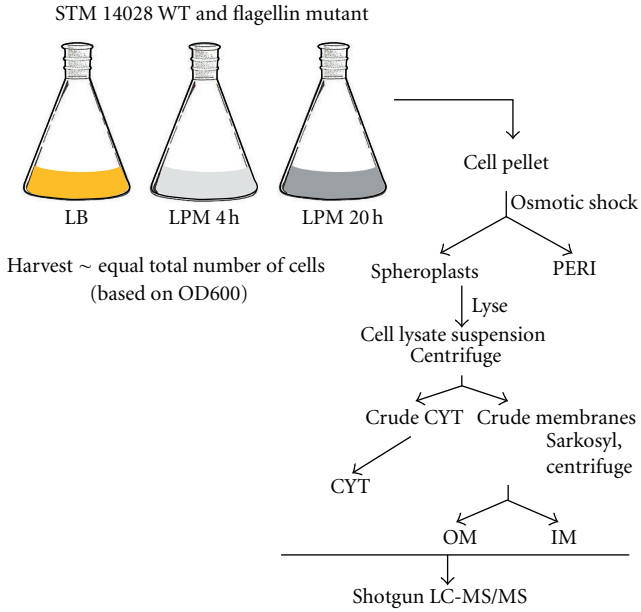

Figure 1: Experimental workflow. A fractionation scheme based on differential centrifugation and Sarkosyl solubilization of membranes was combined with spheroplasting to obtain PERI, CYT, OM, and IM samples from *S.* Typhimurium strain 14028. Subcellular fractions were further processed prior to high-resolution LC-MS/MS analysis.

Agreement between observed and computationally predicted protein localization was assessed. Subcellular predictions were computed using PSORTb [28], with the caveat that ~17% of the observed proteins had no PSORTb subcellular assignment (unknown or unknown with multiple possible localizations). Each subcellular fractionation was enriched in the types of proteins expected to reside there (Figure 2(a); Table 1). Both the IM and OM contained a large number of predicted CYT proteins. Since many proteins were likely observed in multiple fractions as minor contaminants due to cofractionation, protein abundance contributions were more informative than the absolute number of proteins observed [9]. From this analysis, predicted CYT proteins contributed to 80–86% of the total protein abundance in CYT fractions, predicted OM proteins, to 65–80% in OM fractions, and predicted PERI proteins, to 68–75% in PERI fractions. In contrast to the expected agreement between predicted and observed enrichment, predicted IM proteins contributed to only ~25% of the total protein abundance observed in IM fractions (Figure 2(b)). This relatively limited enrichment was due largely to cofractionation of abundant CYT proteins and to the general low observability of integral membrane proteins by proteomics [29, 30].

As many proteins involved in bacterial pathogenesis are located outside the cytoplasm where they may more readily target and respond to the host environment, we assessed our success in enriching envelope proteins in the appropriate fractions. Cell envelope (IM, PERI, and OM) proteins can be distinguished by physicochemical properties, such as hydrophobicity (IM proteins), amphipathic beta sheets (OM

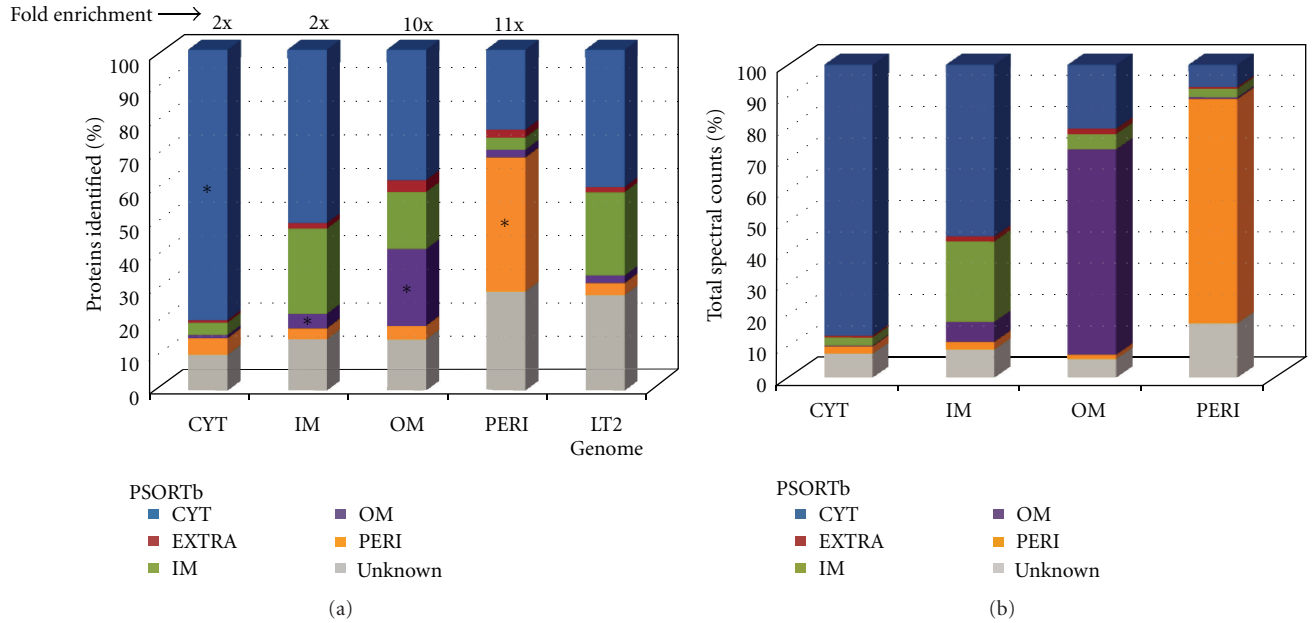

Figure 2: Distribution of proteins observed in subcellular fractions via LC-MS/MS (a). Protein composition of each subcellular fraction, based on number of proteins observed in each fraction sorted according to predicted subcellular location [16]. Data are percentage of proteins observed in each fraction. The fold-enrichment in proteins compared to the genomic potential is noted above each bar. $^*P \leq 0.002$, χ^2 test, compared to genome (b). Summed spectral counts (total abundance) of proteins observed in subcellular fractions.

Table 1: Enrichment of proteins with expected physicochemical properties.

Protein type	CYT	IM	PERI	OM	All observed	In genome	Percentage observed
OM beta barrel	8	27	7	**44**	51	99	52%
Signal Peps	81	120	**130**	100	239	532	45%
TMD > 0	26	**196**	6	54	204	1167	18%
TMD > 1	10	**130**	2	33	130	812	16%
TMD > 2	4	**97**	2	21	97	683	14%
TMD > 3	3	**88**	2	19	88	619	14%
GRAVY > 0	258	**488**	54	140	611	2882	21%
GRAVY > 0.1	158	**335**	31	88	413	2201	19%
GRAVY > 0.2	69	**194**	16	47	231	1637	14%
GRAVY > 0.3	24	**133**	8	34	145	1276	11%
GRAVY ≥ 0.5	3	**66**	0	17	66	890	7%

proteins), and signal peptides (many envelope proteins). The IM, PERI, and OM were significantly enriched in envelope proteins based on observed physicochemical properties. For example, 239 proteins with predicted signal peptides (using PSORTb) were observed (45% of genomic potential). These proteins were mainly identified in the IM, OM, and PERI fractions, with the highest number (130) observed in the PERI (Table 1). Of 51 predicted outer membrane β-barrel proteins [31] observed (51% of genomic potential), 44 of these were in outer membrane fractions. Similarly, proteins with predicted transmembrane α-helices [32], a feature of integral membrane proteins, were concentrated in the IM, as expected. Of 97 proteins with ≥3 transmembrane domains, all were observed in the IM, while only 24 were observed in the other three fractions combined (Table 1). Hydrophobicity, another hallmark of integral membrane proteins [33], correlated well with proteins observed in IM samples. For the 66 proteins that could be considered very hydrophobic (hydrophobicity average ≥0.5) [33], all were observed in the IM with high abundance values (not shown), while 3, 0, and 17 were observed in the CYT, PERI, and OM, respectively.

3.3. Determination of Primary Observed Localization. For proteins observed in multiple subcellular fractions, it was useful to identify the fraction in which each protein was observed at its highest level (i.e., the likely true subcellular location of the protein). Primary localization was determined within each growth condition by calculating the Z-score of protein abundance in each subcellular fraction. Z-scores

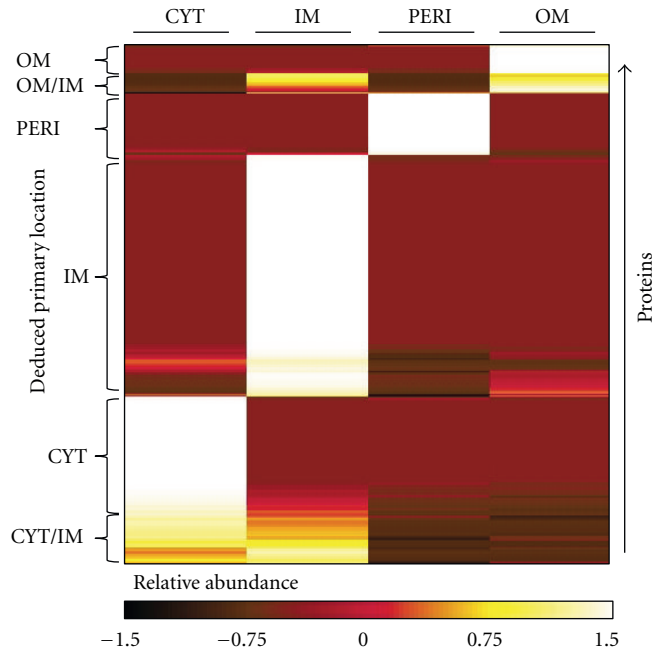

Figure 3: Use of Z-scores and K-means clustering to assign primary subcellular locations to proteins. Since many proteins were observed in two or more subcellular fractions, Z-scores of spectral counts across the four fractions were calculated to highlight the primary observed localization of each protein. K-means clustering was used to group proteins with similar profiles.

Table 2: Two-component regulators showing localization changes depending on growth conditions.

Protein Description (PhoP/Q)	Gene	PSORTb v3	LB 1°Loc	LPM4 1°Loc	LPM20 1°Loc
Sensor protein PhoQ	PhoQ	IM	IM*	IM*	IM*
DNA-binding transcriptional regulator PhoP	PhoP	Cyt	IM/CYT	CYT	CYT
Protein Description (ArcA/B)	Gene	PSORTb v3	LB 1°Loc	LPM4 1°Loc	LPM20 1°Loc
Aerobic respiration control sensor protein ArcB	ArcB	IM	IM*	IM*	IM*
Two-component response regulator	ArcA	Cyt	IM*	IM	CYT

* Indicates that a protein is observed exclusively in one location.

were clustered using the K-means algorithm to group similar profiles of subcellular localization (Figure 3; Supplemental Table 3). Note that similar approaches have been described previously [7, 9]. Using the LB culture as an example, 91% of proteins could be assigned a single primary localization using this scheme.

Some proteins (~9%) were highly observed in two or more subcellular fractions and usually occurred between the CYT and IM or IM and OM. It is noteworthy that six of the 22 IM/OM proteins were lipoproteins, which likely reflects the increased hydrophobicity and tendency to partition with the Sarkosyl-soluble IM. Other members of the IM/OM class included membrane-bound portions of type 3 secretion systems (T3SS): PrgH and PrgK of the invasion-related T3SS and FliF, FliG, and FlgE that represent the ring, basal body, and hook of the flagellar T3SS. In these cases, cofractionation reflects the association of these supramolecular structures with both membranes.

Of the proteins that were multilocalized or had secondary locations, several have been implicated in strong physiologically relevant protein-protein and protein-membrane interactions that can influence localization. For example, seven of the eight subunits of ATP synthase were observed primarily in the IM fraction (Figure 4). While only two subunits are integral to the IM, close protein-protein interactions likely mediated the cofractionation of the entire complex to the IM. Peripheral membrane proteins and multisubunit cytoplasmic proteins made up a majority of the known CYT proteins that had IM or IM/CYT as their primary observed location. Using a combination of available subunit information in Uniprot (http://www.uniprot.org/) and published literature, 45 of the 50 IM/CYT proteins were justified in their observed location due to their multimeric forms or peripheral membrane association that are tied to protein function (Supplemental Table 4).

Another group of proteins in this class were the two-component regulatory systems. These systems consist of a membrane-bound sensor-kinase protein and a cytoplasmic response regulator that interacts with, and is phosphorylated by, the sensor-kinase at the membrane, which promotes DNA binding and regulation of gene expression [34]. In both the PhoP/PhoQ and ArcA/ArcB systems, the sensor-kinases

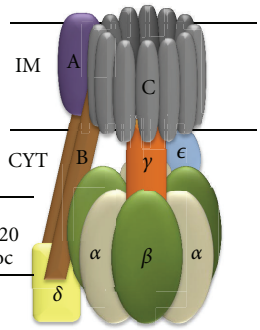

F0F1 ATP synthase subunit	Gene	PSORTb v3	LB 1° Loc	LPM4 1°Loc	LPM20 1°Loc
ϵ	*atpC*	CYT		CYT/IM	IM*
β	*atpD*	CYT	IM	IM	IM
γ	*atpG*	CYT	IM	IM	IM
α	*atpA*	CYT	IM	IM	IM
δ	*atpH*	CYT	IM	IM	IM
A	*atpB*	IM	IM	IM	
B	*atpH*	IM	IM*	IM*	IM

Figure 4: ATP synthase complex exemplifies observed protein-protein and protein-membrane interactions. Schematic representation of membrane-bound ATP synthase, modeled after KEGG Bacterial F-type ATPase Color-coded table shows protein observations in subcellular fractions. n/a: protein not observed. C: AtpE (not observed in this study). *Protein was exclusive to one subcellular fraction in a given growth condition.

were observed exclusively in the IM, while the response regulators were observed either in the IM (i.e., presumably bound to the kinase) or in the CYT (i.e., presumably interacting with DNA), depending on growth condition (Table 2). Our results iterate that PhoP is bound to DNA during growth in LPM (for either 4 or 20 h), which is supported by known activation of the PhoP regulon within acidified macrophage phagosomes [35] and during growth under phagosome-mimicking conditions [26]. Conversely, the response regulator ArcA is IM-localized in cells grown in LB or those grown in LPM for a short duration, but is CYT-localized in cells grown overnight in LPM. These results provide insight into the function of this regulatory system under these specific growth conditions.

We note that some instances of multilocalized proteins may be due to the inability of our methods to perfectly resolve subcellular fractions, or may be artifacts of fractionation. As an example of the latter, DnaK and Ef-Tu can be translocated out of the cytoplasm during osmotic shock [36]. In our study, Ef-Tu was observed at high levels in both the IM and CYT. While DnaK was observed primarily in the CYT, DnaJ, a cochaperone with DnaK, was observed primarily in the IM in all growth conditions in this study.

For those proteins annotated as "putative" ($n = 274$) or "hypothetical" ($n = 92$), we were able to confidently assign localization to a majority based on protein abundances in subcellular fractions (Supplemental Table 5). For many of these proteins, the assignment of subcellular localization as well as data on relative expression levels in different growth conditions represents the most extensive characterization available to date.

3.4. Putative Moonlighting Proteins. Some proteins were observed in unexpected subcellular locations regardless of growth condition, while the location of other proteins appeared to be influenced by growth condition. Several proteins with well-characterized housekeeping roles (e.g., enolase and glyceraldehyde-3-phosphate dehydrogenase) have been observed on the cell surfaces of pathogens, where they have secondary functions such as adhesion and immune modulation [3]. The term "moonlighting" refers to proteins that exhibit more than one biological function [1–3]. Here too, proteins that were observed in unexpected locations based on predictions, annotations, and known functions could point to novel interactions or functions yet to be characterized. In these cases, proteins with higher spectral counts (relative abundance) and greater numbers of unique peptides (more confident identifications) were considered more reliable candidates for assignment of localization.

One of the best moonlighting protein candidates observed in this study is Dps (DNA protection during starvation). This protein has been well characterized as a cytoplasmic DNA-binding protein (reviewed in [37]) and has no predicted signal peptide. In each growth condition tested, we observed Dps significantly enriched in the OM fraction (Figure 5), which shows for the first time that this protein is OM-localized in *Salmonella*. Dps is a known virulence determinant of *Salmonella* [38], but how it translocates to the OM and its role(s) at the cell surface remain to be investigated. Interestingly, Dps was recently observed on the cell surface of *Escherichia coli* [38, 39], where it may play a role in attachment to abiotic surfaces [38]. We observed >2-fold increase in the relative abundance of OM-localized Dps between LB and LPM20 growth conditions, which indicates that *Salmonella* Dps is responsive to growth under phagosome-mimicking conditions (Figure 5).

Because the CYT and OM are the two most physically separated subcellular locations studied here and contain proteins with fairly distinct physicochemical properties, we considered known cytoplasmic proteins observed in the OM as the most promising moonlighting candidates.

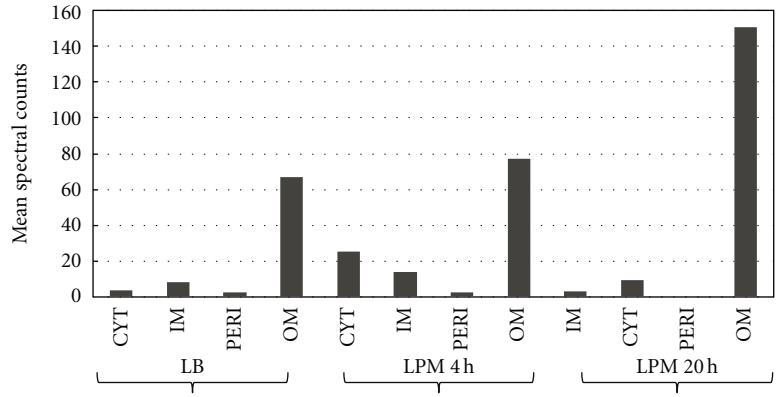

Figure 5: Localization and relative abundance of potential moonlighting protein, Dps. Spectral counts of Dps in each subcellular fraction in each growth condition. Values are means of 3 replicates.

These candidates included a (3R)-hydroxymyristoyl-ACP dehydratase (FabZ), a curved DNA-binding protein (CbpA), an imidazole glycerol-phosphate dehydratase/histidinol phosphatase (HisB), and an ATP-dependent RNA helicase (SrmB). All of these cases included proteins generally accepted to be cytoplasmic, with no detectable signal peptides, transmembrane helices, or beta barrel predictions that were confidently observed in OM or in a mix of OM and IM fractions (Supplemental Table 6). These proteins represent the first candidates for an investigation of moonlighting activities in *Salmonella*.

3.5. Subcellular Responses to Growth Conditions. Although not a perfect replica of the *in vivo* environment, defined *in vitro* synthetic growth media provide valuable insights into the pathogenic strategies of *Salmonella* [40, 41]. Growth in LB to mid-exponential phase induces genes of the *Salmonella* pathogenicity island 1 (SPI-1) involved in host cell invasion [42–44], while genes of the *Salmonella* pathogenicity island 2 (SPI-2) can be induced by growth in LPM that simulates the environment of the *Salmonella*-containing vacuole (phagosome) [45, 46]. We used these growth conditions to probe the subcellular-level responses of *Salmonella* to phagosome-mimicking conditions.

When qualitatively assessed, similar numbers of proteins were observed in the three growth conditions: 993 in LB, 1102 in LPM-4h, and 1006 in LPM-20h. Approximately 10% of the proteins identified in each growth condition were unique to a given culture: 175 in LB, 100 in LPM-4h, and 92 in LPM-20h (Supplemental Figure 2), and less than half of all identified proteins (688) were observed in all growth conditions, which underscores the utility of using multiple growth conditions for improved coverage of a bacterial proteome.

We have previously investigated the proteome response of *Salmonella* to phagosome-mimicking *in vitro* conditions [19, 26]; however, the use of subcellular fractionation presented an opportunity for obtaining better proteome coverage, especially of proteins that are typically under-represented in global proteomic strategies, in addition to highlighting the subcellular location of proteins of interest. Based on studies of *Salmonella* grown in acidic minimal media [19, 26], we confirmed the expected increases in abundance of proteins associated with the SPI-2 T3SS (SsaC, SseA, and SsaJ), the SsrB regulon (SsrA, SsrB, and SrfN), and the PhoP regulon (PhoP, PhoQ, PagC, MgtA, and MgtB) during growth in LPM (Supplemental Table 7). Conversely, proteins related to the invasion-associated SPI-1 T3SS (SipA, B, C, D, SopB, SicA, InvG, PrgK, and PrgL) decreased in abundance with growth in LPM. Further analyses focused on envelope proteins because the proteins primarily detected in previous global analyses were cytoplasmic proteins and because envelope proteins have high potential for host-pathogen interactions.

OM proteins whose abundance increased during growth in LPM included iron transporters (FepA, FhuA, IroN, and FoxA), ABC transporters, and virulence-related proteins (PagC; T3SS-related SsaC and SseC), which reflects the nutrient-limited and virulence gene-inducing nature of LPM (Figure 6(a)). A notable OM protein was the outer membrane protease PgtE that was increased 13- and 89-fold in LPM4 and LPM20, respectively ($P < 0.001$). PgtE is involved in cleavage of serum complement during the extracellular phase of *Salmonella* systemic infection [47], but its induction under phagosome-mimicking conditions suggests an intracellular role as well. In addition to the importance of OM proteins that increase in abundance in LPM, those that decrease in abundance may be indicative of immune evasion or virulence-related OM remodeling. For example, putative outer membrane lipoprotein maltoporin and outer membrane protein N were significantly decreased during growth in LPM for 20 h (Supplemental Table 7). Known SPI-1 T3SS-related surface proteins such as PrgK, PrgI, and InvG were also significantly decreased in the OM during growth in LPM, indicating the expected shift away from SPI-1 T3SS expression during growth in LPM.

Notable in the IM was a decrease in chemotaxis-related proteins (CheA, B, M, and Z; Tsr, Trg, and Tcp) and motility-related proteins (FliF, FliI, FliN, and MotA) in LPM compared to LB. A range of IM-integral and peripheral IM proteins of various functions were enriched during growth in LPM, including expected functions such as magnesium

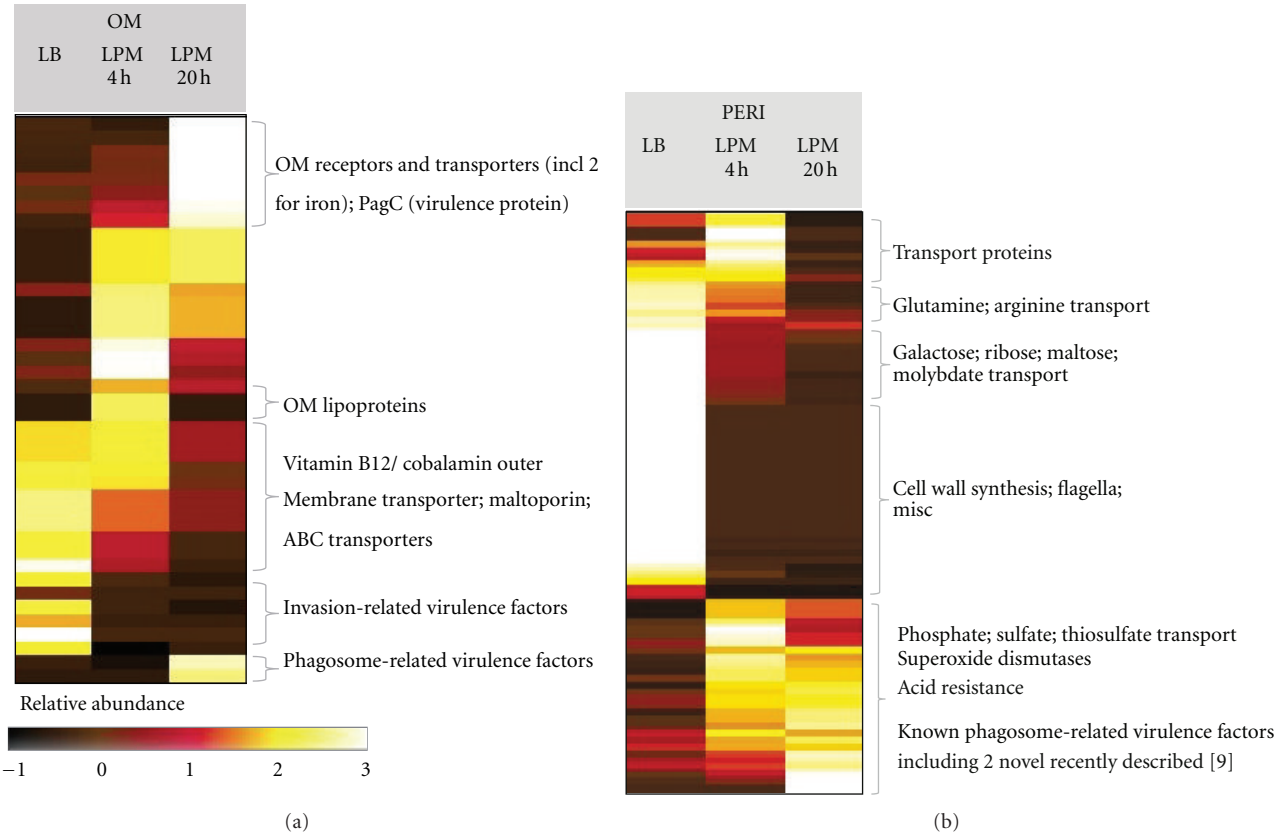

Figure 6: Heat map representation of differentially expressed OM and PERI proteins. Z-scores of protein abundance were calculated across the 3 growth conditions for proteins observed at their highest levels in the OM (a) and PERI (b) fractions. Each protein showed ≥ 2-fold difference in abundance in any two growth conditions.

transport (MgtA and MgtB), virulence proteins (PhoQ and SsaC), and various transporters, enzymes, and proteins of unknown function (Supplemental Table 7).

The PERI shifted from transport of sugars (galactose, ribose, and maltose), oligopeptides, dipeptides, aminoacids, and related compounds (arginine and putrescine) in LB to transport of phosphate, sulfate, and thiosulfate in LPM (Figure 6(b)). Also showing increased abundance in LPM were PERI proteins involved in superoxide and acid resistance (SodC and PhoN) and known secreted factors CigR [14] and SrfN [48, 49] for which the subcellular location prior to being translocated into infected mammalian cells was previously unknown.

4. Discussion

Comparative proteomics is an emerging tool for studying bacterial pathogenesis both *in vitro* and during infection [19, 26, 50]. Subcellular fractionation complements such analyses by providing a means to resolve physiologically relevant protein location in the bacterium. Our analysis of CYT, IM, PERI, and OM fractions of *S.* Typhimurium grown under laboratory and phagosome-mimicking conditions yielded ~1400 unique proteins, most of which could be confidently localized to a single subcellular fraction in a given growth condition. Each subcellular fraction contained a unique protein profile (Figures 1 and 3 and Supplemental Figure 1) and protein physicochemical properties generally agreed well with their observed localization (Table 1).

To our knowledge, this study represents the most comprehensive global survey of subcellular localization in *Salmonella* to date. In earlier work, Coldham and Woodward [51] assessed cytosolic, cell envelope, and outer membrane protein preparations of *Salmonella* by extensive chromatographic fractionation followed by mass spectrometry. They observed 816 proteins, with 371 in the CYT, 565 in the envelope, and 262 in the OM samples. Of the latter 262, only 20 were OM proteins. Recently, the OM proteome of *S. enterica* was identified using a lipid-based method [52]. In that study, 54 OM proteins were identified with ≥2 peptides, using a multistep digest procedure on outer membrane vesicle preparations. In an early attempt to catalogue the OM proteome of *Escherichia coli*, Molloy and colleagues [27] identified ~30 proteins in the OM fraction, using 2D gel electrophoresis and MS approach. In our present study, at least 74 OM proteins were identified in OM fractions (deduced by PSORTb prediction, annotation, or by the presence of OM β-sheets). In addition to high coverage of OM proteins, confident assignment of CYT, IM, and PERI proteins was presented (Supplemental Table 3).

Among the challenges in any subcellular fractionation endeavor are to maximize fraction purity and correctly assign proteins to a subcellular location. Due to the close proximity of fractions, protein-protein interactions between fractions, or to the presence of protein domains that span multiple fractions, proteins sometimes copurify to two or more fractions. These biological phenomena are difficult to distinguish from experimental noise. In our analysis, large multi-subunit cytoplasmic complexes often concentrated in the membrane fractions (particularly the IM); likewise, many protein complexes that are known to be peripherally IM-associated also co-fractionated with the IM (e.g., ATP synthase). In cases where a protein was observed in multiple fractions, we were able to use relative abundance data to deduce the primary observed localization (Figure 3). However, some fractions posed more of a challenge than others; for example, the IM was more ambiguous than the OM, PERI, or CYT. Over 40% of proteins whose primary observed location was the IM were predicted by PSORTb to be cytoplasmic. It is important to note that this localization prediction does not take into account the many potential IM-interacting proteins. While the IM fraction is a good potential source of novel protein-protein and protein-membrane interactions, a clearer picture of the integral IM landscape could emerge upon high-pH buffer treatment of the IM fraction to remove peripherally bound proteins [27].

An aspect of this study that may be helpful to others interested in subcellular proteome characterization was our use of a mutant that was depleted in an abundant cell envelope component, flagellin (Δ*fliC*Δ*fljB*). Because flagellin was one of the most abundant proteins observed in the PERI (and contaminated all envelope fractions) in a preliminary subcellular proteomic analysis (Supplemental Table 1), we hypothesized that deleting flagellin genes would enable better detection of low abundance of PERI proteins and likely increase the signal of most other proteins in the PERI fraction. Flagella are not essential for survival in macrophage phagosomes [53] and are downregulated under the environmental conditions simulated by our mLPM culture condition [20]. Thus, deleting flagellins should not interfere with the physiological responses we were interested in. In addition, flagella are nonessential for growth in LB (not shown). Proteomic analysis of the wild type versus Δ*fliC*Δ*fljB* mutant PERI fractions showed no differences in presence of "housekeeping" proteins such as elongation factor Tu, elongation factor G, chaperonin GroEL, and ribosomal proteins that co-fractionated with the PERI (Supplemental Table 2). Also, IM and OM proteins that co-fractionated with the PERI were observed at similar (low) levels in both the wild type and mutant. Most importantly, we observed higher spectral counts of PERI proteins in the mutant relative to wild type, and several PERI proteins were detected only in the flagellin mutant (Supplemental Table 2). Thus, we advocate the use of relevant mutations in abundant nonessential proteins for improved subcellular proteome coverage.

The availability of experimentally observed subcellular localization data for such a large number of *Salmonella* proteins provides opportunities for further study. Among these opportunities are using high-confidence localization information for training subcellular localization prediction tools and for computationally predicting *Salmonella* function in host cells through the use of genome-scale models [4]. In addition, localization data for hypothetical or uncharacterized proteins (Supplemental Table 5) is a first step towards functional characterization of these unknown proteins. To extend the utility of these data, our future study will focus on multilocalized proteins and those that changed localization depending on growth condition. Both categories present the possibility of exciting discoveries in terms of protein function. Moonlighting protein candidates are included in this class; determining the transport mechanism and secondary function of our candidates are challenges for future study.

In summary, we presented a comparative subcellular proteomic analysis of *Salmonella* representative of laboratory growth and infection-like states. We cataloged the confident localization of over 1000 proteins and provided evidence of differential protein movement and the appearance of some proteins in unexpected subcellular compartments. These results imply the existence of unknown transport mechanisms and novel functions for a subset of *Salmonella* proteins.

Abbreviations

IM:	Inner membrane
OM:	Outer membrane
CYT:	Cytoplasmic
PERI:	Periplasmic
WCL:	Whole cell lysate
LC-MS/MS:	Liquid chromatography-tandem mass spectrometry
TTSS:	Type III secretion system
SPI:	*Salmonella* pathogenicity island.

Acknowledgments

The authors thank Robbie Heegel and Dr. Joseph Brown for their contributions to this research. Support for this work was provided by the National Institute of Allergy and Infectious Diseases NIH/DHHS through interagency agreement Y1-A1-8401-01. Proteomic analyses were performed in the Environmental Molecular Sciences Laboratory, a U.S Department of Energy Office of Biological and Environmental Research (DOE/BER) national scientific user facility on the Pacific Northwest National Laboratory (PNNL) campus in Richland, Washington. PNNL is a multiprogram national laboratory operated by Battelle for the DOE under Contract DE-AC05-76RL01830. This work used instrumentation and capabilities developed with funds provided by NIH grants from the National Center for Research Resources (5P41RR018522-10) and the National Institute of General Medical Sciences (8 P41 GM103493-10) and by DOE/BER. Mass spectrometry results are available via http://SysBEP.org/ and http://omics.pnl.gov/.

References

[1] N. R. Smalheiser, "Proteins in unexpected locations," *Molecular Biology of the Cell*, vol. 7, no. 7, pp. 1003–1014, 1996.

[2] V. Pancholi and G. S. Chhatwal, "Housekeeping enzymes as virulence factors for pathogens," *International Journal of Medical Microbiology*, vol. 293, no. 6, pp. 391–401, 2003.

[3] B. Henderson and A. Martin, "Bacterial virulence in the moonlight: multitasking bacterial moonlighting proteins are virulence determinants in infectious disease," *Infection and Immunity*, vol. 79, no. 9, pp. 3476–3491, 2011.

[4] I. Thiele, D. R. Hyduke, B. Steeb et al., "A community effort towards a knowledge-base and mathematical model of the human pathogen *Salmonella* Typhimurium LT2," *BMC Systems Biology*, vol. 5, p. 8, 2011.

[5] M. Dreger, "Subcellular proteomics," *Mass Spectrometry Reviews*, vol. 22, no. 1, pp. 27–56, 2003.

[6] M. Dreger, "Proteome analysis at the level of subcellular structures," *European Journal of Biochemistry*, vol. 270, no. 4, pp. 589–599, 2003.

[7] S. J. Callister, M. A. Dominguez, C. D. Nicora et al., "Application of the accurate mass and time tag approach to the proteome analysis of sub-cellular fractions obtained from Rhodobacter sphaeroides 2.4.1. aerobic and photosynthetic cell cultures," *Journal of Proteome Research*, vol. 5, no. 8, pp. 1940–1947, 2006.

[8] M. Thein, G. Sauer, N. Paramasivam, I. Grin, and D. Linke, "Efficient subfractionation of gram-negative bacteria for proteomics studies," *Journal of Proteome Research*, vol. 9, no. 12, pp. 6135–6147, 2010.

[9] R. N. Brown, M. F. Romine, A. A. Schepmoes, R. D. Smith, and M. S. Lipton, "Mapping the subcellular proteome of *Shewanella* oneidensis MR-1 using sarkosyl-based fractionation and LC-MS/MS protein identification," *Journal of Proteome Research*, vol. 9, no. 9, pp. 4454–4463, 2010.

[10] E. Jung, M. Heller, J.-C. Sanchez, and D. F. Hochstrasser, "Proteomics meets cell biology: the establishment of subcellular proteomes," *Electrophoresis*, vol. 21, no. 16, pp. 3369–3377, 2000.

[11] C. Bell, G. T. Smith, M. J. Sweredoski, and S. Hess, "Characterization of the mycobacterium tuberculosis proteome by liquid chromatography mass spectrometry-based proteomics techniques: a comprehensive resource for tuberculosis research," *Journal of Proteome Research*, vol. 11, no. 1, pp. 119–130, 2012.

[12] D. Becher, K. Hempel, S. Sievers et al., "A proteomic view of an important human pathogen-towards the quantification of the entire staphylococcus aureus proteome," *PLoS One*, vol. 4, no. 12, p. e8176, 2009.

[13] E. Carlsohn, J. Nyström, H. Karlsson, A. M. Svennerholm, and C. L. Nilsson, "Characterization of the outer membrane protein profile from disease-related *Helicobacter pylori* isolates by subcellular fractionation and nano-LC FT-ICR MS analysis," *Journal of Proteome Research*, vol. 5, no. 11, pp. 3197–3204, 2006.

[14] G. S. Niemann, R. N. Brown, J. K. Gustin et al., "Discovery of novel secreted virulence factors from *Salmonella enterica* serovar Typhimurium by proteomic analysis of culture supernatants," *Infection and Immunity*, vol. 79, no. 1, pp. 33–43, 2011.

[15] U. Silphaduang, M. Mascarenhas, M. Karmali, and B. K. Coombes, "Repression of intracellular virulence factors in *Salmonella* by the Hha and YdgT nucleoid-associated proteins," *Journal of Bacteriology*, vol. 189, no. 9, pp. 3669–3673, 2007.

[16] D. M. Cirillo, R. H. Valdivia, D. M. Monack, and S. Falkow, "Macrophage-dependent induction of the *Salmonella* pathogenicity island 2 type III secretion system and its role in intracellular survival," *Molecular Microbiology*, vol. 30, no. 1, pp. 175–188, 1998.

[17] J. Delwick, T. Nikolaus, S. Erdogan, and M. Hensel, "Environmental regulation of *Salmonella* pathogenicity island 2 gene expression," *Molecular Microbiology*, vol. 31, no. 6, pp. 1759–1773, 1999.

[18] B. K. Coombes, N. F. Brown, Y. Valdez, J. H. Brumell, and B. B. Finlay, "Expression and secretion of *Salmonella* pathogenicity island-2 virulence genes in response to acidification exhibit differential requirements of a functional type III secretion apparatus and SsaL," *Journal of Biological Chemistry*, vol. 279, no. 48, pp. 49804–49815, 2004.

[19] J. N. Adkins, H. M. Mottaz, A. D. Norbeck et al., "Analysis of the *Salmonella* Typhimurium proteome through environmental response toward infectious conditions," *Molecular and Cellular Proteomics*, vol. 5, no. 8, pp. 1450–1461, 2006.

[20] L. A. Knodler, B. A. Vallance, J. Celli et al., "Dissemination of invasive *Salmonella* via bacterial-induced extrusion of mucosal epithelia," *Proceedings of the National Academy of Sciences of the United States of America*, vol. 107, no. 41, pp. 17733–17738, 2010.

[21] K. A. Datsenko and B. L. Wanner, "One-step inactivation of chromosomal genes in *Escherichia coli* K-12 using PCR products," *Proceedings of the National Academy of Sciences of the United States of America*, vol. 97, no. 12, pp. 6640–6645, 2000.

[22] Y. Shen, N. Tolić, R. Zhao et al., "High-throughput proteomics using high-efficiency multiple-capillary liquid chromatography with on-line high-performance ESI FTICR mass spectrometry," *Analytical Chemistry*, vol. 73, no. 13, pp. 3011–3021, 2001.

[23] T. Jarvik, C. Smillie, E. A. Groisman, and H. Ochman, "Short-term signatures of evolutionary change in the *Salmonella enterica* serovar Typhimurium 14028 genome," *Journal of Bacteriology*, vol. 192, no. 2, pp. 560–567, 2010.

[24] S. Kim, N. Gupta, and P. A. Pevzner, "Spectral probabilities and generating functions of tandem mass spectra: a strike against decoy databases," *Journal of Proteome Research*, vol. 7, no. 8, pp. 3354–3363, 2008.

[25] J. Peng, J. E. Elias, C. C. Thoreen, L. J. Licklider, and S. P. Gygi, "Evaluation of multidimensional chromatography coupled with tandem mass spectrometry (LC/LC-MS/MS) for large-scale protein analysis: the yeast proteome," *Journal of Proteome Research*, vol. 2, no. 1, pp. 43–50, 2003.

[26] L. Shi, C. Ansong, H. Smallwood et al., "Proteome of *Salmonella enterica* serotype Typhimurium grown in a low Mg^{2+}/pH medium," *Journal of Proteomics and Bioinformatics*, vol. 2, no. 9, pp. 388–397, 2009.

[27] M. P. Molloy, B. R. Herbert, M. B. Slade et al., "Proteomic analysis of the *Escherichia coli* outer membrane," *European Journal of Biochemistry*, vol. 267, no. 10, pp. 2871–2881, 2000.

[28] N. Y. Yu, J. R. Wagner, M. R. Laird et al., "PSORTb 3.0: improved protein subcellular localization prediction with refined localization subcategories and predictive capabilities for all prokaryotes," *Bioinformatics*, vol. 26, no. 13, pp. 1608–1615, 2010.

[29] V. Santoni, M. Molloy, and T. Rabilloud, "Membrane proteins and proteomics: un amour impossible?" *Electrophoresis*, vol. 21, no. 6, pp. 1054–1070, 2000.

[30] T. Rabilloud, "Membrane proteins and proteomics: love is possible, but so difficult," *Electrophoresis*, vol. 30, supplement

1, pp. S174–S180, 2009.

[31] F. S. Berven, K. Flikka, H. B. Jensen, and I. Eidhammer, "BOMP: a program to predict integral β-barrel outer membrane proteins encoded within genomes of Gram-negative bacteria," *Nucleic Acids Research*, vol. 32, pp. W394–W399, 2004.

[32] L. Käll, A. Krogh, and E. L. L. Sonnhammer, "A combined transmembrane topology and signal peptide prediction method," *Journal of Molecular Biology*, vol. 338, no. 5, pp. 1027–1036, 2004.

[33] J. Kyte and R. F. Doolittle, "A simple method for displaying the hydropathic character of a protein," *Journal of Molecular Biology*, vol. 157, no. 1, pp. 105–132, 1982.

[34] R. B. Bourret, K. A. Borkovich, and M. I. Simon, "Signal transduction pathways involving protein phosphorylation in prokaryotes," *Annual Review of Biochemistry*, vol. 60, pp. 401–441, 1991.

[35] C. M. Alpuche Aranda, J. A. Swanson, W. P. Loomis, and S. I. Miller, "*Salmonella* Typhimurium activates virulence gene transcription within acidified macrophage phagosomes," *Proceedings of the National Academy of Sciences of the United States of America*, vol. 89, no. 21, pp. 10079–10083, 1992.

[36] C. Berrier, A. Garrigues, G. Richarme, and A. Ghazi, "Elongation factor Tu and DnaK are transferred from the cytoplasm to the periplasm of *Escherichia coli* during osmotic downshock presumably via the mechanosensitive channel MscL," *Journal of Bacteriology*, vol. 182, no. 1, pp. 248–251, 2000.

[37] L. N. Calhoun and Y. M. Kwon, "Structure, function and regulation of the DNA-binding protein Dps and its role in acid and oxidative stress resistance in *Escherichia coli*: a review," *Journal of Applied Microbiology*, vol. 110, no. 2, pp. 375–386, 2011.

[38] R. M. Goulter-Thorsen, I. R. Gentle, K. S. Gobius, and G. A. Dykes, "The DNA protection during starvation protein (Dps) influences attachment of *Escherichia colis* to abiotic surfaces," *Foodborne Pathogens and Disease*, vol. 8, no. 8, pp. 939–941, 2011.

[39] A. Lacqua, O. Wanner, T. Colangelo, M. G. Martinotti, and P. Landini, "Emergence of biofilm-forming subpopulations upon exposure of *Escherichia coli* to environmental bacteriophages," *Applied and Environmental Microbiology*, vol. 72, no. 1, pp. 956–959, 2006.

[40] S. Löber, D. Jäckel, N. Kaiser, and M. Hensel, "Regulation of *Salmonella* pathogenicity island 2 genes by independent environmental signals," *International Journal of Medical Microbiology*, vol. 296, no. 7, pp. 435–447, 2006.

[41] C. R. Beuzón, G. Banks, J. Deiwick, M. Hensel, and D. W. Holden, "pH-dependent secretion of SseB, a product of the SPI-2 type III secretion system of *Salmonella* Typhimurium," *Molecular Microbiology*, vol. 33, no. 4, pp. 806–816, 1999.

[42] E. A. Miao and S. I. Miller, "A conserved amino acid sequence directing intracellular type III secretion by *Salmonella* Typhimurium," *Proceedings of the National Academy of Sciences of the United States of America*, vol. 97, no. 13, pp. 7539–7544, 2000.

[43] K. Eichelberg and J. E. Galán, "Differential regulation of *Salmonella* Typhimurium type III secreted proteins by pathogenicity island 1 (SPI-1)-encoded transcriptional activators InvF and HilA," *Infection and Immunity*, vol. 67, no. 8, pp. 4099–4105, 1999.

[44] K. Ehrbar, B. Winnen, and W. D. Hardt, "The chaperone binding domain of SopE inhibits transport via flagellar and SPI-1 TTSS in the absence of InvB," *Molecular Microbiology*, vol. 59, no. 1, pp. 248–264, 2006.

[45] B. K. Coombes, M. J. Lowden, J. L. Bishop et al., "SseL is a *Salmonella*-specific translocated effector integrated into the SsrB-controlled *Salmonella* pathogenicity island 2 type III secretion system," *Infection and Immunity*, vol. 75, no. 2, pp. 574–580, 2007.

[46] X. J. Yu, K. McGourty, M. Liu, K. E. Unsworth, and D. W. Holden, "pH sensing by intracellular *Salmonella* induces effector translocation," *Science*, vol. 328, no. 5981, pp. 1040–1043, 2010.

[47] P. Ramu, R. Tanskanen, M. Holmberg, K. Lähteenmäki, T. K. Korhonen, and S. Meri, "The surface protease PgtE of *Salmonella enterica* affects complement activity by proteolytically cleaving C3b, C4b and C5," *FEBS Letters*, vol. 581, no. 9, pp. 1716–1720, 2007.

[48] S. E. Osborne, D. Walthers, A. M. Tomljenovic et al., "Pathogenic adaptation of intracellular bacteria by rewiring a cis-regulatory input function," *Proceedings of the National Academy of Sciences of the United States of America*, vol. 106, no. 10, pp. 3982–3987, 2009.

[49] H. Yoon, C. Ansong, J. E. McDermott et al., "Systems analysis of multiple regulator perturbations allows discovery of virulence factors in *Salmonella*," *BMC Systems Biology*, vol. 5, p. 100, 2011.

[50] L. Shi, J. N. Adkins, J. R. Coleman et al., "Proteomic analysis of *Salmonella enterica* serovar Typhimurium isolated from RAW 264.7 macrophages: identification of a novel protein that contributes to the replication of serovar Typhimurium inside macrophages," *Journal of Biological Chemistry*, vol. 281, no. 39, pp. 29131–29140, 2006.

[51] N. G. Coldham and M. J. Woodward, "Characterization of the *Salmonella* Typhimurium proteome by semi-automated two dimensional HPLC-mass spectrometry: detection of proteins implicated in multiple antibiotic resistance," *Journal of Proteome Research*, vol. 3, no. 3, pp. 595–603, 2004.

[52] D. Chooneea, R. Karlsson, V. Encheva, C. Arnold, H. Appleton, and H. Shah, "Elucidation of the outer membrane proteome of *Salmonella enterica* serovar *Typhimurium* utilising a lipid-based protein immobilization technique," *BMC Microbiology*, vol. 10, p. 44, 2010.

[53] C. K. Schmitt, J. S. Ikeda, S. C. Darnell et al., "Absence of all components of the flagellar export and synthesis machinery differentially alters virulence of *Salmonella enterica*serovar Typhimurium in models of typhoid fever, survival in macrophages, tissue culture invasiveness, and calf enterocolitis," *Infection and Immunity*, vol. 69, no. 9, pp. 5619–5625, 2001.

Hindawi Publishing Corporation
International Journal of Proteomics
Volume 2012, Article ID 838630, 15 pages
doi:10.1155/2012/838630

Research Article

Method for Recovery and Immunoaffinity Enrichment of Membrane Proteins Illustrated with Metastatic Ovarian Cancer Tissues

Luke V. Schneider,[1] Varsha Likhte,[1] William H. Wright,[1] Frances Chu,[1] Emma Cambron,[1] Anne Baldwin-Burnett,[1] Jessica Krakow,[1] and Gary B. Smejkal[2, 3]

[1] *Target Discovery, Inc., 4030 Fabian Way, Palo Alto, CA 94030, USA*
[2] *Pressure Biosciences, Inc., 14 Norfolk Avenue, South Easton, MA 02375, USA*
[3] *Hubbard Center for Genome Studies, University of New Hampshire, Durham, NH 03824, USA*

Correspondence should be addressed to Luke V. Schneider, luke_schneider@targetdiscovery.com

Received 1 March 2012; Accepted 30 April 2012

Academic Editor: Winston Patrick Kuo

Integral membrane proteins play key biological roles in cell signaling, transport, and pathogen invasion. However, quantitative clinical assays for this critical class of proteins remain elusive and are generally limited to serum-soluble extracellular fragments. Furthermore, classic proteomic approaches to membrane protein analysis typically involve proteolytic digestion of the soluble pieces, resulting in separation of intra- and extracellular segments and significant informational loss. In this paper, we describe the development of a new method for the quantitative extraction of intact integral membrane proteins (including GPCRs) from solid metastatic ovarian tumors using pressure cycling technology in combination with a new (ProteoSolve-TD) buffer system. This new extraction buffer is compatible with immunoaffinity methods (e.g., ELISA and immunoaffinity chromatography), as well as conventional proteomic techniques (e.g., 2D gels, western blots). We demonstrate near quantitative recovery of membrane proteins EDG2, EDG4, FASLG, KDR, and LAMP-3 by western blots. We have also adapted commercial ELISAs for serum-soluble membrane protein fragments (e.g., sVEGFR2) to measure the tissue titers of their transmembrane progenitors. Finally, we demonstrate the compatibility of the new buffers with immunoaffinity enrichment/mass spectrometric characterization of tissue proteins.

1. Introduction

Integral membrane proteins, particularly G-protein-coupled receptors (GPCRs), are the biological targets for half of all the small molecule pharmaceuticals on the market today [1–3]. Membrane transport proteins, such as P-glycoprotein and related efflux pumps, are thought to impart chemotherapy agent resistance by transporting the drugs from the cytoplasm faster than they can diffuse back, thus lowering the effective drug concentrations at the site of action [4]. Even the common cold (rhinovirus) invades the cell by first binding to specific cell surface proteins [5–7], at least some of which are thought to involve glycosylated and sialylated extracelluar domain recognition sites [7, 8]. Clearly, integral membrane proteins play key biological roles in cell signaling, transport, and pathogen invasion. As such, membrane proteins also play key clinical roles in drug efficacy and resistance and should have a larger role in clinical diagnostics and personalized medicine. However, quantitative clinical assays (e.g., immunosorbent assays) for this important class of proteins remain elusive and are generally limited to serum-soluble extracellular fragments. Many serum markers for cancer detection and treatment monitoring—such as CA-125 (a serum-soluble fragment of mucin-16 approved for recurrence monitoring of ovarian cancer), CA 15-3 (a serum-soluble fragment of mucin-1 approved for recurrence monitoring of breast cancer), sVEGFR (a serum-soluble fragment of the vascular endothelial growth factor receptor that is implicated as a prognostic marker in lung cancer) [9], and sEGFR (a serum-soluble fragment of endothelial growth

factor receptor that is implicated as a theranostic marker for trastuzumab treatment in breast cancer) [10]—are currently only accessible for clinical assays once extracellular fragments are shed from the tumor cell membranes into the circulatory system. Other membrane protein biomarkers—such as HER-2/neu (an oncogenic growth factor receptor approved for use in herceptin therapy guidance) [11] and the estrogen receptor (an indicator for hormonal therapy in breast cancer) [12]—are currently only accessible through gene-based assays. Yet, genetic assays are unable to detect potentially clinically relevant posttranslational modifications, such as glycosylation, phosphorylation, acetylation, ubiquitination, and editing. Furthermore, as has been well established for more than a decade, measurements of mRNA levels, which are produced transiently, do not correlate well to protein levels, which accumulate over time [13, 14].

1.1. Membrane Protein Recovery and Purification. Classically, detergents are used to extract membrane proteins from biological membranes. Detergents also mediate membrane protein solubility in aqueous solutions, which is a prerequisite for further protein purification [15]. The surfactant concentrations required to keep most membrane proteins in aqueous solution also typically denature immunoglobulins, precluding their use for immunoaffinity purification and enrichment. Therefore, purification of membrane proteins is often very tedious and is made more so because surfactants can only partially mimic the lipid bilayer environment of the protein in nature [16]. Thus, many membrane proteins no longer retain their native biological conformations or activities in surfactant solutions [17], except in isolated cases [18]. Furthermore, not all proteins can be recovered efficiently with the same surfactant. Mitic et al. showed how the recovery of claudin-4 (with four transmembrane sequences) from insect cell cultures failed to consistently track total protein recovery over 37 different surfactants tested, ranging from 0 to 169% of the sodium dodecyl sulfate (SDS) control [19]. Surfactants also create limitations on further proteomic analysis of membrane proteins, since subsequent polyacrylamide gel electrophoresis of the recovered proteins generally requires SDS, or other ionic surfactants such as perfluorooctanoic acid [20]. With the exception of newer acid-cleavable forms [21], surfactants can produce ionization problems for mass spectrometric analyses, except at very low concentrations [22, 23], which are too low to support solubility of membrane proteins. Surfactants also bind to surfaces, significantly altering the behavior of liquid chromatographic media [24].

Because of the problems surfactants pose in chromatographic and mass spectrometric proteomic analyses, several membrane protein extraction schemes have been reported based on chaotropic agents and organic solvents. Jacks et al. report a 4 : 1 : 1 mixture of ethanol : acetonitrile : water as being useful for recovering membrane proteins of mitochondrial and spherosomal origin in a system that is optically transparent in the range of 200–700 nm [25]. The lower end of this optical range is particularly useful for studying protein structure by circular dichroism or quantification by absorbance. Zhang et al. report on the use of aqueous methanol, trifluoroethanol, and aqueous urea for the extraction of membrane proteins from red blood cells, finding that each solvent system liberated different membrane proteins [26]. Cordwell has advocated the use of a series of potent chaotropic agents and detergents (increasing progressively in strength) for protein extraction and fractionation, ending with thiourea and amidosulfobetaine-14 [27]. He applied this method to Gram-negative bacteria, cultured mammalian cells, and heart tissue.

In all these cases, the more readily soluble proteins are generally recovered first from the patient sample in standard aqueous buffers from which they can be more readily purified and assayed since all the solvents, detergents, and chaotropic agents necessary to recover and solubilize the integral membrane proteins are incompatible with the downstream separation and purification schemes. Therefore, the only applicable immunoaffinity technique that can be used on most membrane proteins after surfactant extraction is western blotting [28], which has only been sparing applied in clinical settings (e.g., early human immunodeficiency virus testing [29], early bovine spongiform encephalopathy testing [30], and Lyme disease [31]). Even these were quickly replaced when more robust nucleic acid or enzyme-linked immunosorbent assay (ELISA) alternatives became available.

1.2. Proteolysis of Intra- and Extracellular Domains. Another classic proteomic approach to membrane protein analysis involves digestion of the generally soluble intra- and extracellular domains from the generally insoluble transmembrane regions. Nühse et al. used this approach in combination with immobilized metal ion affinity chromatography (IMAC) to study the phosphopeptides resulting from trypsin treatment of the plasma membrane fraction isolated from cultured Arabidopsis cells [32]. However, membrane proteins can be refractory to digestion, particularly to trypsin, and nonspecific digestion enzymes (e.g., pepsin and elastase) are more commonly employed for this purpose [33]. The challenge, therefore, is to control the degree of digestion so that optimal recoveries are obtained. The resulting mixtures of partially digested peptides limit detection of the subsequent peptides by distributing the available signal over more distinct, but related, mass spectrometric species. Furthermore, this approach is generally only suited for global proteomic analysis by liquid chromatography and mass spectrometry since the resultant peptides are often not immunologically active and mixtures of peptides are created from all the membrane proteins found in the sample (both diagnostic and nondiagnostic).

With the exception of qualitative immunohistochemistry, clinical exploitation of integral membrane proteins has heretofore been limited by our ability to recover these proteins in a form suitable for quantitative immunoassays and rapid proteomic characterization. In this paper, we describe a new approach for the combined quantitative recovery of both cytosolic and integral membrane proteins in a buffer system immediately suitable for direct use in immunosorbent assays and subsequent mass spectrometric analyses. This approach

uses the commercial ProteoSolve-TD1 and -TD2 extraction buffers, developed in our laboratory and commercialized by Pressure Biosciences (PBI), in combination with PBI's pressure cycling technology (PCT). This new approach is demonstrated by extraction and analysis of several different biomarker proteins from fresh frozen human metastatic ovarian tumor tissues.

2. Material and Methods

2.1. Tissue Preparation and Protein Extraction. Fresh frozen samples of metastatic ovarian tumors (surgically isolated from the omentum of several different individuals) were purchased from Bio-Options (Fullerton, CA). All samples were reported to have been obtained from surgical resections of stages III and IV ovarian cancer patients. The frozen tumor samples were finely diced and mixed prior to extraction to provide better sample homogeneity.

2.2. Cryogenic Grinding. Diced tumor tissue (200 mg) was weighed into an aluminum weigh boat, precooled over dry ice, to keep the samples frozen during processing. A mortar and pestle were precooled by addition of liquid N_2 until a permanent lake of liquid N_2 could be maintained in the mortar. The tissue sample was added to the lake of liquid N_2 and cryogenically ground under liquid N_2 to a fine powder (about the consistency of corn starch). Additional liquid N_2 was added as necessary. After grinding, the liquid N_2 was allowed to evaporate, and the frozen tissue along with any frozen condensate was transferred to a PULSE tube (an integral part of the Barocycler device), which was precooled in a bed of dry ice.

2.3. Extraction Buffers. Three different buffer systems were used to extract proteins from the ground tumor tissue samples. The control extraction buffer, adapted from Song et al. for the homogenization of liver tissue for subsequent protein recovery and analysis, consisted of 20 mM HEPES adjusted to pH 7.5 with NaOH [34]. This buffer also forms the basis of the ProteoSolve-TD1 extraction buffer (Pressure Biosciences, South Easton, MA), which contains additional agents for membrane protein extraction and stabilization. The ProteoSolve-TD2 extraction buffer (Pressure Biosciences) was subsequently formulated with additional agents to stabilize the ground tissue dispersion during Barocycler operation, improving the reproducibility of protein extraction between samples. All these buffers were formulated to be compatible with subsequent protein labeling chemistries (e.g., aldehyde Schiff-base, N-hydroxysuccinimide, or iodoacetamide) to facilitate quantitative stable isotope work, such as isotope-coded affinity tags (ICATs) [35], isobaric tags for relative and absolute quantitation (iTRAQ) [36], and mass defect (isotope-differentiated binding energy shift tags, IDBEST) [37].

2.4. Barocycler Extraction. The NEP2320 Barocycler (Pressure Biosciences) was precooled with a circulating water bath to 4°C prior to use. All extraction buffers were refrigerated (0–4°C) overnight prior to use and used cold. Commercial protease and phosphatase inhibitor cocktails (P8340, P5726, and P2850, Sigma Aldrich, St. Louis, MO) were added to each buffer according to package directions immediately prior to use. PULSE tubes were loaded according to the manufacturer's instructions using 1.3 mL of the appropriate buffer in each tube. The tubes were immediately processed in the Barocycler (20 cycles from 0 to 35,000 psi for 20 sec on each cycle).

The resulting extracts were viscous and were treated with 25 μL of micrococcal nuclease from *Staphylococcus aureus* (New England Biolabs, Ipswich, MA) reconstituted at 1,000 units per mL per the manufacturer's instructions, for 15 min on ice. The resulting extract was recovered with a transfer pipette and placed in a 2 mL microfuge tube along with any residual pellet. The pellets with HEPES and TD1 extraction buffers appeared as soft sticky disks generally pressed against the center frit of the PULSE tube. Significantly less pellet was formed in the TD2 extraction buffer, and the TD2 postextraction pellet proved to be very friable.

Insoluble materials were recovered from each extract by centrifugation (13,000 ×g for 15 minutes at 4°C). The clarified extracts were recovered by aspiration to a second microfuge tube. The pellets were resuspended in 1 mL of TD1 buffer by passing them through a 21-gauge syringe needle several times to disperse the pellet. Because the pellets were not washed, they contain some residual soluble protein. Both the pellets and clarified extracts were stored in aliquots at −80°C prior to use.

2.5. 2-D Gel Electrophoresis. Aliquots (45 μL) of both the HEPES- and TD1-clarified extracts were diluted into 365 μL of ProteoSolve-IEF buffer (Pressure BioSciences, Inc.). First dimension separation was carried out with 200 μL of each diluted extract on the computer-controlled IsoelectrIQ^2 IEF apparatus (Proteome Systems, Ltd. Sydney, AU) using 11 cm, pH 3–10 ReadyStrip IPG strips (Bio-Rad Laboratories, Inc., Hercules, CA). Separation was programmed with current limited to 50 μA/strip in two steps: twelve hours on a concave voltage ramp set to start at 100 V and end at 10,000 V, followed by a constant voltage for 8 hours at 10,000 V. The strips were removed at 90 kV-h. The second dimension was performed on Criterion 8–16% polyacrylamide Tris-HCl precast gels in a Dodeca Cell (both from Bio-Rad Laboratories), equipped with the Thermo-EC 570–90 power supply at constant current of 60 mA/gel for 2 h. Gels were fixed and stained with a ProteomIQ Blue Colloidal Coomassie gel stain as described previously [38]. Gel images were acquired on a UMAX PowerLook III flatbed scanner as 48-bit color TIFF files and converted to 16-bit grayscale using ImageJ software (NIH). Image analysis was performed using Ludesi REDFIN 3 software (Ludesi AB, Malmö, Sweden).

2.6. Western Blots. Aliquots (17.5 μL) of each clarified extract and corresponding pellet suspension were denatured by the addition of 5 μL of 4x NuPAGE LDS Sample Buffer (Invitrogen), 2 μL of 1 M dithiothreitol, followed by heating to 90°C for 10 minutes. The samples were centrifuged at 13,000 ×g

(5 min) and the entire contents run on precast 4–12% Bis-Tris NuPAGE minigels, using the XCell SureLock system (Invitrogen, Carlsbad, CA), according to the manufacturer's instructions. Both SeeBlue and Magimark (Invitrogen) were used as molecular weight markers on each gel according to package instructions. Proteins were transferred to PVDF membranes at 65 V for 2 hours using a transfer buffer consisting of 20 mM TRIS, 160 mM glycine, and 0.04% SDS.

The PVDF membranes were blocked on a rotary shaker at room temperature with two different blocking buffers. A blocking buffer consisting of 100 mM phosphate buffered saline with 0.05% Tween, 0.01% Thimerosal, and 10% nonfat milk was used for the FASLG, NRP1, KDR, LAMP-3, BCL-2, CCNE2, and AKT blots. These were incubated for 10 min before primary antibody addition. The blocking buffer used for the EDG4, EDG2, GPC3, and TUBB blots consisted of 25 mM Tris, 0.15 M NaCl, 0.1% Tween-20, and 0.01% thimerosal at pH 7.4 containing 2% nonfat milk. The second set of membranes were blocked for 1 h before addition of the primary antibody. In both cases, the blocking buffer used for incubation was removed before addition of fresh buffer with the primary antibody. Primary antibodies were added at a nominal concentration of 1 μg/mL in 10 mL of the respective blocking buffers for FASLG, NRP1, KDR, LAMP-3, BCL-2, CCNE2, and AKT blots, and a nominal concentration of 0.5 μg/mL in 12 mL for the EDG4, EDG2, GPC3, and TUBB blots (except with 1% nonfat milk). Each blot was incubated with the primary antibody overnight on a rotary shaker at 0–4°C. Primary antibodies consisted of affinity-purified polyclonal antibodies against each biomarker purchased from various sources (Table 1). Appropriate cell lysates were used as positive controls for each of the antibodies in the western blots (Table 1).

After overnight incubation with the primary antibody, the blots were washed 4-5 times with their respective blocking buffers (without the nonfat milk). Washed blots were placed in 4 mL of the respective blocking buffer (without the nonfat milk) to which the appropriate antiprimary, secondary HRP-conjugated antibody (Cell Signaling) was added as supplied at a 1 : 1000 dilution for the FASLG, NRP1, KDR, LAMP-3, BCL-2, CCNE2, and AKT blots and 1 : 10,000 dilution for the EDG4, EDG2, GPC3, and TUBB blots. Blots were incubated with the HRP-conjugated secondary antibodies for 1 h at room temperature on a rotary shaker. Blots were again washed as described above and developed using Supersignal West Femto substrate (Pierce, Thermo-Fisher) following the manufacturer's recommendations. The chemiluminescent images were collected using a Fluorchem SP gel imager (Alpha Innotech, San Leandro, CA). The grey scale was inverted during postprocessing.

2.7. Sample Preparation for Immunoaffinity Techniques. Ovarian tumor samples extracted with TD2 buffer using the Barocycler (as described above) were diluted 1 : 10 in ProteoSolve-TDilute (Pressure Biosciences) containing both phosphatase and protease inhibitors (previously described) prior to any immunoaffinity work.

2.8. Enzyme-Linked Immunosorbent Assays. The effect of the diluted TD2 buffer on immunoassays was evaluated in several commercial ELISA kits, including human transferrin kit (Bethyl Laboratories, Montgomery, TX), Quantikine MMP-2 and MMP-3 (R&D Systems, Minneapolis, MN), and PathScan total p53 and PathScan total AKT1 (Cell Signaling, Danvers, MA). Immunoassays were performed following the manufacturer's instructions and in parallel with standards reconstituted in the diluted TD2 buffer (described above). Rate assays (change in absorbance with time) were performed, instead of the standard single time point, to ascertain any residual effects of the TD2 buffer components on the amplification step of the assay (i.e., modulation of horseradish peroxidase [HRP] enzyme kinetics or quenching of substrate color development).

Nonlinear least squares curve fit of the antibody binding (1) to the standards prepared in each buffer system was used to get the apparent affinity constants (K_{aff}). While the total antigen concentration [An] is known in the standard curve, the total antibody concentration [Ab] and the affinity constant were determined simultaneously by nonlinear curve fit. The one sigma error of the estimate in each fitted parameter was determined from the Jacobian matrix.

$$\text{Rate} = k\frac{1 + k_{\text{aff}}[\text{An}] - k_{\text{aff}}[\text{Ab}]}{2k_{\text{aff}}} + \frac{\sqrt{4k_{\text{aff}}^2[\text{An}][\text{Ab}] + (k_{\text{aff}}[\text{An}] - k_{\text{aff}}[\text{Ab}] - 1)^2}}{2k_{\text{aff}}}. \quad (1)$$

The ovarian TD2 extracts (after 1 : 10 dilution in ProteoSolve-TDilute) were also run in each assay to determine the effective biomarker concentrations in the extract. Because of this dilution, the highest tissue concentration tested was 15 mg of tissue/mL, which in a 100 μL ELISA sample well is the equivalent of 1.5 mg of tissue.

2.9. Immunoaffinity Enrichment of Specific Biomarkers. Antibody-conjugated PhyTips (PhyNexus, Sunnyvale, CA) were used for all immunoaffinity enrichment experiments. The experiments were conducted on a PhyNexus MEA robot system (PhyNexus, Sunnyvale, CA) using deep well plates. Each tip contained 100 μL fluidized beds of AminoLink Resin (Pierce Protein Research, Thermo-Fisher Scientific, Rockford, IL) conjugated to affinity-purified polyclonal anti-transferrin antibody (Bethyl Laboratories, Montgomery, TX) and packed in glycerol. The antibody conjugation procedure is described below. The sample consisted of 1 mL of ovarian tumor extract prepared in TD2 buffer and diluted (1 : 10 in ProteoSolve-TDilute) as described above. Nonspecific goat IgG (Equitech-Bio, Kerrville, TX) was added to the sample (9 mg per 10 mL of diluted sample) to suppress histone binding to the antibodies present on the bead surface [39].

Glycerol (used to pack and store the PhyTips) was found to significantly alter flow through the PhyTips and suppress ionization in the subsequent mass spectrometric analyses. This glycerol was removed by washing the PhyTips with 100 mM PBS (pH 7.2) in two stages using 96-well deep well trays (Seahorse Labware, no. S30009, 2 mL per well). The

Table 1: Affinity-purified polyclonal antibodies used for western blots and their sources.

Biomarker	Source	Ab Catalog no.	Control cell lysate
Lysophosphatidic acid receptor 2 (EDG4)	Santa Cruz Biotechnology	sc25490	BT-20
Lysophosphatidic acid receptor 1 (EDG2)	Abcam	ab23698	A549
CD95L, tumor necrosis factor ligand (FASLG)	Cell Signaling	4233S	MDA-MB-231
CD304, neurophilin-1 (NRP1)	Santa Cruz Biotechnology	sc7329	MDA-MB-231
CD309, vascular endothelial growth factor receptor 2 (KDR)	Santa Cruz Biotechnology	sc48161	MOLT-4
CD63, lysosomal-associated membrane protein 3 (LAMP-3)	Santa Cruz Biotechnology	sc15363	MOLT-4
Apoptosis regulator 2 (BCL2)	Cell Signaling	2872	MOLT-4
Cyclin-E2, G1/S-specific (CCNE2)	Strategic Diagnostics	2901.00.02	MOLT-4
Glypican-3 (GPC3)	Santa Cruz Biotechnology	sc11395 (30 kDa) sc10455 (60–80 kDa)	MDA-MB-231
RAC serine/threonine-protein kinases (pan-AKT)	R&D Systems	AF2055	MOLT-4
β-tubulin (TUBB)	Santa Cruz Biotechnology	sc9935	NIH/3T3

first stage wash consisted of four successive quick rinses in single draw and expel cycle each of 1 mL at a 2 mL/min flow rate (with 2 min holds at the top and bottom of each cycle). This removed the glycerol surrounding the bead bed, but left glycerol saturating the beads themselves. Diffusion of the glycerol out of the pores of the beads in the second stage required four additional washes consisting of a 0.5 mL draw followed by 60 cycles of 0.3 mL volume at a 2 mL/min flow rate (with 2 and 10 sec holds at the bottom and top of each cycle). This totaled about 30 min in each 20 mL wash volume (for 12 tips). Immediately following glycerol removal, the tips were immersed in a trough of an 8-row deep trough trays (Seahorse Labware, no. S30020, 32 mL per trough) containing 10 mL of diluted tumor sample. Next, 0.5 mL of sample was drawn into each tip, and 0.3 mL was cycled 240 times at 2 mL/min (with 2 and 10 sec holds at the bottom and top). This totaled about 2-hour for sample binding. Sample binding was immediately followed by a stringency wash in 4.17 M NaCl with 83 mM $NaPO_4$ (pH 7.2) for 60×0.5 mL cycles at 2 mL/min (with 2 and 10 sec holds at bottom and top). This was followed by buffer exchange into 150 mM pyridinium acetate (pH 6). Five washes in 10 mL of pyridinium acetate in a trough (0.5 mL with 48 cycles of 0.3 mL each at 2 mL/min with 2 and 10 sec holds at the bottom and top of each cycle) were required to diffuse all the salts from within the bead pores. Antigens were subsequently eluted directly into 2 mL microfuge tubes containing 0.6 mL of 50% aqueous acetic acid (0.5 mL draw with 30 cycles of 0.3 mL at 2 mL/min). The eluates were dried overnight in a SpeedVac (Savant). The residual pyridium acetate is a volatile buffer, which evaporated with the water in the SpeedVac.

2.10. Antitransferrin Antibody Conjugation to PhyTips. Custom PhyTips were purchased from PhyNexus (Sunnyvale, CA). These were 1.1 mL volume pipette tips packed by PhyNexus with 100 μL of AminoLink beads (ThermoFisher) in a fluidized bed configuration. Affinity-purified, carrier-free, goat polyclonal antitransferrin antibodies (no. A80-128A, Bethyl Laboratories, Montgomery, TX) were dissolved at 83 μg/mL in 100 mM PBS (pH 7.8) with 33 mM sodium cyanoborohydride ($NaCNBH_3$). A 0.6 mL quantity of the antibody solution was placed in the well of a deep-well plate for each tip. A 0.5 mL quantity of the antibody solution was drawn into each glycerol-free PhyTips (washed as described above) and processed for 960 cycles of 0.3 mL at 2 mL/min (6 h). Unreacted AminoLink aldehydes were then quenched with a 0.5 mL draw and 60 cycles of 0.3 mL each at 2 mL/min (0.5 h) in 1 M tris(hydroxymethyl)-aminomethane chloride (pH 7.8) with 33 mM $NaCNBH_3$. Residual TRIS and cyanoborohydride were removed with five washes (0.5 mL draw and 60 cycles of 0.3 mL each) in 100 mM PBS, the last of which contained 0.05% sodium azide. The tips were then packed with glycerol and stored refrigerated. An average of 35 μg Ab was bound to each PhyTip, as determined by UV_{280} absorbance change in the conjugation solution.

2.11. MALDI-MS Analysis. Immunoaffinity-enriched transferrin from ovarian tumor extracts was identified by peptide mass fingerprinting. The dried eluates (described above) were dissolved in 0.1 mL of 20 mM ammonium bicarbonate (pH 8.2), simultaneously reduced and capped by the addition of 2 μL each of 2-vinylpyridine (50 mM in isopropanol) and triethylphosphine (25 mM in isopropanol) at 37°C for 1 h, following the procedure described by Hale et al. [40]. After capping, the eluates were digested by adding 2.5 μL of trypsin (Sequencing Grade-Modified, Promega, Madison, WI), reconstituted at 100 μg/mL in 20 mM ammonium bicarbonate, for 2 h at 37°C. Addition of 0.11 mL of HPLC grade acetonitrile quenched the digestion, and the digest was evaporated overnight in a SpeedVac. The pellet was resuspended in 25 μL of MALDI matrix (α-cyano-4-hydroxycinnamic acid dissolved at 5 mg/mL in 50 : 50 acetonitrile : water with 0.1% trifluoroacetic acid), and 1 μL of the digest was spotted on a stainless steel MALDI plate and analyzed using a Q-TOF Premier (Waters, Milford, MA). The resulting monoisotopic peptide peaks were selected using mMass [41], and matching proteins were identified using MASCOT to search the Swiss-Prot protein database [42].

3. Results and Discussion

3.1. Global Protein Recovery. In order to show equivalence to classic extraction buffers, we performed a global proteomic analysis (2D gel electrophoresis) using separate 100 mg aliquots of a cryogenically ground metastatic ovarian tumor sample pool (sourced from multiple patients). Using the Barocycler, the first aliquot was extracted in HEPES buffer and a second processed in the TD2 buffer. The clarified extracts were diluted to 8.6 mg of tissue/mL in denaturing IEF buffer for 2D gel analysis. Comparison of the resulting gels by image analysis (Figure 1) reveals few differences in the more abundant protein species recovered. Of 585 discrete protein spots identified, 97% were common in both position and abundance between the two gels. Only 14 protein spots were unique to the TD2 extraction buffer gel. One spot was unique to the HEPES extraction buffer. These 15 differences were all in less abundant proteins. Therefore, TD2 buffer appears fully compatible with classic gel electrophoretic methods with little alteration in recovery of the more abundant proteins.

3.2. Recovery of Specific Proteins. Only the most abundant proteins can be seen in Coomassie-stained gels. Thus, the above analysis tells us little about the quantitative extraction of membrane proteins. We, therefore, selected a number of representative biomarkers from different protein classes for more detailed analysis by western blots. In particular, we were interested in determining how much protein of each class was left behind unrecovered in the insoluble pellets. To this end, the insoluble Barocycler pellets from each condition tested were recovered and treated by boiling in SDS-PAGE sample buffer. These SDS extracts of the pellets were run side by side in western blots with the clarified extracts at similar "effective" tissue concentrations.

Tissue extractions were performed with HEPES, TD1, and TD2 buffers at 150 mg tissue/mL buffer concentrations. The Barocycler extracts were centrifuged to recover an insoluble pellet and a soluble protein extract as separate samples. The extracts were diluted directly into 4x LDS-PAGE sample buffer (Invitrogen, Carlsbad, CA) to an equivalent gel loading concentration of 110 mg tissue/mL. All the pellets were resuspended in TDilute buffer to an equivalent concentration of 200 mg of tissue/mL to create a fine suspension. An aliquot of this suspension was diluted in LDS-PAGE sample buffer to an equivalent gel loading concentration of 140 mg tissue/mL. A series of western blots (Figure 2) were prepared from these extracts and pellets. Each blot was probed for a different protein.

Each extract and corresponding pellet sample were obtained from the same PULSE tube (i.e., the same tissue preparation). Therefore, it is possible to determine the relative abundance of each protein seen between the extract and pellet for each buffer. However, different PULSE tubes are used for each of the different extraction buffers tested. Because of water condensation during the weighing of frozen tissues, the amounts of tissue may vary between PULSE tubes. This makes direct cross-comparison of absolute protein recovery between buffers impractical. However, recovery determinations between the clarified extract and its corresponding pellet are possible.

Detailed descriptions of the specific proteins analyzed by western blots (Figure 2) can be found in the Supplementary Materials available online at doi:10.1155/2012/838630. The salient features of these proteins are summarized in Table 2. Key among these features are the number of transmembrane sequences, the theoretical (sequence MW) of the protein and any splice variants, and the reported measured MWs of the protein, including any posttranslational modifications. Alternate gene names are also provided to facilitate searches.

EDG2 and EDG4 are both G-protein-coupled receptors. Two strong overlapping EDG4 bands appear in the gel with nearly equal intensity and differing by less than 2 kDa in weight in the cell line control (lane J) between 50 and 60 kDa. Single strong EDG4 bands are seen in all the ovarian tumor samples at 55 kDa, except the HEPES extract (lane B). Three weak bands are seen in the HEPES extract at 55, 56, and 57 kDa, only one of which may correlate to EDG4. Clearly, little EDG4 is extracted into the HEPES buffer in the Barocycler since the amount extracted from the HEPES pellet (lane C) is in great excess to any of the bands seen in the HEPES extract. It is also possible that all the bands seen in this extract may be cross-reactive protein species because the band pattern is so different from that observed in any of the other samples. The strongest EDG4 band in both the TD1 and TD2 extracts (lanes D and F, resp.) appears at a slightly lower apparent molecular weight than the EDG4 band in the corresponding pellets. We note, however, that the molecular weights for the EDG4 bands observed in the 1/3 dilution of the TD2 extract (lane H) appear at the higher molecular weight observed for both the cell line control and the dominant EDG4 band observed in the TD1 and TD2 pellets. Therefore, we suspect that the EDG4 protein in both the TD1 and TD2 extracts is running at a slightly lower molecular weight, either because the protein load in these lanes is too high or the SDS fails to fully displace bound membrane lipids found in the insoluble pellet fractions. An additional weak band is seen at 56-57 kDa in the 1/3 dilution of the TD2 pellet (lane H), but in none of the other samples, and may be an artifact.

An EDG2 band is seen in all samples at or just below 50 kDa, including the cell line control (lane H). The protein appears to run at a slightly higher molecular weight when recovered with hot SDS from the Barocycler pellets than when isolated from the Barocycler extracts. This may reflect incomplete displacement of adsorbed lipids by SDS from the insoluble protein found in the pellets. However, it may also merely reflect differences in protein concentrations between the gel lanes since the 1/3 concentration sample of the TD2 Barocycler extract (lane H) runs closer to the higher-molecular-weight band and appears less distorted. The EDG2 band in the cell line control (lane J) is similarly distorted as the other extracts. EDG2 recovery seems to improve dramatically from the HEPES to TD buffers. Comparison of the TD2 and TD1 buffers in this sample shows only marginal recovery improvement.

Little or no FASLG appears to be recovered in either the HEPES or TD1 extracts from the Barocycler (lanes B and D in

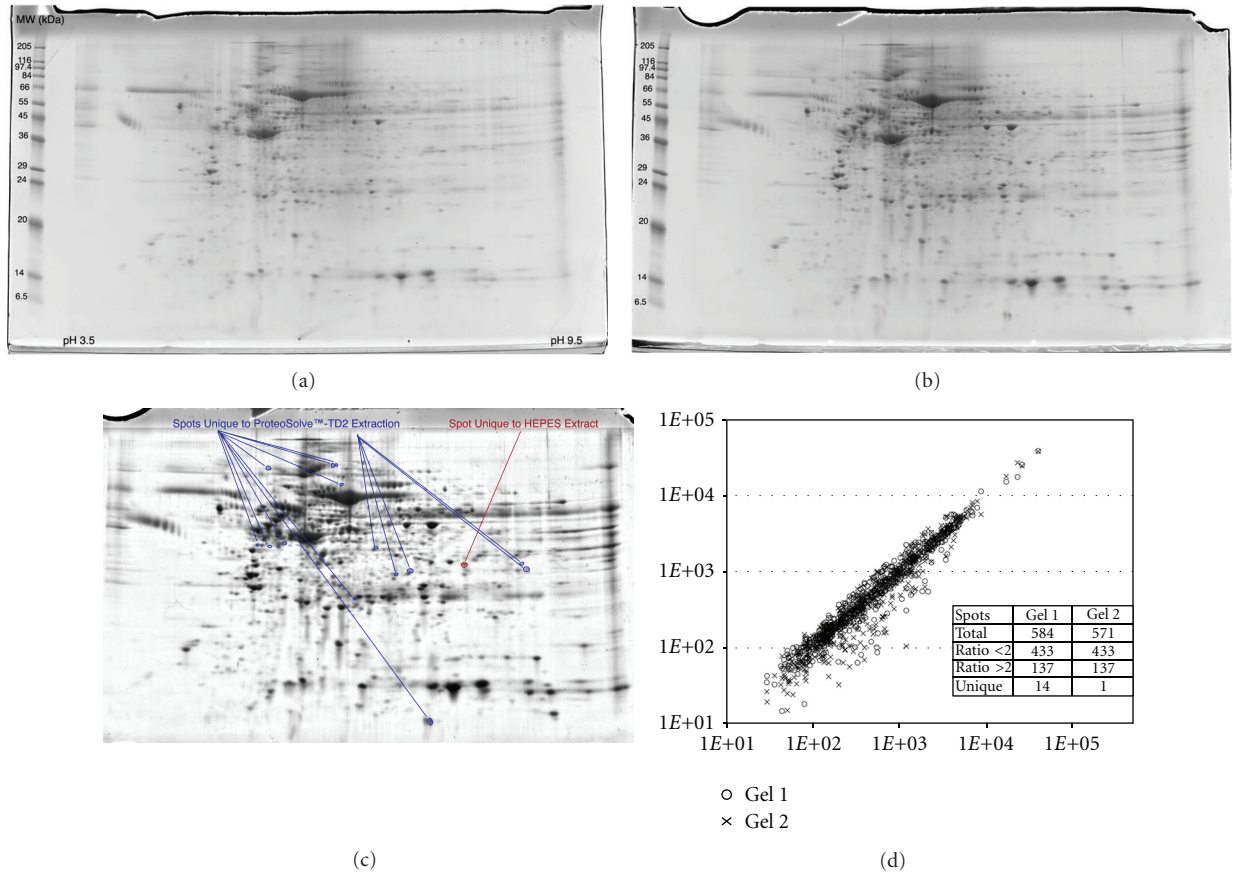

Figure 1: 2D gel analysis of proteins extracted from the same metastatic ovarian tumor sample by (a) HEPES buffer (Gel 1) and (b) TD2 buffer (Gel 2). Each extraction was conducted for 30 pressure cycles (30,000 psi for 20 sec followed by 0 psi for 20 sec) at a concentration of 75 mg tissue/mL of extraction buffer using the Barocycler. The samples were subsequently diluted to 8.6 mg/mL in ProteoSolve-IEF (a denaturing IEF gel buffer) for gel analysis. Automated gel image analysis of the Coomassie-stained gels suggests that 97% of the protein spots are shared between the two gels in position with most (74%) of the same abundance (d). One spot is uniquely found in the HEPES control, and 14 spots are unique to the ProteoSolve-TD2 extraction.

Figure 2). FASLG is seen in high abundance in the insoluble pellets from both of these extracts. However, nearly complete recovery of FASLG is seen in the soluble TD2 extract with little remaining in the insoluble pellet. Other experiments (data not shown) suggested that FASLG recovery was variable with TD1 buffer, but was consistently high in the TD2 buffer. FASLG was not recovered in the extract after several attempts with the HEPES buffer.

No evidence of the 72 kDa soluble form of NRP1 is seen on the western blots. The 140 kDa membrane bound form is present in all extracts (lanes B, D, and F). However, NRP1 recovery into the soluble fraction was lowest in HEPES buffer with most of the protein found in the HEPES pellet. About half of the NRP1 appeared to be recovered in the TD1 extract in this experiment. However, NRP1 recovery in the TD1 buffer was inconsistent between trials (data not shown). Almost complete recovery is seen in the TD2 extract with only a trace of NRP1 left in the pellet. This result was consistent between trials (data not shown). NRP1 was not seen in the cell line control. It is possible that the antibody used in these blots was reactive to a variant of the NRP1 protein that was not present in the cell line control used and which presents an epitope that is removed in the creation of the 72 kDa soluble form.

Both the intermediate and mature KDR proteins are apparent in the western blot for both the cell line control and the tumor samples at 200 kDa and 230 kDa, respectively. Partial recovery of the more abundant mature KDR protein is seen in HEPES extract (lane B) with most of the protein left in the HEPES pellet (lane C). The intermediate glycosylated form was not seen in the HEPES extract or pellet, possibly due to its lower solubility in the HEPES buffer than either the TD1 or TD2 buffers. The aqueous solubility of the mature form is expected to be greater due to the higher level of glycosylation. Most of the intermediate glycosylated form appears to be extracted into both the TD1 and TD2 buffers (lanes D and F) with apparently little left in either pellet (lanes E and G). At least some of the more abundant mature form (230 kDa) was seen in all the extracts (lanes B, D, and F, Figure 2) and both the HEPES and TD1 pellets (lanes C and E, Figure 2). The best relative KDR extraction was observed with the TD2 buffer (lanes F and G, Figure 2).

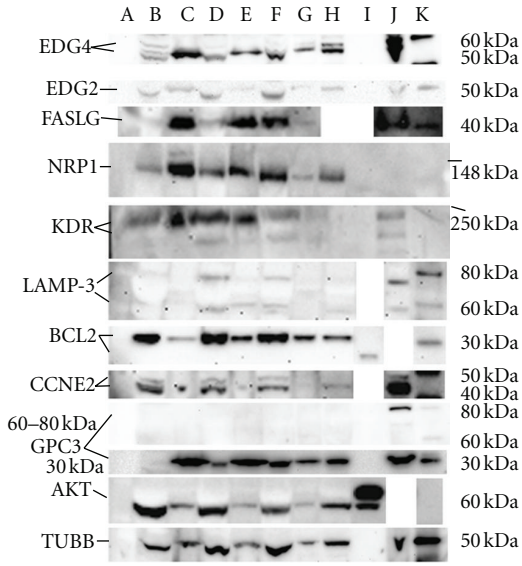

Figure 2: A series of western blots for various membrane, nuclear, and cytosolic proteins (Table 2) extracted from metastatic ovarian tumor samples. The extracts were prepared using 3 different extraction buffers (lane B = HEPES buffer extract, lane D = TD1 buffer extract, and lane F = TD2 buffer extract). Lane H is a duplicate of lane F at 1/3 the protein loading. The corresponding insoluble proteins trapped in the pellets recovered after each extraction are also shown in the adjacent lanes (lane C = HEPES pellet, lane E = TD1 pellet, and lane G = TD2 pellet). Either a purified recombinant protein control (lane I) or a human cell line extract control (lane J) was used in each blot (both were used for EDG4, NRP1, and KDR). Lanes A (see blue, Invitrogen) and K (Magic Mark, Invitrogen) are molecular weight markers. Lane A is only visualized in visible light, not in the chemiluminescent images shown. Both of these markers (see blue from a white light image not shown) were used to determine the molecular weights shown (on the right hand side). Gaps between lanes are provided only for alignment purposes, and the lanes are from the same gels.

Two bands at 58 kDa and 73 kDa are seen for the LAMP-3 protein in the western blot (Figure 2). It is not clear if the upper band is a cross-reactive antigen or a hyperglycosylated version of the protein, but it is found in both the control cell line (lane J, Figure 2) and all tumor extracts. Little of either molecular weight species are seen in any of the pellets, except for a trace of the 73 kDa species in the TD1 pellet. These high apparent recoveries, independent of extraction buffer used, may be due to the hyperglycosylation of this protein, particularly present between the transmembrane helixes. LAMP-3 is found in all the extracts but appears to be in low total abundance overall in the tumor samples because long chemiluminescent substrate exposure times were required to visualize LAMP-3 compared to the other biomarkers tested. Reblotting with higher primary antibody titers did not appear to improve the signal strength (data not shown).

BCL2 is a single-pass apoptosis regulator predominantly found in the outer mitochondrial membrane, but also seen in the nuclear, and endoplasmic reticulum membranes. Recombinant human BCL2 (the first 218 amino acids and nonglycosylated) is used as the antibody control. This truncated recombinant form runs at 24 kDa. Native BCL2 from the tumor samples is seen at 30 kDa [49]. BCL2 recovery was good, but not complete, in all buffers tested, with the best apparent recovery in HEPES buffer. There was no apparent difference in recoveries between the TD1 and TD2 buffers. BCL2 is found in mitochondria. However, because mitochondria are not expected to pellet at the 13,000 ×g used in this experiment [33], it is possible that BCL2 seen in the HEPES extract is actually recovered from intact suspended mitochondria after heating in SDS-PAGE sample buffer. The same may be true of the other buffers, making it difficult to differentiate BCL2 recovery among the Barocycler extraction buffers.

In our work, two CCNE2 bands are seen in the western blot of the cell line control and tumor samples (Figure 2), a dominant band at 45 kDa and a minor band at 47 kDa. These bands probably correspond to the long and short isoforms. As CCNE2 is not a membrane-bound protein, we would expect recoveries to be good in all the buffer systems tested. However, some of the dominant 45 kDa protein remains in the HEPES pellet (lane C). A trace amount is also seen in the TD1 pellet (lane E, Figure 2). These bands might be explained from residual extract present in the unwashed pellets. Extraction appears to be nearly quantitative with the TD2 buffer (lanes F and G, Figure 2). These results could also suggest that one of the components of the TD1 and TD2 buffers may be assisting Barocycler disruption of the nuclear membrane.

When the western blot from our work is probed with a C-terminal-specific GPC3 antibody (i.e., raised against amino acids 303–464) [52], a single strong band is seen in the gel at 30 kDa for all the tumor and cell line samples. The GPC3 protein is lipid anchored to the cell membrane in this C-terminal region. Several splice, or posttranslationally edited, variants are noted in the literature. None of these proteins is extracted into HEPES buffer (lane B, Figure 2). A small amount (≈10%) appears to be extracted into TD1 in the sample shown (lanes D and E, Figure 2). About 75% appears to be extracted into TD2 buffer (lanes F and G, Figure 2). This 30 kDa protein is also seen in the cell line control. No other bands are seen in the blot probed with the C-terminal-specific antibody.

When the blot is stripped and reprobed with an antibody specific to the N-terminal GPC3 region [53], however, a single band is seen near 80 kDa in the cell line control (lane J, Figure 2). The 30 kDa fragment is not detected with the N-terminal-specific primary antibody. No corresponding bands in the 60 to 80 kDa region are seen in the gel. Since the mature protein is exported, it would normally be carried away from the tumor site in the blood; therefore, little mature protein is expected to remain in the solid tumor. These results suggest that the 30 kDa fragment may be the lipid-anchored C-terminus (postmodification), which is only recovered in the TD1 and TD2 buffers and that the 80 kDa band is the full-length protein with its lipid-anchored C-terminus intact.

Table 2: Salient details of the proteins studied by western blots (Figure 2) and their estimated recoveries following the new method using ProteoSolve-TD2 buffer.

Database accession number	Protein name	Number of transmembrane sequences	Gene name(s)	Predicted sequence MW(s)	Apparent MW(s)	Estimated recovery (ProteoSolve-TD2)
Q9HBW0	Lysophosphatidic acid receptor 2	7	LPAR2 EDG4 LPA2	39 kDa	50 kDa [43]	65%
Q92633	Lysophosphatidic acid receptor 1	7	LPAR1 EDG2	41 kDa	43 kDa [44]	90%
Q0VHD7	CD95 ligand	1	FASLG	31 kDa	40 kDa [45]	95%
O14786	Neurophilin-1 (CD304)	1 0	NRP1 VEGF165R	103 kDa 72 kDa	130–140 kDa [46]	95%
P35968	Vascular endothelial growth factor receptor 2 (CD309)	1	KDR FLK1	150 kDa	150 kDa 200 kDa 230 kDa [47]	90%
P08962	Lysosomal-associated membrane protein 3 (CD63)	4	Tspan-30 LAMP-3	26 kDa	53 kDa [48]	100%
P10415	Apoptosis regulator Bcl-2	1 0	BCL2	26 kDa 22 kDa	28 kDa [49]	see text
O96020	Cyclin-E2 (G1/S specific)	0	CCNE2	47 kDa 41 kDa	45 kDa [50]	100%
P51654 Q53H15 Q2L882 Q2L880	Glypican-3	Lipid anchored 0	GPC3	66 kDa <66 kDa	65 kDa [51–53]	60%
P31749 P3175 Q9Y243	RAC serine/threonine-protein kinases α, β, γ	0	AKT PKB RAC	56 kDa 54 kDa	58 kDa [54]	95%
Q6P602 Q9H4B7 Q13885 Q9BVA1 Q9BUF5 P68371 Q13509 Q2NKY5 Q3ZCM7	β-tubulin	0	TUBB [55]	50 kDa	50 kDa [56]	95%

AKT is seen at 60 kDa in the western blot, as determined from the recombinant control (lane I, Figure 2). The second band seen in the recombinant human AKT control sample (at 62 kDa, lane I, Figure 2) is attributed to incomplete cleavage of the His_6 tag used in the purification of this fusion protein. AKT recoveries are high in all the buffers tested, which would be expected for a soluble cytosolic protein, with no apparent differences between the buffers tested.

While TUBB is generally a cytosolic protein, it spontaneously forms dimers with alpha-tubulin (TUBA) and is always in dynamic equilibrium between soluble a/b-dimers and polymerized microtubules, which can be insoluble depending on their size [57]. A single strong band at 50 kDa is seen in all lanes of the TUBB western blot (Figure 2). Based on the relative chemiluminescent intensities, about 50% of the TUBB is recovered in the HEPES extract (comparison of lanes B and C, Figure 2). TD1 appears to extract more than 80% of the TUBB present in the sample (comparison of lanes D and E, Figure 2). TD2 extracts better than 90% of all the TUBB present. In separate time course experiments (data not shown), we have shown that purified bovine tubulin (Cytoskeleton, Denver, CO) remains soluble at 1 mg/mL in TD1 buffer but polymerizes and precipitates nearly quantitatively within 24 hours in 20 mM HEPES buffer. Therefore, we believe that the lower apparent recovery of TUBB in the HEPES buffer is due to microtubule formation and precipitation in this extract.

3.3. Impact of Barocycler and Cryogenic Grinding. Several initial attempts to process diced (unground) metastatic ovarian tumor tissue through the Barocycler with the same extraction buffers did not produce good yields, even for cytosolic proteins (data not shown). Therefore, cryogenic grinding prior to Barocycler extraction appears to be necessary. We speculate that the higher surface-to-volume ratio of the ground tissue allows for better access of the extraction buffer and shorter diffusional paths for the extracted proteins during pressure cycling. Furthermore, as cited above, results

with the TD1 buffer proved inconsistent from sample to sample. Some samples yielded small friable pellets and had good protein yields, and others appeared to leave a large sticky pellet after pressure cycling. These latter samples exhibited poor protein recovery. The addition of a dispersion aid (TD2 buffer) resulted in vastly improved sample-to-sample reproducibility. Furthermore, no appreciable protein could be extracted from ground tumor samples heated at 95∘C for 1 h in either the TD1 or TD2 buffers in the absence of pressure cycling. When SDS was added to these samples, in the form of SDS-PAGE sample buffer (Invitrogen), protein was subsequently recovered on additional heating (data not shown). This demonstrates that pressure cycling is an integral part of the membrane protein extraction process with the ProteoSolve-TD buffers and that the buffers alone do not act as detergents.

3.4. Enzyme-Linked Immunosorbent Assays. Several commercial sandwich ELISA kits (transferrin, MMP2, MMP3, AKT1, VEGF, and sVEGF R2) were used to determine the effect of the TD2 extraction buffer on subsequent immunoaffinity work. In each case, one vial of antigen standards was reconstituted as prescribed in the manufacturer's instructions, and a second vial was reconstituted using the TD2 buffer diluted 1 : 10 by volume in ProteoSolve-TDilute (at pH 7.5). Otherwise, the kits were run as prescribed by the manufacturer with the exception that rate assays were performed to determine any residual effects of the TD2 buffer on the reporter (horseradish peroxidase) activity or substrate color development. The resulting standard curves are presented in Figure 3. The small differences in affinity constants between the buffers used are within the experimental error of the serial dilutions and the curve fitting. Furthermore, there was no consistent trend with K_{aff} being either slightly higher or lower, depending on the assay, and generally within the expected preparation variation of the standards. The lone exception was the VEGF assay, for which no assay response is seen for the recombinant human VEGF_{165} standard reconstituted in the diluted TD2 buffer. Either this standard is not soluble or stable in the TD2 buffer, or the buffer induces a change in the epitope recognized by the ELISA antibodies. Other than the anomalous VEGF assay results, these data suggest that the TD2 extraction buffer has no significant affect on antibody affinity or antigenicity of the recovered proteins. Presumably the kit buffers had been optimized by the manufacturers for each assay. The TD2 extraction buffer was used without optimization in all the assays. We expect, therefore, that better results may be obtained in each assay with further diluent optimization.

The resultant antigen concentrations in the metastatic ovarian tumor TD2 extracts were also determined in these assays and are summarized in Table 3. Holotransferrin (holo-Tf) is a surrogate marker for the blood or serum content of the tumor sample. Serum Tf concentrations are reported to be in the range of $2.9–4.0 \times 10^6$ ng/mL [58, 59]. Assuming all of the serum Tf is recovered in the TD2 extract, we estimate 0.5×10^6 ng Tf per g of tissue, suggesting that the average blood/serum content of the frozen metastatic tumor samples is around 15%. Matrix metalloproteinase 2 (MMP2) is below the detection limits of the ELISA (i.e., <70 ng per g of tissue). Matrix metalloproteinase 3 (MMP3) is detectable above background at the highest extract concentration used, but is below the quantitation limits of the assay (i.e., ≤7 ng per g of tissue. No references to the tumor tissue concentrations of these proteins could be found, so recovery could not be determined. AKT1 is a cytosolic protein for which the western blots (Figure 2) suggest nearly quantitative recovery with the TD2 buffer. The total AKT1 concentrations were determined to be about 20 μg/g of tissue, determined from the single ELISA sample tested. VEGF R2 (also known as KDR) is a heavily glycosylated membrane protein. The glycosylated N-terminal domain, which is often cleaved, becomes a plasma-soluble biomarker species (sVEGF R2). Assuming that the antibodies towards sVEGF R2 will crossreact with the membrane bound version, we thought this ELISA kit might provide a more quantitative measurement of the amount of the membrane protein recovered than the western blot (Figure 2), which suggested high recovery efficiency in the TD2 extraction buffer. Polanski and Anderson report the plasma concentration of sVEGF R2 to be 15 ng/mL [59]. The measured tissue concentration of VEGF R2 is 1 ± 0.1 ng/g of tissue, which is about twice as high as that expected for sVEGF R2 in the 15% blood contamination of the tissue sample. This translates to an expected sVEGF R2 concentration of 0.5 ng/g of tissue. However, the amount of sVEGF R2 measured for the HEPES Barocycler extract was indistinguishable from that seen in the TD2 Barocycler extract. Yet, KDR (VEGF R2) recovery in HEPES buffer was poor compared to that observed in the TD2 extraction buffer (Figure 2). Possible explanations are that the ELISA assay is truly specific to the soluble form of this protein, VEGF R2 recovery differs negligibly between the different extraction buffers (i.e., the western blot results are not quantitative), or the amount of membrane-bound VEGF R2 is low relative to that of the sVEGF R2 in the patients' plasma.

3.5. Immunoaffinity Enrichment/MALDI-MS. Antitransferrin PhyTips were prepared as described in the methods. These were used to recover and enrich transferrin protein from the TD2 ovarian tumor extract. ELISA data indicate that the extract contains 80 μg of transferrin (Table 3). Digest controls prepared with different concentrations of purified buffer-free apotransferrin (Sigma-Aldrich) suggested a limit of detection of about 4 ng of transferrin in a single MALDI-MS spot (1 μL of sample matrix) for protein identification using peptide mapping. No improvement in sequence coverage was seen above 1 μg of apotransferrin in a 1 μL spot. Of the 34 peaks found in the spectrum and submitted to a MASCOT search, 24 mapped to peptides from human transferrin, which was the top-ranked protein (score of 280). Sequence coverage was 36% (Figure 4).

4. Conclusions

4.1. Global Protein Recovery and Analysis. Global proteomic comparison between the HEPES and TD2 extracts (Figure 1) shows few differences from among the higher-abundance

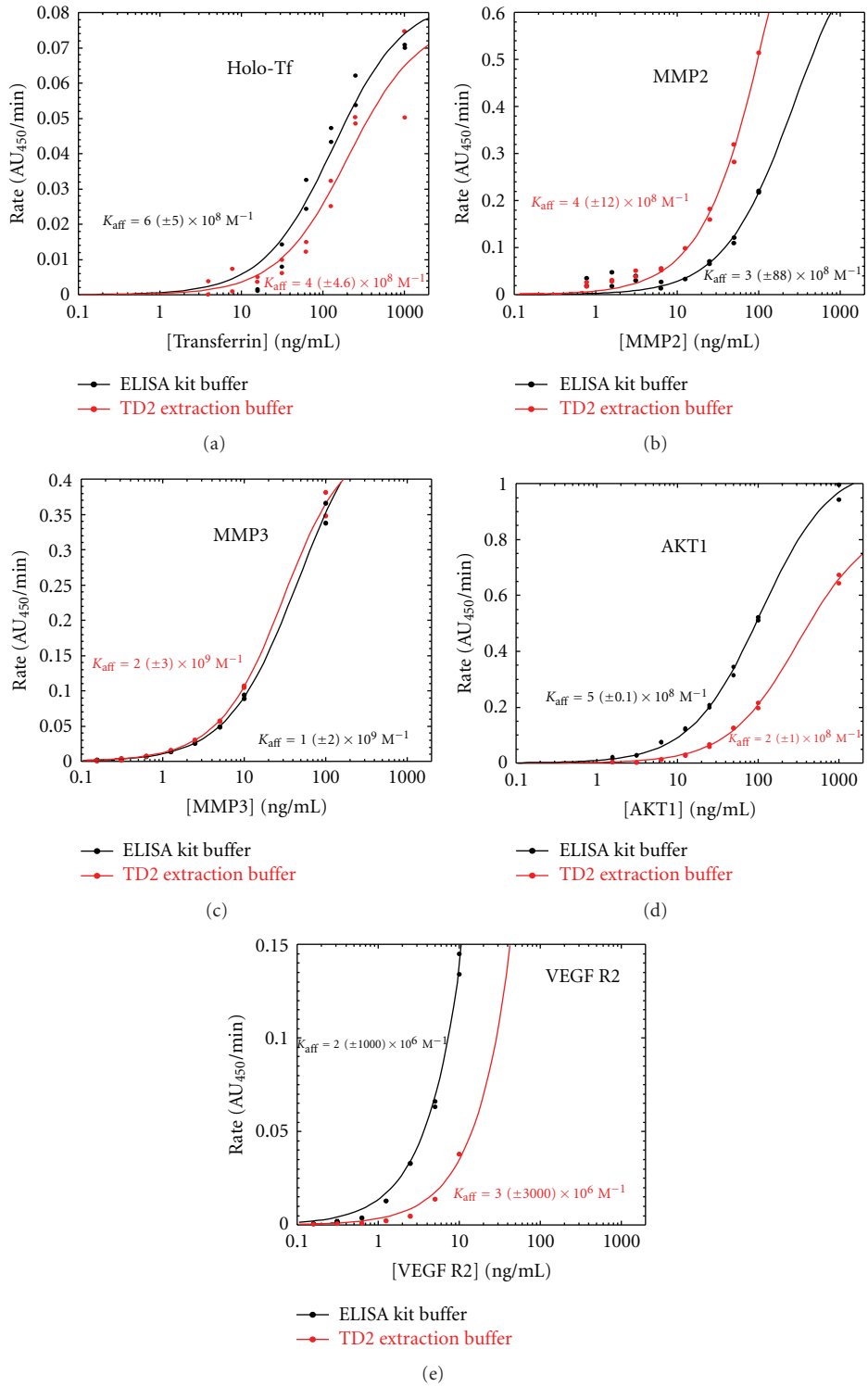

Figure 3: No significant effect of the TD2 buffer was seen in either the rate of color development from the HRP conjugate or antigen affinity in commercial ELISA kits for (a) total human transferrin (Tf), (b and c) total human matrix metalloprotease 2 (MMP2) or 3 (MMP3), (d) total human V-akt murine thymoma viral oncogene homolog 1 (AKT1), or (e) soluble vascular endothelial growth factor receptor (sVEGFR). Apparent affinity constants (±one standard deviation) for separate serial dilutions for the kit standards are shown for each ELISA for both the recommended kit diluent and TD2 buffers. (Standard deviations are determined by partitioning the error of the estimate across the fitted parameters using the Jacobian matrix. In ELISA assays lacking experimental data defining the upper asymptotic limits of quantitation (e.g., VEGF R2 assay of Figure 3), this method produces very large errors when fitting the data with a nonlinear equation (1)).

Table 3: The concentrations of various protein biomarkers extracted from mixed metastatic ovarian tumors obtained from the omenta of various patients during surgical debulking as measured by ELISA. Proteins were extracted from the cryogenically ground tumor samples using a Barocycler with TD2 Buffer. The concentrations (± one standard deviation) of each biomarker are determined from the extract contained using the ELISA assays described in Figure 3 and extrapolated to that present in the tumor assuming 100% recovery. Transferrin was used as a ubiquitous control protein, which is indicative of the serum content of the sample. Some biomarkers were below the detection limits of the assay. MMP3 was below the limits of quantitation of the ELISA.

Biomarker protein	Extract concentration (ng/mL)	Tumor concentration (ng/g)
Holo-Tf	80,000 ± 40,000	$5 \times 10^6 \pm 3 \times 10^6$
MMP2	BDL (<10)	BDL (<70)
MMP3*	≈1	≈7
AKT1	40 (single determinant)	20×10^3
VEGF R2/sVEGF R2	0.2 (only 2 replicates)	1 ± 0.1

BDL: below detection limits (assay detection limits).
*Measurements were below the quantitation limits of the assay.

proteins recovered from the sample. Some 2,000 different proteins have titers greater than 5×10^4 copies in the average mammalian cell [60]. The cellular titers of many cellular receptor (membrane) proteins are reported to be in the range of 10^3–10^5 copies per cell, by comparison [61]. The same dynamic range issues that plague global analysis of the plasma proteome [62] also plague cellular proteomic analysis. With the limited dynamic range for a Coomassie-stained gel [63], we may not see lower-abundance membrane proteins in such a global proteomic analysis. Nonetheless, the 2D gel data are important in that they show virtually that all the same proteins are recovered in the TD2 buffer as are recovered in a more standard aqueous buffer and in similar abundance. Furthermore, the ProteoSolve-TD buffers do not affect either the isoelectric focusing or SDS-PAGE separation coordinates of any proteins. Therefore, we conclude that the ProteoSolve-TD buffers are fully compatible with this time-honored global proteomic technique.

4.2. Membrane Protein Recovery. The western blots (Figure 2) provide definitive evidence for the recovery of seven-different integral membrane proteins. EDG2 and EDG4, both seven transmembrane G-protein-coupled receptors, appeared to be recovered well in the TD2 buffer system and virtually not at all in the HEPES control buffer. EDG4 recovery, however, may not have been quantitative, but this is confounded by apparent cross-reactivity of the primary antibody with proteins of similar size. FASLG, NRP1, and KDR (VEGF R2) proteins, all single transmembrane proteins, were nearly quantitatively recovered in the TD2 buffer but also showed partial recovery in the HEPES control buffer. LAMP-3, an apparently low-abundance protein with four-transmembrane sequences, appeared to be recovered in good yield in all the extraction buffers. LAMP-3 is highly glycosylated (particularly between the transmembrane helixes), potentially improving its aqueous solubility. Neither overnight incubation or boiling of the tissue samples in the ProteoSolve-TD buffers showed any significant transmembrane protein recovery (data not shown), suggesting that extraction of the membrane proteins was primarily due to the pressure cycling process. These observations support a PCT mechanism (a mechanistic discussion can be found in the Supporting Information) in which the pressure cycle itself is primarily responsible for disruption of the lipid membranes and exclusion of the membrane proteins. The data further suggest that the ProteoSolve-TD buffers need only to support the solubility of the pressure-extracted membrane proteins when the sample is returned to ambient conditions.

GPC3 is a lipid-anchored protein. What appears to be a 30 kDa C-terminal domain, which contains the lipid-anchor, only appears to be recovered in the TD1 and TD2 buffers (Figure 2). The soluble 65 kDa mature GPC3 protein, resulting from cleavage of the C-terminal, lipid-anchored domain, was not seen in any of the samples. BCL2, a mitochondrial protein with a single-transmembrane sequence, was the only protein to show better recovery in the HEPES buffer than either TD1 or TD2 buffers. We believe that this was caused by the failure to pellet mitochondria during the centrifugation step (13,000 ×g). Centrifugation at 52,000 ×g is normally required to pellet free mitochondria [33]. If mitochondria were left suspended in the extracts, then BCL2 would have been liberated from the membranes upon sample preparation for SDS-PAGE (i.e., boiling in SDS sample buffer). Higher recoveries of TUBB were evident in both the TD1 and TD2 buffers compared to the HEPES control. We believe this result is due to improved solubility of tubulin microtubules in the TD buffers over that in HEPES control. By contrast, the soluble protein controls (i.e., CCNE2, AKT, and TUBB) appeared to be well recovered in all of the Barocycler buffers.

4.3. Compatibility with Immunoaffinity Techniques. Of particular clinical interest is that the TD extraction buffers appear to stabilize membrane proteins in an aqueous environment that is compatible with subsequent immunoaffinity techniques (e.g., immunosorbent assays or immunoaffinity enrichment). With performance data from five different ELISAs (Figure 3), we can say with good confidence that the TD buffer system can have negligible effect on antibody affinity constants. Nor does the TD buffer system affect subsequent activity of the final ELISA amplification reaction (at least with the commonly used HRP enzyme). Only a single assay (VEGF) failed with the TD2 extraction buffer system. We believe this may be due to a structural difference in the VEGF epitope in the ProteoSolve-TD buffer system. This might be overcome by the selection of alternative capture or reporter antibodies for the ELISA, but was untried.

Unlike the western blot data (Figure 2), we found no significant difference between sVEGF R2/VEGF R2 titers (by ELISA) between the HEPES and TD2 extraction buffer

systems (Table 2). While membrane-bound VEGF R2 (KDR) can be distinguished from sVEGF R2 in a western blot (based on molecular weight differences), these can only be distinguished in an ELISA based on the specificity of the antibodies, which are unknown in the kit used. This ELISA was designed for sVEGF R2 (a plasma marker) and may not be cross-reactive with the membrane-bound version. However, the VEGF R2/sVEGF R2 tissue titers determined (1 ± 0.1 ng/g of tissue) were double the sVEGF R2 titer expected to be present in the entrained blood in the sample [59]. AKT1 (a soluble cytoplasmic protein) was found to be present in the patients' samples at a titer of 20 μg/g of tissue.

We note that both the MMP2 and MMP3 were below the limits of detection or quantitation of the ELISAs used in this study. It seems likely that many cellular proteins of clinical relevance may be similarly too dilute for direct measurement in the small ($\leq$0.2 mL) well volumes of standard ELISA microwell plates. Therefore, we investigated the use of immunoaffinity enrichment to concentrate lower-abundance biomarkers from larger sample volumes for subsequent analysis. Subsequent mass spectrometric analysis was successfully used to confirm the identity of immunoaffinity-enriched transferrin (Figure 4). Not only does this enrichment experiment demonstrate the affinity and avidity of the TUBB antibody in TD2 buffer, but it also shows that none of the buffer components survive the enrichment process to interfere with enzymatic digestion of the sample, peptide ionization (e.g., ion suppression), or mass spectral analysis (e.g., adduct formation).

4.4. Compatibility with Mass Spectrometry. Immunoaffinity enrichment followed by direct mass spectrometric determination of the mass of the intact protein to identify possible clinically relevant isoforms was pioneered by Nelson et al. [64] and has been adapted in our laboratory for biomarker validation. While we illustrate this method with a single protein (Tf) to illustrate the method in this paper, however, we have applied it to enrich 33 different biomarkers from the same ovarian tumor samples (data not shown).

As mentioned previously, the TD1 and TD2 buffers are fully compatible with the common protein labeling chemistries (data not provided). We have applied the described immunoaffinity/MS method using isotope-differentiated binding energy shift tags in our laboratory (data not shown) [65]. This intact protein capture approach allows the detection of novel protein isoforms (either sequence variants or posttranslational modifications) that may be lost in other biomarker validation methods such as multireaction monitoring (MRM) [66] or the use of stable isotope standards with antipeptide antibody enrichment (SISCAPA) [67].

Many solid tumors consist primarily of compact epithelial cells and connective tissue, which can be particularly recalcitrant to protein extraction. We note that the solid metastatic ovarian tumors used in this study had to be cryogenically ground to a fine powder before protein extraction proved effective. A video of the sample preparation process is provided in the Supplementary Materials. We also note that the results were variable with the TD1 buffer, but with the addition of the dispersion they aid to create the TD2 buffer, and this recovery variability was eliminated. We suspect that other softer tissues (e.g., liver) or harvested cell lines may be processed via pressure cycling technology with either the TD1 or TD2 buffers and likely will not require prior cryogenic grinding. Pressure cycling technology combined with the commercial ProtoSolve-TD extraction buffers appears to offer a new approach for protein, particularly membrane protein, extraction from tissues in a format suitable for subsequent clinical immunoaffinity methods and classic proteomic analyses.

```
  1 MRLAVGALLV CAVLGLCLAV PDKTVRWCAV SEHEATKCQS FRDHMKSVIP
 51 SDGPSVACVK KASYLDCIRA IAANEADAVT LDAGLVYDAY LAPNNLKPVV
101 AEFYGSKEDP QTFYYAVAVV KKDSGFQMNQ LRGKKSCHTG LGRSAGWNIP
151 IGLLYCDLPE PRKPLEKAVA NFFSGSCAPC ADGTDFPQLC QLCPGCGCST
201 LNQYFGYSGA FKCLKDGAGD VAFVKHSTIF ENLANKADRD QYELLCLDNT
251 RKPVDEYKDC HLAQVPSHTV VARSMGGKED LIWELLNQAQ EHFGKDKSKE
301 FQLFSSPHGK DLLFKDSAHG FLKVPPRMDA KMYLGYEYVT AIRNLREGTC
351 PEAPTDECKP VKWCALSHHE RLKCDEWSVN SVGKIECVSA ETTEDCIAKI
401 MNGEADAMSL DGGFVYIAGK CGLVPVLAEN YNKSDNCEDT PEAGYFAVAV
451 VKKSASDLTW DNLKGKKSCH TAVGRTAGWN IPMGLLYNKI NHCRFDEFFS
501 EGCAPGSKKD SSLCKLCMGS GLNLCEPNNK EGYYGYTGAF RCLVEKGDVA
551 FVKHQTVPQN TGGKNPDPWA KNLNEKDYEL LCLDGTRKPV EEYANCHLAR
601 APNHAVVTRK DKEACVHKIL RQQQHLFGSN VTDCSGNFCL FRSETKDLLF
651 RDDTVCLAKL HDRNTYEKYL GEEYVKAVGN LRKCSTSSLL EACTFRRP
```

FIGURE 4: The 36% mass spectrometric sequence coverage (underlined) from a tryptic digest of immunoaffinity-enriched transferrin contained in a Barocycler TD2 extract of metastatic ovarian tumor tissue.

Disclosure

The authors have no financial stake in Invitrogen, nor have they received any financial remuneration from Invitrogen for the use of their products in this study (e.g., XCell SureLock, SeeBlue, and Magimark). However, Pressure Biosciences has been licensed by Target Discovery to manufacture and sell the ProtoSolve-TD buffers for the preparation of tissues for scientific analysis, and therefore, both companies employing the authors profit from the sales of these reagents. Pressure Bioscience also profits from the sale of the Barocycler cited in this study.

Acknowledgment

The authors thank Alexander Lazarev of Pressure Biosciences, Inc. for his assistance in the preparation and image analysis of the 2D gel electrophoresis samples and image analysis presented in this paper.

References

[1] J. Drews, "Drug discovery: a historical perspective," *Science*, vol. 287, no. 5460, pp. 1960–1964, 2000.

[2] A. L. Hopkins and C. R. Groom, "The druggable genome," *Nature Reviews Drug Discovery*, vol. 1, no. 9, pp. 727–730, 2002.

[3] J. P. Overington, B. Al-Lazikani, and A. L. Hopkins, "How many drug targets are there?" *Nature Reviews Drug Discovery*, vol. 5, no. 12, pp. 993–996, 2006.

[4] M. M. Gottesman, "How cancer cells evade chemotherapy: sixteenth Richard and Hinda Rosenthal Foundation Award Lecture," *Cancer Research*, vol. 53, no. 4, pp. 747–754, 1993.

[5] G. Abraham and R. J. Colonno, "Many rhinovirus serotypes share the same cellular receptor," *Journal of Virology*, vol. 51, no. 2, pp. 340–345, 1984.

[6] M. G. Rossmann, "Viral cell recognition and entry," *Protein Science*, vol. 3, no. 10, pp. 1712–1725, 1994.

[7] A. T. H. Burness, "Glycophorin and sialylated components as receptors for viruses," in *Virus Receptors, Part 2*, K. Lonberg-Holm and L. Phillpson, Eds., pp. 64–84, Chapman and Hall, London, UK, 1981.

[8] M. G. Rossmann, "Viral cell recognition and entry," *Protein Science*, vol. 3, no. 10, pp. 1712–1725, 1994.

[9] W. Naumnik, T. Izycki, E. Świdzińska, M. Ossolińska, and E. Chyczewska, "Serum levels of VEGF-C, VEGF-D, and sVEGF-R2 in patients with lung cancer during chemotherapy," *Oncology Research*, vol. 16, no. 9, pp. 445–451, 2007.

[10] A. T. Baron, J. A. Wilken, D. E. Haggstrom, S. T. Goodrich, and N. J. Maihle, "Clinical implementation of soluble EGFR (sEGFR) as a theragnostic serum biomarker of breast, lung and ovarian cancer," *IDrugs*, vol. 12, no. 5, pp. 302–308, 2009.

[11] J. S. Winston, J. Ramanaryanan, and E. Levine, "HER-2/neu evaluation in breast cancer are we there yet?" *American Journal of Clinical Pathology*, vol. 121, pp. S33–49, 2004.

[12] J. Thomas, A. Hanby, S. Pinder et al., "Implications of inconsistent measurement of ER status in non-invasive breast cancer: a study of 1,684 cases from the Sloane project," *Breast Journal*, vol. 14, no. 1, pp. 33–38, 2008.

[13] L. Anderson and J. Seilhamer, "A comparison of selected mRNA and protein abundances in human liver," *Electrophoresis*, vol. 18, no. 3-4, pp. 533–537, 1997.

[14] S. P. Gygi, Y. Rochon, B. R. Franza, and R. Aebersold, "Correlation between protein and mRNA abundance in yeast," *Molecular and Cellular Biology*, vol. 19, no. 3, pp. 1720–1730, 1999.

[15] O. T. Jones, J. P. Earnest, and M. G. McNamee, "Solubilization and reconstitution of membrane proteins," in *Biological Membranes: A Practical Approach*, J. B. C. Findlay and W. H. Evans, Eds., pp. 139–177, IRL Press, Washington, DC, USA, 1987.

[16] G. Von Heijne, "A day in the life of Dr K. or how I learned to stop worrying and love lysozyme: a tragedy in six acts," *Journal of Molecular Biology*, vol. 293, no. 2, pp. 367–379, 1999.

[17] T. Arnold and D. Linke, "Phase separation in the isolation and purification of membrane proteins," *BioTechniques*, vol. 43, no. 4, pp. 427–440, 2007.

[18] M. Greenberg and Tian Yow Tsong, "Detergent solubilization and affinity purification of a local anesthetic binding protein from mammalian axonal membranes," *Journal of Biological Chemistry*, vol. 259, no. 21, pp. 13241–13245, 1984.

[19] L. L. Mitic, V. M. Unger, and J. M. Anderson, "Expression, solubilization, and biochemical characterization of the tight junction transmembrane protein claudin-4," *Protein Science*, vol. 12, no. 2, pp. 218–227, 2003.

[20] M. Ramjeesingh, L. J. Huan, E. Garami, and C. E. Bear, "Novel method for evaluation of the oligomeric structure of membrane proteins," *Biochemical Journal*, vol. 342, no. 1, pp. 119–123, 1999.

[21] A. A. Klammer and M. J. MacCoss, "Effects of modified digestion schemes on the identification of proteins from complex mixtures," *Journal of Proteome Research*, vol. 5, no. 3, pp. 695–700, 2006.

[22] T. M. Annesley, "Ion suppression in mass spectrometry," *Clinical Chemistry*, vol. 49, no. 7, pp. 1041–1044, 2003.

[23] D. C. Grant and R. J. Helleur, "Surfactant-mediated matrix-assisted laser desorption/ionization time-of-flight mass spectrometry of small molecules," *Rapid Communications in Mass Spectrometry*, vol. 21, no. 6, pp. 837–845, 2007.

[24] M. Tang and S. N. Deming, "Interfacial tension effects of non-ionic surfactants in reversed-phase liquid chromatography," *Analytical Chemistry*, vol. 55, no. 3, pp. 425–428, 1983.

[25] T. J. Jacks, R. H. Barker, and T. P. Hensarling, "Solubilization of protein with ethanol-acetonitrile-water solvent system," US Patent 3975343, 1976.

[26] H. Zhang, Q. Lin, S. Ponnusamy et al., "Differential recovery of membrane proteins after extraction by aqueous methanol and trifluoroethanol," *Proteomics*, vol. 7, no. 10, pp. 1654–1663, 2007.

[27] S. J. Cordwell, "Sequential extraction of proteins by chemical reagents.," *Methods in Molecular Biology*, vol. 424, pp. 139–146, 2008.

[28] W. N. Burnette, ""Western Blotting": electrophoretic transfer of proteins from sodium dodecyl sulfate-polyacrylamide gels to unmodified nitrocellulose and radiographic detection with antibody and radioiodinated protein A," *Analytical Biochemistry*, vol. 112, no. 2, pp. 195–203, 1981.

[29] O. I. Iweala, "HIV diagnostic tests: an overview," *Contraception*, vol. 70, no. 2, pp. 141–147, 2004.

[30] B. J. Bennionn and V. Daggett, "Protein conformation and diagnostic tests: the prion protein," *Clinical Chemistry*, vol. 48, no. 12, pp. 2105–2114, 2002.

[31] S. M. Engstrom, E. Shoop, and R. C. Johnson, "Immunoblot interpretation criteria for serodiagnosis of early Lyme disease," *Journal of Clinical Microbiology*, vol. 33, no. 2, pp. 419–427, 1995.

[32] T. S. Nühse, A. Stensballe, O. N. Jensen, and S. C. Peck, "Large-scale analysis of in vivo phosphorylated membrane proteins by immobilized metal ion affinity chromatography and mass spectrometry.," *Molecular & Cellular Proteomics*, vol. 2, no. 11, pp. 1234–1243, 2003.

[33] M. Jansson, K. Wårell, F. Levander, and P. James, "Membrane protein identification: N-terminal labeling of nontryptic membrane protein peptides facilitates database searching," *Journal of Proteome Research*, vol. 7, no. 2, pp. 659–665, 2008.

[34] Y. Song, Y. Hao, A. Sun et al., "Sample preparation project for the subcellular proteome of mouse liver," *Proteomics*, vol. 6, no. 19, pp. 5269–5277, 2006.

[35] M. P. Hall, S. Ashrafi, I. Obegi, R. Petesch, J. N. Peterson, and L. V. Schneider, ""Mass defect" tags for biomolecular mass spectrometry," *Journal of Mass Spectrometry*, vol. 38, no. 8, pp. 809–816, 2003.

[36] S. P. Gygi, B. Rist, S. A. Gerber, F. Turecek, M. H. Gelb, and R. Aebersold, "Quantitative analysis of complex protein mixtures using isotope-coded affinity tags," *Nature Biotechnology*, vol. 17, no. 10, pp. 994–999, 1999.

[37] P. L. Ross, Y. N. Huang, J. N. Marchese et al., "Multiplexed protein quantitation in Saccharomyces cerevisiae using amine-reactive isobaric tagging reagents," *Molecular and Cellular Proteomics*, vol. 3, no. 12, pp. 1154–1169, 2004.

[38] G. B. Smejkal, M. H. Robinson, and A. Lazarev, "Comparison of fluorescent stains: relative photostability and differential staining of proteins in two-dimensional gels," *Electrophoresis*, vol. 25, no. 15, pp. 2511–2519, 2004.

[39] U. Groschel-Stewart, P. Heurich, and D. I. H. Stewart, "Non-specific interactions of histones with serum components and

contractile proteins," *Biochemistry International*, vol. 13, no. 6, pp. 927–932, 1986.

[40] J. E. Hale, J. P. Butler, V. Gelfanova, J. S. You, and M. D. Knierman, "A simplified procedure for the reduction and alkylation of cysteine residues in proteins prior to proteolytic digestion and mass spectral analysis," *Analytical Biochemistry*, vol. 333, no. 1, pp. 174–181, 2004.

[41] M. Strohalm, M. Hassman, B. Košata, and M. Kodíček, "mMass data miner: an open source alternative for mass spectrometric data analysis," *Rapid Communications in Mass Spectrometry*, vol. 22, no. 6, pp. 905–908, 2008.

[42] D. N. Perkins, D. J. C. Pappin, D. M. Creasy, and J. S. Cottrell, "Probability-based protein identification by searching sequence databases using mass spectrometry data," *Electrophoresis*, vol. 20, no. 18, pp. 3551–3567, 1999.

[43] Product data sheet, *CD63 (R-13): sc-31213*, Santa Cruz Biotechnology, Santa Cruz, Calif, USA, 2009.

[44] Product data sheet, *EDG2 antibody (ab23698)*, Abcam, Cambridge, UK, 2009.

[45] Product data sheet, *Fas (C18C12) Rabbit mAb*, no. 4233, Cell Signaling Technology, Danvers, Mass, USA, 2009.

[46] Product data sheet, *Anti-human neuropilin-1 antibody*, AF3870, R&D Systems, Minneapolis, Minn, USA, 2009.

[47] Product data sheet, *FLK-1 (6B11):sc-101560*, Santa Cruz Biotechnology, Santa Cruz, Calif, USA, 2009.

[48] Product data sheet, *CD63 (R-13): sc-31213*, Santa Cruz Biotechnology, Santa Cruz, Calif, USA, 2009.

[49] Product data sheet, *Bcl-2 (C-2): sc-7382*, Santa Cruz Biotechnology, Santa Cruz, Calif, USA, 2009.

[50] Product data sheet, *cyclin E2 (C-19): sc-9568*, Santa Cruz Biotechnology, Santa Cruz, Calif, USA, 2009.

[51] Product data sheet, *glypican-3 (C-17): sc-34095*, Santa Cruz Biotechnology, Santa Cruz, Calif, USA, 2009.

[52] Product data sheet, *glypican-3 (H-162): sc-11395*, Santa Cruz Biotechnology, Santa Cruz, Calif, USA, 2009.

[53] Product data sheet, *glypican-3 (W-18): sc-10455*, Santa Cruz Biotechnology, Santa Cruz, Calif, USA, 2010.

[54] Product data sheet, *Affinity-Purified Rabbit Anti-Human Pan Akt Antibody*, R&D Systems, Minneapolis, Minn, USA, 2007.

[55] S. A. Lewis and N. J. Cowan, "Tubulin genes: structure, expression and regulation," in *Microtubule Protein*, J. Avia, Ed., pp. 37–66, CRC Press, Boca Raton, Fla, USA, 1990.

[56] Product data sheet, *beta Tubulin (L-15):sc-31782*, Santa Cruz Biotechnology, Santa Cruz, Calif, USA, 2009.

[57] R. L. Margolis and L. Wilson, "Addition of colchicine tubulin complex to microtubule ends: the mechanism of substoichiometric colchicine poisoning," *Proceedings of the National Academy of Sciences of the United States of America*, vol. 74, no. 8, pp. 3466–3470, 1977.

[58] N. L. Anderson, M. Polanski, R. Pieper et al., "The human plasma proteome," *Molecular and Cellular Proteomics*, vol. 3, no. 4, pp. 311–326, 2004.

[59] M. Polanski and N. Anderson, "A list of candidate cancer biomarkers for targeted proteomics," *Biomarker Insights*, vol. 1, pp. 1–48, 2006.

[60] T. A. Brown, *Genomes*, John Wiley & Sons, New York, NY, USA, 2nd edition, 2002.

[61] D. A. Lauffenberger and J. J. Linderman, *Receptors: models for binding, trafficking, and signaling*, Oxford University Press, New York, NY, USA, 1996.

[62] M. P. Hall and L. V. Schneider, "Isotope-differentiated binding energy shift tags (IDBEST) for improved targeted biomarker discovery and validation," *Expert Review of Proteomics*, vol. 1, no. 4, pp. 421–431, 2004.

[63] G. B. Smejkal, "The Coomassie chronicles: past, present and future perspectives in polyacrylamide gel staining," *Expert Review of Proteomics*, vol. 1, no. 4, pp. 381–387, 2004.

[64] R. W. Nelson, J. R. Krone, A. L. Bieber, and P. Williams, "Mass spectrometric immunoassay," *Analytical Chemistry*, vol. 67, no. 7, pp. 1153–1158, 1995.

[65] L. V. Schneider and M. P. Hall, "Stable isotope methods for high-precision proteomics," *Drug Discovery Today*, vol. 10, no. 5, pp. 353–363, 2005.

[66] N. R. Kitteringham, R. E. Jenkins, C. S. Lane, V. L. Elliott, and B. K. Park, "Multiple reaction monitoring for quantitative biomarker analysis in proteomics and metabolomics," *Journal of Chromatography B*, vol. 877, no. 13, pp. 1229–1239, 2009.

[67] N. L. Anderson, N. G. Anderson, L. R. Haines, D. B. Hardie, R. W. Olafson, and T. W. Pearson, "Mass spectrometric quantitation of peptides and proteins using stable isotope standards and capture by anti-peptide antibodies (SISCAPA)," *Journal of Proteome Research*, vol. 3, no. 2, pp. 235–244, 2004.

Hindawi Publishing Corporation
International Journal of Proteomics
Volume 2012, Article ID 397103, 8 pages
doi:10.1155/2012/397103

Research Article

Plasma Fractionation Enriches Post-Myocardial Infarction Samples Prior to Proteomics Analysis

Lisandra E. de Castro Brás,[1,2] Kristine Y. DeLeon,[1,2] Yonggang Ma,[1,2] Qiuxia Dai,[1,2] Kevin Hakala,[1,3] Susan T. Weintraub,[1,3] and Merry L. Lindsey[1,2]

[1] *San Antonio Cardiovascular Proteomics Center, The University of Texas Health Science Center at San Antonio, San Antonio, TX 78245, USA*
[2] *Division of Geriatrics, Gerontology & Palliative Medicine, Department of Medicine, UTHSCSA, San Antonio, TX 78245, USA*
[3] *Department of Biochemistry, UTHSCSA, San Antonio, TX 78245, USA*

Correspondence should be addressed to Lisandra E. de Castro Brás, decastrobras@uthscsa.edu
and Merry L. Lindsey, LindseyM@uthscsa.edu

Received 15 March 2012; Accepted 9 April 2012

Academic Editor: William C. S. Cho

Following myocardial infarction (MI), matrix metalloproteinase-9 (MMP-9) levels increase, and MMP-9 deletion improves post-MI remodeling of the left ventricle (LV). We provide here a technical report on plasma-analysis from wild type (WT) and MMP-9 null mice using fractionation and mass-spectrometry-based proteomics. MI was induced by coronary artery ligation in male WT and MMP-9 null mice (4–8 months old; $n = 3$/genotype). Plasma was collected on days 0 (pre-) and 1 post-MI. Plasma proteins were fractionated and proteins in the lowest (fraction 1) and highest (fraction 12) molecular weight fractions were separated by 1-D SDS-PAGE, digested in-gel with trypsin and analyzed by HPLC-ESI-MS/MS on an Orbitrap Velos. We tried five different fractionation protocols, before reaching an optimized protocol that allowed us to identify over 100 proteins. Serum amyloid A substantially increased post-MI in both genotypes, while alpha-2 macroglobulin increased only in the null samples. In fraction 12, extracellular matrix proteins were observed only post-MI. Interestingly, fibronectin-1, a substrate of MMP-9, was identified at both day 0 and day 1 post-MI in the MMP-9 null mice but was only identified post-MI in the WT mice. In conclusion, plasma fractionation offers an improved depletion-free method to evaluate plasma changes following MI.

1. Introduction

Acute myocardial infarction (MI) remains a leading cause of morbidity and mortality worldwide. According to the latest report of the American Heart Association, every 25 seconds, an American will have a coronary event, and approximately every minute, someone will die of a coronary event [1]. In 2010, 785,000 Americans experienced an MI, and approximately 470,000 had a recurring MI [1]. Heart failure can result from adverse remodeling of the collagenous scar that replaces the damaged myocardium in the left ventricle (LV) after MI. LV remodeling is mediated by cell survival, inflammation, angiogenesis, and turnover of the extracellular matrix (ECM). Markers of LV remodeling can be either determined in the circulation (e.g., serum or plasma) or detected in the heart by imaging technologies or biopsy. Post-MI, levels of specific matrix metalloproteinases (MMPs) increase and mediate left ventricular remodeling. MMP-9 has been reported as a prognostic indicator of cardiac dysfunction in MI patients [2, 3]. MMP-9 deletion has also been shown to improve remodeling of the LV in mice [4, 5]. We hypothesized that the analysis of plasma proteins post-MI in wild-type (WT) and MMP-9 null mice will identify prospective markers of early MI that are MMP-9 dependent.

Termed as the most complex proteome, plasma is an intricate body fluid, containing a wide diversity of proteins [6]. Plasma has been investigated using targeted evaluations, to measure markers that detect MI or predict outcomes following MI. For examples, the muscle form of creatine

kinase (CK-Mb), troponins, and C-reactive protein are used clinically to determine both presence of MI and extent of myocardial damage [7, 8]. MMP-9, galectin-3, and brain natriuretic peptide have been used to evaluate LV responses to MI [9–11]. Plasma has also been investigated using proteomic approaches, but this has been fraught with technical issues, primarily because the range of protein levels in the plasma is 10^{10}, and the ten most abundant proteins account for 90% of the total protein concentration [12, 13]. Serum albumin is a high abundant protein in plasma, and it is the leading candidate for selective removal prior to proteomics analysis of less abundant proteins in plasma. Several albumin-depletion methods are commercially available, mainly based in immunoaffinity columns. Albumin can also be removed by ligand chromatography [14, 15], and isoelectric trapping [16]. Nonetheless, the use of depletion methods may also result in specific removal of low abundant cytokines, lipoproteins, and peptide hormones of interest [17].

Accordingly, we hypothesized that using a fractionation protocol for the analysis of plasma proteins post-MI in wild-type (WT) and MMP-9 null mice would identify prospective markers of early MI that are MMP-9 dependent. In our study, we performed protein fractionation prior to protein separation by 1D-PAGE and MS analysis. By doing so, we avoided using depletion methods and concomitantly reduced the presence of albumin and enriched for lower abundance proteins.

2. Materials and Methods

2.1. Animals and Surgery. All animal procedures were conducted according to the "Guide for the Care and Use of Laboratory Animals" (NIH Notice Number: NOT-OD-12-020) and were approved by the Institutional Animal Care and Use Committee at the University of Texas at San Antonio. Male 4–8 months old C57BL6/J wild-type (WT) ($n = 3$) and MMP-9 null mice ($n = 3$) were used in this study. Animals were housed at constant temperature ($22 \pm 2^{\circ}$C) on a 12 h light/dark cycle. They were fed *ad libitum* on standard laboratory mice chow and had free access to tap water. MI was made by permanent ligation of the left anterior descending coronary artery as described previously [18]. Animals without MI (day 0) were used as controls ($n = 3$/genotype). At one day post-MI, mice were anesthetized with 5% isoflurane, plasma was collected, the coronary vasculature was flushed with 0.9 M saline, and the hearts were excised. The hearts were separated between right and left ventricles and were stained with 1% 2,3,5-triphenyltetrazolium chloride (Sigma) and photographed for measurement of infarct area.

2.2. Plasma Fractionation. Plasma was collected at days 0 and 1 post-MI, snap frozen and stored at -80°C. At sacrifice, heparin (100 μL of 1000 USP Units/mL) was injected intraperitoneally, and 5 min after heparin injection, blood was collected from the carotid artery of the mouse. Total protein quantification was determined using Quick Start Bradford Protein Assay (Biorad). Plasma was fractionated using the GellFree 8100 Fractionation System (Protein Discovery, Inc.). Five hundred micrograms of total protein were reduced for 10 min at 50°C with 1x acetate sample buffer (Protein Discovery, Inc.) and 0.053 M dithiothreitol (DTT). After samples being cooled down to room temperature, 15 mM iodoacetamide was added, and samples were alkylated in the dark for 10 min.

For protocol optimization, we used six different protocols where samples were either run in an 8%, 10%, or 12% Tris-acetate cartridge combined with one of three fractionation programs. We tested three different fractionation programs shown in Figures 2, 3, and 4. For all of the programs, MES was used as the running buffer (0.05 M MES, 0.05 M Tris, 0.1% SDS pH 7.9). For each of the six protocols tested, twelve fractions (150 μL/fraction) were collected per sample and proteins were visualized on a 12% Bis-Tris gel by SDS-PAGE.

2.3. Mass Spectrometry. The proteins in fraction 1 were separated in a 10–20% Tricine/peptide gel. The gel lane for each replicate was divided into six slices. The gel region containing visually detectable proteins from the lane for fraction 12 (the highest molecular weight fraction) on the Bis-Tris gel was excised into three slices. Each slice was separately destained and dehydrated and the proteins digested *in situ* with trypsin (Promega). The digests were analyzed by capillary HPLC-electrospray ionization tandem mass spectrometry (HPLC-ESI-MS/MS) on a Thermo Fisher LTQ Orbitrap Velos mass spectrometer fitted with a New Objective Digital PicoView 550 NanoESI source. Online HPLC separation of the digests was accomplished with an Eksigent/AB Sciex NanoLC-Ultra 2-D HPLC system: column, PicoFrit (New Objective; 75 μm i.d.) packed to 15 cm with C18 adsorbent (Vydac; 218MS 5 μm, 300 Å). Precursor ions were acquired in the Orbitrap in profile mode at 60,000 resolution (m/z 400); data-dependent collision-induced dissociation (CID) spectra of the six most intense ions in the precursor scan above a set threshold were acquired at the same time in the linear trap. Mascot (versions 2.3.02; Matrix Science) was used to search the uninterpreted CID spectra against a combination of the mouse subset of the NCBInr database (Mus. (145,083 sequences)) and a database of common contaminants (179 sequences). Methionine oxidation was considered as a variable modification; trypsin was specified as the proteolytic enzyme, with one missed cleavage allowed. A secondary search of the CID spectra using X! Tandem, cross-correlation of the X! Tandem and Mascot results, and determination of protein and peptide identity probabilities were accomplished by Scaffold (version 3; Proteome Software). The thresholds for acceptance of peptide and protein assignments in Scaffold were 95% and 99.9%, respectively. The results for the individual slices were combined for presentation purposes.

2.4. Immunoblotting. Proteins of interest were further analyzed by immunoblotting. Total proteins (10 μg) were loaded onto either 4–12% Bis-Tris gels (proteins >50 kDa) or 10–20% tricine gels (proteins <50 kDa) and run by SDS-PAGE. Proteins were transferred to a nitrocellulose membrane

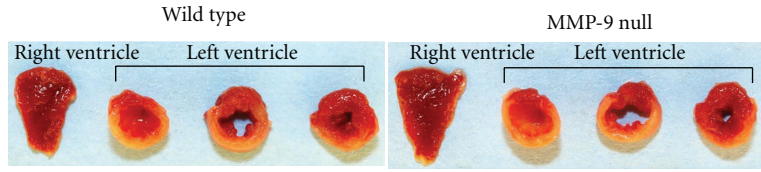

Figure 1: Infarct area was measured in the left ventricle. Infarct areas were similar between WT (52 ± 8%) and MMP-9 null (54 ± 2%) mice ($P = 0.85$).

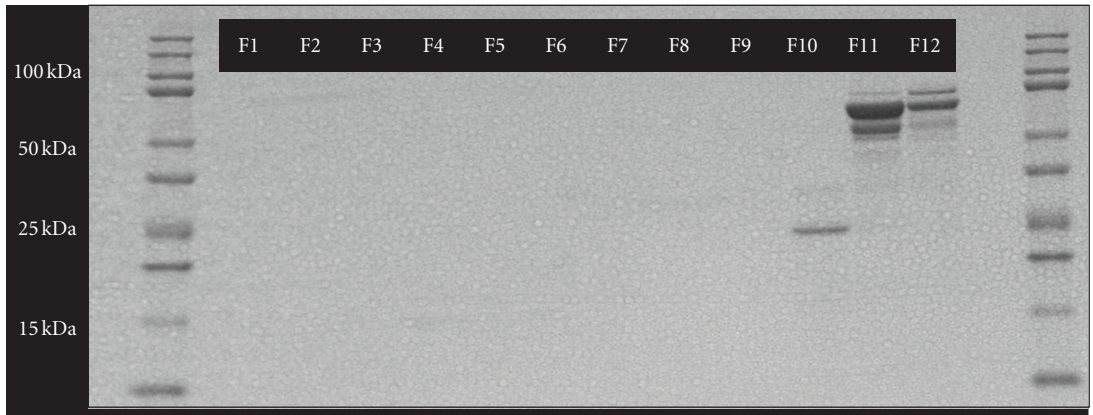

Fractionation program number 1.*during this step, running buffer was replaced with fresh running buffer.

Step	1	2	3	4	5	6	7	8	9	10	11	12	13
Voltage (V)	50	50	50	50	100	100	100	100	100	100	100	100	100
Fraction time (min)	16	41.5	2	2	3	2	2	3	5	7	10	15	20
Fraction number	---	1	2	3*	4	5	6	7	8	9	10	11*	12

Figure 2: Plasma fractionation using an 8% acetate cartridge and program number 1; samples were run on 12% Bis-Tris gel. This fractionation scheme was not optimal because all of the proteins were observed in the last three fractions, rather than being evenly spread across fractions.

which was hybridized overnight at 4°C with primary antibody. Primary antibodies used were antiserum amyloid A1 (number AF2948, R&D), anti-alpha-2 macroglobulin (number ab52651, Abcam) and antineutrophil-associated gelatinase lipocalin (NGAL, aka lipocalin 2; number ab63929, Abcam) (number ab63929, Abcam). Protein quantification was determined by densitometry analysis using ImageJ.

2.5. Statistical Analysis. Data are reported as mean ± SEM. Immunoblot intensities (arbitrary units) were assessed using a one-way ANOVA with Newman-Keuls multiple comparison test. A $P < 0.05$ was considered significant.

3. Results

Infarct areas were similar between WT and MMP-9 null mice ($P = 0.85$; Figure 1), indicating that both groups received a similar injury stimulus. We tested several methods to optimize the plasma fractionation prior to MS analysis. The different fractionation programs are shown in the figures. When using fractionation program number 1 and an 8% acetate cartridge, proteins were only observed in fractions 10 to 12 (Figure 2). By changing voltage intensities and step duration, we were able to visualize proteins in all 12 fractions. The protein' profiles differed depending of the type of cartridge used (Figure 3). Since serum albumin is approximately 66 kDa, we focused on protocols that provided fractions with reduced albumin content. The combination of program number 3 with the 8% acetate cartridge yielded fractions with these characteristics, where most of the albumin was seen in fractions 2 to 11 (Figure 4). These conditions were considered optimal for our examination, and fractions 1 and 12, which showed reduced levels of albumin, were further analyzed by HPLC-ESI-MS/MS on an Orbitrap Velos.

Supplemental Tables 1 and 2 list the proteins identified in both fractions (see Supplementary Material available online at doi:10.1155/2012/397103), per genotype and time point. Of the 145 proteins identified in the WT mice, 12

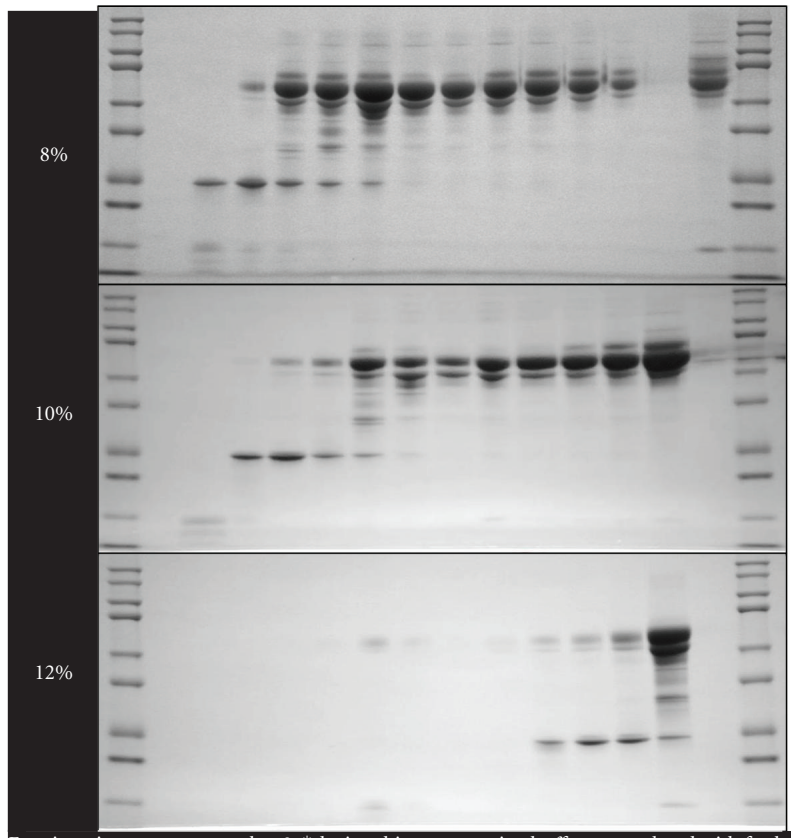

Fractionation program number 2. * during this step, running buffer was replaced with fresh running buffer.

Step	1	2	3	4	5	6	7	8	9	10	11	12	13
Voltage (V)	50	50	60	60	60	80	80	80	50	50	50	80	100
Fraction time (min)	16	44	5	5	5	8	5	3	8	8	8	10	25
Fraction number	---	1*	2	3	4	5	6	7	8	9*	10	11	12

Figure 3: Three cartridges with different acetate percentages were used with the same fractionation program to study fraction protein profile. Program number 2 on 8%, 10% and 12% acetate cartridges and 12% Bis-Tris gels gave interesting results, in that the samples were spread out across fractions, but fraction 12 still showed high albumin abundance.

proteins were present only at day 0, and 45 proteins were just observed 1 day post-MI (Figure 5(a)). In the MMP-9 null mice, 195 proteins were identified; of which 19 were unique to day 0 and 61 proteins were observed only post-MI (Figure 5(b)). The molecular weight of proteins observed in fraction 1 ranged from 7 kDa to 69 kDa, although fragments of higher molecular weight proteins (e.g., C-terminus of alpha-2 macroglobulin) were also present. The majority of proteins observed in fraction 12 had molecular weights ranging from 45 kDa to 263 kDa; nevertheless, lower molecular weight proteins such as transthyretin (16 kDa) were also observed. The UniProt protein database was used to classify proteins by biological function. The unweighted spectrum counts were used to provide measure of relative abundance (Figure 6). Two percent of the proteins identified in WT animals were ECM proteins, while ECM proteins accounted for 3% of the total identified proteins in MMP-9 null mice.

We used immunoblotting as a secondary method to examine the proteins identified by MS. Serum amyloid A (SAA), a marker of inflammation, was observed at both time points. SAA was identified in fraction 1 of both genotypes and levels at day 0 were significantly different ($P < 0.001$) from levels at day 1 post-MI (Figure 7(a)). Eighty nine proteins were identified only post-MI, including NGAL. NGAL levels post-MI were significantly higher than at day 0 ($P < 0.05$) but no differences were observed between genotypes (Figure 7(b)). Alpha-2 macroglobulin, a generic MMP inhibitor and an MMP-9 substrate, was observed only post-MI in the WT group. Nevertheless, alpha-2 macroglobulin precursor was observed in both groups at days 0 and

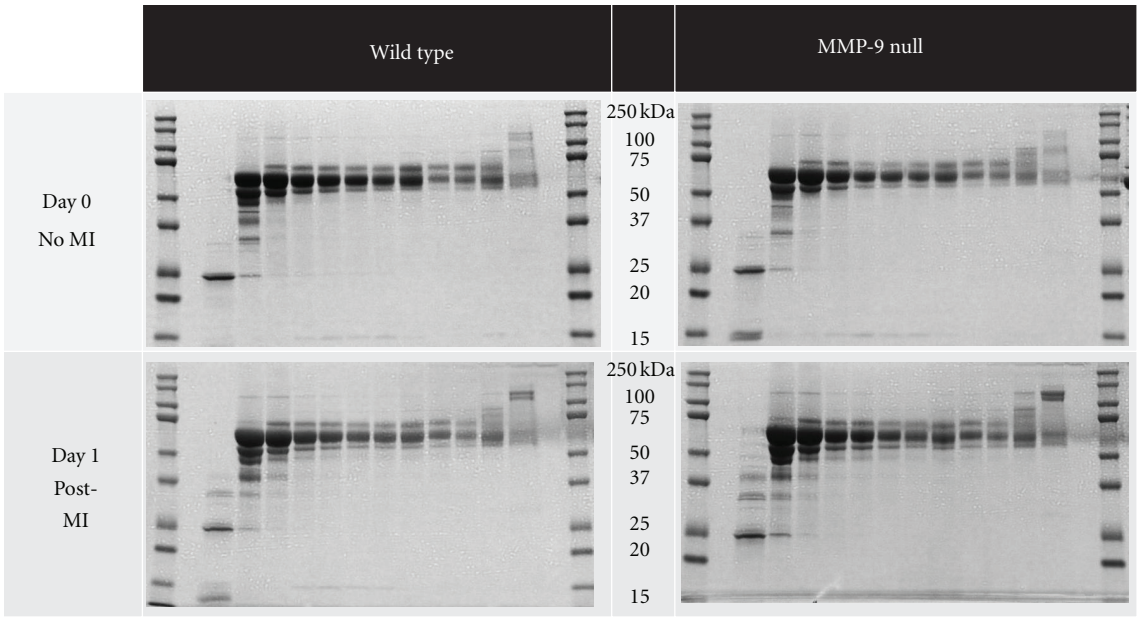

Fractionation program number 3. *during this step, running buffer was replaced with fresh running buffer.

Step	1	2	3	4	5	6	7	8	9	10	11	12	13
Voltage (V)	50	50	100	100	80	80	80	80	80	80	80	100	100
Fraction time (min)	16	44	7	5	3	3	3	3	5	5	5	10	20
Fraction number	---	1*	2	3	4	5	6	7	8	9*	10	11	12

Figure 4: Each plasma sample was separated by electrophoretic mobility into 12 fractions, using fractionation program number 3 on an 8% acetate cartridge and were run on 12% Bis-Tris gels. The figure shows a representative gel from each group ($n = 3$ for each group).

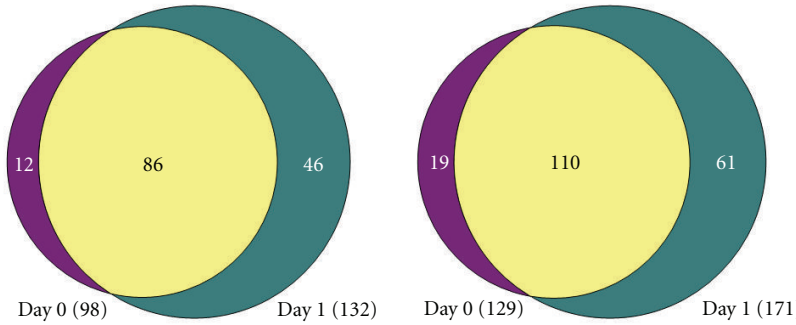

(a) WT (b) MMP-9 null

Figure 5: Venn diagram representing the number of proteins identified in combined fractions 1 and 12 of the plasma from each group. The purple is the number of proteins identified only in day 0. The green is the number of proteins identified at both time points. The Venn diagram was made using Venn Diagram Plotter software.

1 post-MI. Quantification of alpha-2 macroglobulin showed a significant difference between genotypes 1 day post-MI (Figure 7(c)).

4. Discussion

The discovery of plasma markers remains challenging due to the complexity of the samples and the wide range of protein concentrations. In addition, the analysis of proteomics data is a complex multistep process [17]. Therefore, to overcome these problems, effective sample preparation is of outmost importance. Efficient sample preparation will reduce component complexity and enrich for lower abundance proteins while depleting or reducing the most abundant ones. We used a novel fractionation technique to interrogate plasma from WT and MMP-9 null mice at day 1 post-MI. This novel technique provides all of the advantages of 1-D gel electrophoresis, with the additional

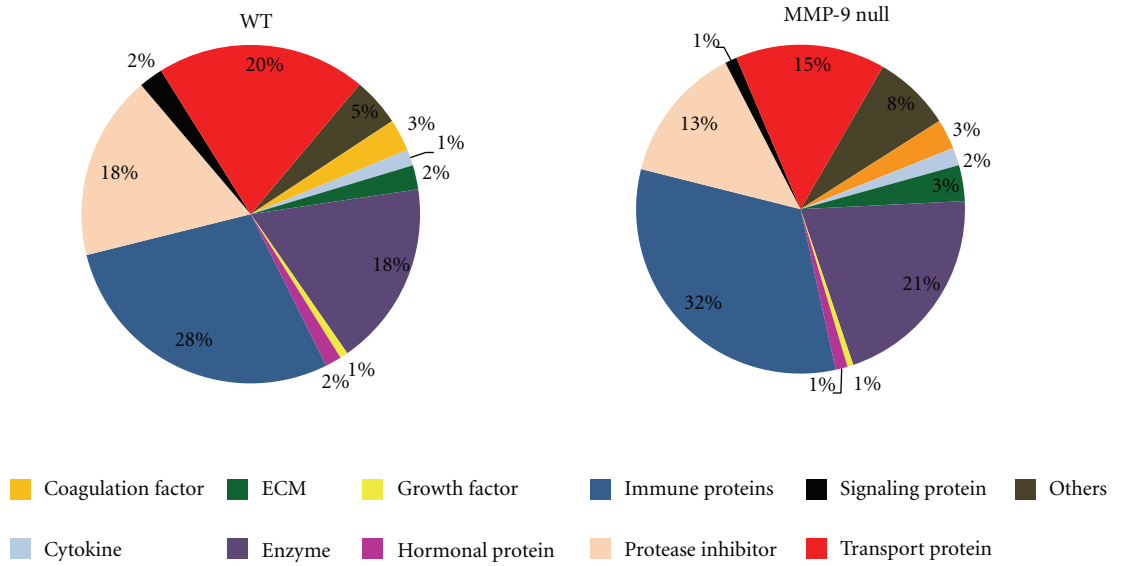

Figure 6: Proteins classification by biological function. The graph was created using the number of unweighted spectrum counts as a measure of relative abundance.

benefits of increased loading capacity and high yield liquid phase recovery. The most significant findings of this study were that (1) multiple proteins were identified in post-MI plasma, compared with day 0 control plasma; (2) serum amyloid A is good marker of early MI but it is not MMP-9 dependent; (3) alpha-2 macroglobulin may be an MMP-9 dependent marker. These results combined indicate that a fractionation followed by 1-D gel/LC/MS analysis strategy is effective to isolate and identify plasma proteins changes in response to MI.

We identified a total of 145 unique proteins in the WT samples and 195 unique proteins in the MMP-9 null samples. Known markers of inflammation, such as haptoglobin and SAA, were among the proteins identified. Studies from the Malmö Preventive Study, Sweden, have shown that elevated plasma levels of haptoglobin are a risk factor for MI [19]. Recently, Devaux's group identified haptoglobin as a potential biomarker of prognosis of heart failure in patients with acute MI [20]. Interestingly, they state that low levels of haptoglobin early post-MI favor heart failure. We identified haptoglobin as a potentially increased post-MI marker; nevertheless, studies with longer time points post-MI will have to be developed to confirm the role of haptoglobin in progression to heart failure. SAA is a known marker of inflammation, and SAA levels inversely correlate with cardiac function [21]. One-day post-MI the levels of SAA were significantly higher, in both genotypes, confirming an association with MI. Our future work involves a temporal study of plasma biomarkers post-MI. We plan to investigate if changes in plasma SAA are correlated with progression to heart failure post-MI.

From the proteins present only post-MI, we performed immunoblots against NGAL and alpha-2 macroglobulin. NGAL is a marker of kidney injury [22], as well as matrix degradation and inflammation [23]. This protein has previously been reported to be associated with MI and heart failure [24, 25]. A recent paper by Akcay and colleagues shows that 1-year mortality rates were significantly higher in patients with high levels of NGAL [26]. Our results were in accordance with the previous reports, showing a robust increase in NGAL levels post-MI. Alpha-2 macroglobulin is a generic proteinase inhibitor with broad specificity [27] and an MMP-9 substrate [28]. Although the association between MMP-9 and alpha-2 macroglobulin has been previously reported, this is the first time that alpha-2 macroglobulin is associated with MMP-9 in the myocardial infarction setting. The higher levels of alpha-2 macroglobulin observed in the MMP-9 mice post-MI suggest that this protein may be an MI biomarker that is MMP-9 dependent.

The protocols developed in this study can be used for other biological samples besides plasma. We are currently developing a fractionation method to investigate secreted proteins in cell culture media. Like in plasma, albumin is highly abundant in the commercially available serums used to supplement culture media. *In vitro*, the levels of secreted proteins are very low compared to the values observed in culture serum, making it very difficult to identify and quantify the proteins produced by the cells. Fractionation of samples is an easy and reproducible technique that can be used in a variety of models and biological samples.

Mouse models of MI are very useful and important given the unique ability to genetically manipulate these animals [29]. However, it is important to remember that the MI mouse model does not fully mimic the human disease. Thus, postinfarct remodeling of the LV likely has differences between the mouse and human that will need to be taken into account before full translation can occur. Acute MI remains a leading cause of morbidity and mortality worldwide. Thus, the discovery and development of biomarkers has high potential for providing a real benefit for screening, diagnosis, prognosis, prediction of recurrence, and therapeutic monitoring of MI patients.

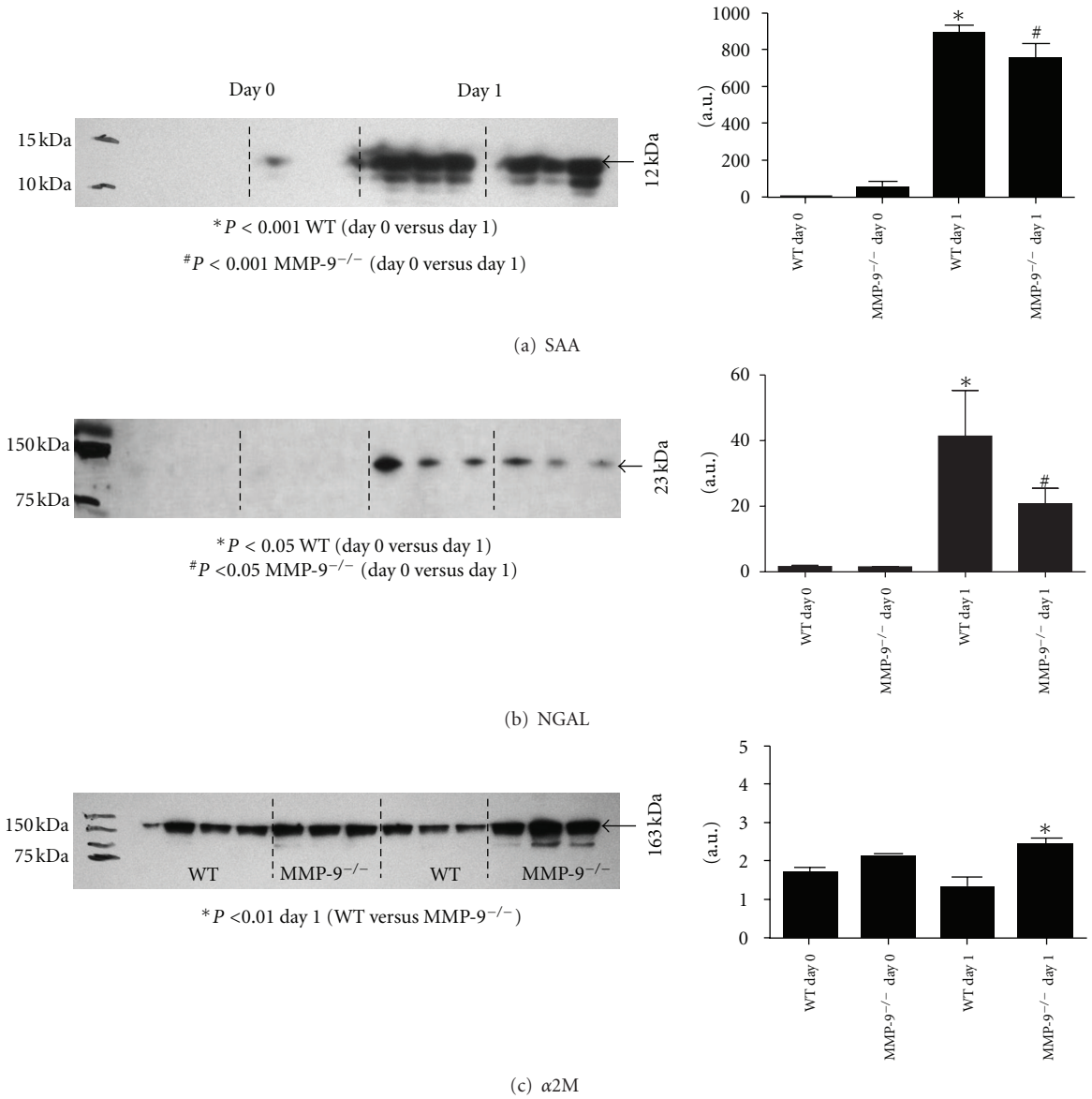

Figure 7: Immunoblots for: (a) Serum amyloid A. Protein levels increased significantly post-MI for both genotypes ($P < 0.001$). (b) NGAL. NGAL was observed only post-MI in both genotypes ($P < 0.05$). (c) Alpha-2 macroglobulin (α2M). MMP-9 null mice showed higher levels of α2M at 1 day post-MI compared to the WT mice counterpart. Densitometry, measured as arbitrary units (a.u.), was used to quantify protein levels in all immunoblots. $n = 3$/group.

In conclusion, by performing plasma fractionation prior to proteomics analysis, we were able to reduce the presence of high abundant proteins, such as albumin, and enrich samples for the detection of lower abundance proteins. We compared plasma samples from wild-type and MMP-9 null mice post-MI, and identified alpha-2 macroglobulin as a prospective MI marker which may be MMP-9 dependent. This technical report revealed that a fractionation approach is a useful technique to evaluate plasma samples.

Acknowledgments

The authors acknowledge support from NIH NHLBI T32 HL07446 to KYD and from NHLBI HHSN 268201000036C (N01-HV-00244) for the UTHSCSA Cardiovascular Proteomics Center and R01 HL075360, the Max and Minnie Tomerlin Voelcker Fund, and the Veteran's Administration (Merit) to M. L. Lindsey. They acknowledge support from the University of Texas Health Science Center at San Antonio for the Institutional Mass Spectrometry Laboratory.

References

[1] V. L. Roger, A. S. Go, D. M. Lloyd-Jones, E. J. Benjamin, and J. D. Berry, "Heart disease and stroke statistics—2012 update: a report from the American Heart Association," *Circulation*, vol. 125, pp. e2–e220, 2012.

[2] A. T. Yan, R. T. Yan, F. G. Spinale et al., "Plasma matrix metalloproteinase-9 level is correlated with left ventricular volumes

and ejection fraction in patients with heart failure," *Journal of Cardiac Failure*, vol. 12, no. 7, pp. 514–519, 2006.

[3] D. Kelly, G. Cockerill, L. L. Ng et al., "Plasma matrix metalloproteinase-9 and left ventricular remodelling after acute myocardial infarction in man: a prospective cohort study," *European Heart Journal*, vol. 28, no. 6, pp. 711–718, 2007.

[4] M. L. Lindsey, J. Gannon, M. Aikawa et al., "Selective matrix metalloproteinase inhibition reduces left ventricular remodeling but does not inhibit angiogenesis after myocardial infarction," *Circulation*, vol. 105, no. 6, pp. 753–758, 2002.

[5] A. Ducharme, S. Frantz, M. Aikawa et al., "Targeted deletion of matrix metalloproteinase-9 attenuates left ventricular enlargement and collagen accumulation after experimental myocardial infarction," *Journal of Clinical Investigation*, vol. 106, no. 1, pp. 55–62, 2000.

[6] N. L. Anderson, M. Polanski, R. Pieper et al., "The human plasma proteome," *Molecular and Cellular Proteomics*, vol. 3, no. 4, pp. 311–326, 2004.

[7] L. Karpinski, R. Płaksej, R. Derzhko, A. Orda, and M. Witkowska, "Serum levels of interleukin-6, interleukin-10 and C-reactive protein in patients with myocardial infarction treated with primary angioplasty during a 6-month follow-up," *Polskie Archiwum Medycyny Wewnetrznej*, vol. 119, no. 3, pp. 115–121, 2009.

[8] N. D. Brunetti, D. Quagliara, and M. Di Biase, "Troponin ratio and risk stratification in subjects with acute coronary syndrome undergoing percutaneous coronary intervention," *European Journal of Internal Medicine*, vol. 19, no. 6, pp. 435–442, 2008.

[9] M. Szulik, J. Stabryla-Deska, J. Boidol, R. Lenarczyk, and Z. Kalarus, "Echocardiography-based qualification and response assessment to cardiac resynchronisation therapy in patients with chronic heart failure. The matrix metalloproteinase-9 substudy," *Kardiologia Polska*, vol. 69, pp. 1043–1051, 2011.

[10] K. Sakata, K. Iida, N. Mochiduki, and Y. Nakaya, "Brain natriuretic peptide (BNP) level is closely related to the extent of left ventricular sympathetic overactivity in chronic ischemic heart failure," *Internal Medicine*, vol. 48, no. 6, pp. 393–400, 2009.

[11] P. A. McCullough, A. Olobatoke, and T. E. Vanhecke, "Galectin-3: a novel blood test for the evaluation and management of patients with heart failure," *Reviews in Cardiovascular Medicine*, vol. 12, pp. 200–210, 2011.

[12] P. G. Righetti, A. Castagna, F. Antonucci et al., "Proteome analysis in the clinical chemistry laboratory: myth or reality?" *Clinica Chimica Acta*, vol. 357, no. 2, pp. 123–139, 2005.

[13] M. Nissum, S. Kuhfuss, M. Hauptmann et al., "Two-dimensional separation of human plasma proteins using iterative free-flow electrophoresis," *Proteomics*, vol. 7, no. 23, pp. 4218–4227, 2007.

[14] J. Travis, J. Bowen, and D. Tewksbury, "Isolation of albumin from whole human plasma and fractionation of albumin depleted plasma," *Biochemical Journal*, vol. 157, no. 2, pp. 301–306, 1976.

[15] A. K. Sato, D. J. Sexton, L. A. Morganelli et al., "Development of mammalian serum albumin affinity purification media by peptide phage display," *Biotechnology Progress*, vol. 18, no. 2, pp. 182–192, 2002.

[16] D. L. Rothemund, V. L. Locke, A. Liew, T. M. Thomas, V. Wasinger, and D. B. Rylatt, "Depletion of the highly abundant protein albumin from human plasma using the Gradiflow," *Proteomics*, vol. 3, no. 3, pp. 279–287, 2003.

[17] K. Chandramouli and P. Y. Qian, "Proteomics: challenges, techniques and possibilities to overcome biological sample 6 complexity," *Human Genomics and Proteomics*, vol. 2009, Article ID 239204, 2009.

[18] M. L. Lindsey, G. P. Escobar, L. W. Dobrucki et al., "Matrix metalloproteinase-9 gene deletion facilitates angiogenesis after myocardial infarction," *American Journal of Physiology*, vol. 290, no. 1, pp. H232–H239, 2006.

[19] S. Adamsson Eryd, J. G. Smith, O. Melander, B. Hedblad, and G. Engström, "Inflammation-sensitive proteins and risk of atrial fibrillation: a population-based cohort study," *European Journal of Epidemiology*, vol. 26, no. 6, pp. 449–455, 2011.

[20] B. Haas, T. Serchi, D. R. Wagner et al., "Proteomic analysis of plasma samples from patients with acute myocardial infarction identifies haptoglobin as a potential prognostic biomarker," *Journal of Proteomics*, vol. 75, pp. 229–236, 2011.

[21] R. Di Stefano, V. Di Bello, M. C. Barsotti et al., "Inflammatory markers and cardiac function in acute coronary syndrome: difference in ST-segment elevation myocardial infarction (STEMI) and in non-STEMI models," *Biomedicine and Pharmacotherapy*, vol. 63, no. 10, pp. 773–780, 2009.

[22] D. Bolignano, V. Donato, G. Coppolino et al., "Neutrophil Gelatinase-Associated Lipocalin (NGAL) as a marker of kidney damage," *American Journal of Kidney Diseases*, vol. 52, no. 3, pp. 595–605, 2008.

[23] S. H. Nymo, T. Ueland, E. T. Askevold, T. H. Flo, and J. Kjekshus, "The association between neutrophil gelatinase-associated lipocalin and clinical outcome in chronic heart failure: results from CORONA," *Journal of Internal Medicine*, vol. 271, no. 5, pp. 436–443, 2012.

[24] A. Şahinarslan, S. A. Kocaman, D. Bas et al., "Plasma neutrophil gelatinase-associated lipocalin levels in acute myocardial infarction and stable coronary artery disease," *Coronary Artery Disease*, vol. 22, no. 5, pp. 333–338, 2011.

[25] A. Yndestad, L. Landrø, T. Ueland et al., "Increased systemic and myocardial expression of neutrophil gelatinase-associated lipocalin in clinical and experimental heart failure," *European Heart Journal*, vol. 30, no. 10, pp. 1229–1236, 2009.

[26] A. B. Akcay, M. F. Ozlu, N. Sen, S. Cay, and O. H. Ozturk, "Prognostic significance of neutrophil gelatinase-associated lipocalin in ST-segment elevation myocardial infarction," *Journal of Investigative Medicine*, vol. 60, pp. 508–513, 2012.

[27] L. C. Cáceres, G. R. Bonacci, M. C. Sánchez, and G. A. Chiabrando, "Activated α2 macroglobulin induces matrix metalloproteinase 9 expression by low-density lipoprotein receptor-related protein 1 through MAPK-ERK1/2 and NF-κB activation in macrophage-derived cell lines," *Journal of Cellular Biochemistry*, vol. 111, no. 3, pp. 607–617, 2010.

[28] L. F. Arbeláez, U. Bergmann, A. Tuuttila, V. P. Shanbhag, and T. Stigbrand, "Interaction of matrix metalloproteinases-2 and -9 with pregnancy zone protein and α2-macroglobulin," *Archives of Biochemistry and Biophysics*, vol. 347, no. 1, pp. 62–68, 1997.

[29] N. A. Trueblood, Z. Xie, C. Communal et al., "Exaggerated left ventricular dilation and reduced collagen deposition after myocardial infarction in mice lacking osteopontin," *Circulation Research*, vol. 88, no. 10, pp. 1080–1087, 2001.